The role of calcium dependent neurotransmission in axon path finding, myelination and maintenance of specified cortical projection neuron populations



Doctor of Philosophy Thesis
Trinity 2018

Kim Virginia Korrell

Linacre College
Department of Physiology, Anatomy and Genetics
Medical Science Division, University of Oxford

Supervised by
Prof Zoltán Molnár and Dr Anna Hoerder-Suabedissen

Abstract

My thesis examines the mechanisms involved in regulation of myelination during mammalian cortical development and the subsequent maintenance of the myelin in cortical projection neurons during adult life. Myelin in the central nervous system is produced by oligodendrocytes to ensure fast saltatory conduction of action potentials at the nodes of Ranvier, the gaps left by myelin. Myelination in the central nervous system is among others dependent on neuronal activity but the underlying mechanism is not yet completely understood. Because myelination plays an important role in many neuronal diseases, such as multiple sclerosis and schizophrenia, it is important to understand the molecular and cellular mechanisms. To do so, I examined the effects of genetically suppressing the neuronal activity in two separate ways in deep cortical layers of the mouse.

One way to reduce neuronal activity was to abolish regulated vesicular release by removing Snap25 (synaptosome-associated protein of 25 kDA), member of the SNARE ((N-ethylmaleimide-sensitive factor) Attachment Protein Receptor) complex in a Snap25-flox mouse in which the essential exon 5a/b is flanked by LoxP sites and therefore truncated in the presence of Cre-recombinase. Since the fusion of neurotransmitter containing vesicles is mediated amongst others by the SNAP25 protein, removal of the functional SNAP25 protein prevented calcium-dependent regulated vesicle exocytosis in a cell-type specific manner. Nrsr1 (for Layer VI) and Rbp4 (for Layer V) conditional Snap25 KO mice were bred on a floxed-stop-tdTomato background such that all affected cells were tdTomato-labelled within the subpopulation of layer V or VI projection neurons. My results for layer VI and Layer V demonstrated that preventing neurotransmitter release in Snap25 cKO mice does not affect the onset of myelination, density of oligodendroglia, nodal structure or thalamic fibre targeting but it has the effect of premature fibre degeneration causing myelin degeneration and decreasing the g-ratio in the dorsal corticospinal tract. The time course of degeneration occurs in a cell type specific manner, layer V being the most sensitive for silencing.

The second way to influence neuronal activity was by introducing the inwardly rectifying potassium channel (Kir2.1) by *in utero* electroporation at the time of the cortical projection neuron generation. The overexpression of Kir2.1 lowers the probability of action potential formation through hyperpolarization of the neurons which leads to a decrease of the membrane resistance so that they are less excitable. Examining this model at various stages did not reveal differences in targeting of projections or myelin in the corpus callosum when assessed by MBP immunohistochemistry at P14.

Together, the results indicate that neuronal activity has little effect on the onset of myelination but has effects on the g-ratio in deep cortical layer projection neurons in mice.

Acknowledgements

This thesis would not have been possible without the support of many individuals, who shared their time, knowledge and wisdom with me. I am deeply grateful for you.

Firstly, I would like to thank Professor Zoltán Molnár for welcoming me into his laboratory and giving me with the opportunity to work on this fascinating project. I greatly appreciate his passion for the developing brain (including mine) during the PhD. Thank you for having confidence in me when I did not have it in myself.

I also would like to thank my Co-Supervisor, Dr Anna Hoerder-Suabedissen, for many project-advice coffee sessions in BioChem. I appreciate the guidance on both basic lab techniques as well as some crucial laboratory 'voodoo' for genotyping. Her patience when teaching me triple genetic animal breeding was remarkable.

Melissa, Navneet, Luigi, and James gave me supervisory advice like older siblings would give parental advice to their little sister. My elder laboratory siblings were invaluable to me.

I would also like to express my gratitude for the support of all the other Molnár lab members, students and collaborators that I have worked, laughed, and cried with over the years: Wei-Zhi, Fernando, Isabel, Kristina, Lance, Patricia, Helen, Eddie, and Sanskrithi.

I am especially grateful for the students Charlotte, Harriet and Mai-Carmen, who supported me both in the Molnár lab and over a bowl of ice-cream at G&D's. Thanks also to Will, with whom I shared as many laughs as deep and meaningful conversations.

The EM-competency of my collaborator, Dr Graham Knott from École Polytechnique Fédérale de Lausanne, came just when it was needed most, helping me with my myelin techniques.

Sharing an office with postdocs from other labs offers the precious opportunity to get diverse advice on a range of topics. It also means that they often eat all of your food. Carlo, Graham, and Raquel - I loved sharing my care packages with you (of course entirely voluntarily). Special thanks to Carlo, who dried my tears, and listened to me not only during the work day but also during late

night/weekend experiments. You are a great father and scientist, I owe you a lot (of chocolate).

Without the scholarship of the Anatomical Society this DPhil would have never been financially feasible for me nor my family. I am equally grateful for both the scholarship and the individuals I met at the Society conferences.

Thanks to the college, department and especially BSB staff, namely Laura, Michael, Angela, and Richard, who regularly made my day by cheering me up with their English lessons and general cheekiness.

In Oxford, your College is your home, and your College friends are family. Thank you to my amazing 9 housemates in my first year and to my college friends/family, including Peter, Boi, Salam, Luana, Tarique, Josh, Jill, Luana and Karrar, who guided me through light and dark times.

There were many people outside the laboratory who also had a significant impact on the success of this thesis.

Firstly, thanks to my family, who believed in me long before my earliest memories. Without the endless support of my father, my mother, and my sister, both before and during my PhD, I never would have made it. It gives me strength to know that you will support me in the yet-unwritten chapters in my life. Thanks also to all Scheidenberger and Korrell family members for their small and large acts of support, and especially to those who have sadly passed away.

Yvonne, by making me god-mother of your son, you made me part of your lively family. Thank you for entrusting me with this most honourable of responsibilities. You and your children have the invaluable talent of distracting me from all of my struggles.

Anna and Anna, our ‘Bastel-Gruppe’ (and all other activities) meant so much to me. You were my constant support for all DPhil-related (and unrelated) questions. Without you, I would have never met Selina, Alex, and Leigh, who have all filled my life with even more kindness.

Thanks to my Italian friends, whom I met near the end of my time in Oxford, but who have and continue to make lasting impressions: Noemie, for all the falafels we shared and the desk we never shared, and Alberto, for the night time myelin (pub) meetings and the launch of ‘myelin – pitfalls and pitfalls’.

Thanks to Kathie and Flo, as well as Nolan and Caitlin, for all the fun pub outings, games and cocktail nights. Thanks to Carina and Raam for sharing a bottle (or two) of wine after a long lab day.

I am grateful for my time at Yoga Quota where I spent so many hours stretching and strengthening, where inspiring teachers became close friends.

While writing up my thesis in Hamburg, I've made many new friends, most through AcroYoga, especially Laura. I enjoyed the jams and classes that distracted me after a long day in the library with my writing partner Tine.

Finally, I had many friends at home who supported me from afar and visited me during my PhD: Kim, Alex, Maike, Paula and Hanna. Our long-lasting friendships mean a lot to me.

Philipp and Ani, without the love and strength I gained through both of you I probably would have never made it through my PhD. You were there during ALL of my highs and lows - no matter how big or small. I am eternally grateful for your daily guidance through both professional and deeply personal successes and crises. It is so precious to have Ani in my life, who has the gift of knowing just what to say when I need it most and envelops me with her pure kindness and honesty. My partner Philipp made the brave move to follow me on my adventure. He was always proud of me and believed in me unconditionally. I am looking forward to all our adventures yet to come.

Thanks to all I mentioned and to the ones I missed.

Statement of Authorship

I contributed to the design, performance and analysis of the experiments for all results included in this thesis with the exceptions and collaborations listed below. My supervisors, Prof Zoltán Molnár and Dr Anna Hoerder-Suabdeissen, discussed and approved the design of experiments and provided guidance on the performance and analysis of them.

Three project students joined our laboratory during my doctorate and I provided day-to-day supervision for them: Miss Charlotte Pollart, an Erasmus master student from Université libre de Bruxelles; Miss Harriet Fodder, Final Honour School undergraduate medical student from Keble College, University of Oxford and Miss Mai-Carmen Requena-Komuro, MSc Neuroscience Program student, University of Oxford. While Miss Harriet Fodder mainly supported me with MBP and Olig2 immunohistochemistry in the LVI mouse line (subchapter 4.2.1.2 and 4.2.3.2), Miss Mai-Carmen Requena-Komuro worked on the same topics in the LV mouse line (subchapter 4.2.1.1 and 4.2.3.2). Miss Jolande Disser continued the analysis of some of the specimen I prepared using Kir2.1 *in utero* electroporation and on Snap25 cKO lines after I moved back to Germany to complete the writing up of my thesis. She contributed to immunohistochemistry and images in Figure 38.

All three students were directly supervised by me and I trained them to be able to do histological processing of the tissue, immunohistochemistry, microscopy and image analysis.

I performed a considerable behaviour tests on LVIb Snap25 cKOs which have not been included in this thesis (presented at SFN in San Diego in 2016: Guidi et al., (2016) SFN Abstract 634.16).

Dr Anna Hoerder-Suabedissen wrote a Cell Profiler script for Olig2 cell counts from which P8 results were included in this thesis (Figure 39 and Figure 41). Additionally, Anna and I shared the workload of genotyping, perfusions and the tissue resulting from it for our experiments. The DiI crystal placements discussed in chapter 5 were performed by Dr Hoerder-Suabedissen with my assistance.

After I left Oxford, Dr Kristina Parley, laboratory technician and manager, obtained animals and immunostained them followed by confocal imaging for me to perform the subsequent image analysis that resulted in Figure 50.

Advice on transmission electron microscopy (TEM) as well as immunogold labelling was provided by Professor Helen Christian, Department of Physiology, Anatomy and Genetics, and Ms Errin Johnson, Sir William Dunn School of Pathology (both Oxford University). The results on g-ratio gained through electron microscopy experiments were performed in collaboration with Professor Graham Knott, EPFL (École polytechnique fédérale de Lausanne, Lausanne, Switzerland) whom I visited to observe and learn some of the methodologies. All the perfusions were performed by me, but occasionally I had to leave Oxford and then I received help from Dr Shuichi Hayashi from our laboratory who used the same animals, but different parts of the CNS for his own experiments. Tissue processing for TEM as well as imaging was performed by Prof Knott at EPFL at Lausanne with my assistance while all subsequent image analysis and quantification was performed entirely by me.

I received training in fibre teasing from Prof Peter Brophy's laboratory members at the University of Edinburg.

All other experiments, including design, performance and analysis, were performed by me with generous guidance from members of the Molnár laboratory and the greater scientific community especially on cloning, sequencing, western blotting. Special thanks belongs to Miss Melissa Bailey and Dr Fernando Gracía-Moreno who trained me in *in utero* electroporations, to Dr Kristina Parley helping with genotyping, to Peter Gyring, PhD-student at Department of Engineering Science, Oxford, for advising me on statistics, to Dr Carlo Rinaldi and his assistance Joana, Department of Physiology, Anatomy and Genetics, Oxford University, for assisting me with tissue processing and qPCR and to Dr Anna Behrens, former at Biochemistry Department, Oxford University, for cloning support and to all group leaders who let us perform some of the experimental work under their Home Office project licences.

Parts of this thesis have been published or submitted to Cerebral Cortex and the Journal of Anatomy, respectively.

Alphabetical List of Abbreviations

AIS	Axon initial segment
AP	Action Potential
bHLH	Basic helix-loop-helix
BMP	Bone morphogenetic protein
bp	Base pair
CASPR	Contactin associated protein
CNP	2',3'-cyclic-nucleotide 3'-phosphodiesterase
CNS	Central nervous system
CP	Cerebral peduncle
CTX	Cortex
D N A	Deoxyribonucleic acid
DREADD	Designer receptors exclusively activated by designer drugs
EPSP	Excitatory postynaptic potential
GAPDH	Glyceraldehyde-3-phosphate dehydrogenase
GFAP	Glial fibrillary acidic protein
IC	Internal capsule
IPSP	Postynaptic potential
IUE	*In utero* electroporation
Kir	Inwardly rectifying potassium (K) channel - IRK or K_{ir}
LGN	Lateral geniculate nucleus
LP	Lateral posterior nucleus
LV	Layer V
LVI	Layer VI
MAG	Myelin associated glycoprotein
MBP	Myelin basic protein
MOBP	Myelin-associated oligodendrocyte basic protein
MOG	Myelin oligodendrocyte glycoprotein
MRF	Myelin gene regulatory factor
MS	Multiple sclerosis
Myrf	Myelin regulatory factor
NCAM	Neuronal cell adhesion molecule
NG2	Neural/glial antigen 2 proteoglycan
NoR	Node of Ranvier
OPC	Oligodendroyte progenitor cell
PCR	Polymerase chain reaktion
PDGF	Platelet-derived growth factor
PDGFaR	Platelet-derived growth factor α receptor
PLP	Myelin proteolipid protein
PNS	Peripheral nervous system
RNA	Ribonucleic acid

SHH	Sonic hedgehog
SNAP25	Synaptosome-associated protein of 25 kDA
SNARE	Soluble NSF (N-ethylmaleimide-sensitive factor) Attachment Protein Receptor
TH	Thalamus
TRN	Thalamic reticular nucleus
VAMP	Vesicle-associated membrane protein
VPM	Ventral posterior nucleus
LB	Lysogeny broth
PFA	Paraformaldehyde
PBS	Phosphate buffered saline
EDTA	Ethylenediamine tetraacetic acid
TRIS	Tris(hydroxymethyl)aminomethane
NaCl	Sodium chloride
nH_2O	Deionized water with
PCR	Polymerase chain reaction
MgCl	Magnesium chloride
dNTP	Deoxynucleotide
PBSA	Phosphate buffered sodium azide
PCR	Polymerase chain reaction
TEM	Transmission electron microscopy
PBSea	Phosphate buffered saline egg albumin
EM	Electron microscopy
RIPA	Radioimmunoprecipitation assay buffer
LDS	Lithium dodecyl sulfate
PVDF	Polyvinylidene difluoride
TBST	Tris buffered saline
ECL	Chemiluminescence
ATP	Adenosine 5'-triphosphate
cDNA	Complementary DNA
qPCR	Quantitative realtime PCR
Ct	Cycle of threshold
GOI	Gene of interest
ROI	Region of interest
H_2O	Water
PBSA	Phosphate buffered sodium azide
DAPI	4’,6-Diamidin-2-phenylindol
RFP	Red fluorescent protein

List of figures

Figure 1: Summary of the developmental sequence (target selection, somatodendritic differentiation and electrophysiological characteristics) of the two major classes layer V pyramidal neurons 27
Figure 2: Subtypes of pyramidal LVI cells and their main connections 31
Figure 3: Thalamocortical circuits in the adult mouse brain and schematic representation of the two major sets of thalamic projection neurons 33
Figure 4: Signals influencing oligodendrocyte development in the spinal cord and in the telencephalon 38
Figure 5: Insulation of nerve cells by oligodendrocytes in the CNS 44
Figure 6: Stylized diagram of cross-section through a myelinated segment of a nerve fibre in the CNS 45
Figure 7: Calcium mediated regulated vesicle release at synapse 65
Figure 8: tdTomato conditional Snap25 knock out 100
Figure 9: Normal thalamic targeting of cortical LV Snap25 cKO fibres 106
Figure 10: Premature axonal disintegration in the dorsal corticospinal tract 109
Figure 11: LV Type I and Type II neurons express Rbp4-Cre in controls and LV Snap25 cKOs at P8 110
Figure 12: Similar expression of tdTomato in LV of M1 at P21 111
Figure 13: Visibility of barrel field pattern in LV Snap25 cKOs is similar to controls in primary somatosensory cortex at 2 months 112
Figure 14: Extra-cortical labelling of Ntsr1-Cre is consistent across genotypes at P7 115
Figure 15: Similar weights of 4 months old LVI Snap25 cKO and control males 117
Figure 16: Normal thalamic targeting of cortical LVI Snap25 cKO fibres compared to control 118
Figure 17: Similar tdTomato fluorescent intensity in LVI of M1 at P21 120
Figure 18: Premature axonal disintegration of LVI Snap25 cKO axons 121
Figure 19: tdTomato signal and cell loss in the brain of LVI Snap25 cKOs 123
Figure 20: Visibility of barrel field pattern in LVI Snap25 cKOs similar to controls in primary somatosensory cortex at 2 months 124
Figure 21: Initial dsRed signal in control brains is markedly reduced compared to dsRed signal in experimental Kir2.1 brains at P14 127
Figure 22: Discontinuous dsRed signal in the P12 corpus collosum of E13.5 electroporated brains 128
Figure 23: Fluorescent electroporation side visible after dissection 128

Figure 24: Plasmid map of pCAG-Kir2.1-IRES-Cre 130
Figure 25: Plasmid map of stop-flox dsRed 131
Figure 26: Plasmid map of MutKir2.1-T2A-tdTomato 132
Figure 27: Plasmid map of Kir2.1-T2A-tdTomato 133
Figure 28: In utero electroporation in E13.5 embryos resulted in expression of experimental vectors in deep and superficial cortical layers at P14 134
Figure 29: At P14 tdTomato/dsRed signal is visible in the cerebral peduncle after in utero electroporation at E13.5 135
Figure 30: tdTomato/dsRed signal is not visible in the dorsal corticospinal tract after in utero electroporation at E13.5 examined at P14 136
Figure 31: Timeline of Cre-expression and degenerative processes in the Rbp4-Cre (LV) and Ntsr1-Cre (LVI) strains following Snap25 knockdown 147
Figure 32: Stages of oligodendrocyte development and their markers in the oligodendroglial lineage 155
Figure 33: Myelin basic protein (MBP) immunoreactivity in a wildtype brain at P14 (medial cross section) 163
Figure 34: MBP immunoreactivity in LV Snap25 cKOs in M1 at P8, P14 and P21 165
Figure 35: MBP immunoreactivity in striatal tissue of LV Snap25 cKOs and controls between P8 and P21 167
Figure 36: MBP immunoreactivity in LVI Snap25 cKOs and controls in M1 at P8, P14 and P21 169
Figure 37: MBP immunoreactivity in the striatum at P8, P14 and P21 in LVI Snap25 cKOs and controls 171
Figure 38: MBP immunoreactivity in LV Snap25 cKOs and LV controls as well as Kir2.1 and MutKir2.1 electroporations in the corpus callosum (CC) at P14 174
Figure 39: Expression of oligodendroglial markers Olig2 and CC1 in LV Snap25 cKOs at P8 in M1 and striatum 178
Figure 40: Expression of oligodendroglial markers Olig2 and CC1 in LV Snap25 cKOs at P21 in M1 and striatum 181
Figure 41: Immunoreactivity of Olig2 and CC1 in LVI Snap25 cKOs at P8 in the striatum 185
Figure 42: Immunoreactivity of Olig2 and CC1 in LVI Snap25 cKOs at P21 in M1 and striatum 188
Figure 43: Transmission electron microscopy artefacts of myelin disintegration due to inefficient fixation on a coronal section through the spinal cord 219
Figure 44: Lower g-ratio of LV Snap25 cKOs in comparison to controls in dorsal corticospinal tract at P18 222

Figure 45: Attached teased fibres from the dorsal spinal cord after immunohistochemistry for MBP and Caspr at P18 of control animals..... 225
Figure 46: Regular Caspr immunoreactivity at nodes of Ranvier in the corpus callosum of LVI Snap25 cKO at P14..... 227
Figure 47: Nodal segmentation along axons is not affected at P14 in the corpus callosum when analysed based on Caspr immunoreactivity..... 229
Figure 48: Quantitative western blot of myelin constituent MBP did not reveal a difference in MBP protein levels when normalised against the housekeeping gene GAPDH in striatal tissue at 6 months..... 232
Figure 49: qPCR of mRNAs coding for myelin proteins or oligodendrocyte and inflammation markers of cortical tissue revealed significant difference in some mRNA levels..... 234
Figure 50: Reduced tdTomato signal intensity at 6 months in LVI Snap25 cKOs in the striatum..... 237
Figure 51: Reduced tdTomato and MBP signal intensity at 9 months in LVI Snap25 in primary motor cortex and striatum..... 239

Table of Content

Abstract 3

Acknowledgements 4

Statement of Authorship 7

Alphabetical List of Abbreviations 9

List of figures 11

Table of Content 14

1 Introduction 18

1.1 Central Nervous System 20

1.2 Cortex 22

1.3 Anatomy of the deeper layers of the cortex 25

1.3.1 Anatomy of LV 25

1.3.2 Anatomy of LVI 29

1.4 Cell types of the CNS 34

1.5 Oligodendrocytes and myelin in the central nervous system 35

1.5.1 Oligodendrocytes and their development 35

1.5.2 Myelin sheath 42

1.5.3 MBP 46

1.6 Activity dependent myelination in the CNS 48

1.6.1 Influence of cognitive, motor and sensory activity on myelination 49

1.6.2 Influence of stimulating environment on myelination 53

1.6.3 Mechanisms of activity dependent myelination 55

1.6.4 Competition created by neuronal activity influences myelin formation 57

1.6.5 Myelination in information integration 58

1.7 Action potential propagation and regulated synaptic vesicle release 61

1.7.1 Action potential propagation at nodes of Ranvier 61

1.7.2 Regulated synaptic vesicle release 63

1.7.3 The role of Snap25 in the SNARE complex 64

1.7.4 Other roles of Snap25 and its family members 67

1.7.5 Snap25 mutants 69

1.8 Inward-rectifier potassium channels 70

1.8.1 Structure, location and function of K_{ir}2.1 and its family members 71

1.8.2 Neuronal activity and axonal development 73

1.8.3 Studying the role of neuronal activity by introducing Kir2.1 via *in utero* electroporation 74

1.9 Aims of this thesis 76

2 Methods ***80***

2.1 Animals 80

2.1.1 Breeding and maintenance 80

2.1.2 Genotyping 81

2.1.3 *In utero* electroporation 82

2.1.4 Tissue collection 83

2.2 Histology 83

2.2.1 Vibratome sectioning 83

2.2.2 Longitudinal flat-mounting of spinal cords 84

2.2.3 Fibre teasing of spinal cord tissue 84

2.2.3 Fluorescent immunohistochemistry 85

2.2.4 Tissue preparation for transmission electron microscopy (TEM) 85

2.2.5 Immuno-gold and contrast stain 86

2.2.6 Tissue preparation for tiled electron microscopy 86

2.3 Image acquisition and analysis 88

2.3.1 Epifluorescence and confocal microscopy 88

2.3.2 Electron microscopy 88

2.3.3 Fluorescence intensity analysis 89

2.3.4 Electron microscopy image analysis 89

2.3.5 Node of Ranvier quantification 90

2.3.6 Cell counts 90

2.4 Molecular techniques 90

2.4.1 Western blots 90

2.4.2 Miniprep 91

2.4.3 Sanger sequencing 91

2.4.4 DNA restriction digest 92

2.4.5 DNA extraction from agarose-gel and ligation 92

2.4.6 Maxiprep 93

2.4.7 Tissue homogenisation and RNA extraction for qPCR 93

2.4.8 c-DNA synthesis 94

2.4.9 Quantitative Realtime PCR (qPCR) 94

2.5 Frequently used solutions and antibody list 96

2.6 Statistics 97

3 Fibre targeting and maintenance of silenced neurons ***98***

3.1 Introduction 98

3.1.1 Transgenic mice to label subcortically projecting cortical LV and LVI neurons 99

3.1.2 Whisker Barrel cortex 101

3.1.3 Nomenclature 103
3.1.4 Aims of Chapter 3 103

3.2 Results 106
3.2.1 Normal thalamic targeting, but impaired maintenance of LV Snap25 cKO projections 106
3.2.2 Characterisation of Layer VI Snap25 cKO 114
3.2.3 Targeting of projection neurons electroporated with Kir2.1 125

3.3 Discussion 138
3.3.1 Targeting of LV and LVI Snap25 cKO fibres 138
3.3.2 Impaired fibre maintenance in LV and LVI Snap25 cKOs after the third postnatal week 144
3.3.3 Targeting of projections originating from Kir2.1 electroporated cortical neurons 149
3.3.4 Conclusion 152

4 Onset of myelination under the influence of genetically reduced neuronal activity 153

4.1 Introduction 153
4.1.1 Marker of oligodendrocyte lineage 154
4.1.2 Neuronal activity and the influence on oligodendrocyte development and myelinogenesis 158
4.1.3 Aims of this chapter 161

4.2 Results 163
4.2.1 Onset of myelination assessed by MBP in LV and LVI Snap25 cKOs 163
4.2.2 Comparison of myelination in the Corpus Callosum around LV Snap25 cKO and Kir2.1 electroporated fibres measured by MBP immunoreactivity 173
4.2.3 Expression of oligodendrocyte lineage markers in LV and LVI Snap25 cKO 177

4.3 Discussion 191
4.3.1 Onset of myelination under the influence of genetically reduced neuronal activity 191
4.3.2 Oligodendrocyte lineage markers in LV and LVI Snap25 cKO 201
4.3.3 Conclusion 208

5 Myelin characteristics and myelin maintenance surrounding axons originating from silenced cortical neurons 209

5.1 Introduction 209
5.1.1 Conduction velocity in myelinated nerve fibres 210
5.1.2 Contactin associated protein 1 215
5.1.3 Aims of this chapter 216

5.2 Results 218
5.2.1 Testing post embedding immuno-gold stain for tdTomato on TEM sections for myelin quantification in LV Snap25 cKOs 218
5.2.2 Reduced g-ratio in the dorsal corticospinal tract of LV Snap25 cKOs 220
5.2.3 Nodes of Ranvier in LV Snap25 cKOs 224
5.2.4 Protein and mRNA levels after degeneration of LVI Snap25 cKOs fibres 231

5.3 Discussion 241
5.3.1 Decreased g-ratio in LVI Snap25 cKOs in the dorsal corticospinal tract at P18 241
5.3.2 Unchanged nodal parameters in the CC of LV Snap25 cKOs 247
5.3.3 Protein and mRNA levels after degeneration of LVI Snap25 cKOs fibres 250
5.3.4 Conclusion 256
6 Discussion ***257***
6.1 Importance of activity dependent myelination **258**
6.2 What are the mechanisms of activity-dependent myelination? **259**
6.3 Various ways of myelin plasticity **261**
6.4 Hypoactivity and activity independent mechanisms **262**
6.5 The role of diffusible molecules in activity-dependent myelination **263**
6.6 Future possibilities of influencing neuronal vesicular release **266**
6.7 The influence of regional differences in adaptive myelination **269**
6.8 Changes in myelin characteristics following changes in neuronal activity **271**
6.9 Conclusion **273**
References ***275***

1 Introduction

The focus of this thesis is to observe the effects of reduced neuronal activity on myelination of deeper cortical projection neurons in mice.

The conceptual work of this thesis started in 2013 with a research proposal. Therefore, the proposal was based on the literature about activity dependent myelination that had been published so far. Changes in anatomical features like internodal distance, nodal structure, myelin thickness that could influence conduction velocity (or oligodendroglia), were not well examined in the context of activity-dependent plasticity (Fields 2005).

During the time of this project, the knowledge and therefore also the body of literature regarding this topic has highly expanded. This allowed me to discuss the findings of the thesis with the recent evidence about activity dependent myelination. Since many aspects we know now have not been known by the start of the project, the original rational will be introduced in the following paragraphs. However, it is to keep in mind that before I started the project, no publication on genetic alteration of neuronal activity with focus on myelination had been published. Most studies used *in vitro* models (Demerens et al. 1996; Stevens et al. 2002), injected toxins *in vivo* (Colello et al. 1995; Colello and Pott 1997; Hayes and Meyer 1989) or raised kittens in the dark/premature eye opening to influence sensory input and observe myelin in the optic nerve (Gyllensten and Malmfors 1963; Omlin 1997; Tauber, Waehneldt, and Neuhoff 1980; Moore, Kalil, and Richards 1976; Fukui et al. 1991), (for a more detailed review see Zalc and Fields 2000). The evidences from these experiments were the basis of my work, knowing that this might not reflect more sophisticated *in vivo* outcomes with more defined

methods. Therefore, we did not strongly predict any particular outcomes but rather kept an open mind about possible results.

Despite little detailed *in vivo* evidence, the project was also pursued because of the known functional importance that myelination has on cognitive as well as physical capabilities during development of children (Schmithorst et al. 2005; Meyersburg and Post 1979; Travis 1998) and in pathological conditions (Steck and Hartung 1998; Kubicki et al. 2005; Steingard et al. 2002; Chari and Blakemore 2002).

Our hypothesis that neuronal activity can regulate oligodendrocyte development and myelin, was based on findings that oligodendrocytes exhibit neurotransmitter receptors (Verkhratsky and Steinhäuser 2000; Káradóttir and Attwell 2007). Additionally, it was reported in 2007 that glutamate can also be released at discrete sites along axons in white matter after action potential propagation by vesicular fusion under the involvement of calcium, like observed at synapses. The released neurotransmitters can then be detected by ionotropic AMPA glutamate receptors in oligodendrocyte precursor cells (Kukley, Capetillo-Zarate, and Dietrich 2007; Ziskin et al. 2007).

Additionally to neurotransmitter regulating oligodendroglia, it was also known that premyelinated axons release ATP (and adenosine as one of its disassembly products) when electrical active that can also be detected by oligodendrocytes with their purinergic membrane receptors and influence oligodendroglia development, proliferation, and myelination (Stevens et al. 2002; Stevens, Tanner, and Fields 1998; R.Douglas Fields and Stevens 2000).

In this thesis two mechanisms have been used reduce neuronal activity in the murine central nervous system followed my several myelin analyses. The rationale

for choosing two different methods was to draw conclusions in the end about the effect when neurotransmitter release is reduced but spontaneous activity still occurring versus reduced excitability with no spontaneous activity. One way of reducing neuronal activity was by using a triple transgenic mouse line where Snap25 was abolished in parts of layer V (LV) or layer VI (LVI) of the cortex. The other way was by introducing a potassium channel (Kir2.1) via *in utero* electroporation in deeper layers of the cortex. Therefore, the introduction of this thesis focuses on presenting the central nervous system including the cortex with deeper layers V and VI. Additionally, myelinating glia cells (oligodendrocytes) as well as myelin itself will be introduced before current evidence of activity dependent myelination will be discussed. The last part of the introduction focusses on basic principles of neuronal activity, including the role of Snap25, and how its manipulation, especially with Kir2.1, affects the development.

1.1 Central Nervous System

Our nervous system enables us to integrate diverse sensations and respond accordingly. Integration of sensory information is taking place in different brain areas and where necessary a response is sent back to the brainstem or spinal cord to elicit movement. From there, the information is passed on to the peripheral nerves that innervate skeletal or smooth muscles. In addition, the nervous system regulates vital processes in the entire body and coordinates them including proper function of inner organs.

For the central nervous system to fulfil its task of information processing and to enable us to interact with our environment, a rapid nerve conduction speed is

necessary. Information is passed on by neurons through action potentials. However, neurons are not the only cells in the nervous system. Indeed, in primates there are probably as many glial cells (glia, Greek = glue) in the central nervous system as there are neurons (Azevedo et al. 2009; Herculano-Houzel 2009). Glia do not fire action potentials but can change their depolarisation level and conduct various forms of activity patterns. In contrast to neurogenesis, where most neurons are born before birth, glial cells are generated during the whole life span of an individual (Rieske et al. 2007; Yamaguchi et al. 2016). Glial cells are in close contact which each other as well as with neurons by various interaction mechanisms and are dependent on each other. Glial cells were discovered in 1856 by the German pathologist Rudolf Virchow (Virchow 1856) and astrocytes were named by Hungarian anatomist von Lenhossék (1891). During the 19th century glial cells were thought to have just a minor role in the CNS. Since then, robust research results show that in addition to an important supportive role, glial cells are also essential for maintaining many functions in the nervous system and its information processing (Jäkel and Dimou 2017). Oligodendrocytes are one subtype of glia cells and are a crucial part of a mechanism called myelination. Myelin was developed by jawed vertebrates during the course of evolution to increase nerve conduction speed in a spatially economic way by insulating axons instead of increasing their diameter (Castelfranco and Hartline 2015; Baraban, Mensch, and Lyons 2016). This allowed the development of more complex nervous systems (Hartline and Colman 2007). This insulation is achieved by multiple wrappings of extended and specialised processes from oligodendrocytes in the central nervous system. Visually, the CNS can be divided into white and grey matter. Grey matter refers to an area where mostly cell bodies are located (such as cerebral cortex, nuclei in the

CNS, ganglia in the PNS). In the underlying white matter myelinated fibre tracts are located giving it its characteristic appearance and colour on unstained tissue.

1.2 Cortex

A mammalian brain can be divided into three large parts based on the initial compartmentalisation of the neural tube: forebrain, midbrain and hindbrain. The forebrain (prosencephalon) can be furthermore subdivided into diencephalon and telencephalon. The latter one is also called cerebrum and in humans it is relatively large in relation to their body. Prosencephalon with the large cerebral cortex is meant to be accountable for higher cognitive functions, such as logical thinking, moral perception in decision making as well as planning, controlling and organising of complex social behaviours. Furthermore, information is processed from sensory organs to produce perception, such as hearing, seeing and touch as well as produce sensation of taste. The cerebrum is comprised of two hemispheres, the surfaces of which are covered by the grey matter of the cortex. The human cortex consists of circa 16 billion neurons and additional glial cells (Herculano-Houzel 2009). Modularity is a common organizational principle in all parts of the brain. The cerebral cortex exhibits a laminar and a radial organization. Cortical columns are sometimes regarded as the “basic functional units” in cerebral cortical processing, development and evolution. The cortex is functionally organised in horizontal layers and vertical columns as well as areas which group several columns that process the same tasks and form the functional units of the cortex (Jones and Rakic 2010). For example, all the information of one whisker is processed by all neurons in the same barrel of the same column of that barrel in the somatosensory cortex (Mountcastle 1997; Mountcastle 1956). “Cortical column” is a historic term that can

refer to a vertically arranged cell constellation, dendritic bundling, a pattern of connectivity, myelin distribution, metabolic characteristics, staining property, vasculature, magnitude of specific gene expression, embryonic origin or functional properties. The columnar organization reflects the intermittently recursive mapping of several variables under the two-dimensional surface of the neocortex in a variably independent or combined (e.g. hypercolumn manner (Molnár 2013).

The cortical neuron population consists of two types with a distinct quantity, origin and migration (Molyneaux et al. 2007; Kriegstein and Noctor 2004). Excitatory glutamatergic neurons are making up for around 80% of the neurons and are generated in the ventricular zone, a proliferative zone lining the lateral ventricles of the pallium (Noctor et al. 2001; Angevine and Sidman 1961). By undergoing asymmetric division, they create another radial glia as well as a cortical neuron (Noctor et al. 2004; Noctor et al. 2002; Malatesta, Hartfuss, and Götz 2000; Malatesta et al. 2003; Miyata et al. 2001; Anthony et al. 2004)**.** The radial glia then serves as a scaffold for migrating neurons on their way to the cortical plate by having processes contacting the surface of the ventricular zone as well as the pial surface (Kriegstein and Noctor 2004; Hatanaka and Murakami 2002; Misson et al. 1991; Rakic 1972).

The remaining 20% are inhibitory GABAergic interneurons which are generated in the ventricular zone of the subpallium from where they migrate tangentially into the cortex (Kriegstein and Noctor 2004; Sahara et al. 2012; Anderson et al. 1997; Carlos, López-Mascaraque, and Valverde 1996; Tamamaki, Fujimori, and Takauji 1997). Interneurons establish more local connections within their layer of location whereas glutamatergic neurons form local as well as long ranging projections out of the cortex (Markram et al. 2004; Sahara et al. 2012).

Different cortical neurons with a distinct morphology and size are grouped in six to seven layers, dependent on definition. The different layers can also be distinguished by their cell density and connectivity of afferent and efferent projections to different brain areas (Brodmann 1909; Economo and Koskinas 1927; Gilbert 1983). The seventh layer is referred to as LVIb or subplate and consists of a thin and heterogenous cell population forming the boundary between cortex and the white matter (Price et al. 1997; Hoerder-Suabedissen and Molnár 2013; Hoerder-Suabedissen and Molnár 2012). Many of the neurons in this layer undergo cell death after development (Price et al. 1997). The subplate layer is generated when the early generated preplate splits into marginal zone and subplate by more neurons migrating from the ventricular zone past subplate and settling between them (Marin-Padilla 1971; Luskin and Shatz 1985; Antonio et al. 2000). Thus, the layer development of the cortex processes from inside out by adding more and more neurons, with the exception of marginal zone and subplate. Newly born neurons need to migrate along the radial glia through the earlier generated layers (Angevine and Sidman 1961; Kriegstein and Noctor 2004; Hatanaka and Murakami 2002; Misson et al. 1991; Berry and Rogers 1965; Luskin and Shatz 1985).

Most of the peripheral sensory information is transmitted to the cortex by a relay structure called thalamus that is strongly connected to layer IV (Frost and Caviness 1980). There are three modality specific areas which get input directly from the thalamus and therefore are called visual (V1), somatosensory (S1) or auditory (A1) primary sensory areas. Furthermore, areas which are associated with the primary areas but do not receive direct input from their modality are called secondary cortical areas (visual: V2; somatosensory: S2; and auditory: A2) (Brodmann 1909; Jones and Powell 1970).

The incoming information is processed and passed on to layer II/III, V and VI in which both latter ones are the main output layer of the cortex. Therefore, those layers have efferent connections back to the thalamus and LV additionally forms connections to the spinal cord (Beeman 2014). These fibres bundle in the white matter underlying the cortex and extend through the internal capsule to the brain stem, forming the corticospinal tract in the spinal cord which is responsible for voluntary motor movement (Leary and Louis 1988). Additionally, cortico-cortical projections form the corpus callosum, a fibre bundle connecting both cortical hemispheres (Innocenti and Clarke 1983; Schmidt and Lent 1987).

1.3 Anatomy of the deeper layers of the cortex

The deeper layers of the mammalian cortex are built out of many different cell types which influence neuronal activity locally as well as in other structures with their long-range projections. Within the layers, there are further differences between various regions. Here, I focus on general principles in the rodent neocortex of deeper cortical layers (LV and LVI) since they will be studied in this thesis.

1.3.1 Anatomy of LV

LV is characterised by its diverse pyramidal cells which are among the largest cells of the neocortex (Molyneaux et al. 2007; Molnár and Cheung 2006). They have long-range projections to cortical as well as subcortical areas (Aronoff et al., 2010; Hattox & Nelson, 2018; Lavesque et al., 1996; Veinante et al., 2000). This anatomical feature establishes LV as the main cortical output layer which controls other brain areas. However, it has been shown that LV pyramidal cells also receive direct thalamocortical input and can be activated by it (Agmon & Connors, 1992;

Constantinople & Bruno, 2013; Rah et al., 2013). Additionally, LV is receiving input from all other cortical layers allowing integration of local and efferent signals in the cortex (Markram et al. 2015). LV also contains inhibitory interneurons which can be roughly divided into three mainly non-overlapping groups based on their expression of the following molecular markers: parvalbumin (PV), somatostatin (SOM) or serotonin receptor 5HT3aR (Rudy et al. 2011). Each subgroup can be further divided into multiple cell types (Naka and Adesnik 2016).

LV can be broadly subdivided into two layers, an upper layer a (LVa) and a lower layer b (LVb). The subdivision is mainly related to the targets the different pyramidal cells in LVa and LVb project to but they can also be distinguished by their intrinsic properties, plasticity and morphology (see Figure 1) (Hattox & Nelson, 2018; Agmon & Connors, 1989; Agmon & Connors, 1992; Chagnac-Amitai et al., 1990; Jacob et al., 2012; Schubert et al., 2001; Greenhill et al., 2015). LVa neurons for example tend to have a larger soma than LVb cells which correlates with their projection area, physiological property and dendritic morphology (Mason and Larkman 1990; Hallman, Schofield, and Lin 1988; Klein et al. 1986). LVa is characterised by intratelencephalic neurons (Type II neurons) that mainly project to the contralateral hemisphere or the ipsilateral striatum as well as other cortical regions from which it also receives strong input (Hattox & Nelson, 2007, 2018; Lavesque et al., 1996; Larsen et al., 2008; Veinante et al., 2000; Wise & Jones, 1977). Type II neurons also receive input from the thalamus. These neurons often have smaller dendrites that usually end in layer II/III of the cortex and a less complex dendritic morphology than neurons in LVb (Kasper, Larkman, and Lubke 1994).

LVb neurons are called pyramidal tract neurons (Type I neurons) and have thick-tufted apical dendrites ending in layer I. They project to subcortical regions like the brainstem, spinal cord, superior colliculus, basal pons, ipsilateral striatum and thalamic nuclei with their multiprojectional axons. (Leary and Louis 1988; Hattox and Nelson 2007; Lévesque et al. 1996; Larsen, Wickersham, and Callaway 2008; Veinante et al. 2000; Wise and Jones 1977). Electrophysiologically, LVb cells can be distinguished from LVa cells by the detection of burst firing patterns which cannot be detected in LVa cells (Kasper, Larkman, and Lubke 1994). Within layer V, intratelencephalic neurons of LVa form excitatory synapses onto LVb cells as well as LVa cells whereas LVb cells preferentially to connect to other LVb cells (Brown and Hestrin 2009; Lefort et al. 2009; Perin, Berger, and Markram 2011; Kiritani et al. 2012; Harris and Shepherd 2015). Cell types of both layers can be further subdivided based on their specific targeting regions (Hattox and Nelson 2007).

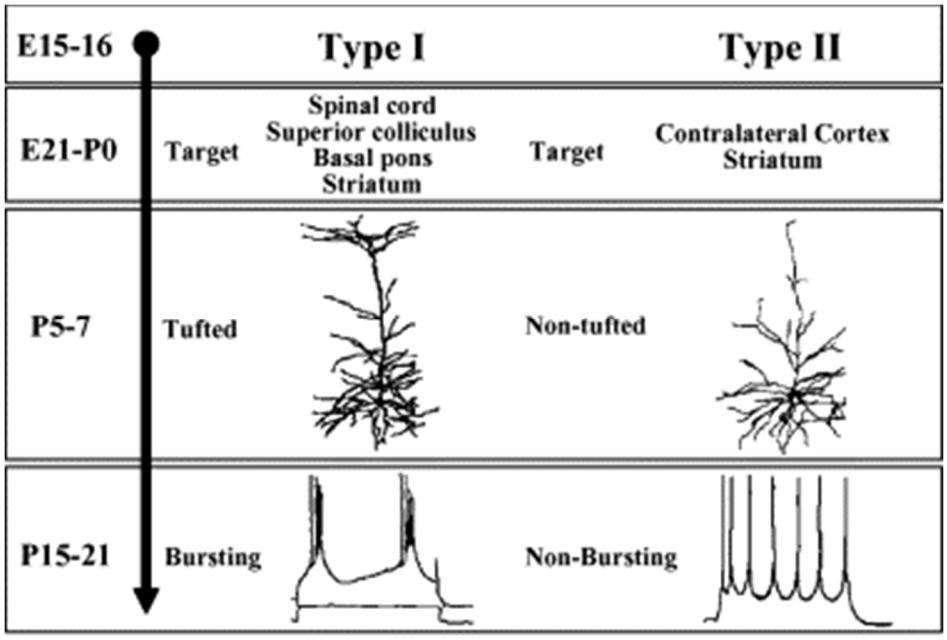


Figure 1: Summary of the developmental sequence (target selection, somatodendritic differentiation and electrophysiological characteristics) of the two major classes layer V pyramidal neurons

LV pyramidal cells can be broadly subdivided into two major classes: Type I and Type II. The subdivision is mainly related to the targets the different pyramidal cells project to but they can also be distinguished by their intrinsic properties, plasticity and morphology. Before P5, both cell types display a tufted dendrite morphology before Type II cells undergo an extensive remodelling of their dendritic area.
From Molnár & Cheung 2006

During migration, LVa and LVb cells cannot be distinguished by their morphology nor by their firing patterns (Kasper et al. 1994; Christophe et al. 2018). In the beginning, both cell types display a tufted dendrite morphology before LVa cells undergo an extensive remodelling of their dendritic area (Koester and O'Leary 1992). LVb cells also undergo a remodelling of their morphology. All LVb cells tend to extend their unbranched axons into the spinal cord passing through the striatum, internal capsule, cerebral peduncle and the basal pons. During early postnatal development axons start branching into the areas where they passed through before and additionally into cerebellar nuclei (Stanfield and O'Leary 1985a). By P7, the main descending axon is still quite simple while between P7 and P10 a rapid progression in complexity of axonal branching can be seen (Larsen and Callaway 2006). Additionally, a selective elimination and maintenance is taking place of those long-range axons depending on the specific region the cell body is located in the cortex. For example, cell bodies located in the motor cortex will retain their projections to the spinal cord while visual cortex will keep its projections to the superior colliculus but not the spinal cord (O'Leary and Stanfield 1989; Koester and O'Leary 1992).

In rats the timepoint of this selective degeneration can be determined to the second to third postnatal week (O'Leary and Koester 1993). This elimination is happening by degeneration through fragmentation of the axon (Hoopfer et al. 2006). Little is known about the exact process of this elimination. Otx1 has been found to be

involved by being translocated into the nucleus where it presumably regulates the transcription of molecules that are involved in axon pruning (Weimann et al. 1999). However, Otx1 is not region specific and therefore it is unclear how region-specific axon degeneration is regulated. Local clues of cortical areas might be involved in this process as demonstrated by rat cortical transplants. When parts of the rat foetal occipital cortex were transplanted into more rostral cortical areas of newborn rats, several neurons extended and maintained projections beyond timepoints when they normally get eliminated (Stanfield and O'Leary 1985a; Stanfield and O'Leary 1985b; O'Leary and Stanfield 1989).

1.3.2 Anatomy of LVI

LVI receives input from other layers as well as from the thalamus but also projects to the thalamus, making it a cortical output as well as input layer. Yet, the role of LVI is not yet completely understood (Thomson 2010). So far it seems that LVI integrates already processed information of layer V pyramidal cells and from other LVI cells with the input it receives from the thalamus. The effects of layer VI might be subtle but due to its morphology and position in the cortex it will control the information flow in and out of the cortical network. It is well established that LVI influences the thalamus but to which extent is still debated due to the complexity of the system (Thomson 2010; Briggs 2010).

Compared to other cortical layers, Layer VI contains the most diverse cell population. However, some of the different cell types can be grouped: (1) excitatory pyramidal cells (2) a minority of excitatory cells which are non-pyramidal with various shapes which are mainly connected within layer VI and (3) diverse

inhibitory cells which can project outside of LVI (then mainly inhibit layer IV) but are mainly interneurons with local projections (Kumar and Ohana 2008).

In LVI pyramidal cells can be distinguished into three subtypes based on their projection sites, morphology and electrophysiological properties (see Figure 2): Corticocortical (CC) pyramidal cells with long axons to connect across the cortex, corticothalamic (CT) cells that project to the thalamus and cells projecting to the claustrum.

Simplified, CC cells are short and can be upright pyramids but are often inverted pyramids and bipolar cells. Additionally, they have long horizontal axons that stay in LV and LVI of the cortex (Thomson 2010). CT cells are short and upright pyramids that have local axon arbours projecting into more superficial layers. Depending on the superficial layer they terminate in and their projection areas, CT cells can be further subdivided into: (1) CT cells projecting to primary sensory thalamic nuclei from which they also receive direct input and terminating in layer IV and are mainly located in the upper part of layer VI (Bourassa et al., 1995, Zhang & Desche, 1997) or (2) CT cells that also project to non-primary sensory areas of the thalamus and terminate in LV which are located in the lower part of layer VI (Zhang and Desche 1997; Chevée and Brown 2018). However, they also project to primary sensory thalamic nuclei.

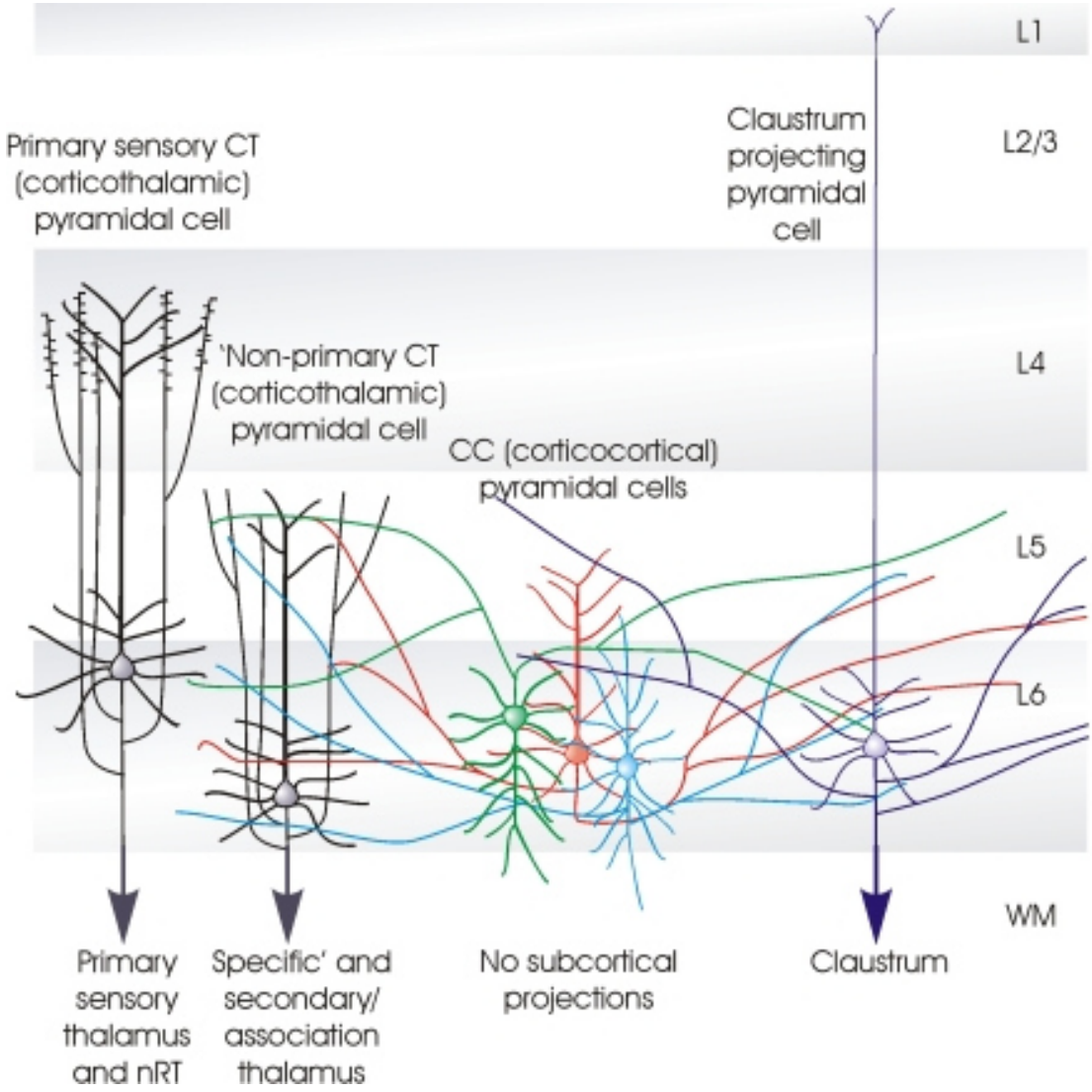


Figure 2: Subtypes of pyramidal LVI cells and their main connections

From left to right: 1) corticothalamic (CT) cells that project primary sensory regions and to the nucleus reticularis thalami (nRT). Apical dendrites as well as their axons branch in LIV. 2) corticothalamic (CT) cells also project to non-primary sensory areas of the thalamus and have axons mostly branching in LV and LVI. 3) Corticocortical (CC) pyramidal cells with long axons to connect across the cortex. Their dendrites and axons ramify in cortical LV and LVI. 4) LVI claustrum cells project to the claustrum with axons placed horizontally in deep layers of the cortex, have a simple apical dendrite reaching LI and strongly innervate other layer VI pyramidal cells.
From Thomson 2010

Another class of LVI pyramidal neurons are cells projecting to the claustrum with axons placed horizontally in deep layers of the cortex and a simple apical dendrite reaching LI (Chen et al., 2009; Katz, 1987). LVI claustrum cells as well as LVI CC

cells strongly innervate other layer VI pyramidal cells whereas CT cells rarely form connections to other LVI pyramidal cells (Bremaud et al., 2007).

In mice, cortical projections reach the thalamus between embryonic day 14 and 15 whereas thalamic fibres reach the cortex one to two days earlier (López-Bendito and Molnár 2003). Already at birth, thalamocortical cells have branched in deeper layers of the cortex (Auladell et al. 2000).

Several transcription factors have been shown to influence the development of LVI cells as well as their projections. Especially for corticothalamic cells, the following transcription factors and their influenced genes have been investigated: neuroD2, SOX5, influencing Fezf2 and Bcl11b, Ctip2 and Tbr1 (Ince-Dunn et al. 2006; Hevner et al. 2001). Disruption of these factors result in misallocation of pyramidal axons and thereby to anomalous targeting and inaccurate connections.

LVI gets input from all layers (Briggs and Callaway 2001; Binzegger et al. 2004; Zarrinpar and Callaway 2005; Llano and Sherman 2009) but does not provide any input to superficial layers (Dantzker and Callaway 2000; Barbour and Callaway 2008; Weiler et al. 2008; Lefort et al. 2009; Petreanu et al. 2009). LIV has a strong inhibitory input to layer VI but layer VI also inhibits LIV via interneurons (Kumar and Ohana 2008). LIV and LVI are linked by large, inhibitory basket cells which are supposedly responsible for the synchrony between the two layers that receive thalamic input while the thalamic input itself has an influence on this synchrony (Staiger, Zilles, and Freund 1996). LVI CC cells provide a strong excitatory input to pyramidal neurons from LV and vice versa.

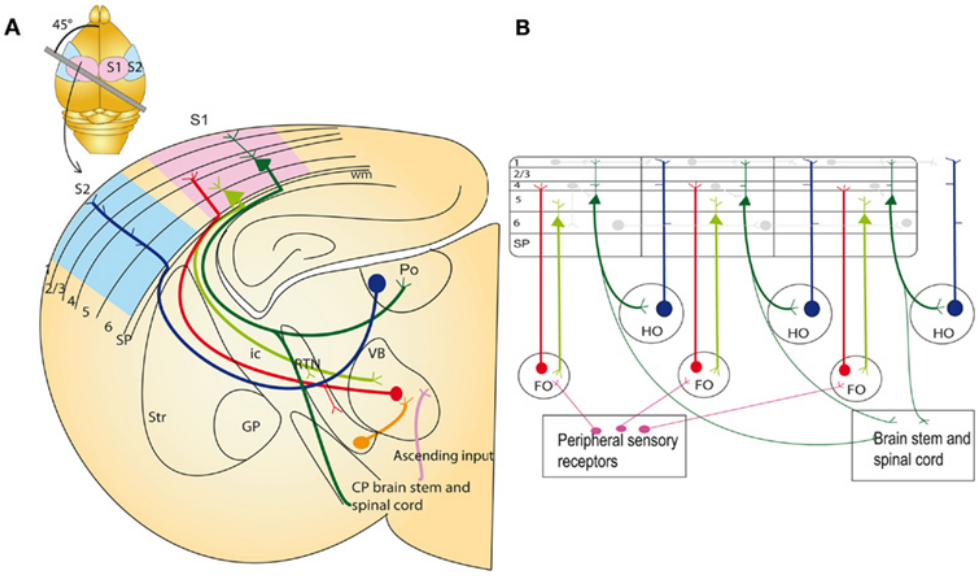


Figure 3: Thalamocortical circuits in the adult mouse brain and schematic representation of the two major sets of thalamic projection neurons

(A) Overview: outline of mouse brain with the line indicating the plane of section to obtain S1 and S2 thalamocortical slice containing intact thalamocortical somatosensory projections. Coronal cross-section: connections between cortex and thalamus using the somatosensory system as an example. The first order thalamic nucleus VB receives somatosensory peripheral input (pink) and then projects axons (red) to LIV of the primary somatosensory cortex (S1; light blue). LVI "modulator" neurons (light green) in S1 project back to the VB. LV neurons (dark green) in S1 project to subcerebral regions and make a collateral branch to a higher order thalamic nucleus. The higher order nuclei then project (dark blue) to an area of cortex that is different from the one they received input from generating an open loop. (B) Sensory information is relayed through the first order thalamic nucleus to the cortex (red). This cortical area then projects from LVI reciprocally back to the first order nucleus (light green). Each area is also non-reciprocally connected to a higher order thalamic nucleus. The LV input to the thalamus (dark green) is an "efference copy" of the layer 5 output to the motor system in the brainstem and spinal cord. This copy is forwarded to a higher cortical area (blue). Direct cortico-cortical connections between cortical layers and cortical areas are indicated in pale gray lines.
From Grant et al. 2012, based on Sherman & Guillery 2002. CP, cerebral peduncle; FO, first order thalamic nuclei; GP, globus pallidus; HO, higher order thalamic nuclei; ic, internal capsule; RTN, reticular thalamic nuclei; SP, subplate; Str, striatum; S1, primary somatosensory cortex; S2, secondary association somatosensory cortex; Po, posterior thalamic nuclei; VB, ventrobasal thalamic nuclei; wm, white matter.

Synapses from projections ending in the primary sensory thalamic region differ from those terminating in non-primary sensory areas. The modulatory synapses from LVI in primary sensory areas are smaller than their counterpart synapses called driver originating from LV. Modulatory synapses are also more distally

located around dendrites they connect to while driver synapses in non-primary sensory areas are larger and more proximal (Sherman and Guillery 1998).

1.4 Cell types of the CNS

The central nervous system contains neurons and glia cells. Neurons are electrically active cells which process and shape the information that they forward. There are many specialised types of neurons regarding their shape and function. However, simplified, they share four basic structures: 1) dendrites – where incoming information is detected 2) cell bodies - where the cell nucleus is located 3) axons – where action potentials are propagated 4) synaptic endings – where signals are passed on to the next neurons (Purves, Augustine, and Fitzpatrick 2001).

Glia cells in the central nervous system have very diverse tasks like supporting neurons with nutrients, insulation of axons as well as creating a balanced environmental milieu. Those tasks are executed by specialised types of glial cells. Glia communicate with neurons as well as with each other by various mechanisms like ion fluxes, cell adhesion molecules and signalling molecules (Fields & Stevens-Graham 2002).

Glial cells can be grouped by their size into micro glia and macro glia. The latter ones can be further distinguished into oligodendrocytes, astrocytes and ependymal cells (Allen and Barres 2009).

The epithelial layer of the ventricles and the spinal cord central canal is formed by ependymal cells. They produce and regulate cerebrospinal fluid for which they are equipped with cilia and microvilli on their apical surface and they even have the potential of neuroregeneration (Johansson et al. 1999).

Microglia serve as the immune system of the CNS by acting like macrophages. By phagocytosis they clear cell debris from atopic cells to reduce infections when detected by their processes. Furthermore, they abolish misplaced synapses or provide support to create accurate contact between cells by releasing growth factors (Paolicelli et al. 2011; Allen and Barres 2009).

Astrocytes are named after their stellar morphology and present the biggest glia cell population in the brain by number. They are mainly necessary for homeostasis due to their important role in providing nutrients to neurons and removing metabolic products. Their end feet are in direct contact with the endothelial cells of blood vessels and thereby they are involved in the induction and maintenance of the blood brain barrier (Ballabh, Braun, and Nedergaard 2004). Additionally, astrocytes control the formation, modulation and stability of synapses and protect them by their influence on extracellular ion- and neurotransmitter concentration (Ullian et al. 2001; Miller 2002). One special feature of astrocytes is their ability to form a syncytium by gap junctions and play an active role in information processing when communicating by calcium waves (Cornell-Bell et al. 1988; Brightman & Reese 1969).

Myelinating oligodendrocytes are of main interest in this thesis and will therefore be given more detailed attention in the next paragraphs.

1.5 Oligodendrocytes and myelin in the central nervous system

1.5.1 Oligodendrocytes and their development

One task of oligodendrocytes in the central nervous system is to ensure fast conduction of electrical impulses by insulating axons with multilamellar membranes called myelin. Oligodendrocytes carry out the job that is done by Schwann cells in

the PNS. Mature, myelinating oligodendrocytes develop from oligodendrocyte precursor cells (OPCs) via a pre-oligodendrocyte state to a mature, myelinating oligodendrocyte (see Figure 4). OPCs can also differentiate into astrocytes and it is still debated whether OPCs differentiate into neurons as well. OPCs are referred to as neural/glial antigen 2 (NG2) cells or polydendrocytes and can be identified by expression of the proteoglycan NG2 and the platelet-derived growth factor receptor α (PDGFRα). Therefore, they proliferate in response to platelet-derived growth factor (PDGF) and fibroblast growth factor (FGF). OPCs can detect neurotransmitters by their glutamate receptors (Patneau et al. 1994). They have a higher abundance in white matter but can also be found in grey matter. OPCs have their origin in the neuroepithelium of the neural tube. During early development they proliferate and migrate along blood vessels from ventral and dorsal regions of the brain, as well as the spinal cord to their target axons where they become postmitotic and thereby stop migrating (for reviews see: Goldman and Kuypers 2015; Takebayashi and Ikenaka 2015; Bergles and Richardson 2019). When OPCs start differentiating, pre-oligodendrocytes are forming more and more processes before myelinating neurons (Cai et al. 2014; Vallstedt et al. 2014; Richardson et al. 2006). Later during development, OPCs are also generated in the subventricular zone (SVZ) where they form a reservoir of remyelinating cells (Franklin and Ffrench-Constant 2008; Chang et al. 2000). Besides this spatial separation there is also a temporal difference during OPC generation. Ventral OPCs are born first (around P12 in the mouse) whereas dorsal ones are generated a few days later (Cai et al. 2014). Knockout experiments with one or the other cell type have proven that despite their divergent origin they can replace each other

without any influence on number, distribution or function (Richardson, Kessaris, and Pringle 2006; Kessaris et al. 2006).

Mature oligodendrocytes express myelin specific proteins which can be used as cell-specific markers like Myelin Basic Protein (MBP), Myelin-associated Glycoprotein (MAG) und Myelin-Oligodendrocyte Glycoprotein (MOG). Similarly, proteins expressed during other maturation stages can be used as markers for these developmental milestones (Miron, Kuhlmann, and Antel 2011).

Intrinsic as well as extrinsic factors, including signals from neurons and astrocytes, are influencing maturation stages from an OPC to a premyelinating oligodendrocyte until ultimately myelin can be formed by a mature oligodendrocyte (Zuchero and Barres 2013). Already during OPCs' very early development from multipotent neuronal stem cells in the neural tube morphogens like sonic hedgehog (Shh) and bone morphogen proteins (BMPs) act on them (Poncet et al. 1996; Pringle et al. 1996; Mekki-Dauriac et al. 2002). Shh indirectly increases the basic helix-loop-helix transcription factor Olig2 (Oligodendrocyte transcription factor) via the Nk homeobox proteins Nkx6.1 and Nkx6.2 (Novitch, Chen, and Jessell 2001; Liu et al. 2003). Olig2 is additionally regulated by sulfatase 1 and Indian hedgehog b and in turn regulates Sox10 (Sry-related HMG box) (Chung et al. 2013; Touahri et al. 2012). Olig2 and Sox10 can induce genes via Nkx2.2 which are needed for the development into a mature oligodendrocyte like PLP expression (Zhou, Choi, and Anderson 2001; Qi et al. 2001). Additionally, Sox10 induces MBP expression as well as the transcription factors myelin gene regulatory factor and zinc finger protein 191 (Koenning et al. 2012; Stolt et al. 2002; Howng et al. 2010).

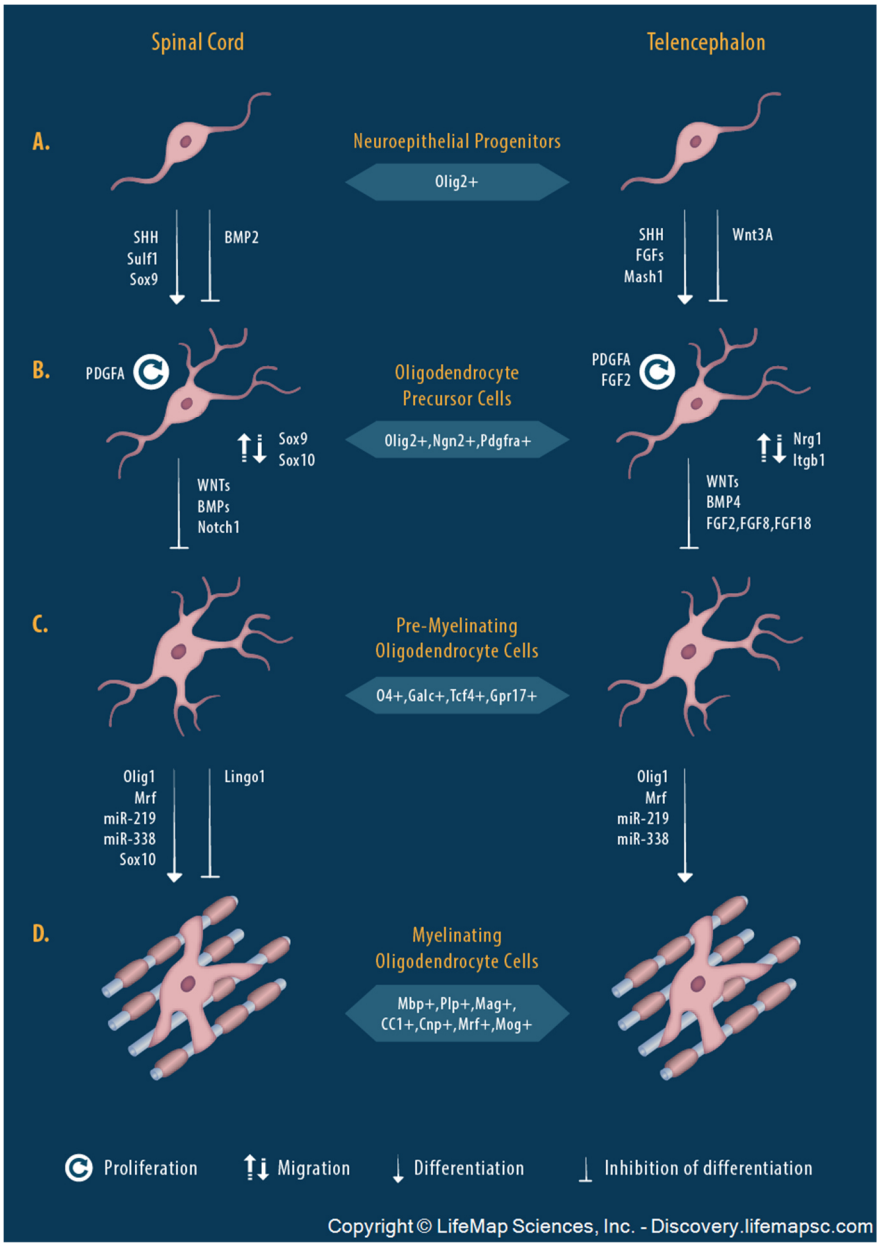


Figure 4: Signals influencing oligodendrocyte development in the spinal cord and in the telencephalon

Markers indicated for identifying oligodendrocyte stages and signals influencing oligodendrocyte development. Progenitor cells arising from the spinal cord or the telencephalon (A) differentiate into OPCs (B). OPCs are proliferative and migratory cells in the white matter. They develop into pre-myelinating oligodendrocytes (C) that finally mature into myelinating oligodendrocytes (D).
(Edgar et al. 2013, https://discovery.lifemapsc.com/library/images/prominent-markers-and-signals-during-oligodendrocyte-development)

Growth factors which are known to be involved in the maturation from OPCs to oligodendrocytes are Insulin-like growth factor 1, ciliary neurotrophic factor and

thyroid hormone T3 (McMorris and McKinnon 1996; McMorris and Dubois-Dalcq 1988; Mayer, Bhakoo, and Noble 1994; Barres et al. 1996; Baas et al. 1997). Furthermore, known involved intrinsic factors are for example different transcription factors or the Myelin Gene Regulatory Factor (MRF) (Emery et al. 2009). Established transcription factors can have inhibitory as well as promoting effect during OPC development. Olig1, Olig2, Sox8, Sox9, Sox10, Nkx2 and Nkx2.6 are needed for maturation whereas Sox5 and 6 have an inhibitory effect (Collarini et al. 1991).

An important role during different phases has also been assigned to microRNAs (Galloway and Moore 2016; Zhao et al. 2010). Additionally, a variety of microRNAs are necessary for maintaining lipid homeostasis in mature oligodendrocytes as well as for their final development by regulating temporal and local protein biosynthesis (Shin et al. 2009).

Even though most OPC maturation is taking place during an early postnatal phase in mice, there is continuous maturation of OPCs into oligodendrocytes through life. However, some OPCs remain undifferentiated and some mature oligodendrocytes will never myelinate an axon (Dawson et al. 2003). During development, more oligodendrocytes mature in the beginning than needed before excess cells will become apoptotic. This process is regulated for example by the amount of available growth factors to finetune the number of actually needed oligodendrocytes (Barres et al. 2018). The exact process to initiate myelination is not yet completely understood. So far it is known that axonal signals that are known to be involved in the process have an inhibitory as well as promoting effect. This indicates a combinatory role of both signals. Neuregulin proteins and plasma membrane bound L1-CAM are both promoting myelination. After electrical

stimulation L1 levels were raised. L1 binds to oligodendric F3/contactin and thereby activates Fyn kinase which initiates myelination (White et al. 2008b; Wake, Lee, and Fields 2011a). Another CAM (PSA-NCAM) was found to have an inhibitory effect on myelination along with LINGO-1 and Jagged1 (Wang et al. 1998; Charles et al. 2000; Jepson et al. 2012).

However, this dependence of oligodendrocytes on extrinsic factors for their development is not a one-way system. Neurones also need the support of oligodendrocytes especially in axonal areas far away from the soma. In 2010, Nave suggested that myelin causes a metabolic isolation and therefore oligodendrocytes are needed for trophic support especially in long-range axons. This might be an explanation why in neurodegenerative disease like multiple sclerosis where oligodendrocytes are affected, an impairment of long-term survival of axons can be observed (Nave 2010; Trapp and Nave 2008). Furthermore, using several mouse models it has been implicated that oligodendrocytes have neuroprotective characteristics. In mice lacking the proteins CNP and PLP, myelin ultrastructure is rarely changed but axonal degeneration can be observed. The underlying mechanisms for this still need to be further explored (Griffths et al. 1998; Lappe-Siefke et al. 2003).

Adding to the evidences that oligodendrocytes play an important role in energy support of neurons, are the studies published by Lee and colleagues (2013) and by Fünfschilling and colleagues (2012). Lee et al. showed that the most common lactate transporter in the CNS, monocarboxylate transporter 1 (MCT1), is strongly expressed in oligodendroglia. Disruption or reduction of the transporter causes axonal damage as well as neuronal loss *in vitro* and *in vivo*, demonstrating its importance (Lee, Morrison, et al. 2012). Following, Fünfschilling proposed a

mechanism by which lactate, as a possible glycolysis product, can be transferred by monocarboxylic acid transporters when axon energy levels are low. Lactate is transported from oligodendrocytes to neurons by the transporters located in the internodal myelin as well as in the axonal compartment, providing a metabolic coupling (Fünfschilling et al. 2012). A more recent study then discovered a connection between neuronal energy metabolism and neuronal activity in fast spiking neurons (Saab et al. 2016). It was described that activity dependent glutamate release enhanced the uptake of glucose and glycolytic support in oligodendroglia. This mechanism works via oligodendroglial NMDA receptors that regulate Glucose Transporter 1 (GLUT 1) trafficking and thereby glucose import. In mice lacking the oligodendroglial NMDA receptor, a delayed myelination can be observed as well as late-onset axonopathy and neuroinflammation. When oligodendroglial NMDA receptor is activated, axonal energy metabolism is supported by stimulating GLUT1 export and lactate release while also being incorporated into the myelin compartment.

In 2007 Krämer-Albers and colleagues showed that another way of communication between oligodendrocytes and axons is via micro vesicles called exosomes. They enable cells to communicate by transporting molecules like proteins and RNAs in exosomes (Krämer-Albers et al. 2007). Furthermore, it has been shown that neuroprotective molecules can be transmitted from oligodendrocytes to axons via this process (Krämer-Albers et al. 2007). Frühbeis and colleagues showed that release of oligodendroglial exosomes is dependent on activity-dependent release of glutamate facilitated by activating ionotropic glutamate receptors *in vitro* (Frühbeis et al. 2013).

1.5.2 Myelin sheath

Myelin sheaths in the central nervous systems are formed by oligodendrocyte processes to increase nerve conduction speed when wrapping axons. Loss of myelin causes several symptoms dependent on the region of loss. Symptoms are caused by impaired signalling and axonal loss. Multiple sclerosis is the most common disease which affects myelin damage in humans (Multiple Sclerosis Society, January 2016).

In the CNS, not all axons and axonal segments are myelinated (Tomassy et al. 2014). Myelin thickness is partially depended on axonal diameter. The axon diameter is also known to be a deciding factor whether an axon becomes myelinated. Axons in the CNS must be above 0.2μm to be myelinated but that does not mean that all axons above this diameter are going to be myelinated (Foster, Connors, and Waxman 1982; Vojvodic 1989). The number of wraps around an axon is roughly determined by its calibre resulting in a constant g-ratio (axonal diameter divided by fibre diameter including axon as well as surrounding myelin) especially in the PNS (Friede 1972). Several factors like NCAM (neuronal cell adhesion molecule), L1, F3/contactin and notch receptors have been shown to be involved in the onset of myelination in vitro and especially in the PNS (Hu et al. 2003; Barbin et al. 2004; Popko 2003; Charles et al. 2000). Interestingly, for the CNS the selection mechanism by which axons are myelinated and which stay without myelin has not yet been identified despite much research. Surprisingly, oligodendrocytes form myelin like structures around carbon fibres but for mature myelin neuronal axons are needed (Lubetzki et al. 1993; Althaus, Montz, and Neuhoff 1984; Althaus et al. 1987). It is expected that positive as well as negative

signals are needed to determine location, onset and maturation of myelin. Neuronal activity has been proposed to have an influence on myelination for a long time but came into focus of renewed interest in recent years (Tauber, Waehneldt, and Neuhoff 1980; Omlin 1997; Demerens et al. 1996; Gyllensten and Malmfors 1963) (see chapter 1.6 for details).

Once myelination starts, a vast biosynthetic performance of oligodendrocytes is necessary due to the enormous amount of lipids and proteins that are needed at the right time and place to form the myelin sheath. Additionally, the formation of a mature oligodendrocyte from an OPC is based on vast remodelling of the cytoskeleton.

Myelin membranes are characterised by their high ratio of lipids compared to proteins (roughly 70/30) (Finean, Hawthorne, and Patterson 1957). Most of the lipids are glycosphingolipids (circa 35%), cholesterol (circa 27%) and phospholipids (circa 17%) (Norton and Oduslo 1973). In addition to lipids, there are specific myelin proteins. The most abundant protein is an integral protein called proteolipid protein (PLP, 25kDa) and its splicing variant DM20 (20kDa) followed by myelin basic protein (MBP) and myelin-associated oligodendrocytic basic protein (MOBP). Other important myelin proteins are myelin-associated glycoprotein (MAG), myelin oligodendrocyte glycoprotein (MOG) and cyclic nucleotide phosphodiesterase (CNP) (Baumann and Pham-Dinh 2001).

Interestingly, some areas of neurons like dendrites and nodes of Ranvier are kept unmyelinated. The signals and mechanisms for this avoidance is not yet completely know. Nodes of Ranvier (NoR) are gaps between myelinated internodes and are left unmyelinated by oligodendrocytes (Ranvier 1871). These nodes are important for fast saltatory conduction of action potentials along an axon.

Nodes are distributed along axons with a size of 1-2 µm whereas internodes, myelinated areas between nodes, can be up to 1.5mm long (Salzer 1997).

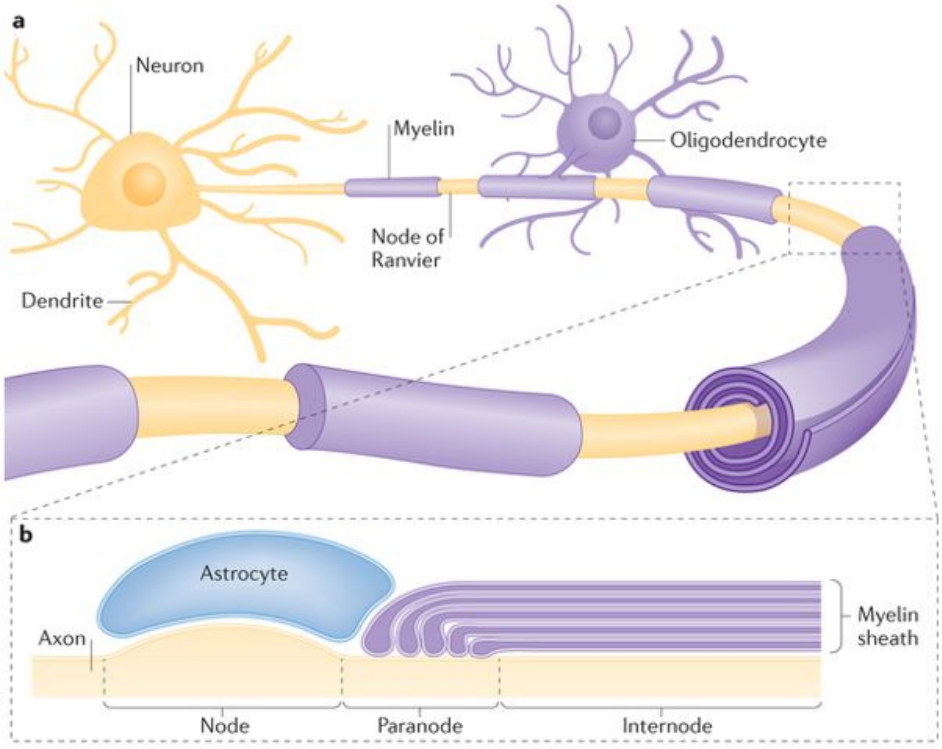


Figure 5: Insulation of nerve cells by oligodendrocytes in the CNS
a) Myelin sheaths in the central nervous systems are formed by oligodendrocyte processes to increase nerve conduction speed when wrapping axons by insulating axons with multilamellar membranes. b) Nodes of Ranvier (NoR) are gaps between myelinated internodes where perinodal astrocytes are in axonal contact. Nodes are important for fast saltatory conduction of action potentials along axons.
Adapted from Fields 2015

It has been shown that a single oligodendrocyte in the cortex can form up to 60 internodes on different axons (Chong et al. 2012). This is in strong contrast to the PNS where the myelinating glia cells, called Schwann cells, wrap only one axonal segment.

The marginal area between internode and node can be further differentiated into the juxtaparanode, next to the internode, and paranode, closer to the node. Juxtaparanodes are characterised by the localisation of voltage-gated potassium

channels. These channels are needed for the resting potential and repolarisation after action potentials (AP). During an action potential, depolarisation is caused by sodium influx through voltage-gated sodium channels at the nodes (Squire, Allaman, and Magistretti 2013). Adjacent to this region the paranode with its paranodal loops can be found. In this less compacted region myelin is in direct contact with the underlying axon. This enables not only anchoring of the myelin loop to the axon and prevents lateral diffusion of membrane compounds but also bidirectional material exchange (Peles and Salzer 2000). Therefore, only structures that have membrane compaction as well as this structured nodal region can be considered as mature myelin. A very specific ultrastructural composition is another myelin characteristic.

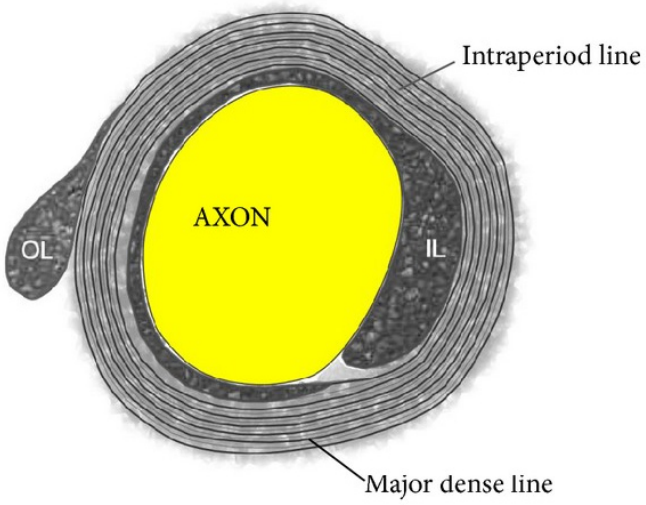


Figure 6: Stylized diagram of cross-section through a myelinated segment of a nerve fibre in the CNS

Myelin sheaths are formed from oligodendrocyte processes which get compacted by reducing the cytoplasmic content. Some cytoplasm remains in processes in small pockets. These pockets are called inner loop (IL) when adjacent to the axon or outer loop (OL) adjacent when they are at the outer edge of the myelin membrane. The major dense line represents the compacted cytoplasm while the intraperiod line is formed by close proximity of the membrane layers.
(Adapted from Greer 2013)

It can be seen in myelin cross section by transmission electron microscopy appearing as lighter and darker bands (see Figure 6). The bands consist of darker major dense lines and lighter intraperiod lines. The latter are formed by two extracellular membrane surfaces facing each other whereas major dense lines are two membrane surfaces facing the cytoplasm (Colello 2011).

1.5.3 MBP

The membrane protein myelin basic protein (MBP) is the second most abundant myelin protein after proteolipid protein (PLP). In this thesis, MBP was used as mature myelin marker. Therefore, it will be the focus of this introduction.

MBP's alkaline property is vital for its main function, membrane compaction, to enable interaction with negatively charged membrane phospholipids (Wood, Vella, and Moscarello 1984). Supposedly, the mature protein cannot be transported through the cell due to this basic characteristic since it could cause compaction of intracellular membranes. Therefore, the protein is synthesised where needed, at the axon-glia contact side, by transporting MBP-mRNA into oligodendrocyte processes (Ainger et al. 1993). MOBP is also transported in mRNA whereas other myelin proteins like PLP, MAG and MOG are packed in endosomal vesicles to be readily transported where needed (Holz and Schwab 1997; Kramer, Schardt, and Nave 2001; Winterstein and Trotter 2008).

The heterogeneous nuclear ribonucleoprotein (hnRNP) A2 is responsible for the transport of MBP mRNA to the periphery by binding to an 11 base pair (bp) long A2 response element (A2RE). The A2RE is present in all isoforms and located in exon 7 at the 3'UTR of the MBP-mRNA (Aigner et al. 1997). The mRNA is transported in an RNA-granule and is kept in a translationally inactive state

probably by the small non-coding RNA 715 (Bauer et al. 2012). Subsequently, local MBP-synthesis is dependent on membrane-bound tyrosine kinase Fyn which is activated when axonal L1 protein binds to oligodendroglial F3. Fyn phosphorylates different granule-compounds such as hnRNP A2 to dissolves the granule so that translation can be initiated (White et al. 2008). Depending on the species, different isoforms can be synthesised based on splicing variants. For temporal expression exon 2 seems to have an important role. Isoforms expressing exon 2 will be synthesised earlier than the ones without (Staugaitis, Smith, and Colman 1990; Pedraza et al. 1997). In mice six different isoforms from 14 to 21.5 kDa can be found. All isoforms are combinations of eleven different exons (Harauz and Boggs 2013). In humans only four different isoforms between 17.2 and 21.5 kDA have been reported (Boggs 2006; Kamholz, Toffenetti, and Lazzarini 1988).

A further variability is introduced to the MBP protein by posttranslational modifications. These modifications are mainly influencing how MBP interacts with phospholipids in the membrane (Polverini et al. 2003; Pointer-Keenan et al. 2004). Thereby, also MBP's spatial allocation in compact and non-compact regions can be altered. For example, phosphorylated MBP is more present in non-compacted regions of myelin than the non-phosphorylated form (Schulz, Cruz, and Moscarello 1988).

In addition to its main function, membrane compaction, MBP is involved in several other processes indicating the importance of MBP for oligodendrocyte homeostasis. For example, MBP is functioning as a size-dependent molecular filter in the myelin sheath and thereby determines the composition of compact myelin (Aggarwal et al. 2011). Within the oligodendrocyte, MBP has been shown to interact with cytoskeleton proteins. It is involved in the assembly of the cytoskeleton

in times of restructuring due to differentiation and myelination (Boggs et al. 2011). Furthermore, MBP interacts with membrane bound Phosphotyrosin-Kinase Fyn which influences differentiation and myelination of oligodendrocytes (Smith et al. 2012). One membrane-bound isoform of MBP, 18.5-kDa, is even involved in the calcium response in oligodendrocytes. This isoform of MBP reduces calcium influx through interaction with voltage-gated calcium channels (Smith et al. 2011).

The importance of MBP can be seen in naturally occurring shiverer mice where a major part of the MBP-gene on chromosome 18 is deleted. Subsequently, these mice show a deficient myelination which fails completely ultimately in the CNS (Readhead et al. 1987). Failure to produce compact CNS myelin leads to a premature death in these mice (Chernoff 1981; Rosenbluth 1980). In contrast, PLP and CNP deficient mice show a relatively mild myelination phenotype but axonal swellings. These swellings are caused by organelles stuck at nodes of Ranvier which ultimately leads to axonal degeneration (Griffths et al. 1998; Klugmann 1997; Lappe-Siefke et al. 2003).

1.6 Activity dependent myelination in the CNS

Myelination is taking place mainly during development and has been thought to be static until degradation with age or in demyelinating diseases like Multiple Sclerosis (MS) (Marner et al., 2003). Early experiments raised the controversial hypothesis that myelination can also be altered by changes in neuronal activity (Colello et al., 1995; Demerens et al., 1996; Fukui et al., 1991; Gyllensten & Malmfors, 1963; Hayes & Meyer, 1989; Moore et al., 1976; Omlin, 1997; Shrager & Novakovic, 1995; Tauber et al., 1980). New studies, using more refined methods developed in

recent times, are in progress to shed light on these apparently contradictory findings, as outlined in the following the subsections.

1.6.1 Influence of cognitive, motor and sensory activity on myelination

Brain imaging studies using magnetic resonance imaging (MRI) in humans have shown that white matter microstructure can be changed by a wide range of activities such as learning how to juggle, practising a new language or playing the piano (Bengtsson et al., 2005; Carreiras et al., 2009; Pujol et al., 2006; Scholz et al., 2010). This indicates that white matter changes cannot only be observed after learning a new motor skill but also after learning cognitive tasks (Kaller et al. 2017). Unfortunately, the techniques used do not allow to conclude which cellular mechanisms lead to the observed changes. A key recent study (Sampaio-Baptista and colleagues, 2013) addressed this gap in the literature through combined a diffusion MRI study on mice performing a single-pellet reaching task with MBP quantitative immunohistochemistry. The study shows that in the sensorimotor cortex the changes observed with the imaging technique correlated with the increased intensity in myelin stains. By using a control group which performed a similar motor task but without a learning effect, they showed that the higher motor activity itself did not lead to increased myelination (Sampaio-Baptista et al. 2013). A similar result was also observed in a previous study when rats where trained in a Morris water maze for spatial learning with a control group that only swam (Blumenfeld-Katzir et al., 2011). This suggests that also spatial learning involves adaptation of myelin. A key unresolved issue is what morphological changes in the myelinated axons lead to the observed increases in myelin quantity – future studies will likely address whether increased myelin thickness, elongation or formation of

new internodes or myelination of new fibre tracts (or a combination of them) are responsible.

Despite these correlational studies showing a link between white matter remodelling, improved behaviour performance, and increased myelin stain intensity, there is the possibility that variations in neuronal factors like alterations in axon branching or calibre are responsible for the observed effects in imaging studies. In short, the direction of causality between these three factors is not clear. To rule this out, McKenzie and colleagues used tamoxifen at P60 or P90 to conditionally delete myelin regulatory factor (MRF) in OPCs of adult mice. The tamoxifen-exposed mice were then exposed to a complex wheel where several rungs were missing leading to unequal gaps. In the control group with functioning MRF, an increase in OPC density as well as more mature oligodendrocytes were described. This increase correlated with better performance in the complex running wheel task compared to MRF deficient mice from day 1 of testing. Interestingly, despite there being a difference in average and maximum speeds between groups from day 1 onwards, the rate of speed increase stayed the same in both groups. Consequently, they concluded that at least partial, OPC recruitment seems necessary for motor learning. Interestingly, when MRF was removed after learning the task, no difference was observed between both groups indicating that recalling of a pre-learned motor task does not involve recruitment of OPCs (McKenzie et al. 2014).

To follow up their reported results that as early as day 1 of testing a difference was observed, they looked at this early phase more closely by a similar experimental paradigm, examining M1 and the underlying white matter (Xiao et al. 2017). For this, they reported and utilised a novel marker for early-differentiating

oligodendrocytes: ecto-enzyme Enpp6 (choline-specific ecto-nucleotide pyrophosphatase/phosphodiesterase). By doing so, they confirmed their earlier finding that fast production of new, immature oligodendrocytes, labelled by Enpp6, is needed in the early stages of motor skill learning in M1 as well as the underlying white matter. The conclusion of this paper refined the former one by stating that surprisingly, new oligodendrocytes are recruited within 2-3 hours resulting in a significant, measurable behaviour change and thereby acting in the time frame when also synaptic modification is taking place (Xu et al. 2010). For this to happen, presumably direct differentiation of oligodendrocytes occurs as observed by the accelerated differentiation of OPCs into newly forming oligodendrocytes after just 2-3 hours on the complex wheel. Later, a second wave of OPCs proliferation and differentiation contributes to a continued improvement over days and weeks. Xiao and colleagues presumably increased neuronal activity by learning a motor task and then studied oligodendroglia in the motor cortex and the adjacent white matter (Xiao et al. 2017). Gibson and colleagues studied the reverse experimental paradigm by stimulation the motor cortex and then looking at oligodendroglia in the motor cortex and the underlying white matter (also after 3 hours, as done by Xiao, and additionally at later stages) followed by behaviour analysis. Via optogenetics, they stimulated layer V neurons in one hemisphere of the murine motor cortex. Their observations included increased OPC proliferation by examining Olig2 and PDGFRα cells, differentiation within 3 hours, as seen by Xiao, (and at later stages) and myelin thickness which correlated with improved swing speed of the contralateral forelimb in a gait assessment paradigm. Similar to Xiao's results, these changes were not only observed in the motor cortex but also in the corpus callosum through which these neurons project to the contralateral hemisphere.

Thus, their findings demonstrate that neuronal activity induced remodelling is not limited to the soma or synaptic endings. Analysis of oligodendroglia revealed major differences between control and stimulated animals (e.g.: Olgi2 positive cells in M2 after 3hours increased roughly 8 times, and so did PDGFRalpha positive cells). G-ratio analysis however, revealed a rather small but significant difference (controls: 0.75 vs stimulated: 0.70), indicating that later observed behaviour phenotype could also be due to adaption of other parts of the circuit. Never the less, it is to keep in mind that g-ratio analysis was performed in all neurons rather than in only stimulated ones, which could strongly reduce an affect. Testing conduction speed might have given more information about the question if the small changes observed in g-ratio could have been responsible for the improved behaviour results.

No effects on oligodendrogenesis or myelin and behavioural changes were observed when blocking OPC differentiation pharmacologically. This is in line with the finding of the two aforementioned studies, where mice lacking the transcription factor MRF performed not as good on a complex wheel due to impaired OPC recruitment in the early training phase (McKenzie et al. 2014; Xiao et al. 2017).

Strikingly, seizures did not increase myelination in a similar way, thus suggesting that specific stimulation rather than undirected activity is needed for myelin plasticity (Stevens, Tanner, and Fields 1998). The observation that undirected activity is not sufficient to see strong effects on myelination, was further recapitulated in zebrafish despite a previous study showing increased OPC proliferation and differentiation after unphysiological electrical stimulation in the adult rat corticospinal tract (Li et al. 2010; Gibson et al., 2014; Hines et al., 2015).

Additionally to the studies focused on the influence of changes in motor activity on myelination, there are also studies about the effect of sensory deprivation on myelination. Three different ways of sensory deprivation in mice were used, whisker trimming, monocular deprivation or ear plugging, followed by myelin analysis (Etxeberria et al. 2016; Sinclair et al. 2017; Barrera et al. 2013; Mangin et al. 2012). In the auditory system, the development of myelin within a central auditory fiber tract was characterized to determine the influence of sensory experience. It was shown that earplugs introduced at hearing onset to induce elevation in auditory thresholds caused thinner axons and myelin compared to controls. Earplugs introduced during adulthood resulted in myelin decrease around the thickest fibers reinforcing the importance of sensory experience for myelination in the auditory system (Sinclair et al. 2017; Lazari et al. 2018).

Whisker trimming in neonatal mice led to a spatial alteration in OPC distribution and diminished myelination in the barrel cortex (Barrera et al., 2013; Mangin et al., 2012). However, monocular deprivation actually increased oligodendrogenesis without changes in OPC proliferation. Myelin thickness and the number of myelinated axons were also unaffected. Nevertheless, conduction speed in the optic nerve was reduced after monocular deprivation which was accompanied with observed shorter internodal length. The group was able to mimic these effects when glutamate release was attenuated indicating that this might be a mechanism by which activity dependent myelination can be regulated (Etxeberria et al. 2016).

1.6.2 Influence of stimulating environment on myelination

Neuronal activity, which has been shown to alter myelination, is influenced by our surroundings. Therefore, it is not surprising that several groups have demonstrated

that changes in a rodent's environment lead also to modifications in myelination. So far, this has been shown for alterations in the social relationships as well as when enriching the cage environment by being housed with seven cage mates and replacement of a novel toy every 48 hours. Interestingly, the observed effects on myelination were dependent on the age of the studied cohort. Isolation after weaning led to irreversible reduction of myelin protein expression and thinner myelin sheaths in the medial prefrontal cortex even after re-socialising (Makinodan et al., 2012). Similar effects were observed after isolation in adulthood although myelination could be restored in these animals after reintroduction to co-housing (Liu et al. 2012).

Older rats (14 month) living in an enriched cage environment for 4 months showed a delayed loss of white matter during ageing with increased myelin thickness (Yang et al. 2013). Additionally, a study performed on elderly humans with a mean age of 61 years revealed changes in white matter structure after memory training for several weeks. Similarly, in another study, altered white matter structures have been shown to correlate with improved memory performance (Engvig et al. 2010; Kennedy and Raz 2009). Taken together, it can be concluded from these observations that white matter plasticity is not restricted to developmental ages or adulthood, but can be achieved during aging as well.

Furthermore, these findings could have important implications for treatment of MS patients where deficits in motor and cognitive abilities often lead to depression and fatigue. Later symptoms are then accompanied by decreased interest in activities and social engagement (Jensen and Yong 2016).

1.6.3 Mechanisms of activity dependent myelination

One important question in the research area of activity dependent myelination remains largely unanswered: what are the mechanisms in the CNS by which activity dependent myelination is regulated *in vivo*? Most of the molecular candidates that are expected to be involved in this process have been discovered *in vitro* and are now being tested in different model organisms. One class of putative regulators of myelination are cell adhesion molecules (CAMs) which are localised on the axonal surface. Their expression can be regulated by specific action potential firing patterns and their recognition by myelinating glia cells occurs directly at the axon glia contact side (Itoh et al, 1997). For example, the protein L1 CAM plays an important role during the initiation of CNS myelination and its expression is regulated by action potential firing via synaptic glutamate release. By increasing Fyn kinase activity by electrical stimulation of neurons, local myelin protein synthesis is increased (Barbin et al., 2004; Wake et al., 2011). Additionally, Chen and colleagues demonstrated in zebrafish that N-cadherin, another CAM, is involved in activity dependent myelination by acting via a cAMP pathway. They increased neuronal activity by using pentylenetetrazol which led to elevated cAMP levels and an accumulation of N-cadherin that was accompanied by an increase in myelinating capacity of individual oligodendrocytes (Chen et al. 2017).

The importance of cAMP as a messenger to promote myelination has been already described in cell cultures of dorsal root ganglia. cAMP levels were increased three-fold following electrical stimulation promoting the formation of myelin segments. This effect was mimicked by adding artificial cAMP to the cultures and supressed by inhibiting the cAMP pathway (Malone et al. 2013).

In addition, it is known that OPCs as well as oligodendrocytes have a variety of receptors for growth factors and neurotransmitters but also ion channels in their cell membrane (for reviews see: Verkhratsky & Steinhäuser 2000; Káradóttir & Attwell 2007; Park et al. 2001). These receptors are crucial to detect soluble molecules like glutamate, adenosine and ATP, released by active axons into their surroundings which have the potential to influence all stages of OPC development via calcium signalling (Ishibashi et al., 2006; Stevens et al., 2002; Hiroaki et al., 2011). Additionally, other glial cells like astrocytes, are also able to sense these molecules released in an activity dependent-release mechanism. Astrocytes themselves then release the growth factor leukaemia inhibitory factor in response to which oligodendrocytes mature (Ishibashi et al. 2006). Nevertheless, most often OPCs and oligodendrocytes are located far away from synaptic endings where soluble factors were traditionally thought to be released during neuronal activity. More recent studies have shown that neurotransmitters are also secreted along the axolemma in a vesicle dependent as well as independent fashion (Fields and Ni 2010; Kukley, Capetillo-Zarate, and Dietrich 2007). ATP for example, is released through volume-activated anion channels after action potential firing (Fields and Ni 2010). The same channels are also permeable for glutamate which, upon release, can stimulate OPC migration by activating AMPA (α-amino-3-hydroxy-5-methyl-4-isoxazolepropionic acid) and NMDA (N-methyl-D-aspartat) receptors (Gudz et al., 2006; Xiao et al., 2013). Adenosine additionally influences OPC development by inhibiting their proliferation and thereby increasing myelination (Stevens et al. 2002). In zebrafish, an accumulation of vesicles has been reported at axon-glia contact sides suggesting an importance of their cargo for myelination initiation (Hines et al. 2015).

An interesting finding was made by Bergles and colleagues, who discovered transient functional synapses projecting from neurons to OPCs (Bergles et al., 2000). However, in a further study by the same group, it was shown that those synapses are not essential for proliferation and differentiation of those OPCs so that their function remains unknown (Biase et al. 2011).

1.6.4 Competition created by neuronal activity influences myelin formation

Although the studies mentioned thus far seem to support the existence of activity-dependent myelination, they are difficult to reconcile with other findings from the cell culture literature, which show that oligodendrocytes can, for instance, grow on inert synthetic nano fibres when they exceed a certain diameter (Lee et al. 2012). Two studies which have been performed in zebrafish have helped reconcile these seemingly opposing findings. One study showed that initial wrapping is independent of the neuronal activity of a specific axon, but that sheath stabilisation occurs in an activity dependent manner (Hines et al. 2015). The authors found that this was due to a higher frequency of retracted sheaths as well as shorter sheaths if stabilized. Mensch et al concluded that oligodendrocytes can adapt the amount of myelin sheaths they produce in response to decrease or increase in synaptic vesicle release. However, the study by Hines and colleagues did not observe the same effect when neuronal activity was enhanced by optogenetics. This could be due to the fact that specific firing patterns are needed in order to stimulate myelin formation like it has been shown for affecting myelin regulating CAMs (Itoh et al. 1997). It is also possible that changes in neuronal activity only affect myelination during a narrow time window as proposed before (Stevens et al., 1998; Zalc & Fields, 2000). One of the groups then further investigated their previous findings

by looking at different neuronal subtypes. Strikingly, they showed that distinct types of neurons show variable sensitivity to vesicular dependent myelination. This could not be explained by their properties since the analysed neuronal subgroups were very similar in neurotransmitter use, axon calibre, birth time and projections and even become myelinated by the same oligodendrocytes (Koudelka et al. 2016).

Together, these results led to the hypothesis that synaptic vesicle exocytosis in neurons is not necessary for the initial wrapping of oligodendrocytes. However, it can bias axon selection in some neuronal subtypes in a competitive way for nascent sheath stabilization during a distinct period of time. This hypothesis allows co-existence of activity dependent myelination with the finding of myelinated nano fibres in culture in the absence of neuronal activity (Lee, Leach, et al. 2012).

1.6.5 Myelination in information integration

In the discussion about adaptive myelination it is important to keep in mind, that an increase in myelination that may lead to an increase in conduction speed does not necessarily result in improved circuit function. Synchronous firing patterns, oscillation frequency or coupling, as well as propagation of brain waves to generate a rhythm, are important factors for complex and proper information processing. The disturbance of these factors, for example by changes in myelin that result in asynchronous arrival of action potentials, can influence attention, sleep and memory or even may contribute to disorders like dyslexia, schizophrenia and epilepsy (Pajevic, Basser, and Fields 2014).

Although it is not clear how myelin plasticity may influence network dynamics, several mechanisms have been proposed. In one scenario, myelin plasticity allows to tweak timing of action potentials across axons. To strengthen connectivity,

signals (APs) must arrive at synapses simultaneously (Kistler 2002). Alterations in conduction speed along myelinated axons can be achieved by altering myelin thickness, internodal length and distance or even the nodal structure. Additionally, the length of the axon initial segment (AIS) can influence action potential firing and can be remodelled in response to changes in neuronal activity (Grubb and Burrone 2010; Yamada and Kuba 2016).

By changing conduction speed, synchronous arrival of signals may be out of balance and result in a reduced performance of the network. Especially in complex circuits, like in in large brains, delays in conduction speed could have significant influence in processing complex cognitive actions. For example, research showed the importance of neuronal synchrony in neurological disorders (reviewed in Uhlhaas & Singer 2006). Another example that has been known for a long time where synchronous arrival of action potentials is influenced by myelin, is the electric fish. Synchronous arrival of action potentials at electrocytes in electric organs is influenced by different myelination patterns in axons of different lengths (Bennett 1971). A further instance is the auditory system, in which encoding the spatial location of a stimulus is essential. To achieve uniform conduction times for simultaneous arrival of information in both hemispheres from the cochlear, longer collaterals display longer myelin sheaths (Seidl 2014; Seidl and Rubel 2016). Ford and colleagues studied the specific parts of the auditory system in gerbils that are responsible for sound localisation using *in silico* as well as *in vivo* and *in vitro* experiments. By doing so, they provided deeper insights into how structural specializations of myelin contributes additionally to tune conduction velocity and therfore timing of action potentials. They discovered that individual anatomical parameters of myelin sheaths and nodes can vary significantly along a single axon

as well as between axons with different firing frequencies, to optimise pathways which contribute to temporal processing. Interestingly, they observed that myelination properties were significantly different from traditionally assumed structures. Surprisingly, it was shown that axons responding best to low-frequency sounds had a larger diameter but shorter internodes, leading to higher conduction velocities in electrophysiological recordings (*in vivo* and *in vitro*). Additionally, it was described that the closer to the distal end of an axon nodes and internodes are located, the greater the diameter of the node and the shorter the internode length gradually get. This allows for shorter heminodes (which they observed) than previously predicted for reliable depolarisation of presynaptic terminals**.** In simulations they predicted that these changes may adjust conduction velocity, ensure precisely timed depolarisation and timing of action potentials within the circuit in vivo. However, in their predictions they did not look at ion channel density, which is also a factor that takes part in processing of temporal information for sound localisation (Ford et al. 2015).

An alternative to modify conduction speed more effectively than in changing existing myelin, is by myelination of axons which were not myelinated before (*de novo* myelination). In the adult rodent corpus callosum for example, only 30-50% of all axons are myelinated. Strikingly, there is a 10 fold increase in conduction speed compared to non-myelinated axons (30 to 300ms) (Swadlow 1985). Tomassy and colleagues showed in 2014 that myelin is not uniform along one axon and that different types of neurons display distinct myelination patterns. Partial myelination would be one possibility of changing conduction speed in a gradual way to ensure circuit adaptation when new myelin is formed (Tomassy et al. 2014).

Further studies are needed to obtain deeper insights into how synaptic and myelin plasticity are integrated to optimise network function and on the type of functional feedback that would coordinate myelin changes.

1.7 Action potential propagation and regulated synaptic vesicle release

1.7.1 Action potential propagation at nodes of Ranvier

Action potentials are generated at the axon initial segment (AIS) and propagate along the downstream axon. In myelinated axons this is happening in a saltatory fashion at the Nodes of Ranvier (Huxley and Stampfli 1948). In unmyelinated axons, a continuous transmission is taking place.

Action potentials are generated following an all-or-none law, meaning that a threshold value for cell membrane depolarisation needs to be reached and the amplitude stays unchanged (Adrian 1912).

A continuous depolarisation along the whole axon membrane is a relatively slow process of 0.5 to 10 m/s dependent on axon diameter compared with the saltatory propagation of up to 150m/s in myelinated axons (Purves, Augustine, and Fitzpatrick 2001). Since the conduction speed limits the information processing within the nervous system, fast propagation is essential for many organisms. The up to 300 times quicker propagation in myelinated axons can be explained by a higher membrane resistance through insulation which allows a fast current flow of ions (Gasser and Erlanger 1927). This ion flow creates an electrical field that causes enough membrane depolarisation at the following Node of Ranvier to reach the threshold and thereby renewing the action potential. Most neurons showing this threshold around -50 to -30 mV while having resting potentials around -90 to -70

mV. Hence, this way of action potential propagation is called saltatory conduction (Latin saltare = jump) when jumping from one node to the next one (Hartline and Colman 2007; Huxley and Stampfli 1948). Renewing action potentials permanently would be time consuming as well as energy consuming for the axon and therefore would likely result in a less complex nervous system (Attwell and Laughlin 2013). After each action potential ATP-driven Na^+/K^+ ATPase pumps work to restore the ionic concentration gradients (Skou 1957). Therefore, myelination is often considered as energy saving. However, this is only true for neurons but not in sum for the white matter when myelin sheath production by oligodendrocytes are also included into the calculation (Harris and Attwell 2012).

An increased conduction speed cannot only be achieved by insulation of the axon membrane but also by an increased axon diameter. This mechanism is well studied in vertebrates like squids that did not develop axon insulation during the course of evolution. However, when an increased axon diameter is compared with myelin insulation it is relatively ineffective regarding space and speed (Haydon and Hendry 1982).

The resting potential originates in the different distribution of cations and anions in the extra- and intracellular space along the semi-permeant cell membrane with support of the potassium/sodium-ATP-pump. The initial distribution of more sodium ions outside and more potassium ions inside the cell creates in addition to the electrical gradient along the cell membrane a chemical gradient. This gradient allows a fast ion flux during action potentials at nodes of Ranvier where ion channels are clustered (Purves, Augustine, and Fitzpatrick 2001).

1.7.2 Regulated synaptic vesicle release

In order for the nervous system to be able to process information, neurons need to communicate with each other. Communication in the nervous system is achieved by two different mechanisms. Within neurons information is passed on by propagation of electrical signals (action potentials) along axons. Those signals are converted into a chemical signal using neurotransmitters stored in vesicles at synapses to be sensed by neighbouring neurons which convert it back into an electrical signal (Squire, Allaman, and Magistretti 2013).

In 1970, the Nobel Prize in Medicine and Physiology was given to Katz, Euler and Axelrod for their work on neurotransmitter and synaptic transmission. Katz's work was focusing on neurotransmitter release in quantal units at neuromuscular junctions when electrically active (Fatt and Katz 1951; Castillo and Katz 1954). In 1968 Dodge and Rahamimoff added the role of calcium in regulated vesicle release to formulate today's understanding of regulated synaptic transmission: the arrival of an action potential at the presynapse leads to a series of events initiated by membrane depolarisation (Dodge and Rahamimoff 1967). Opening of voltage gated calcium channels leads to an influx of calcium ions along their concentration gradient. Calcium then triggers the beginning of vesicle fusion with the presynaptic cell membrane by binding to a calcium sensor attached to the synaptic vesicle. This process lowers the energy barrier of vesicle and cell membrane fusion and thereby vesicle exocytosis probability is significantly increased. When fusion occurs, neurotransmitters stored in the synaptic vesicles are released into the synaptic cleft. By diffusion, neurotransmitters bind to and thereby open ion channels at the postsynaptic membrane which causes an influx of ions. Depending on which kind of neurotransmitter is released from the presynapse and binds to

specific receptors, either cations or anions flow across the postsynaptic cell membrane. When the membrane potential decreases even further an inhibitory postynaptic potential (IPSP) is created whereas an increase the potential causing an excitatory postynaptic potential (EPSP) (Purves, Augustine, and Fitzpatrick 2001). Since dendrites of one single neuron have synapses with many different neurons the different incoming signals need to be integrated. The final temporal and spatial summation happens in proximity to the soma just after the axon hillock, the axon initial segment (AIS) (Squire, Allaman, and Magistretti 2013). This is also the area action potentials are generated and send through the axon to the next synaptic endings (Hedstrom and Rasband 2006).

How much an individual synapse contributes to the summation at the AIS is dependent on its distance from the soma and synaptic strength which can be modulated in adaption to necessity. This synaptic plasticity enables the storage of information like learnt behaviours and memories. Synaptic plasticity can be achieved by pre- or post-synaptical changes when altering neurotransmitter release and receptor availability or even by forming new synapses and retracting already established ones (Citri and Malenka 2008).

1.7.3 The role of Snap25 in the SNARE complex

In this thesis, activity dependent myelination will be studied in Snap25 conditional knockout mice, therefore, Snap25 will be introduced in the following paragraphs.

The neuron-specific protein Snap25 was discovered by Michael Wilson and his colleagues in 1989 (Oyler et al. 1989). The name derives from the compound it was first studied in, synaptosomes, and its size of 25 kDA, which form together the name of synaptosome-associated protein of 25 kDA (Snap25). *Snap25* is

differentially expressed in the CNS where it is part of the SNARE complex (Soluble NSF (N-ethylmaleimide-sensitive factor) Attachment Protein Receptor) (see Figure 7). The involvement of the SNARE complexes in intracellular membrane fusion is highly preserved between mammalian species and considered universal for eukaryotes (Jahn and Südhof 1999).

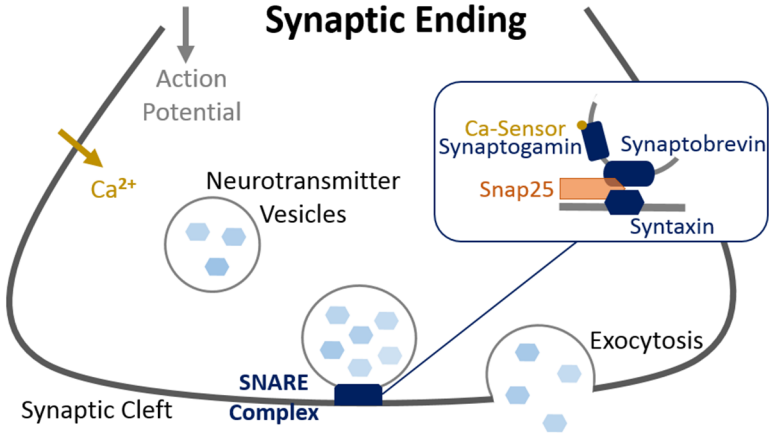


Figure 7: Calcium mediated regulated vesicle release at synapse
Action potentials are transmitted between neurons at presynaptic endings through exocytosis of neurotransmitter containing vesicles. Vesicle fusion is mediated by the SNARE protein complex, which contains the essential protein Snap25. Regulated neurotransmitter release is prevented by the lack of Snap25.
Adapted based on research of Rothman and Südhof (e.g. Südhof & Rizo 2011)

At the presynaptic ending, the SNARE complex is located at the membrane facing the cytosol and responsible for vesicle docking and membrane fusion by creating a complex that creates proximity between vesicle and plasma membranes. This creates a so-called 'readily releasable pool' of vesicles for exocytosis (Rosenmund & Stevens 1996). All SNARE family members share a 60-70 amino acid conserved domain called SNARE motif (Weimbs et al. 1997). Members of this family are targeted by the neurotoxins tetanus and botulinum toxin of which botulinum toxin A and E specifically target Snap25 (Washbourne et al. 1997). This feature has been used to show essentiality of Snap25 for vesicle exocytosis at the synapse (Bain, et al., 1994).

There are two isoforms of Snap25, A and B, differing in 9 amino acids. The *Snap25* gene consists of 9 exons in total but exon 5 is duplicated resulting in exon 5a and 5b. By alternative splicing, the two isoforms are formed differently in an area important for palmitoylation suggesting differences in reaction with membranes (Slavena et al. 2008). *In vivo* and *in vitro* it has been shown that *Snap25A* is mainly expressed during development whereas *Snap25B* is the major isoform of adult neuronal tissue (Bark, et al., 1995; Boschert et al., 1996).

Snap25 contributes 2 out of 4 alpha helices to the neuronal trans-SNARE complex. All 4 helices build a metastable coiled coil structure due to heptad repeats (Chapman, et al, 1994). The other two helices are contributed by synaxin-1 and synaptobrevin (also named: vesicle-associated membrane protein, VAMP2) which is associated with the vesicle membrane (Based 1998). In Snap25, one of the two SNARE motifs is located at the N-terminus where syntaxin-1 binds, the other one at the C-terminus where contact with synaptobrevin is established (Chapman, et al., 1994). In between those two motifs, a central linker domain can be found. This domain contains 4 cysteines which are responsible for the binding of Snap25 to the plasma membrane due to their palmitoylation (Oyler et al. 1989; Lane and Liu 1997).

Besides the SNARE proteins, for a fast release of primed vesicles at synapses, a further protein is important. This protein, synaptotagmin-1, is responsible for reacting to the rapid and transient influx of calcium through voltage-gated calcium channels which is triggered by the arrival of an action potential at the synapse. Synaptotagmin is the calcium sensor associated with the SNARE complex due to its two C_2-domains and their function of binding calcium (Brose, et al., 1992). In the event of calcium binding, those C_2-domains are partially inserted into the plasma

membrane, leading to a perturbation and thereby facilitating vesicle fusion (Damer and Creutz 1994). After the fusion event, the SNARE complex is in a cis-state and will be disassembled for recycling involving a protein called alphaSNAP and eventually will be recycled in the cytoplasm (Hayashi, et al., 1995, Hanson, et al., 1995).

1.7.4 Other roles of Snap25 and its family members

It is well known that Snap25 is involved in the SNARE complex and thereby enables synaptic vesicle exocytosis. But vesicle fusion to cell membranes is not only important for neurotransmitter release but also believed to be important for other neuronal functions like axonal elongation and the involved membrane expansion during development (Osen-Sand, Catsicas, Staple, Jones, Ayala, and Knowles 1993). Additionally, in mature synapses, when a growth cone reaches and recognises its target cell, vesicle fusion is essential for remodelling of nerve terminals to guarantee plasticity (Mochida 2011).

Axonal elongation is taking place at the growth cone, a structure that is important for axon guidance. It is distinguished from mature synapses by the inability to release synaptic vesicles despite already having SNARE proteins present (Igarashi, et al, 1996; Igarashi, et al., 1997). Snap25 is evident before synaptogenesis but strongly induced during synapse formation in excitatory synapses with the opposite effect in inhibitory synapses (Baudry, et al., 1991; Frassoni et al., 2005; Catsicas et al., 1991; Oyler, et al., 1991).

Osen-Sand (1996) and colleagues studied the selective inhibition of *Snap25* expression during development *in vivo* and *in vitro*, using two different model organisms. Selective inhibition of amacrine cells in culture and in developing chick

retinas *in vivo* was achieved by using modified antisense phosphorothioate oligonucleotides (PONs) (Osen-Sand, et al. 1993). They showed that inhibition of *Snap25* during development blocks axonal elongation in those two systems studied. Using botulinum toxin to disrupt Snap25 showed a similar effect (Osen-Sand et al. 1996). Two further studies proved that Snap25 increases neurite number and length in PC12 cells (Shirasu, et al., 2000; Zhou, et al., 2000).

Further areas where Snap25 plays a major role is the modulation of voltage-gated calcium channels (VGCCs) and its involvement in receptor trafficking like N-methyl-D-aspartate receptor (NMDAR) where it contributes to synaptic plasticity (Lau et al. 2010; Catterall 1999). Snap25 is especially known for a negative regulation of specific VGCCs in glutamatergic cells and thereby decreases a calcium response of neurons to react to action potential driven depolarisation (Condliffe, et al., 2010). The most likely candidate to substitute for Snap25 is Snap23. Snap23 shows a 59% similarity in amino acids to Snap25 (Ravichandran, et al., 1996; Wang et al., 1997). The next closest member in the Snap25 family is Snap29 with a similarity of only 17%. Snap29 is mainly located at intracellular membranes (Hohenstein and Roche 2001; Steegmaier et al. 1998). Unlike Snap25, Snap23 is not neuron specific but also expressed in glial cells (Hepp et al. 1999). It has a similar cysteine containing structure to bind to plasma membranes and to participate in SNARE complexes (Vogel and Roche 1999; Wang et al. 1997). Sørensen and colleagues showed in murine experiments that the homologue Snap23 can substitute for Snap25 only very partially since it fails to create a pool of readily releasable vesicles in PC12 cells (Sørensen et al. 2003).

1.7.5 Snap25 mutants

The functional importance of Snap25 can be studied in Snap25 null-mutants. The mutants show a morphological abnormal development even though the brain development during embryogenesis is unaltered until birth. No abnormality of the thalamocortical or corticofugal targeting was observed during the prenatal period. Additionally, no abnormal thalamic ingrowth or abnormal branching was observed when a Snap25-/- thalamus was co-cultured with a Snap25 +/+ cortex for several days (Molnár et al. 2002). Cortical slices of Snap25 KO mice still exhibit spontaneous neurotransmitter release in the absence of Snap25 but calcium dependent release triggered by action potentials is prevented (Washbourne et al. 2002). Slice cultures of Snap25 KOs allow insight into early postnatal stages of development since the homozygous deletion of *Snap25* is perinatal lethal at birth (Blakey, Wilson, and Molnár 2012; Washbourne et al. 2002).

Viable Snap25+/- mice show no overt behavioural phenotypes despite a 40% decrease in SNAP25 protein levels (Sharma et al. 2012; Washbourne et al. 2002). The viable blind-drunk mouse possesses a I67T missense mutation in a highly conserved domain of the Snap25 B-isoform (Jeans et al. 2007). The described complex behavioural phenotype displays similar patterns that have been linked to schizophrenia like ataxia and impaired sensorimotor gating. On the cellular level, impaired exocytotic vesicle recycling and a reduced amplitude of evoked cortical excitatory postsynaptic potentials was described in the brain (Jeans et al. 2007). Coloboma mice, which are heterozygous deficient of a larger chromosomal area including Snap25, show similar phenotypes as ADHD patients (Hess, et al., 1992; Heyser, et al., 1995).

The findings from the previous studies about Snap25 mutations fit in with finding in humans. Polymorphisms in the *SNAP25* gene in humans have been associated with hyperactivity as observed in patients with attention deficit hyperactivity disorder (ADHD) (Barr et al. 2000; Mill et al. 2002). Furthermore, milder forms of Snap25 alterations can be found in patients with specific neuronal disorders like schizophrenia where a Snap25 deficiency in the hippocampus was detected (Fatemi, et al, 2001; Young et al., 1998). Additionally, a genome-wide metaanalysis of schizophrenia-susceptibility genes reported a significant link between schizophrenia and the chromosomal region that contains SNAP25 but no other known susceptibility loci (Lewis et al. 2003).

1.8 Inward-rectifier potassium channels

In this thesis, activity dependent myelination will be studied utilising an Inwardly Rectifying Potassium (K) channel (IRK or Kir). Kir2.1 can be utilised as a tool to influence neuronal activity. Therefore, the following paragraphs will focus on introducing Kir2.1.

Inward-rectifier potassium channels are a subset of potassium channels consisting of 7 subfamilies. Each subfamily consists of several members (Kir1.X – Kir7.X). These channels function in a way that they transport more potassium cations into cells than they export (Hibino et al. 2018). Blockage of Kir channels by Barium (Ba) in an isolated axon showed depolarisation followed by action potential firing (Day et al. 2005; Guo and Lu 2003). The strength of the inwardly directed transport is regulated by the channels varying sensibility to bind magnesium and polyamines (Stanfield et al. 1994; Lu and MacKinnon 1994; Lopatin, Makhina, and Nichols 1994; Matsuda, Saigusa, and Irisawa 1987). The channels consist of a pore

domain and two flanking transmembrane segments with both, the N- and C-terminal, facing the cytosol. The pore domain contains the sequence Gly–Tyr–Gly which makes ion channels specific for potassium (Dart et al. 1998). Potassium inward rectifiers play a role in establishing and maintaining the membrane resting potentials in many cell types. Additionally, they can play a role in determining the duration of an action potential as well as in the excitability to generate action potentials (Sakmann and Trube 1984). Four subunits are needed to form a functioning channel that assemble in homo- as well as heterooligomers in membranes (Hibino et al., 2010).

1.8.1 Structure, location and function of K_{ir}2.1 and its family members

In 1993 Kubo and colleagues identified Kir2.1 as the first member of this subfamily (Kubo et al. 1993). Since then, 3 more family members have been added: Kir2.2 (KCNJ12 (Takahashis et al. 1994; Koyamaa et al. 1994)), Kir2.3 (KCNJ4 (Morishige et al. 1994; Bond et al. 1994; Bredt et al. 1995)), and Kir2.4 (KCNJ14 (Do et al. 1998)). Kir2.2 shows a similarity of 70% to Kir2.1 on the amino acid level whereas Kir2.3 shows 61% similarity. Kir2.4 and Kir2.1 have an overlap of 63%.

Kir2.1 is encoded by the KCNJ2 gene. By immunohistochemistry and in situ hybridisation it has been shown that Kir2.1 is weakly and diffusely expressed in the whole brain (Horio et al. 1996; Pruss et al. 2005). However, the expression pattern is limited to dendrites and somata (Pruss et al. 2005). Furthermore, Kir2.1 is expressed in the heart, blood vessels, kidney and skeletal muscles. Knock out mice of Kir2.1 showed no obvious phenotype of neuronal abnormality but vasodilation (Zaritsky et al. 2000). An explanation for this phenomenon is the fact that most neurons express several types of the Kir2.X channels which could compensate for

each other. This assumption is made because it is known that a channel can be formed of different subunits of the Kir2.X family in vitro as well as in vivo. For example, a combination of Kir2.1 and Kir2.4 can be detected in native tissue of the brain (Schram et al. 2002). These heteromers have distinct properties from their homomeric channel relatives (Goerge et al. 2002).

This finding is consistent with human phenotypes where mutations in KCNJ2 are mainly associated with cardiac diseases like Andersen's syndrome (LQT type 7) and short Q-T syndrome. However, short QT3 as well as Andersen's syndrome can be associated with neurodevelopmental disorders like autism-epilepsy phenotype (Ambrosini et al. 2014; Plaster et al. 2001). Most of the known mutations causing Andersen's syndrome are due to incorrect heteromeric assemblies (Tristani-Firouzi et al. 2002; Goerge et al. 2002; Donaldson et al. 2003; Hosaka et al. 2018). Their position is mostly in the cytoplasmic domain (Davies et al. 2005). Also located in the cytoplasmic domain, close to the C-terminus, the region responsible for the trafficking of Kir2.1 can be found. This amino acid sequence is conserved in all Kir2.X subfamily members and necessary for Kir2.1 to get from the endoplasmic reticulum to the cell surface (Ma et al. 2001; Stockklausner et al. 2001). It has been shown that mutations in this area are responsible for Kir2.1 remaining in the cytosol. However, mutations close to the N-terminus have also been shown to have an effect on Kir2.1 trafficking. Mutations in this area lead to Kir2.1 remaining in the Golgi apparatus where posttranslational modification is taking place. The N-terminus sequence for Golgi trafficking can also be found in all Kir2.X channels (Hofherr, Fakler, and Klöcker 2005; Ma et al. 2001; Stockklausner and Klo 2003). The exact localisation of Kir channels might be determined by the

PDZ domain located at the C-terminus which has been shown to interact with different PSDs (post synaptic density proteins) (Songyang et al. 1997).

It is known that some glia cells express Kir2.1. Oligodendrocytes do not belong to the glia cells that express Kir2.1 channels but Schwann cells in the PNS do. By immunohistochemistry in the PNS, it has been shown that Kir2.1 is clustered around Nodes of Ranvier at microvilli. Due to the location of the villi and channels, their function might be buffering of excess potassium ions when a neuron fires action potentials and thereby changing extracellular potassium concentrations (Mi et al. 1996; Wilson and Chiu 1990). Overexpression of inward-rectifying Kir2.1 channel decreases neuronal excitability by lowering the resting membrane potential (Okada and Matsuda 2008; Hartman et al. 2006).

1.8.2 Neuronal activity and axonal development

It has been shown that spontaneous as well as evoked neuronal and synaptic activity is important for the development of neurons in the developing sensory system (Katz and Shatz 1996).

In the visual system, evoked neuronal activity due to visual experience is needed to refine and mature connections that have been initialised through spontaneous neuronal activity before eye opening (Maffei and Galli-Resta 1990; Galli and Maffei 1988; Sernagor and Grzywacz 1996; Katz and Shatz 1996). Monocular deprivation experiments in kittens showed that neuronal arbours of thalamocortical axon shrink when the visual information is missing (Antonini and Stryker 1996; Antonini and Stryker 1993; Haruta and Hata 2007). Additionally, the eye-specific segregation of thalamocortical axons in kittens and monkeys is disrupted after blockage with retinal activity during development (Hubel et al. 1977; Levay, Stryker, and Shatz

1978). Further, suppression of neuronal activity by introducing Kir2.1 in a subset of retinal ganglion cells in zebrafish lead to less neuronal growth and fewer axon branches (Hua et al., 2005).

Also for motor neurons neuronal activity has been shown to have an important effect on pathfinding in the spinal cord of chick embryos. Normal patterns of spontaneous activity were necessary for correct motor axon guidance as well as for the expression of specific guidance cues (Hanson and Landmesser 2004).

Furthermore, Yu and colleagues used Kir2.1 to show that the establishment of the sensory map in the murine olfactory system needs spontaneous neuronal activity (Yu et al. 2004).

During the development of ferrets, spontaneous activity in LV pyramidal neurons is needed for layer-specific and ipsilateral axonal branching in the somatosensory cortex (Dantzker and Callaway 1998; Butler et al. 2001).

In addition to neurite formation, neuronal activity, especially of neighbouring neurons, influences the number and characteristics of GABAergic synapses in rat hippocampal neurons *in vitro* (Hartman et al. 2006). In thalamocortical cells originating from rat, overexpressing Kir2.1 was found to reduce the numbers of synapses to LVI neurons (Matsumoto et al. 2016).

1.8.3 Studying the role of neuronal activity by introducing Kir2.1 via *in utero* electroporation

Kir2.1 has been used in several studies to reduce electrical excitation to study the role of neuronal activity on different systems by *in utero* electroporation. Introducing Kir2.1 has been proven to be an effective method to reduce neuronal excitability non-reversibly and chronically by increasing the potassium leakage current (Burrone, Byrne, and Murthy 2002; Johns et al. 1999). Kir2.1 overexpression does

not only reduce excitability but also spontaneous activity (Hagihara et al. 2015; Yu et al. 2004; Johns et al. 1999). However, Burrone and colleagues reported that due to the constant change in membrane potential, the hyperpolarisation leads to an increase of synaptic input. This homeostatic adaptation may even lead to neuronal excitability (Burrone, Byrne, and Murthy 2002). Though, several other studies looked at neuronal excitability at postnatal ages. These studies showed that neurons expressing Kir2.1 constantly still show a lower excitability than non-affected neurons making Kir2.1 a valid tool to use (Mizuno, Hirano, and Tagawa 2007; Cancedda et al. 2007).

Wang and colleagues were interested in the influence of neuronal activity on callosal projections in the murine somatosensory cortex (Wang et al. 2007). They supressed neuronal excitation by introducing Kir2.1 via *in utero* electroporation. By using this method, they achieve to label a subpopulation of cortial layer II/II neurons to trace their axons into the contralateral hemisphere. It was observed that the less active neurons often do not reach their predetermined target. Either, they did not reach the right area or if they did, they failed to hit the right layer within their area (Wang et al. 2007). In a similar study, Kir2.1 electroporated interhemispheric projections of the neonatal mouse visual cortex were examined. They also reported a disturbance in axonal and arbour growth (Mizuno, Hirano, and Tagawa 2007).

Kir2.1 *in utero* electroporation has also been used to demonstrate the importance of neuronal activity in cortical integration of specific GABA-producing interneurons. Before P3, neuronal activity is needed for correct migration and after P3 for axonal and dendritic development. This process is dependent on the engulfment and cell motility 1 (Elmo1) gene (García, Karayannis, and Fishell 2013). Additionally, when Cancedda and colleagues overexpressed Kir2.1 in rat excitatory GABAergic

cortical LII/III neurons, they found that the morphological maturation was noticeably affected. Kir2.1 transfected cells exhibited shorter dendritic processes, shorter neurite length as well as reduced branch number in neurites (Cancedda et al. 2007). Furthermore, it has been shown that not only the morphology of Kir2.1 expressing cells themselves is affected. Axonal branching in thalamic cells was also affected when Kir2.1 was overexpressed in their input (cortical) cells (Yamada et al. 2010).

1.9 Aims of this thesis

In this introduction I have reviewed the current existing body of literature focusing on the development of the cortex, on neuronal conduction of information and reviewed evidence for activity dependent myelination. Over the last years, the interest in activity dependent myelination has drastically increased based on several seminal studies (examples: Sampaio-Baptista et al. 2013; Gibson et al. 2014; Mensch et al. 2015; Hines et al. 2015). While I was working on my thesis, *in vivo* studies utilising newest advances in genetical techniques were conducted, reducing side effects such as inflammation that can have major effects on myelination. Using transgenic mice models to study activity dependent myelination offers a great potential to gain deeper insights into myelinating processes which can be transformed into regenerative therapies, e.g. in multiple sclerosis patients. However, before we can contemplate any therapeutic intervention, we need to understand the basic mechanisms that influence myelination during development and myelin maintenance during adulthood.

Despite the expansion of the current literature, some of the main research areas are still unexplored such as the influence of reduced neuronal activity in

subpopulations of deep cortical projection neurons in mice. Therefore, my work is focussed on decreasing neuronal activity in two different manners.

The first way of altering neuronal activity is by abolishing *Snap25* from selected populations of cortical projection neurons either in cortical layer V or layer VI that are also labelled with a reporter gene expression. These mouse lines enabled me to monitor selective deep cortical projection populations that differ in their ability to release synaptic vesicles in a calcium dependent regulated manner.

My second way to influence neuronal activity is by introducing the inwardly rectifying potassium channel (Kir2.1) by in utero electroporation at the time of the cortical projection neuron generation. By overexpressing Kir2.1 the probability of action potential formation is lowered through hyperpolarization of the neuron which leads to a decrease of membrane resistance so that they are less excitable.

By using these two techniques two different models can be compared; on the one hand vesicular release will be reduced without influencing spontaneous activity and on the other hand neuronal excitability will be reduced additionally to spontaneous activity.

Hence, in my thesis I attempt to understand the role of various forms of neuronal activities in developmental onset and subsequent maintenance of myelination. Using different projection neuron populations, I can also compare the susceptibility of different cortical projection neuron populations to the experimental manipulations.

In chapter 3, I will investigate whether reducing activity from early stages of development onwards changes the axon elongation and targeting. In particular, I shall study the cortico-thalamic ingrowth and maintenance of LV and LVI Snap25 cKO projections and targeting of projections originating from Kir2.1 electroporated

cortical neurons. For the *in utero* electroporation method I prepared vectors that will also be presented in this chapter. Additionally, I shall present the characterisation of LVI Snap25 cKO and compare it to LV Snap25 cKOs. The results from this chapter will form the basis for my analysis in the next two experimental chapters.

In chapter 4, I will describe the timing of myelination onset for projections originating from LV and LVI Snap25 cKO neurons as well as from neurons that were electroporated by MutKir2.1 or Kir2.1 in various parts of the CNS. Additionally, oligodendroglial lineage marker density will be analysed in LV and LVI Snap25 cKOs. I will focus on the area where neuronal cell bodies are located that are affected by altered neuronal activity as well as the striatum where LV and LVI fibres project through.

In chapter 5, I will analyse myelin characteristics that influence conduction velocity such as g-ratio and parameters of nodes of Ranvier in axons originating from cortical projection neurons lacking Snap25. The formation of nodes of Ranvier as well as compact membrane structures are typical characteristics of myelin. Myelin thickness will be determined in relation to fibre diameter (g-ratio) in electron microscopy images of the dorsal corticospinal tract before the onset of degeneration in LV Snap25 cKOs. Furthermore, I shall analyse the nodes of Ranvier by assessing different paranodal measurements such as paranodal width, nodal width as well as number of nodes in a selected arbitrary unit field of view. Additionally, I shall study mRNA as well as protein levels of myelin and inflammation markers to see alterations during premature aging of myelin ensheathed fibres originating from cortical neurons lacking Snap25.

After each experimental chapter the specific implications of the findings will be discussed. Finally, in chapter 6, I will connect the findings of each experimental chapter and additionally discuss them in the broader context as well as speculating on future research directions.

2 Methods

2.1 Animals

2.1.1 Breeding and maintenance

All experiments were performed with local ethical review committee approval and conducted in accordance with the Animals (Scientific Procedures) Act, 1986 (ASPA), UK, under valid personal and project licences.

Animals were held in individually ventilated cages (IVCs) on a standard diet with 12 hours light/dark cycles in the Biomedical Sciences Building, Oxford.

Due to irregular expression of Cre in the germline when the gene is passed on by the father, Cre can only be transmitted via the mother in Rbp-4-Cre (LV) and Ntsr1-Cre (LVI) lines.

LV Snap25 cKO animals (conditional Snap25 KO from subpopulation of layer V neurons) were obtained by crossing Rbp4-Cre (Tg(Rbp4-cre)KL100Gsat/Mmucd), Snap25-flox (B6- Snap25tm3mcw) and tdTomato (B6;129S6-Gt(ROSA)2-6Sortm14(CAG-tdTomato_Hze/J(Ai14)) mice (Rbp4-Cre::floxed Snap25::tdTomato) (Gerfen, Paletzki, and Heintz 2013; Madisen et al. 2009; Gong et al. 2003; Gong et al. 2007). Rbp4-Cre;Snap25flox/flox;R26RtdTomato females were neglecting their pups and could therefore not be used for breeding purposes. Thus, Rbp4-Cre/+;Snap25fl/+;Ai14/Ai14 females were crossed with Rbp4-Cre+/+;Snap25fl/fl;Ai14/Ai14 males.

Controls were obtained from crossing Rbp4-Cre with tdTomato mice (Rbp4-Cre::tdTomato).

LVI Snap25 cKO animals were obtained by crossing Ntsr1-Cre (Tg(Ntsr1-Cre)220Gsat/Mmucd), Snap25-flox (see above) and tdTomato (see above) mice (Ntsr1-Cre::floxed Snap25::tdTomato). Controls were obtained by crossing Ntsr1-

Cre with tdTomato mice (Ntsr1-Cre::tdTomato) (Gerfen, Paletzki, and Heintz 2013; Madisen et al. 2009; Olsen et al. 2012).

Cre positive animals were identified by using fluorescent goggles (Biological Laboratory Equipment Maintenance and Service, BLS) and genotyping for tdTomato and Cre was therefore not necessary.

2.1.2 Genotyping

Samples for *Snap25* genotyping were either obtained by tail tips (from perfused animals) or ear clips (from living animals). Samples were digested overnight at 55°C in 200-400 µl Proteinase K (1:100, Roche) containing tail-buffer (10mM Tris pH 8.0 (tris(hydroxymethyl)aminomethane), 10mM EDTA pH 8.0 (ethylenediamine tetraacetic acid), 50mM NaCl, 0.5% SDS (sodium dodecyl sulfate) in H_2O). Before chromosomal DNA was used, Proteinase K was inactivated for 10 minutes at 99°C. Samples were cooled down to 4°C, diluted 1:10 in nano water (nH_2O, deionized water with >18.2MOhm resistance) and centrifuged. 1 µl DNA was utilised for PCR (polymerase chain reaction) with 24 µl of PCR-Mix:

Compound	Amount (µl)	Company
Taq 10x PCR buffer	2.5	Invitrogen
2 mM $MgCl_2$	1.5	Invitrogen
0.5 mM dNTPs	0.5	Roche
0.5 µM primer F	1	Sigma
0.5 µM primer R	1	Sigma
Platinum Taq DNA Polymerase	0.2	Invitrogen
nH_2O	17.3	Merck Millipore

Name	Primer Sequence
Lox P Forward	5’ CCC TGG GGA ACC ACG GCA GA 3’
LoxP Reverse	5’ TCC CAG GAA ACA GCA CAG CGT 3’

PCR-Programme was run on the Veriti 96 well Thermal Cycler (Applied Bioscience) as follows:

Cycles	Duration	Temperature °C
1	3 min	95
40	20 sec 30 sec 45 sec	95 61 72
1	10 min	72

4 µl of 6x Loading Dye was added to the PCR-samples and the mix was loaded onto a 1.5% agarose (Bioline) gel. For DNA counterstaining GelRed (1:1000, VWR) was used and to identify DNA fragment length DNA ladder (NEB, 100bp) applied. Gel electrophoresis was performed for 35 minutes at 130V in Tris Acetate-EDTA (ethylenediamine tetraacetic acid) buffer (TAE, 0.04 M tris-acetate and 0.001 M EDTA, pH 8.3) which was also used for the gel preparation. Gel imaging was carried out with a Dual Intensity Transilluminator (UVP Bioimaging systems).

2.1.3 *In utero* electroporation

In utero electroporations were performed 13 days after timed matings on pregnant C57/BL6 females. The protocol was adapted from García-Moreno and Molnár 2015 and Martínez-Garay et al. 2016 with minor adjustments. Animals were anesthetised with vaporised Isofluorane and kept in deep anesthesia until the end of the surgery. Additionally, Vetergesic (0.08 mg/kg) and Meloxicam (NSAID, 1 mg/kg) were injected for pain management.

Females underwent a midline laparotomy so that both horns of the uterus could be exposed. Plasmid (Kir2.1 or control plasmid, 350ng/µl in endotoxin free water, Qiagen) DNA alongside with Fast Green (Sigma) was injected into one of the lateral ventricles of each embryo using pulled glass needles (Harvard Apparatus). 40V Pulses (5x50 ms with 950 ms intervals, Electro Square Porator) were delivered using tweezer electrodes (CUY650P3, Sonidel Limited) before placing the horns of the uterus back into the abdominal cavity. The peritoneal incision was closed by using Vicryl 6/0 (Ethicon) whereas skin incision was closed by using surgical clips. Postoperative recovery took place in a preheated recovery chamber until normal activity was regained. Females were monitored daily post-operative including a three days period with Metacam and Vetergesic jelly provided for postoperative pain management. Clips were removed 10 days post-surgery. Females were sacrificed when pups were perfused between P12 and P22.

2.1.4 Tissue collection

Animals were anaesthetized with 0.6ml/kg Pentobarbitone (animalcare) administered via intraperitoneal (IP) injection and transcardially perfused with 0.1M phosphate buffered saline (PBS, pH7.4) and 4% paraformaldehyde (PFA, diluted in PBS, Sigma Aldrich). After dissection, brains were kept in PFA overnight at 4°C.

2.2 Histology

2.2.1 Vibratome sectioning

For cutting, brains were embedded in 5% low melting agarose (Bioline, in PBS) and sectioned with a vibrating microtome (VT1000S, Leica Systems). Brains were sectioned coronally to a thickness of 50 µm and spinal cords to 80µm (pia removed

prior to cutting) and stored in 1x PBS with 0.05% sodiumazide in 96 well plates (Costar).

2.2.2 Longitudinal flat-mounting of spinal cords

To determine axon integrity in the spinal cord, cervical spinal cord was dissected out of the spinal canal and the tdTomato positive area (corresponding to the location of dorsal corticospinal tract) flat-mounted longitudinally or cut coronally. For identification and dissection of tdTomato positive dorsal column area dissection took place under a fluorescence dissection microscope (Leica) using a scalpel or microsurgical knife (WPI) to remove excess of surrounding spinal cord tissue.

2.2.3 Fibre teasing of spinal cord tissue

After perfusions, spinal cords were dissected out of the spinal canal and 30 minutes postfixed in same fixative (4% PFA in PBS). Using forceps (Fine Science Tools, FST) and a petri dish filled with PBS, a bundle of nerve fibers (from the ventral spinal cord to check if method is working or from the dorsal part to target the dorsal corticospinal tract where tdTomato positive fibres from LV project through) were taken out and placed on an adhesive slide surface (superfrost plus, VWR). By using forceps (FST) or acupuncture needles (provided by laboratory of Prof Peter Brophy), single fibres were separated from the nerve fibres in drops of PBS to stick on the glass slide. PBS was let to dry off.

By using a wax pen (Sigma) a hydrophobic circle was drawn around the slide-mounted tissue. Slides could either be stored frozen (-20°C) or vertical immunohistochemistry in a moist chamber directly started with the protocol stated for free floating brain sections.

2.2.3 Fluorescent immunohistochemistry

Selected sections were pre-incubated at room temperature for 2h in blocking solution (3% goat/donkey serum, Sigma, with 0.1% Triton X-100, Sigma, in PBS). Incubation with primary antibody (see table below) diluted in blocking solution was carried out for 24-48 hours at 4°C. Subsequently, sections were washed three times for 10 minutes each with PBS before incubation with a fluorescently-labelled secondary antibody in blocking solution for 2 hours at room temperature. In the last step, sections were washed another three times and counterstained for 5- 10 minutes with DAPI (4',6-diamidino-2-phenylindole, 5 µg/ml, Invitrogen). Slides were mounted with glass coverslips using FluorSave Reagent (Merck Millipore). In CC1 immunohistochemistry, wash steps were prolonged to 1.5 hours after antibody incubations.

When MBP mean fluorescence intensity was analysed for an experiment, all sections were processed alongside to guarantee similar solutions used and comparable incubation times.

2.2.4 Tissue preparation for transmission electron microscopy (TEM)

Animals were anaesthetized with 0.5 ml Pentobarbitone (20%w/v, Animalcare) administered via intraperitoneal injection and transcardially perfused with phosphate buffer saline (PBS) and 4% paraformaldehyde (PFA, Sigma-Aldrich). After dissection, spinal cords were kept in PFA overnight at 4°C. Spinal cords were cut into thin sections (circa 1-2 mm) with a razor blade by hand. Washes were conducted between each step 1-3 times for 5-10 minutes with nH2O or 0.1M PB-Buffer pH 7.2 which was also used to prepare solutions. First, sections were washed followed by a 1% osmium tetroxide (Agar Scientific) stain for 1 hour. After that, sections were incubated in 2% uranyl acetate (in H2O, Agar Scientific) for

another hour. Following that, several dehydrating steps were conducted with increasing alcohol concentrations for 10 – 15 minutes each (70%, 80%, 90%, 100% Ethanol, 2x 100% absolute Acetone, SIGMA, in H_2O). For the next two days sections were placed on a rotation wheel changing 50/50 Resin/Acetone to pure Spurr Resin (Agar Scientific) after one day and then placed into embedding moulds for baking overnight at 60°C. Ultra-thin sectioning (70 nm, Reichert ultracut S microtome) was performed by Mrs Lynne Scott (practical teaching technical manager at Department of Physiology, Anatomy and Genetics).

2.2.5 Immuno-gold and contrast stain

Ultra-thin sections were stained on 200 mesh nickel grids (EMS) using uranyl acetate, lead and immuno-gold antibody labelling. 0.1 M PB-Buffer with saline pH7.2 and egg albumin (PBSea, SIGMA) was used for solution preparation. Washes were conducted with PBSea or nH2O between each step 1-3 times for 5-30 minutes. First, grids were incubated with primary antibody for 2 hours and, secondly, incubated with proteinA gold (Agar Scientific, 15 nm) for 1 hour. For high contrast stain, grids were placed in uranyl acetate (in H2O) for 20 minutes. After centrifuging lead solution (3% Reynolds' Lead Citrate, Electron Microscopy Science) it was dispensed in drops in a CO_2-free chamber and grids placed in lead-droplets before drying.

2.2.6 Tissue preparation for tiled electron microscopy

Tissue for tiled imaging was obtained by following a slightly altered perfusion protocol to the one stated above.

Animals were anaesthetized with IP administration of 0.5 ml Pentobarbitone (20%w/v, Animalcare) and transcardially perfused by using a perfusion pump

(model 77120-62, Cole Parmer). Flow rate was set to under 50% of maximum cardiac output for 12 minutes. First, dependent on the age, 5-10 ml of phosphate buffered saline (0.1M PBS, pH7.4) was used before switching to fixative. Fixative was prepared with 2.5% room temperature glutaraldehyde (EM grade from Electron Microscopy Scientific, EMS) and 2% paraformaldehyde (EMS) in 0.1M PB pH 7.4, which was also used to prepare solutions. After the perfusion, animals were left for 2 hours at room temperature before dissection to facilitate fixation. Fixed spinal cords were sent to Bio EM Facility of Ecole Polytechnique Federale de Lausanne (EPFL), Switzerland, where they were embedded in 5% agarose (Bioline, in PBS) for sectioning (80 µm) with a Vibroslicer (VT1000S, Leica Systems). Sections were washed three times for 10 minutes each in cacodylate buffer (0.1M, pH7.4, EMS) before postfixing on ice in freshly prepared 1.5% potassium ferrocyanide, 0.13M cacodylate buffer and 2% osmium (diluted in PB-Buffer pH 7.2) for 1 hour. Subsequently, sections were washed 5 times for 3 minutes each in water between all following steps starting with staining sections in filtered thiocarbohydrazide (1%, Sigma Aldrich) for 20 minutes before transferring them into 2% osmium tetroxide (Agar Scientific) for further 30 minutes. Sections were then placed in 1% uranyl acetate at 4ºC overnight. The next day, sections were washed in 50ºC water for three times 10 minutes each followed by a contrast stain with Walton's lead aspartate solution (10ml water heated to 50ºC, 0.04 g aspartic acid, 0.066 % lead nitrate, pH 5.0) at 50ºC for 2 hours. During the following three wash steps, water temperature was gradually lowered from 50ºC to room temperature before dehydration was started using graded alcohol series of 5 minutes each (1x50%, 1x70%, 1x96%, 2x100% in H_2O). Sections were then transferred to increasing concentrations of epoxy resin (Durcupan, Sigma-Aldrich)

in ethanol, and left in 100% resin overnight. They were finally placed in an 60° C oven for 24 hours between glass microscope slides coated with mold separating agent (Glorex, Switzerland).

Semi-thin (500 nm) sections were cut with a diamond knife (Diatome, Switzerland) using an ultramicrotome (UC7, Leica Microsystems). These sections were toluidine blue stained for 4 minutes at 60ºC and imaged using a microscope with transmitted light (Zeiss Axioskop 2) to check the quality of the tissue and to localise the precise region to be prepared for thin sectioning. Thin sections (250 nm thickness) were cut in the same manner and collected onto silicon wafers of 10 mm diameters.

These sections were imaged inside a scanning electron microscopy (Merlin, Zeiss NTS) with a beam voltage of 1.8 kV, pixel size of 8 nm and dwell time of 1 µsec per pixel. The entire corticospinal tract was imaged by tiling multiple images captured using custom software (SBEM Image, Benjamin Titze, FMI, Basel, Switzerland).

2.3 Image acquisition and analysis

2.3.1 Epifluorescence and confocal microscopy

Fluorescence images were taken with a laser-scanning confocal (Zeiss LSM710) or an epifluorescence (Leica DMR) microscope equipped with a digital camera (DC-500, Leica Microsystems). Fluorescence images during dissections were taken by a Leica MZFLIII microscope. Images were compiled using Image J (1.48v, Java, NIH).

2.3.2 Electron microscopy

Single images were taken with a JEOL transmission electron microscope (JEM-1010, JEOL) and tile images with a Merlin, Zeiss NTS electron microscope.

2.3.3 Fluorescence intensity analysis

Mean fluorescence intensity was measured using ImageJ (NIH) measuring mean grey value (Schindelin et al. 2012). tdTomato mean fluorescence intensity was measure in a comparable field of view (whole images or box of same size). MBP mean fluorescence intensity was measured either in a comparable field of view (whole images or box of same size) or where indicated in tdTomato positive areas only by creating a selection after manual thresholding. At 6 months, when MBP signal seemed discontinuous without changes in fluorescence intensity, a particle count was additionally conducted in M1 for MBP as well as tdTomato. Therefor, the whole field of view was analysed in imageJ using the Particle Analyser with following settings: size (μm^2) – 5-infinity, circularity 0.25-1, count masks.

2.3.4 Electron microscopy image analysis

Electron Microscopy (EM) tiled images of the dorsal corticospinal tract were analysed blindly using ImageJ (Schindelin et al. 2012). Two boxes of the size 32.5 x 42.5 µm were drawn on each side of the midline within the dorsal corticospinal tract. All axons completely within this area were measured utilising the line tool. Per axon 4 measurements were taken: shortest inner diameter (axon only), shortest outer diameter (axon including myelin) as well as longest inner diameter (axon only), longest outer diameter (axon including myelin). The g-ratio was calculated by dividing the average of the inner measurements by the average of the outer measurements (Pesaresi et al. 2016).

2.3.5 Node of Ranvier quantification

Node of Ranvier analysis was conducted blindly on image stacks (taken with 40x objective) using ImageJ (NIH) (Schindelin et al. 2012). Rectangular Tool was used to draw a box around a node on the plane where intensity of Caspr stain was highest on both sides of the node. Only nodes where both paranodes were parallel to the focal plane were included in the analysis. A plot profile was generated from which 6 points per node were measured to identify the beginning, maxima and end of each paranode. Half maxima were calculated between these measurements and taken as beginning and end of each paranode.

2.3.6 Cell counts

Blinded manual cell counting was done by using ImageJ (NIH), combined with its cell counter plugin (Schindelin et al. 2012). Olig2 P8 counts were done by using a Cell Profiler pipeline designed by Anna Hoerder-Suabedissen (Jones et al. 2008).

2.4 Molecular techniques

2.4.1 Western blots

For protein detection, western blots (protein immunoblots) were prepared using the BioRad system following the instructions provided by the manufacturer.

Striatal tissue was dissected from brains obtained from animals killed with cervical dislocation and dissected tissue was kept at -80°C until lysates were prepared. Tissue was homogenised with a disposable pellet mixer and cordless motor (both from VWR) in cold radioimmunoprecipitation assay (RIPA) buffer (50 mM Tris-HCl pH 7.5, 150 mM NaCl) containing protease inhibitor cocktail (Roche) and incubated for 30 minutes. Subsequently, the lysates were centrifuged (10 minutes, 5000 rpm, 4°C) and the supernatant transferred into a fresh tube. Pierce bovine serum

albumin (BSA) Assay (Thermo Fisher Scientific) was utilised to determine protein concentrations. Lysates were processed by adding NuPAGE lithium dodecyl sulfate (LDS) sample buffer (4X, Thermo Fisher Scientific) and heated for 10 minutes at 70°C before loading onto precast 4-12% BioRad gels alongside with a protein standard (Dual Color, Biorad). Proteins were blotted onto a polyvinylidene difluoride (PVDF) membrane (Invitrogen) for 1 hour at 120 volt. Dilutions of primary and secondary antibodies (see table) were prepared in 1% milk in TBST (10x Tris Buffered Saline, BioRad, 0 .1% Tween20, Sigma) after conditions were validated for used antibodies. Signal detection was performed by using chemiluminescence (ECL) plus western blot detection reagent (GE Healthcare).

Image acquisition was conducted by using Chemi Doc XRS+ and Image Lab software.

2.4.2 Miniprep

Colonies were picked from agar-plates and incubated overnight in 2 ml LB-medium containing ampicillin (100 µg/ml, Thermo Fisher Scientific). On the next day, 500 µl bacterial solution was used to generate a glycerol (500 µl of 50% glycerol in H_2O) stock to be stored at -80°C. With the remaining 1500 µl a Mini-prep was conducted using a QIAprep Spin Miniprep Kit according to the manufacturer's instructions (Qiagen).

2.4.3 Sanger sequencing

DNA obtained during Miniprep was analysed by Sanger sequencing. 100ng/µl H_2O Plasmid DNA was sent to Source BioScience Sequencing and analysed with following primers:

Name	Primer Sequence
pCAG forward	5’ GCAACGTGCTGGTTATTGTG 3’
EGFP CR	5’ GTT CAG GGG GAG GTG TG 3’

Sequence analysis was conducted using APE (A Plasmid Editor) software.

2.4.4 DNA restriction digest

To control for correct plasmid amplification and for preparing the following ligation of pCAG-Kir2.1-IRES-Cre, a restriction digest was undertaken.

In pCAG-Kir2.1-IRES-Cre, Kir2.1 is flanked on both sides by EcoRI restriction sides. Consequently, EcoRI was applied to cut Kir2.1 out of the vector to generate a control vector only containing pCAG-IRES-Cre.

pCAG-Kir2.1-T2A-tdTomato and pCAG-MutKir2.1-T2A-tdTomato were digested using two different restriction enzymes cutting once each (EcoRI and HindIII).

20 µl of each mixture contained 2 µl 10x NEB Buffer 4, 1 µl of each enzyme and 1 µl DNA in H_2O. Before analysing the digested DNA was applied on a 1% agarose-gel in TAE buffer. Both restriction mixes were incubated at 37°C for 1 hour and enzymes were inactivated for 20 minutes at 65°C.

2.4.5 DNA extraction from agarose-gel and ligation

Linear vector backbone of pCAG-IRES-Cre was excised from the agarose-gel and purified by using QIAquick Gel Extraction Kit (Qiagen) following manufacturer’s instructions. 2 µl of purified DNA was used in a 10 µl ligation mix including 1 µl T4 Ligase and corresponding 1 µl T4 Ligase Buffer with 10 mM ATP (Adenosine 5'-Triphosphate, New England Biolabs). The subsequent incubation (3 hours) took place at room temperature.

The ligated construct was transformed into competent *E. coli* DH5 alpha bacteria (Invitrogen, see protocol above), positive clones were confirmed by sequencing.

The correct clone was cultivated in LB-medium and plasmid DNA was purified by Maxiprep (Qiagen) as described below.

2.4.6 Maxiprep

For a Maxiprep, pre-cultures were inoculated by transferring part of the glycerol stock into 5 ml LB-medium containing ampicillin and incubated shaking (300 rpm) at 37°C. After 6-8 hours, the bacteria solution was transferred to 200 ml of LB-medium to continue growth overnight under the same conditions. Next, bacteria were pelleted and a Maxiprep was conducted using the EndoFree Plasmid Maxi kit (Qiagen). Finally, DNA concentration was measured photometrically (Nano Drop, Thermo Fischer Scientific).

2.4.7 Tissue homogenisation and RNA extraction for qPCR

Cortical tissue was dissected from brains obtained from animals killed by cervical dislocation and dissected tissue was kept at -80°C until lysates were prepared. Tissue was homogenised with Bead Ruptor Pre-Filled Bead Tubes (Thomas Scientific) using a tissue homogeniser (Precellys24, VWR). Following that, 500 µl of TRIzol (Thermo Fischer Scientific) and 100 µl of Chloroform (same source) were added to each sample, vortexed and incubated for 5 minutes at room temperature. Samples were centrifuged for 15 minutes at 12,000 g at 4°C. The newly formed upper aqueous phase layer was transferred into a new tube and RNA in it was precipitated by adding 250 µl Isopropanol per tube. To gain RNA pellet, samples were centrifuged for 15 minutes at 12,000 g at 4°C again. After supernatant was disposed, 400 µl of 75 % Ethanol needed to be added and samples inverted several times. After a further centrifugation step of 5 minutes at 7500 g at 4°C supernatant was disposed and pellet dried. Pellet resuspension was conducted in

52 µl of RNAse-free water (Qiagen). 2 µl were used to determine the RNA concentration by Nano Drop (Thermo Fischer Scientific).

2.4.8 c-DNA synthesis

cDNA was synthesised by using High-Capacity cDNA Reverse Transcription Kit (Thermo Fischer Scientific) following instruction manual.

2.4.9 Quantitative Realtime PCR (qPCR)

Prior to testing all samples, optimal cDNA concentration was determined and the functionality of primers checked by running several control cDNA dilutions. 1ng/µl was set to be used in the following qPCR experiments with all samples. Per sample 5 µl of DNA was added to 0.6 µl of forward and reverse primers (10 µM each), 3.8 µl H_2O and 10 µl SYBR Green (Thermo Fischer Scientific).

Name	Primer Sequence
tdTomato F	5’ GCC CCG TAA TGC AGA AGA AG 3’
tdTomato R	5’ GTG TAG TCC TCG TTG TGG GA 3’
MBP F	5’ CTT TCT CAG ACG GCC TCA GA 3’
MBP R	5’ GAC TCT GAG GGC CTG TCT TT 3’
Olig2 F	5’ CCC CAG AAC CCG ATG ATC TT 3’
Olig2 R	5’ GGT GCT GGA GGA AGA TGA CT 3’
CNP F	5’ GCT GCA GTT CCC TTT CCT TC 3’
CNP R	5’ CAG CAG CGG AVA CCA TCT TG 3’
CD68 F	5’ GCA GCA CAG TGG ACA TTC AT 3’
CD68 R	5’ TTG CAA GAG AAA CAT GGC CC 3’
CC1 F	5’ ATT GCC CAG CTC TTC TTC CT 3’
CC1 R	5’ AAC TTC TGT CGT CCT GGG AG 3’
Iba1 F	5’ ATG CTG GAG AAA CTT GG GT 3’
Iba1 R	5’ CCA GTT GGC CTC TTG TGT TC 3’
GAPDH F	5’ CAACTCCCACTCTTCCACCT 3’
GAPDH R	5’ GAGTTGGGATAGGGCCTCTC 3’

Samples were measured in duplicates and negative controls (DNA substituted with water) run alongside. qPCR-Program was run on the StepOnePlus™ Real-Time PCR System (Thermo Fisher Scientific) as followed:

Cycles	Duration	Temperature °C
1	10 min	95
40	30 sec	95
	60 sec	60
	30 sec	72
1	15 sec	95
	60 sec	60 + 0.5
	15 sec	90

Results were displayed using the StepOne v2.2 software and cycle of thresholds (Ct) determined. Ct is defined as the cycle number at which the PCR product amplification curve intersects a threshold (background fluorescence) of detection set by the software algorithm. A standard curve for each experiment is generated by plotting the Ct values versus the logarithmic concentration. The relative concentration of an unknown sample will be assessed by comparing its Ct with the Cts used for generating the standard curve. Ct values are inverse to the amount of nucleic acid in a sample and correlates with the number of copies in a sample. The individual Cts were used to normalise the genes of interest (GOI) against the housekeeping gene (GAPDH) by subtracting $Ct_{housekeeping\ gene}$ of the Ct_{GOI} to gain Δ CT. The relative expression of the gene of interest was then determined by $2^{\Delta Ct}$.

2.5 Frequently used solutions and antibody list

Table 1: Frequently used solutions

Phosphate Buffer 0.5 M PB, pH7.4	72.1 g Na_2HPO_4*2 H_2O 14.8 g NaH_2PO_4*2 H_2O H_2O added up to 1 l
Phosphate Buffer Saline 0.1 M PB, pH7.4	200 ml PB 9 g NaCl 800 ml H_2O
Phosphate Buffered Sodium Azide 0.05 % PBSA	1 ml 5 % sodium azide (diluted in H_2O) in 1 l PBS
4',6-Diamidin-2-phenylindol Solution 5 µg/ml DAPI	50 µl concentrated DAPI 50 ml 0.1 M PBS
LB Medium (sterilised by autoclaving)	10 g Trypton 5 g Yeast extract 10 g NaCl Dissolved in 1 l H_2O

Table 2: Frequently used antibodies

Antibody	Antigen	Source	Dilution	Company (order number)
Primary	MBP	rat	1:500	Abcam (7349)
	MBP	goat	1:500	Santa Cruz (271524)
	Olig2	rabbit	1:500	Millipore (9610)
	CC1	mouse	1:500	Abcam (16794)
	dsRed	rabbit	1:500	Clontech (632496)
	RFP	chicken	1:500	Rockland (600-901-379)
	RPF	rabbit	1:500	MBL (PM005)
	Caspr	rabbit	1:2000	Abcam (34151)
Secondary	AlexaFluor488	donkey	1:500	Molecular Probes (21208)
	AlexaFluor568	donkey	1:500	Invitrogen (10042)
	AlexaFluor488	goat	1:500	Molecular Probes (11008)
	AlexaFluor568	goat	1:500	Invitrogen (1041)
	Biotinylated	goat	1:250	Vector Laboratories (9400)
Tertiary	streptavidin-cy5		1:200	Molecular Probes (434316)

2.6 Statistics

Statistical analysis and graph visualisation were conducted in GraphPadPrism (GraphPad Software, CA, USA). To determine statistical significance either unpaired two-tailed U-test (Mann-Whitney test, non-parametric test) was used or unpaired one-tailed U-test when degeneration was examined since we tested our hypothesis that the signal will decrease. U-test is more suitable (than t-test) when small sample sizes were tested, as done several times in this thesis that cannot be tested for normality like bigger sample sizes. In figure 44 (Reduced g-ratio in the dorsal corticospinal tract of LV Snap25 cKOs) a two-tailed, unpaired t-tests was conducted, due to the normal distributed myelinated axons that were measured within one animal. This t-test was also conducted in Figure 15 'Similar weights of 4 months old LVI Snap25 cKO and control males' due to normal distributed samples and sufficient sample size (n= 7 & 8).

Only where more than 2 factors per brain were tested (see Figure 49 'qPCR of mRNAs coding for myelin proteins or oligodendrocyte and inflammation markers of cortical tissue revealed significant difference in some mRNA levels'), multiple t-test with adjustment of p-values was performed (Holm-Sidak method). P-values where adjusted to lower the possibility of a false positive test when conducting several tests with one hypothesis.

For NoR analysis (Figure 47), a nested t-test was conducted due to the many data points within a single animal.

Throughout the thesis significance was stated when $p \leq 0.05$.

3 Fibre targeting and maintenance of silenced neurons

3.1 Introduction

This chapter describes the thalamic targeting and maintenance of cortical LV and LVI projections that lack the ability to release synaptic vesicles in a regulated fashion due to the deficiency of Snap25. Additionally, the generation of plasmids that have been used for *in utero* electroporation is discribed, as well as targeting of projections from cortical neurons that express Kir2.1 after the procedure.

Therefore, the first part of this chapter introduces the two transgenic mouse lines studied as well as the basic principle of the barrel cortex.

The aim of this chapter is to characterise the two used models (Snap25 abolishing and Kir2.1 introduction) to test their suitability for further myelin analysis in the following two chapters. This was essential especially due to contradicting results about axonal outgrowth in the absence of functioning Snap25 (Molnár et al. 2002; Osen-Sand et al. 1993). The two Snap25 cKO mouse lines have also been studied for some general anatomical features like thalamic targeting and visibility of the barrel field since these are of major interest in our laboratory. The thalamic targeting in particular was also studied, because previous experiments in our laboratory showed that peripheral activity (reduced by monocular enucleation) is essential for correct timing and correct thalamic targeting of LV and LVI axons during development (Grant, Hoerder-Suabedissen, and Molnar 2016; Grant 2014). The results from this chapter will be the basis to analyse myelination around these fibres in the following two result chapters.

3.1.1 Transgenic mice to label subcortically projecting cortical LV and LVI neurons

Corticothalamic axons innervating the thalamus arise from cells in layer V (LV) and layer VI (LVI) of the cortex (Rouiller et al. 1998; Guillery 1995; Sherman and Guillery 2002). However, they do not innervate the same regions of the thalamus nor do they provide the same input at their target site. LV corticothalamic fibres provide large and powerful (driver) input to the thalamic neurons that is mediated through ionotropic glutamate receptors whereas LVI cells provide smaller and weaker (modulator) input that is mediated through metabotropic glutamate receptors (Sherman and Guillery 1998). Thalamic nuclei can be divided into two basic categories. First order thalamic nuclei receive input from the sensory periphery, whereas higher order thalamic nuclei receive most of their input from the cortex and relay this information back to other cortical areas. Regarding the distinct thalamic nuclei they innervate, one can observe that LV fibres target higher order nuclei like lateral posterior and posterior thalamic nucleus. In contrast, LVI is not exclusively innervating the other type of nuclei, first order nuclei (including ventral posterior-medical and dorsal lateral geniculate nucleus), but both of them (Sherman and Guillery 2002).

To study projections of cortical neurons innervating subcerebral areas I used two transgenic mouse lines in which one specific deeper layer of the cortex is selectively labelled by restricted Cre expression. In Rbp4-Cre (Tg(Rbp4-cre)KL100Gsat) Cre expression is driven in a subset of LV of cortical neurons (GENSAT; Gong et al. 2007; Gong et al. 2003; Gerfen et al. 2013). In Ntsr1-Cre (Tg(Ntsr1-Cre)220Gsat) Cre expression is driven in LVI of cortical neurons (GENSAT; Gerfen et al. 2013; Olsen et al. 2012).

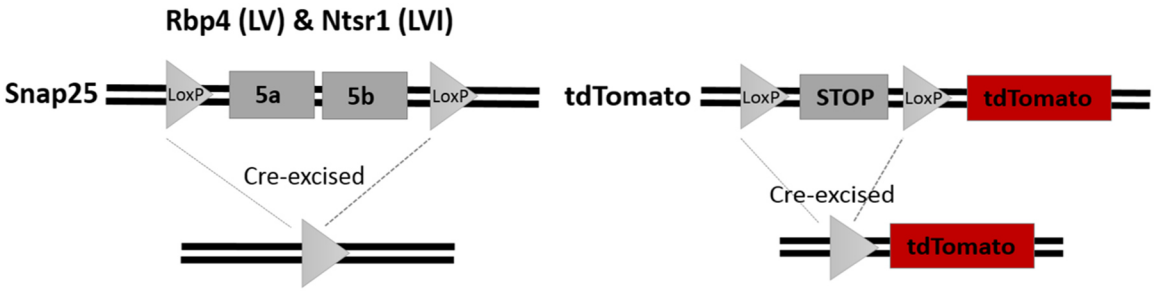


Figure 8: tdTomato conditional Snap25 knock out
In presence of Cre exon 5a/b of *Snap25* and a stop-codon upstream of the *tdTomato*-gene is excised leading to a cell-type specific knock-down of *Snap25* labelled red.

Both mouse lines were crossed with a STOP floxed tdTomato reporter line (B6;129S6-Gt(ROSA)2-6Sortm14(CAG-tdTomato_Hze/J(Ai14)) enabling transcription of tdTomato and labelling of all Cre expressing cells including their neurites. In the presence of Cre the loxP-flanked STOP cassette is excised which prevented the transcription of CAG driven fluorescent protein tdTomato before (Madisen et al. 2009).

It has been reported that Cre-mediated excision of loxP-flanked STOP occurs before P2. This is visible by tdTomato expression in LV of the Rbp4-Cre::tdTomato mouse line and layer VI of the Ntsr1-Cre::tdTomato already at P2 (Hoerder-Suabedissen, Korrell et al. 2018). In both mouse lines pyramidal cell bodies, dendrites as well as axons are labelled with tdTomato.

It has been shown that 15% of LV cells express Cre at P6 in the somatosensory cortex (Grant 2014). Those cells can be found in both subregions, LVa and LVb, as well as both pyramidal subtypes, Type I (corticospinal and corticothalamic) and II (corticocortical and corticostriatal).

Table 3: Summary of LV neuronal subtypes

Sublayer	Apical dendrite	Apical dendrite ends	Projection area	Type
VA	simpler	LII/III	corticocortical and corticostriatal projecting	II
VB	tufted	LI	corticospinal and corticothalamic projecting	I

In LVI, Olsen and colleagues reported that Ntsr1-Cre is expressed in two morphological distinct LVI pyramidal neurons which can be distinguished by their apical dendrites. The bigger population of pyramidal cells had dendrites reaching LI of the cortex whereas the minority of cells had dendrites extending into LIV and LV (Olsen et al. 2012; Bortone, Olsen, and Scanziani 2014; Chevée et al. 2018). Olsen and colleagues also characterized how many cells in LVI express Ntsr1-Cre. They showed that in adult mice 65% of LVI neurons express Ce in the primary visual cortex (Olsen et al. 2012). However, another study done by Grant in our laboratory found that at P6 only 35% of neuronal cells expressed Cre in the somatosensory cortex. Grant concluded that this difference might be due to the difference in age and cortical region or due to the difference in staining intensity of neuronal cells and counting method. Grant and colleagues also demonstrated that the thalamic nuclei are innervated differentially by the two neuronal populations in Rbp4-Cre and Ntsr1-Cre lines (Grant et al. 2016; Hoerder-Suabedissen, Korrell et al. 2018). Projections from Rbp4-Cre expressing neurons target higher order and avoid first order thalamic nuclei, whereas projections from Ntsr1-Cre neurons have no such selectivity.

3.1.2 Whisker Barrel cortex

The whisker barrel field is a region in the primary somatosensory area of the rodent cortex where LIV is patterned, forming barrels according to the pattern of the

sensory periphery of the whiskers. The cell sparse centre of a barrel, called hollow, is of a cylindrical shape and is separated from its neighbouring barrel by a septum (Woolsey and Loos 1970). The barrels receive somatosensory inputs from the thalamus. A single barrel in the brain represents a single whisker of the body (Woolsey & Van der Loos 1970; Diamond et al. 2008). The pattern of the barrels in layer IV of S1 matches the representation of the whiskers in the sensory periphery and barrels correspond to one whisker each. Therefore, neurons within a barrel respond to whisker-related input. LIV neurons of a particular barrel most often respond exclusively to one single whisker and some neurons only respond if the whisker moves to one specific direction (Swadlow 1994). The response of neurons in the barrels can differ from firing only at the initial deflection of the whisker to a response that is continuous throughout the deflection (Wilent and Contreras 2004; Shoykhet, Doherty, and Simons 2000).

The whisker barrel field is organised in a somatotopic map where brain regions are adjacent in the way their corresponding body parts are. The barrels of the major facial whiskers are located in the posteromedial barrel subfield and topographically organised like the whiskers: in 5 rows of 4-7 barrels, corresponding to the five rows of whiskers on the snout (Woolsey and Loos 1970).

Despite the relatively small body area the whisker barrels represent, the barrels dominate the somatotopic map of the somatosensory cortex due to the importance as main sensory organs for the rodents (Hoover et al. 2018; Enriquez-Barreto et al. 2012). Sensory information arrives in various layers of the primary and secondary somatosensory cortex via the thalamus and the brain stem after starting at the whisker follicles.

3.1.3 Nomenclature

In all following chapters of this thesis, Rbp4-Cre+;Ai14;Snap25+/+ and Rbp4-Cre+;Ai14;Snap25fl/+ will be referred to as LV controls. Ntsr1-Cre+;Ai14;Snap25+/+ will be named LVI controls.

Rbp4-Cre+;Ai14;Snap25fl/fl will be called LV Snap25 cKO and Ntsr1-Cre+;Ai14;Snap25fl/fl will be called LVI Snap25 cKO.

3.1.4 Aims of Chapter 3

A previous study reported that SNAP25 expression during development is crucial for axonal growth and can be inhibited when using SNAP25 antisense oligonucleotides. Osen-Sand and colleagues used this technique in cortical neurons originating from rats *in vitro* and the developing chick retina *in vivo* (Osen-Sand, Catsicas, Staple, Jones, Ayala, Knowles, et al. 1993). However, Washbourne and colleagues demonstrated that during mouse embryogenesis genetic ablation of SNAP25 is not necessary for nerve growth. This study also showed that global genetic ablation of SNAP25 is lethal postnatally due to respiration failure (Washbourne et al. 2002; Molnár et al. 2002). Organotypic co-cultures of E16 Snap25 KO thalamus and early postnatal WT cortex suggested that thalamic projections could grow, stop and arborize in WT cortex without the ability of regulated synaptic vesicular release if cultured for a few days (Blakey, Wilson, and Molnár 2012).

However, it was unclear whether postnatal axonal outgrowth and targeting in a subpopulation of murine cortical projection neurons is affected when abolishing Snap25 expression and what influence reducing neuronal activity has on fibre targeting.

Therefore, the aim of this chapter is to examine thalamic targeting during the postnatal periods by using Rbp4 (LV) and Ntsr1 (LVI) Cre Snap25 conditional knock out mice and to observe axonal targeting from neuronal cohorts electroporated with Kir2.1. In Snap25 cKOs regulated vesicular release following an action potential is prevented but spontaneous activity still occurrs whereas in Kir2.1 expressing neurons excitability is reduced including spontaneous activity.

Firstly, I will characterise the extra-cortical Ntsr1-Cre expression at P7 to P21 in the brain.

Secondly, I will study developmental targeting in specific regions of LV and LVI Snap25 cKO projections by analysing tdTomato positive fibres. LV fibres will be analysed in the thalamus, corpus callosum and S1 barrel field. LVI fibres will be analysed in the S1 barrel field cortex as well as in the thalamus (since LVI tdTomato expression in the corpus callosum is very weak). These regions have been chosen since the thalamus as well as the barrel field is of major interest in our laboratory. Additional reasons for studying these areas are that long range projections like corticothalamic as well as corticocortical will later be used for myelin examination and that these regions have been reported to be strongly influenced by neuronal activity.

Furthermore, I will study maintenance of LV and LVI Snap25 cKO projections by analysing tdTomato positive fibres. LV fibres will be analysed by examining the dorsal corticospinal tract at P21 to P44 in longitudinal sections and at P80 in cross sections for measuring tdTomato fluorescence intensity. TdTomato positive fibres from LV project through the dorsal corticospinal tract. It is of interest to study projections in the spinal cord since these are the longest projections studied in this thesis and this allows comparison of their maintenance to shorter LV and LVI fibres

with projection targets in the brain. Additionally, the dorsal corticospinal tract with fibres lacking Snap25 will be later analysed for myelin thickness. Therefore, a good understanding of the timing of degeneration is necessary to choose the right time point for this examination.

LVI fibres will be analysed in the brain of 2 to 9 months old animals. At 9 months, cell numbers will be analysed in primary motor cortex and tdTomato fluorescence intensity measured in the thalamus.

Additionally, I will compare the targeting of projection neurons electroporated at E13.5 by Kir2.1 or MutKir2.1 (as control) at P14 in the brain as well as in the spinal cord.

This chapter, including the analysis of fibres and cells from manipulated cortical neurons, will form the basis for the following two results chapters where myelination, the myelinating cell lineage as well as myelination around degenerating fibres will be studied.

3.2 Results

3.2.1 Normal thalamic targeting, but impaired maintenance of LV Snap25 cKO projections

Knock down of Snap25 with siRNA has been previously reported to influence axonal outgrowth (Osen-Sand, et al. 1993). In order to investigate whether this is also the case in LV Snap25 cKO mice, I examined axonal targeting of thalamic nuclei in LV Snap25 cKO mice in the first three postnatal weeks as a basis for investigating their myelination in the following chapters. Additionally, spinal cord axons of Snap25 cKO mice were monitored until 2.5 months after development to investigate their maintenance.

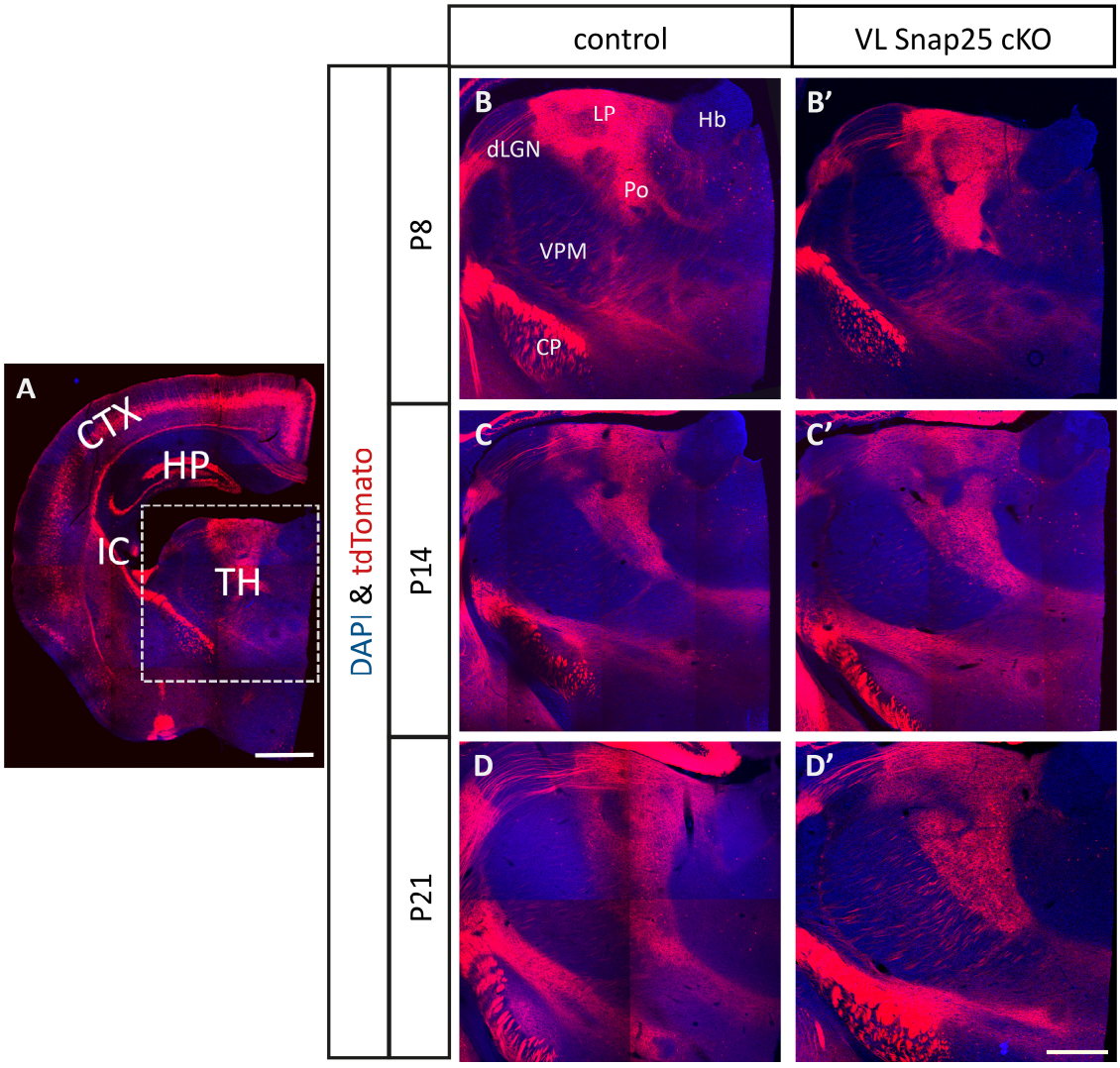


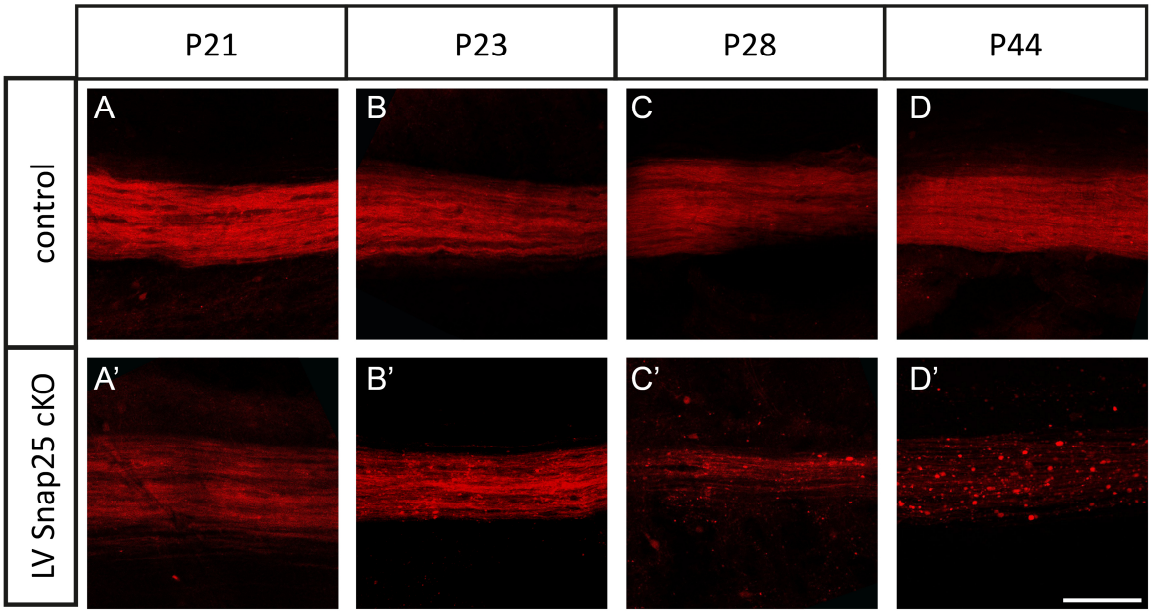
Figure 9: Normal thalamic targeting of cortical LV Snap25 cKO fibres

Rbp4-Cre expressing cell bodies are located in LV of the cortex (CTX). These large neurons have tufted dendrites that extend into the marginal zone, and their axons project through the striatum and internal capsule (IC) to the thalamus (TH) and some descend further through the cerebral peduncle (CP) towards the basal pons and spinal cord. Developing corticothalamic fibres target thalamic nuclei normally at all postnatal ages assessed. A) Representative coronal section of a P21 brain. LV cell population extends their dendrites into superficial layers until LI of the cortex (CTX). B-D') LV cells project to numerous thalamic nuclei, such as posterior thalamic nucleus (Po), lateral posterior nucleus (LP) but not thalamic reticular nucleus (TRN). LV fibres run through the dorsal lateral geniculate nucleus (dLGN) and ventral posterior nucleus (VPM) without innervating them. The cerebral peduncle is strongly labelled by LV corticospinal projections.
Further abbreviations: HP: Hippocampus, Hb: Habenula
Scale bar A overview: 1000µm, magnifications B-D': 500µm, n=3/genotype and age

LV axons from Rbp4-cre neurons target higher order nuclei in the thalamus as observed by utilising a confocal microscope. Figure 9 shows the thalamic targeting of LV Snap25 cKO axons compared to controls at P8, P14 and P21 as well as a representative image of a P21 control brain. Rbp4-Cre-expressing cells are located in LV of the cortex and project through the striatum and internal capsule to the thalamus. Rbp4-Cre is also expressed in the dentate gyrus of the hippocampus. At all three age points, the same nuclei are innervated and spared by tdTomato expressing axons in the control as well as the LV Snap25 cKO. LV axons project through the dorsal lateral geniculate nucleus (dLGN) and ventral posteromedial nucleus (VPM) in large fasculated bundles without substantial innervation. They defasciculate and innervate the posterior thalamic nucleus (Po) and the lateral posterior nucleus (LP).

Furthermore, LV axons are the only axons that project out of the brain and into the spinal cord. To get there, they need to project through the cerebral peduncle (CP). In the spinal cord, tdTomato expressing axons are bundled in the dorsal corticospinal tract. This can be seen in LV Snap25 cKO mice as well as in the control group where cross and longitudinal sections where analysed for

degeneration at different ages (P21 to P80) by fluorescence microscopy. Longitudinal sections, in contrast to cross sections, were not obtained by vibratome cutting but by squeezing the dorsal corticospinal tract between two glass slides to retain all fluorescent fibres. tdTomato mean fluorescence intensity was measured in cross sections of the dorsal corticospinal tract at P80 to quantify disappearing tdTomato signal using ImageJ (Figure 10).



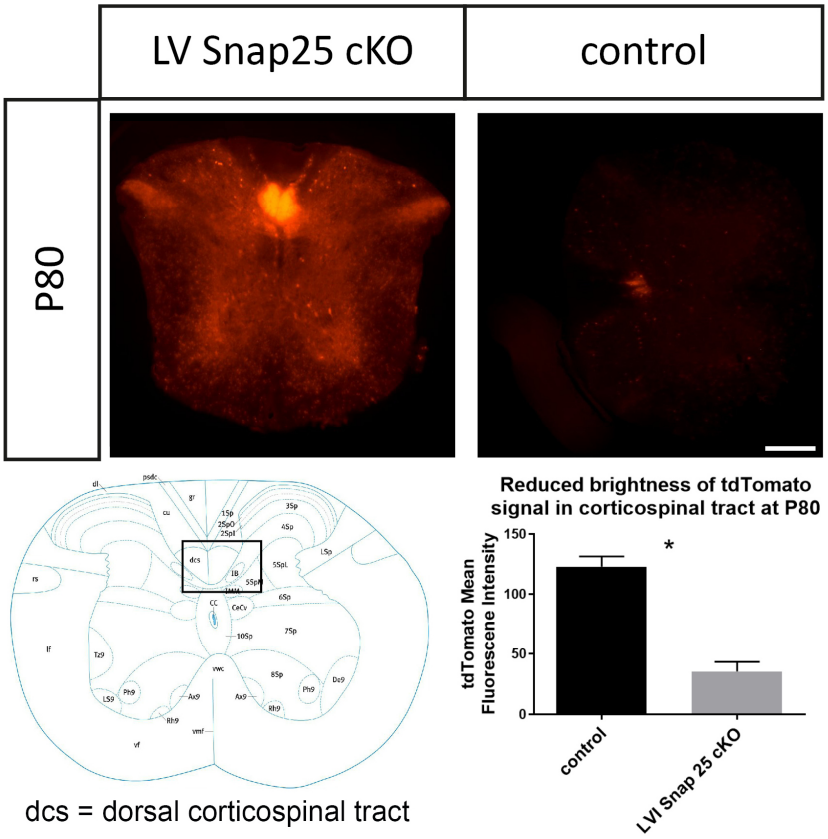


Figure 10: Premature axonal disintegration in the dorsal corticospinal tract

A-D') Disintegration of LV Snap25 cKO fibres in spinal cord. A-A') At P21 control and LV Snap25 cKO fibres in the dorsal corticospinal tract are indistinguishable. B-B') By P23 tdTomato positive axons appear discontinuously labelled with large punctae forming in LV Snap25 cKO but not in controls. C-C') By P28 less continuous fibres are apparent in LV Snap25 cKOs compared to P23 but tdTomato punctae are more prominent. D-D') By P44 hardly any continuous fibres are visible. E-E)' Loss of tdTomato signal in the dorsal corticospinal tract at P80. n=2-4/genotype and age

Cross sections of LV Snap25 and control spinal cords shown. tdTomato positive axons extending in the dorsal corticospinal tract. F) Schematic drawing of spinal cord cross section with corticospinal tract highlighted with a square (from Allen Brain Atlas). G) Mean fluorescence intensity of tdTomato signal in the dorsal column of the spinal cord is significantly reduced by P80 in LV Snap25 cKOs (35.4 ± 8.0) compared to control (122.9 ± 8.5) (p= 0.050, 3 animals/genotype, 2-3 sections/animal)

One-tailed Mann-Whitney test, values given are mean ± SEM. Scale bar longitudinal view A-D': 100 µm, Cross section: 200 µm

When examining tdTomato expressing fibres in longitudinal sections of the dorsal corticospinal tract, a discontinuous labelling can be observed at P23 (see Figure 10). At P21, this difference was not yet apparent. Over time, the discontinuous

tdTomato labelling seems to emerge into bigger swellings and punctae until continuous fibres are almost completely vanished at P44 (Figure 10).

When measuring mean fluorescence intensity of the dorsal corticospinal tract at P80 in cross sections, a strong and significant signal reduction of 71.2% was observed in LV Snap25 cKOs compared to controls (p= 0.050) (see Figure 10 E-G). This timepoint was chosen because there was enough signal left to detect the dorsal corticospinal tract where measurement was conducted.

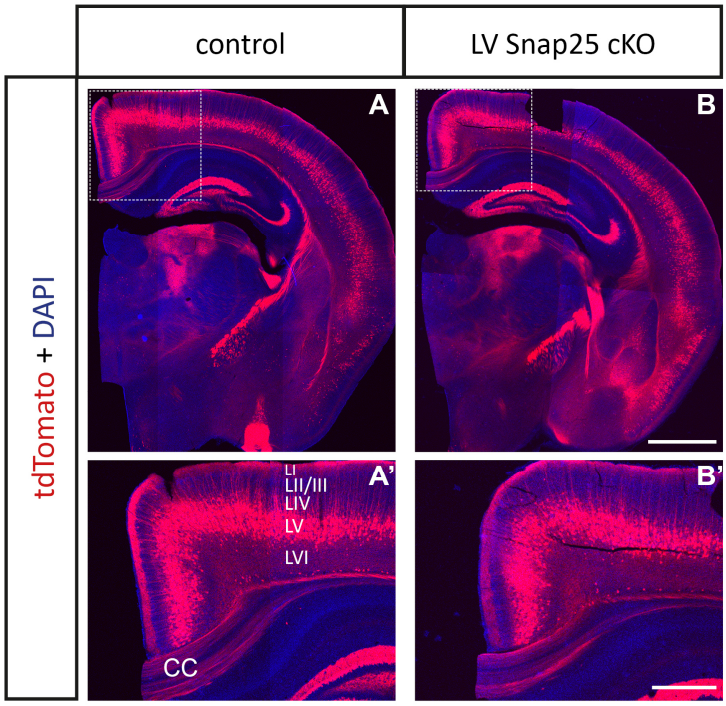


Figure 11: LV Type I and Type II neurons express Rbp4-Cre in controls and LV Snap25 cKOs at P8

Fibres expressing tdTomato, initiated by Rbp4-Cre expression, are visible in the corpus callosum (CC) of controls and LV Snap25 cKO in confocal images. LV neurons projecting through the corpus callosum to the contralateral hemisphere are cortico-cortical Type II projection neurons. Tufted LV neurons after P7 are Type I neurons and can also be found in controls as well as LV Snap25 cKOs.
Scale Bar Overview: 1000 µm, magnification: 500 µm, n=3/genotype

The tdTomato positive fibres in the corpus callosum indicate that Rbp4-Cre expressing cells are cortico-cortical projection neurons (see Figure 11). These neurons are Type II LV neurons that are located in LVa and are distinct from Type

I LVb neurons by their morphology as well as their electrophysiology. Tufted dendrites of Type I LV cells are kept whereas Type II neurons have remodelled their dendrites by P7 (Koester and O'Leary, 1992; Molnár and Cheung, 2006; Hattox and Nelson, 2007). Figure 11 shows callosal projections as well as fibres ending in LI. Therefore, the results indicate that Rbp4 expression occurs by LV Type I as well as Type II neurons and thus is not solely restricted to LVa or LVb in controls as well as Snap25 cKOs.

Next, it will be tested if Rpb4-Cre expression is similar between conditions when to Rpb4-Cre and stop-flox tdTomato additionally stop-flox Snap25 is breed into the mouse line.

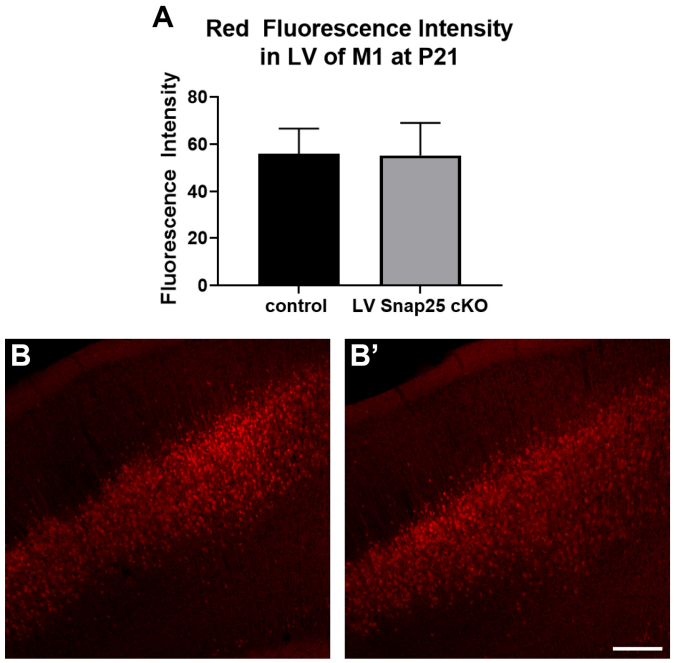


Figure 12: Similar expression of tdTomato in LV of M1 at P21

A) Fluorescence intensity analysis of LV projection neurons expressing tdTomato in LV of M1 at P21 showing that Stop-flox excision from tdTomato by Rbp4-Cre is similarly between controls (55.9 ± 10.8) and LV Snap25 cKOs (55.3 ± 23.8, p >0.9999). B-B') Fluorescent images showing tdTomato positive LV in M1 of the cortex at P21 of control (B) and LV Snap25 cKO (B')

Scale Bar: 200 µm, n=3/genotype, Mann-Whitney test, 2-3 sections/animal, values given are mean

Figure 12 shows tdTomato in LV of M1 in controls and LV Snap25 cKOs at P21 (B-B'). Analysis of tdTomato indicates that there is no difference in tdTomato and therefore also in Rbp4-Cre expression when stop-flox Snap25 is additionally breed into the control mouseline (Figure 12, A).

3.2.1.1 Visibility of barrel field pattern in LV Snap25 cKOs

It has been reported that the correct formation of the barrel field in the somatosensory cortex in LIV is dependent on transmission of periphery related activity. Even though barrels and septa of the whiskers are formed in LIV, the barrel formation can also be seen indirectly in the surrounding layers. Hence, I investigated in tiled confocal images if the formation of barrels is visible in LV Snap25 cKO like in controls by the tdTomato signal in S1 (see Figure 13) or if the absence of regulated vesicle release in parts of LV changes the visible pattern.

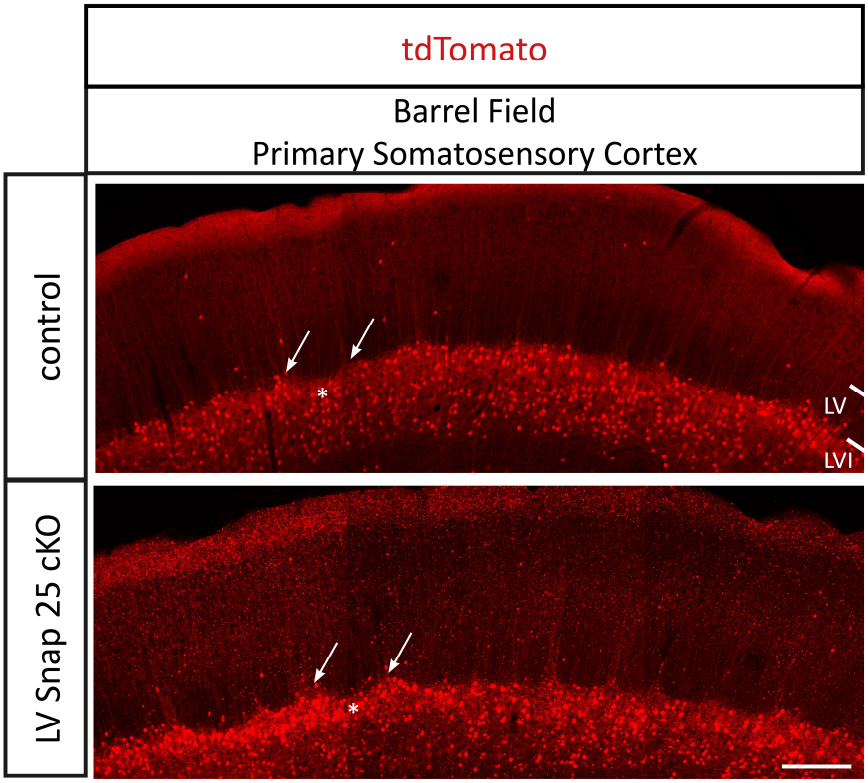


Figure 13: Visibility of barrel field pattern in LV Snap25 cKOs is similar to controls in primary somatosensory cortex at 2 months

The formation of tdTomato positive cell bodies located in LV and their neurite bundles enable the visualisation of the bottom of barrels (white asterisk) and septa (white arrows) in between each barrel which are located in LVI of the cortex despite the clearly visible decline of tdTomato signal at 2 months.
Scale bar: 200 µm, n=3/genotype

By 2 months, the murine barrel field is well established. In LV Snap25 cKOs tdTomato signal shows signs of degeneration at this time point. Despite this, the septa between barrels in the superficial LIV can be seen by dense neurite bundles similar to controls (in Figure 13, arrows). The lower edge of the septa between barrels is formed by the upper boundary of tdTomato cells in LV that form an undulating line corresponding to the barrels (asterisk). The barrels were present in both control and LV Snap25 cKO brains.

To conclude, the characterisation of LV Snap25 cKO animals in comparison to controls, it is to say that thalamic targeting was not altered by abolished regulated vesicular release by the lack of Snap25. By additionally introducing Snap25 to the Rbp4-Cre tdTomato control mouse line, both LV cell types, I and II, are still targeted. The expression of tdTomato in LV cells allowed to identify the barrel field in LIV even when vesicular released was supressed in LV Snap25 cKOs.
Fibre outgrowth was taking place in similar areas between cKOs as well as controls, like the CP and spinal cord but impaired maintenance was only observed in Snap25 cKOs.

3.2.2 Characterisation of Layer VI Snap25 cKO

After the characterisation of LV Snap25 cKOs and controls has been conducted, LVI Snap25 cKOs and their controls should also be conducted, since similar experiments on myelin onset and oligodendroglial cells during development will be conducted in the following chapter.

3.2.2.1 Extra-cortical Ntsr1 expression in LVI Snap25 cKOs

Within the brain, Ntsr1-Cre is mainly expressed in LVI cells from E16 onwards and maintained throughout life (Grant, Hoerder-Suabedissen, and Molnar 2016; Grant 2014). My investigation focuses on the projections of these neurons. However, Ntsr1-Cre is not only expressed in LVI of the cortex. Additionally, there is some extra-cortical expression as well (see Figure 14). Therefore, I examined extra-cortical Ntsr1-Cre expression by epi-fluorescence microscopy in LVI Snap25 cKO brains as well as controls by looking at cellular tdTomato signals to determine if the expression is consistent between genotypes at P7 and does not interfere with my following myelin examination.

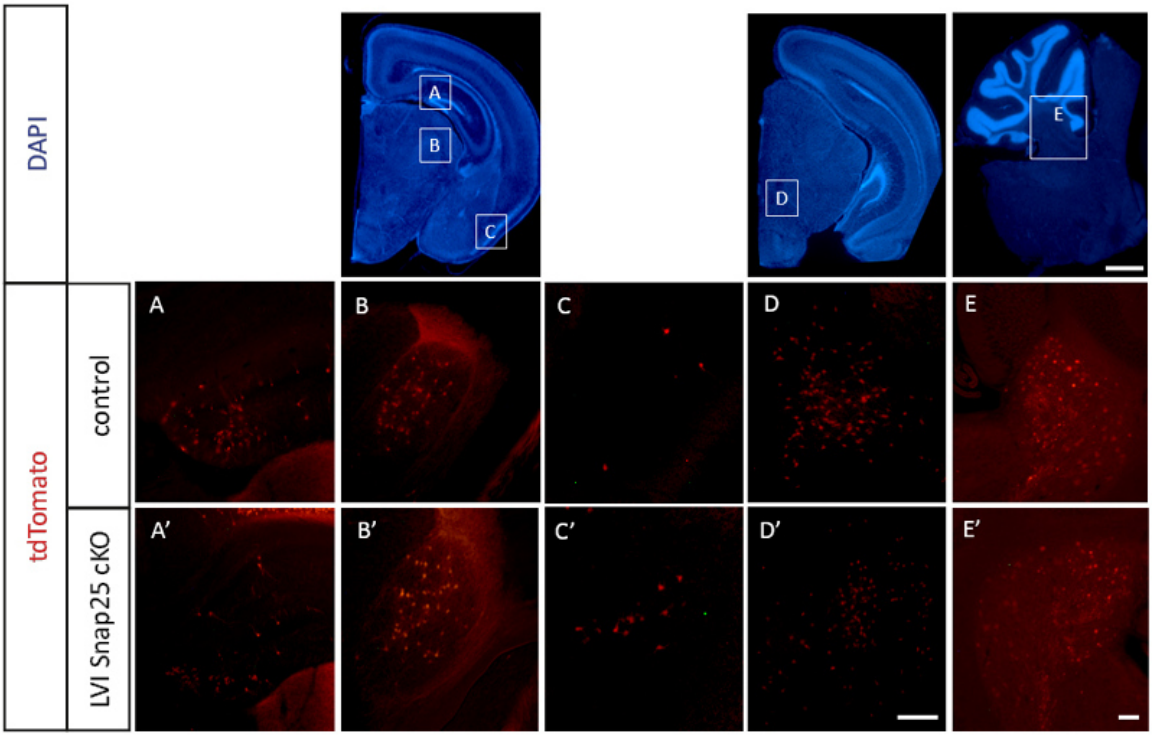


Figure 14: Extra-cortical labelling of Ntsr1-Cre is consistent across genotypes at P7
White boxes with letters A-E indicate magnified regions in the panels below.
Cellular labelling was consistently shown in: A-A') hippocampus where the sparse labelling was not restricted to a specific subregion or layer, B-B') ventral posterior-medial thalamic nucleus, C-C') endopiriform cortex, D-D') ventral tegmental area of the midbrain and E-E') deep cerebellar nucleus.
Scale bars DAPI overviews: 1000 µm, A-D: 200 µm, E: 500, n=3/genotype and age

In the hippocampus sparse labelling of Ntsr1-Cre was seen which was not restricted to any particular subregion or layer. Further, there were sparse cells in the ventral posterior-medial nucleus, endopiriform cortex and ventral tegmental area of the midbrain (Figure 14 A-D). The Ntsr1-Cre labelled cells in the thalamus were sparse with short projections and therefore unlikely to account for the strong tdTomato signal observed between cortex and thalamus. Even more sparsely distributed cells were observed in lateral geniculate nucleus, cerebral peduncle and substantia nigra (not shown). When examining sagittal sections of the brain, a densely labelled cluster of deep cerebellar nuclei was found (Figure 14 E).

The Ntsr1-Cre labelling was consistent between genotypes at P7. Ntsr1-Cre labelling was studied since many cells in the murine brain undergo apoptosis during early postnatal development and it was of interest, if Cre positive cells are differentially affected by the apoptosis process.

Despite the labelling of Ntsr1-Cre outside of the cortex the small number of cells affected by it makes this Cre-expressing strain a suitable tool for assessing long range projections from layer VI.

3.2.2.2 Similar body weight of LVI Snap25 cKOs and controls

In LV Snap25 cKOs it has been found that the body weight differs from controls as early as P21. This reduced weight in LV Snap25 cKOs compared to controls persists throughout adult life. So far, the cause for this is not known. There is no obvious behaviour phenotype in LV (or LVI) Snap25 cKOs that could explain the difference in weight (Monteggia et al. 2018; Hoerder-Suabedissen, Korrell et al. 2018). To see if this phenotype is also apparent in LVI Snap25 cKOs male mice were weighed at 4 months of age, the medium time point of how long animals were kept for experiments.

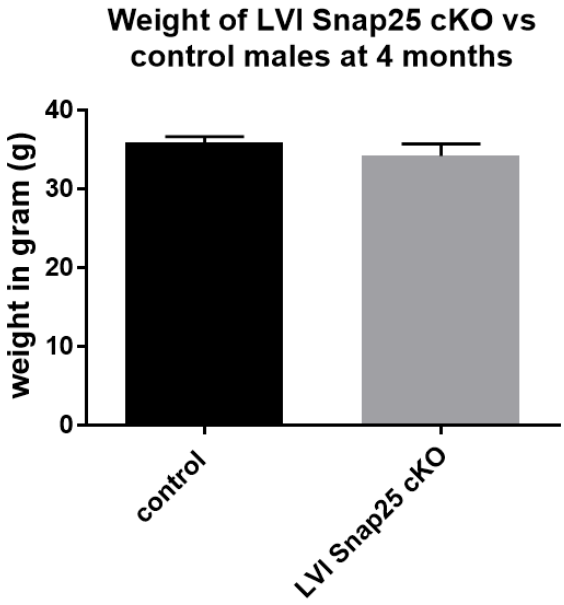


Figure 15: Similar weights of 4 months old LVI Snap25 cKO and control males
At 4 months of age, both control (n=8) and LVI Snap25 cKO males (n=7), weigh around 35g (LVI controls: 35.9 ± 0.8, LVI Snap25 cKOs: 34.2 ± 1.5) with no significant difference. Unpaired t-test p=0.33, values given are mean ± SEM.

The results show that there is no difference in weight between LVI Snap25 cKO males and control males at 4 months, in contrast to observations in LV Snap25 cKOs (Figure 15).

3.2.2.3 Regular thalamic targeting but impaired maintenance of Layer VI projections in Snap25 cKOs

As reported above, in LV Snap25 cKO mice, axonal targeting of cells lacking Snap25 in the thalamus was not influenced and axonal outgrowth took place despite previous reports by Osen-Sand (Osen-Sand et al. 1993). The experiment was repeated in LVI Snap25 cKOs to examine if axons reach and target the correct areas in the thalamus. Additionally, LVI Snap25 cKO and control projections were monitored after development until 9 months of age, and various aspects of the tdTomato signal were assessed.

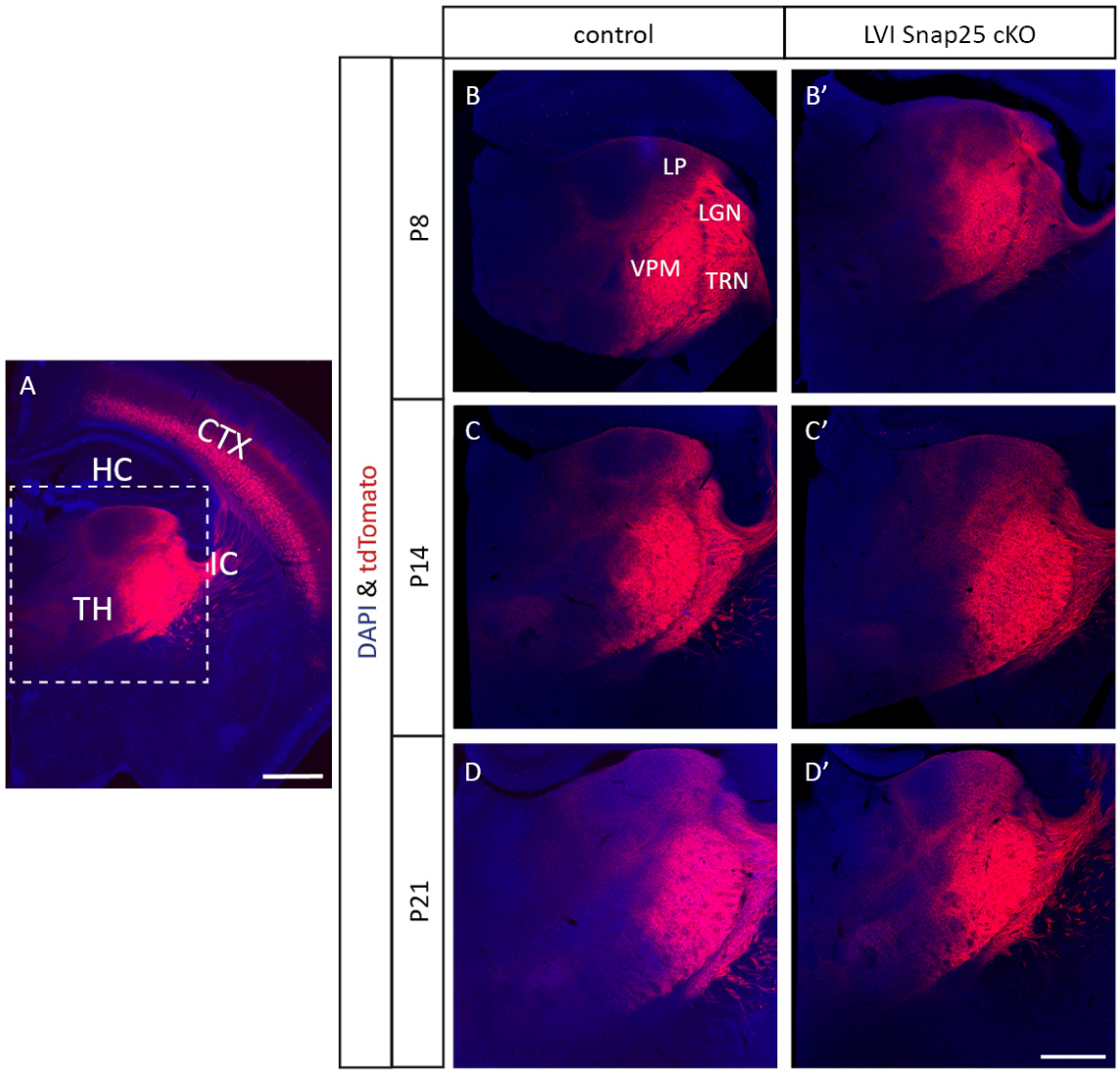


Figure 16: Normal thalamic targeting of cortical LVI Snap25 cKO fibres compared to control

Ntsr1-Cre expressing cell bodies are located in LVI of the cortex (CTX) with dense fibre labelling in LV and apical dendrites extending even further towards the marginal zone. Axons project through underlying white matter, striatum and internal capsule (IC) to the thalamus (TH). Developing corticothalamic fibres target thalamic nuclei normally during the postnatal period assessed by confocal microscopy. A) Representative section of a P8 brain. LVI cell population extends their dendrites within LVI as well as to the overlaying LV of the cortex. White box indicates magnifications shown in B-D'. B-D') LVI projects to numerous thalamic nuclei like lateral geniculate nucleus (LGN), ventral posterior nucleus (VPM), thalamic reticular nucleus (TRN) and lateral posterior nucleus (LP) but not into the cerebral peduncle.
Scale bar overview A: 1000 µm, magnifications B-D': 500 µm, n=3/genotype and age

Figure 16 shows the thalamic targeting of LVI Snap25 cKO axons compared to controls at P8, P14 and P21 as well as a representative image of a P8 control brain.

Unlike LV, LVI fibres project not only to higher order but also to first order thalamic

nuclei (Gilbert & Kelly 1975; Diamond et al. 1969; Jones & Powell 1968; Lózsádi & Guillery 1996; Hoogland et al. 1987). Ntsr1-Cre-expressing cells are located in LVI of the cortex and project through the striatum and the internal capsule to the thalamus. At all three age-points, the same nuclei are innervated or spared by tdTomato expressing axons in control as well as LVI Snap25 cKO (Figure 15). LVI fibres of controls and LVI Snap25 cKOs are visible in the thalamic reticular nucleus (TRN), ventral posteromedial nucleus (VPM), lateral geniculate nucleus (LGN) and the lateral posterior nucleus (LP). They also innervate posterior thalamic nucleus (Po, not shown). Unlike LV cells, LVI cells do not project out of the brain and therefore no tdTomato signal is visible in the cerebral peduncle and there is little tdTomato signal from Ntsr1-Cre expressing cells in the corpus callosum.

It was also of interest in the LVI mouse line, if breeding in stop-flox Snap25 additionally to Ntsr1-Cre and stop-flox tdTomato, changes the expression of Ntsr1-Cre and therefore tdTomato. In 3.2.2.1 it was already shown, that areas affected by extra-cortical labelling were not affected when stop-flox Snap25 was introduced into the control mouse line. Here it will be tested, if the number of cells, measured indirectly by tdTomato fluorescent intensity, is affected by introducing stop-flox Snap25.

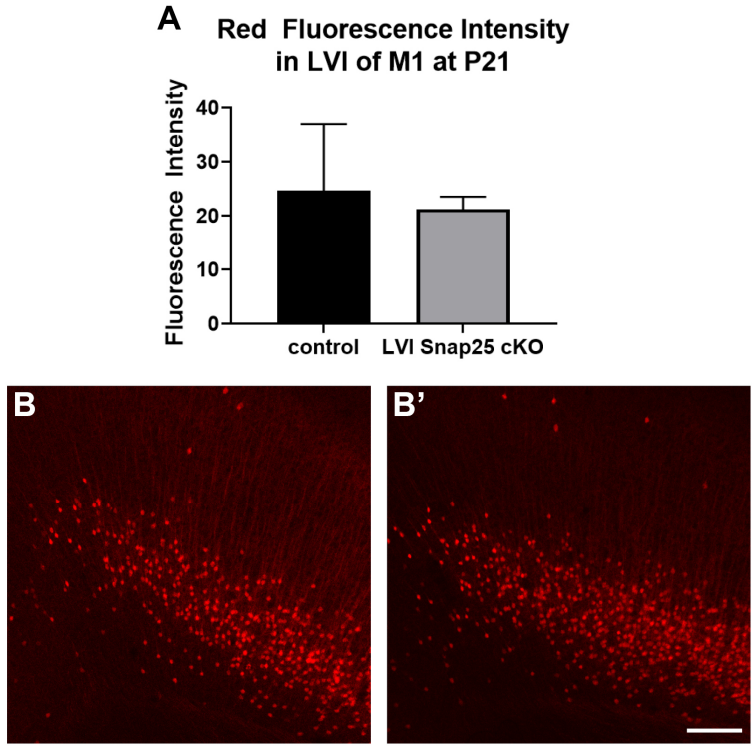


Figure 17: Similar tdTomato fluorescent intensity in LVI of M1 at P21

A) *Analysis of tdTomato in LV of M1 at P21 indicates that introducing Stop-flox Snap25 to Ntsr1-Cre and stop-flox tdTomato, does not significantly influence expression of tdTomato between controls (24.6 ± 21.4) and LV Snap25 cKOs (21.2 ± 4.0, p= 0.700). B-B') Fluorescent images showing tdTomato expressing LV projection neurons in M1 of control (B) and LVI Snap25 cKO (B')*

Scale Bar: 200 µm, Mann-Whitney test, n=3/genotype, 2-3 sections/animal, values given are mean ± SEM

Figure 17 shows tdTomato expression in LVI of controls and LVI Snap25 cKOs at P21 in M1 (B-B'). Analysing tdTomato expression by fluorescence intensity as an indirect measurement of cells expressing Ntsr1-Cre demonstrates that there is no difference between conditions when stop-flox Snap25 is introduced into the LVI control mouse line (Figure 17, A).

Similar to LV Snap25 cKO mice when monitored further into adulthood, the tdTomato signal in LVI Snap25 cKO mice shows punctae over time as shown in Figure 18. At 9 months the number of tdTomato positive cells in M1 was determined

in confocal images since in LV Snap25 cKOs a cell loss has previously been reported around this time (Hoerder-Suabedissen, Korrell et al. 2018). Additionally, mean tdTomato fluorescence intensity in the thalamus was analysed to assess changes in ageing between LVI Snap25 cKOs and controls. The thalamus was chosen for this analysis due to the fact that in LVI Snap25 cKOs and controls this structure shows an intense and relative uniform tdTomato labelling where reduced fluorescence was first evident.

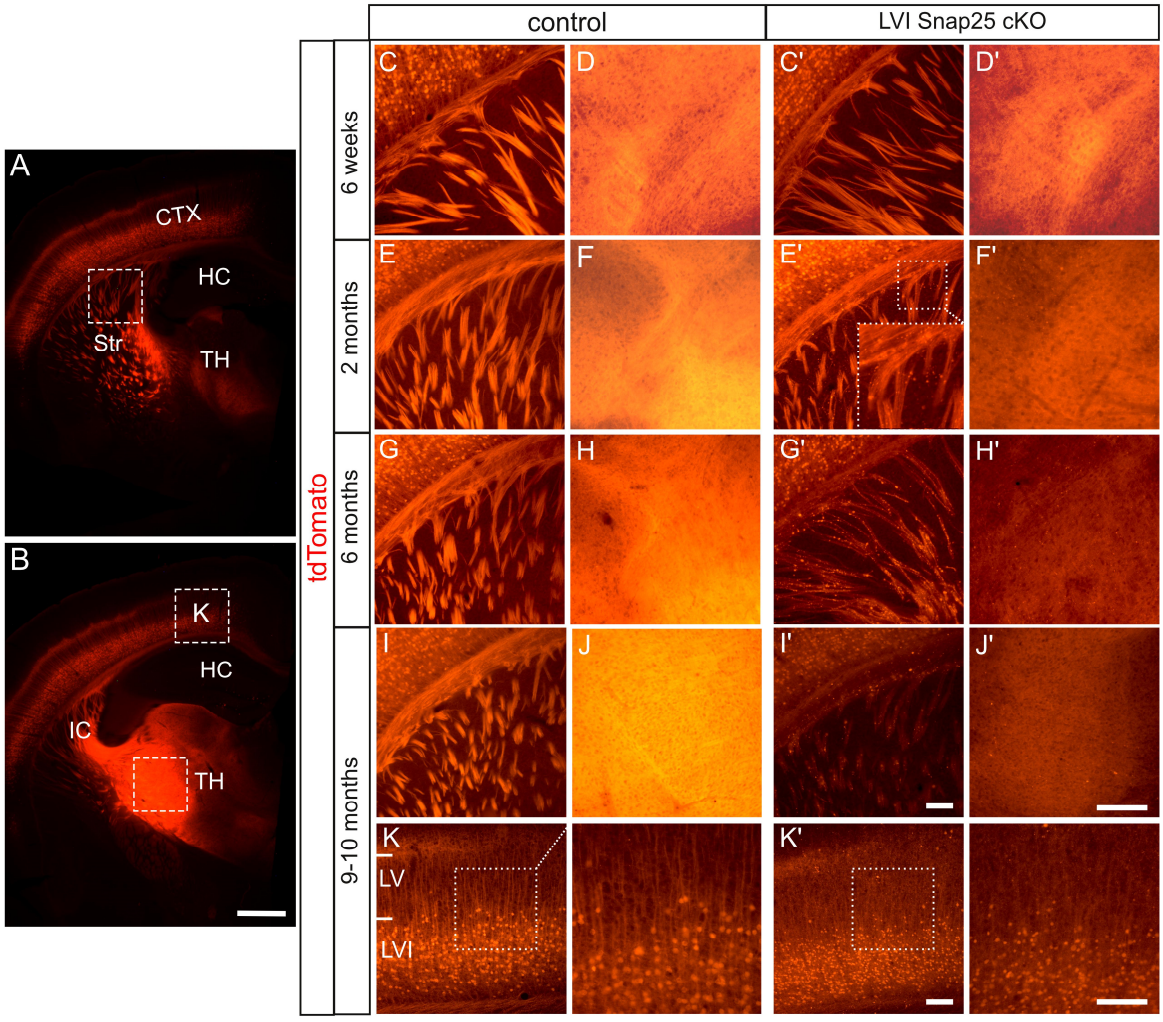


Figure 18: Premature axonal disintegration of LVI Snap25 cKO axons

A) anterior overview of 6 months old control brain. Cell bodies located in LVI of the cortex (CTX) and projecting through the underlying white matter and striatum (Str) to the thalamus (TH). B) medial overview of 6 months old control brain. Cell bodies in cortical LVI project through the internal capsule (IC) to reach the thalamus. C-C') At 6 weeks, the white matter as well as the striatum, where LVI fibres project through, appear intact in control as well

as LVI Snap25 cKO. E-E') At 2 months, punctae in the tdTomato signal become visible in the white matter as well as the striatum in LVI Snap25 cKO whereas controls continue to be continuously labelled. G-G') At 6 months, many punctae in the tdTomato signal are apparent in LVI Snap25 cKO but not in controls. I-I') At 9 months, less punctae are apparent and the overall tdTomato signal is decreased in LVI Snap25 cKO without similar observations in controls. D-D') At 6 weeks, tdTomato signal brightness in the thalamus of LVI Snap25 cKOs is comparable to controls. F-F') However, at 2 months, tdTomato signal in the thalamus starts to be reduced in LVI Snap25 cKOs compared to controls. A couple of tdTomato punctae are visible. H-H') At 6 months, brightness of tdTomato signal in the thalamus is noticeably reduced, few punctae visible. J-J') At 9 months, there is a reduced signal in thalamic brightness of tdTomato signal and rarely any tdTomato punctae are apparent anymore. K-K') Cell bodies in primary motor cortex (white box indicates magnification). Dendrites are extended into superficial LV. In LVI Snap25 cKOs tdTomato signal intensity is reduced and punctuated.
Further abbreviations: HC: Hippocampus
Scale bar overview B: 1000 µm, striatum I': 200 µm, cortex K': 200 µm, cortex magnification: 200 µm, thalamus J': 100 µm, n=3/genotype and age

Between 6 weeks and 2 months of age, tdTomato signal in LVI Snap25 cKOs starts to differ from controls. In the white matter underlying the cortex and in the striatum, through which axons project from LVI to their target destinations, tdTomato punctae become visible. Punctae are not very apparent in the thalamus at this age. However, the tdTomato signal in the thalamus appears slightly less bright in LVI Snap25 cKOs compared to controls. This difference in thalamic brightness of the tdTomato signal becomes even more apparent at 6 months when also red punctae are visible. At the same time, the tdTomato punctae and the discontinuous labellings are very prominent in the white matter and the striatum. At 9 months, it appears as there are fewer punctae compared to 6 months in the striatum. The tdTomato signal is reduced in the striatum as well as the thalamus. Analysis of the reduction in thalamic brightness of the tdTomato signal at 9 months showed that the mean fluorescence intensity has decreased significantly over half the mean value from 121 to 55 (see Figure 19 B). The abnormal tdTomato signal in LVI Snap25 cKOs can not only be observed in subcortical areas but also in the cortex

(see Figure 18 K-K'). Neurites from cell bodies located in LVI expressing tdTomato appear discontinuously labelled with punctae formation in LVI Snap25 cKOs.

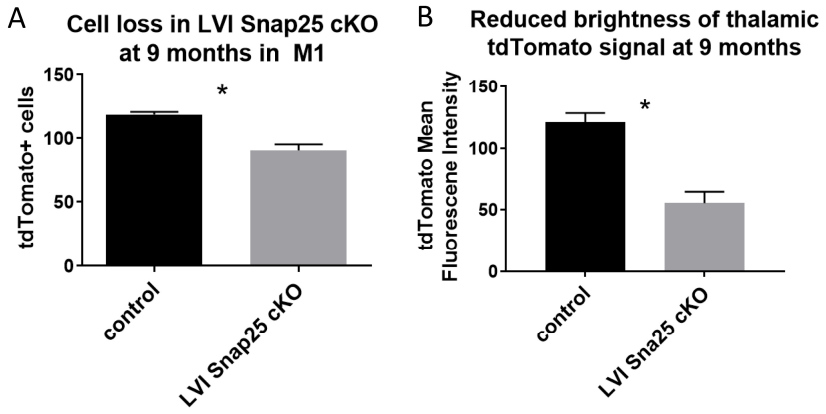


Figure 19: tdTomato signal and cell loss in the brain of LVI Snap25 cKOs
A) Cell loss in LVI Snap25 cKOs at 9 months in primary motor cortex. At 9 months, the average number of tdTomato positive cell bodies located in LVI of the cortex is significantly reduced from 118 cells ± 3.0 in controls to 91 cells ± 4.7 in LVI Sna25 cKOs (p= 0.050) (n=3/genotype, 3 sections/animal). B) Reduced thalamic brightness of tdTomato signal in LVI Snap25 cKOs at 9 months. tdTomato mean fluorescence intensity is significantly reduced in LVI Snap25 cKOs (55.3 ± 9.1, n=3, 2 sections each) compared to controls (121 ± 7.5, n=4, 2 sections each) at 9 months (p= 0.029).
One-tailed Mann-Whitney test, values given are mean ± SEM

At 9 months of age, quantification of tdTomato expressing cell bodies located in LVI of the primary motor cortex in LVI Snap25 cKOs revealed a significant cell loss compared to controls (see Figure 19 A). tdTomato positive cell bodies were reduced by nearly one quarter in LVI Snap25 cKOs. M1 was chosen for quantification since myelin analysis following in the next chapter will also be conducted in an area where cell bodies are located (for which M1 was chosen to compare results with LV mouse line that projects from M1 to the spinal cord, also an area of major interest in this thesis).

In LV Snap25 cKOs cell loss was quantified at 4 and 8 months. Since no cell loss was found at the earlier timepoint (at 4 months), I only assessed cell loss at a late

stage in LVI Snap25 cKOs and LVI controls since the degeneration process was found to be slower in LVI Snap25 cKOs compared to LV Snap25 cKOs.

3.2.2.4 Visibility of barrel field pattern in LVI Snap25 cKOs

As a last characterisation in the LVI mouse line, the visibility of the barrel field will be examined like previously done in LV control mice and LV Snap25 cKOs. Unlike LV, LVI is not adjacent to LIV where the whisker barrels are located in the primary somatosensory cortex. However, there is dense LVI fibre labelling in LV that ends at the upper border of LV and some of the apical dendrites terminate according to the barrel pattern, thus the barrels are indirectly visible. Hence, I investigated if the formation of barrels is visible in the LVI Snap25 cKO like in controls by the tdTomato signal in S1 (see Figure 20).

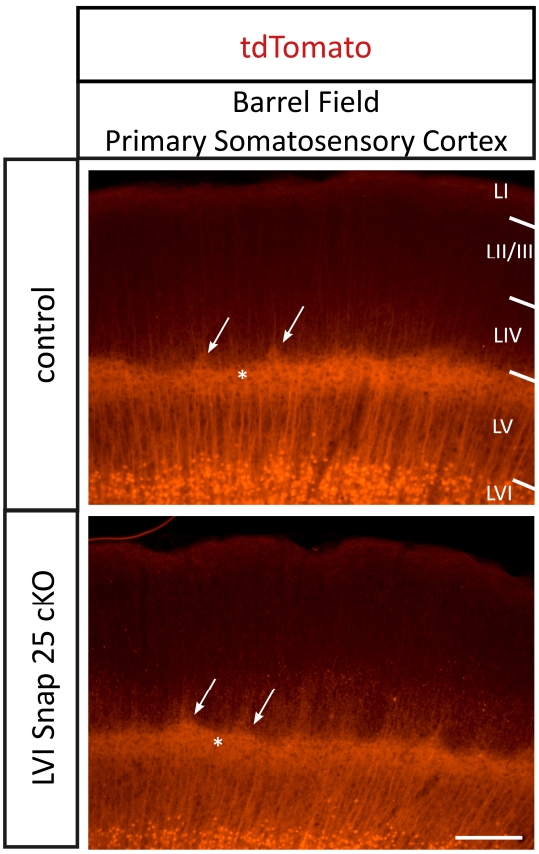


Figure 20: Visibility of barrel field pattern in LVI Snap25 cKOs similar to controls in primary somatosensory cortex at 2 months

The formation of tdTomato positive neurites from cell bodies located in LVI enables the visualisation of the bottom of barrels (marked with asterisk) and septa (marked with arrows) in between each barrel which are located in LIV of the cortex.
Scale bar: 200 µm, n=3/genotype

The septa between barrels in LIV can be seen by denser neurite bundles that extend through LV (in Figure 20 marked with arrows) into LIV in both genotypes. Additionally, the lower boundaries of the barrels are recognisable between the septa bundles (in Figure 20 marked with an asterisk) and between the septa there is a less stained hollow. The hollow becomes visible by LVI tdTomato positive fibres ending at the upper edge of LV in controls as well as LVI Snap25 cKO. Additionally, the upper edge of the cortex is visible by tdTomato fibres ending in LI. Unlike LV, there are no signs of degeneration apparent in the tdTomato signal of LVI Snap25 cKO mice at 2 months.

In summary, characterisation of LVI Snap25 cKOs versus controls showed that cKOs have a similar pattern of extra-cortical labelling, a similar body weight as well as regular thalamic targeting compared to controls. The visibility of the barrel field by neurits from tdTomato positive LVI cells was also not influenced by the lack of Snap25 and its outcomes. However, similar to LV Snap25 cKOs, it was observed that fibre maintenance was impaired when studied by fluorescence intensity and cell counts.

3.2.3 Targeting of projection neurons electroporated with Kir2.1

Manipulating electrical activity by Kir2.1 has been reported to influence axonal targeting (see 1.8.2). Kir2.1 is an inwardly rectifying (ir) potassium (K) channel that allows more potassium influx into the cell than in the outwards direction. Overexpression of inward-rectifying Kir2.1 channel decreases neuronal excitability

by lowering the resting membrane potential as well as spontaneous activity (Okada and Matsuda 2008; Hartman et al. 2006). Introducing Kir2.1 plasmid DNA by *in utero* electroporation has been used in this thesis to influence neuronal activity to study myelination around Kir2.1 expressing fibres in the following chapters. Therefore, vectors and their preparation will be introduced in the following paragraphs, as well as neuronal targeting after Kir2.1 *in utero* electroporation will be studied as a base for following myelin analysis.

3.2.3.1 Vector preparation

First experimental vectors were kindly provided by Professor Nobuhiko Yamamoto, Osaka University, Japan (pCAG-Kir2.1-IRES-Cre and stop-flox dsRed) and Fernando Garcia-Moreno, Oxford UK (pCAG-Cre). Experimental condition was as following:

Control:	pCAG-Cre	+	pCAG-stop-flox dsRed
Experiment:	pCAG-Kir2.1-IRES-Cre	+	pCAG-stop-flox dsRed

Before analysis, all brain sections were immunohistochemically stained with anti-dsRed to reinforce intrinsic dsRed signal. First experiments showed that dsRed expression in control experiments were considerably lower than in experimental condition (Figure 21). A dsRed signal was only observable in cell bodies of electroporated cells but not in their axons which I wanted to study afterwards. The expression vectors pCAG-Cre and pCAG-Kir2.1-IRES-Cre were not of the same backbone. Therefore, I decided to excise Kir2.1 via restriction enzymes to gain a pCAG-Cre control with the same backbone as the experimental vector pCAG-Kir2.1-IRES-Cre (for all vector maps see Figure 24 to Figure 27).

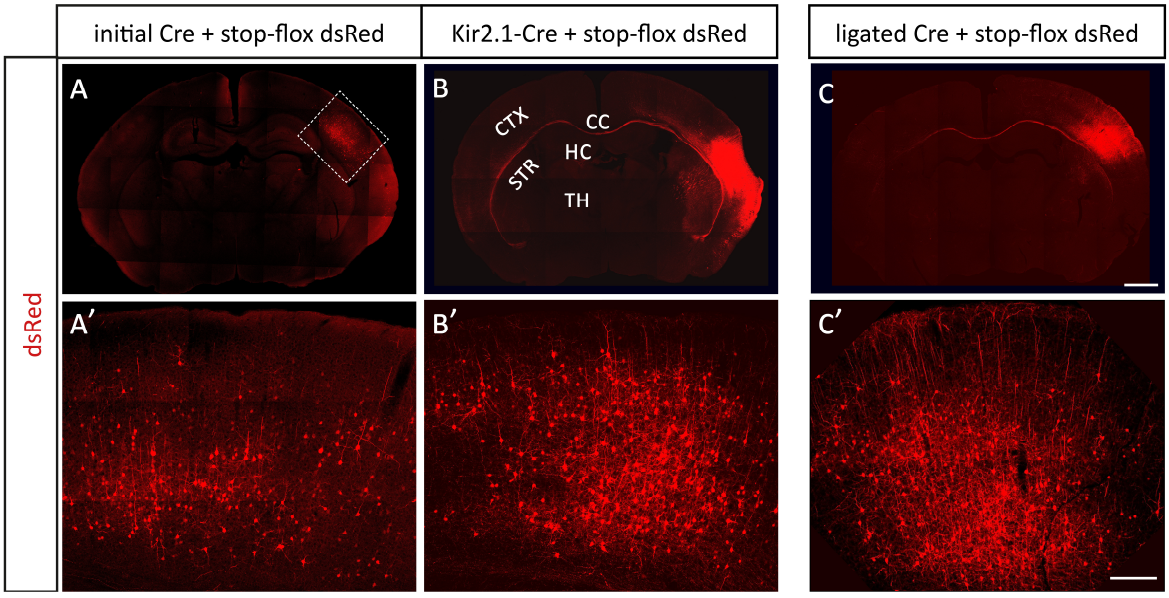


Figure 21: Initial dsRed signal in control brains is markedly reduced compared to dsRed signal in experimental Kir2.1 brains at P14

In utero electroporation at E13.5 with initial control plasmid Cre + stop-flox dsRed did not result in a comparable intensity of tdTomato signal as experimental plasmid Kir2.1-Cre + stop-flox dsRed (3-4 animals/genotype). A-A') In control brains, less cells seem to be affected and there is no detectable fibre signal projecting out of the cortex (white box indicates magnified region shown in A', B' and C'). B-B') In experimental brains, a strong fibre signal can be detected in the striatum, the corpus callosum as well as the contralateral hemisphere of the electroporation side. C-C') *In utero* electroporation with ligated Cre + stop-flox dsRed plasmid to ensure the same vector backbone resulted in a comparable intensity of tdTomato signal as experimental plasmid Kir2.1-Cre + stop-flox dsRed (n=5). Abbreviations used: CTX: Cortex, TH: Thalamus, STR: Striatum, HC: Hippocampus, CC: Corpus Callosum. Scale bar overview: 1000 µm, magnification: 200 µm

Using the described set of plasmids, where control and experimental vector had the same backbone, still led to an unsatisfying expression of dsRed in axons. The red signal appeared discontinuous in controls as well as experimental brains (Figure 22).

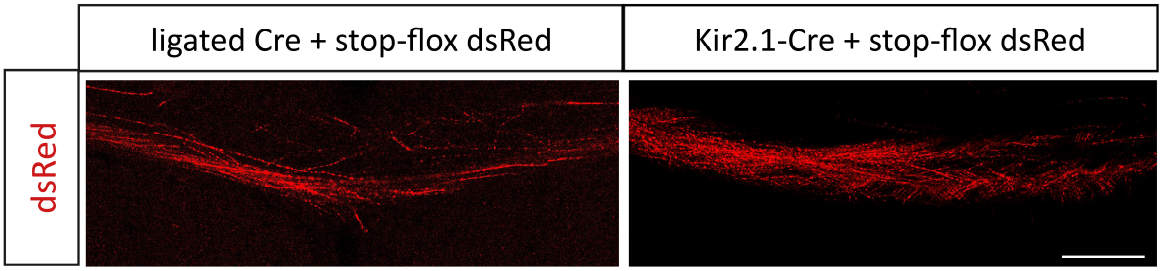


Figure 22: Discontinuous dsRed signal in the P12 corpus collosum of E13.5 electroporated brains

Examination of the corpus callosum revealed a discontinuous dsRed signal in controls (ligated Cre + stop-flox dsRed) as well as experimental animals (Kir2.1-Cre + stop-flox dsRed) (3-4/genotype).
Scale bar: 100 µm

Further experiments were therefore conducted with plasmids obtained from Addgene (MutKir2.1-T2A-Tom and Kir2.1-T2A-Tomato) originally deposited by Massimo Scanziani's laboratory. After IUE with MutKir2.1-T2A-Tom and Kir2.1-T2A-Tomato the tdTomato signal was strong enough to be detected by examining the entire brain with a fluorescence dissection microscope prior to sectioning (Figure 23).

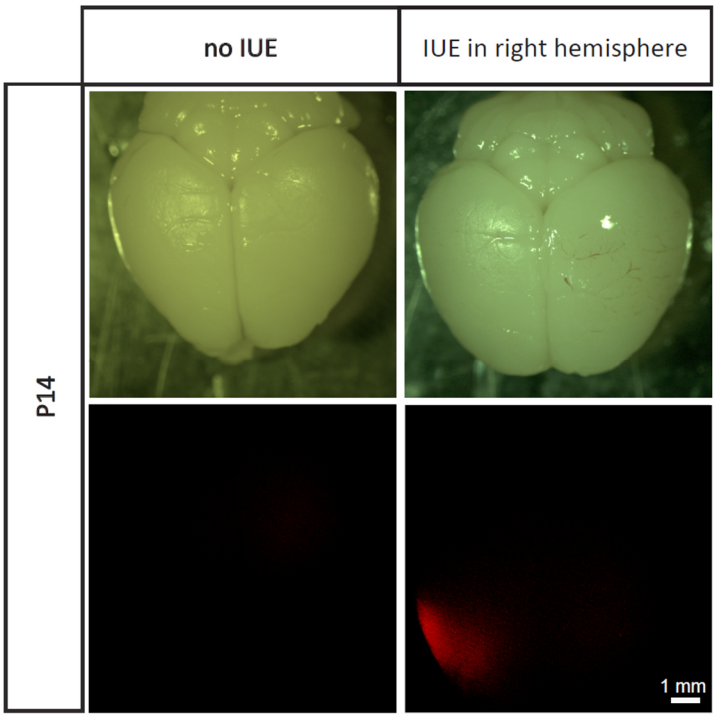


Figure 23: Fluorescent electroporation side visible after dissection

At P14, brains electroporated with MutKir2.1-T2A-Tom or Kir2.1-T2A-Tom at E13.5, have been dissected and electroporation side was examined under fluorescence dissection microscope prior to vibratome sectioning. This process could locate electroporation side in electroporated hemispheres.

pCAG-Kir2.1-IRES-Cre

The plasmid (Figure 24) was kindly provided by the laboratory of Professor Nobuhiko Yamamoto, University of Osaka, Japan (Yamada et al. 2010; Matsumoto et al. 2016). DNA was extracted from filter paper by incubating with 50 µl H_2O for 1 hour.

For the transformation of plasmid DNA into competent cells (*Escherichia coli*, DH5α, Invitrogen), 10 µl purified plasmid DNA was incubated for 30 minutes on ice together with 50 µl bacteria. The bacteria then underwent a 30 seconds heat shock at 42°C, followed by 2 minutes of incubation on ice. Subsequently, 900 µl LB-Medium (lysogeny broth) was added and bacterial growth enabled by placing mixture for 30 minutes at 37°C on a shaker. Next, the transformed bacteria were spread on ampicillin (100 µg/ml, Thermo Fisher Scientific) containing agar-plates and incubated overnight at 37°C.

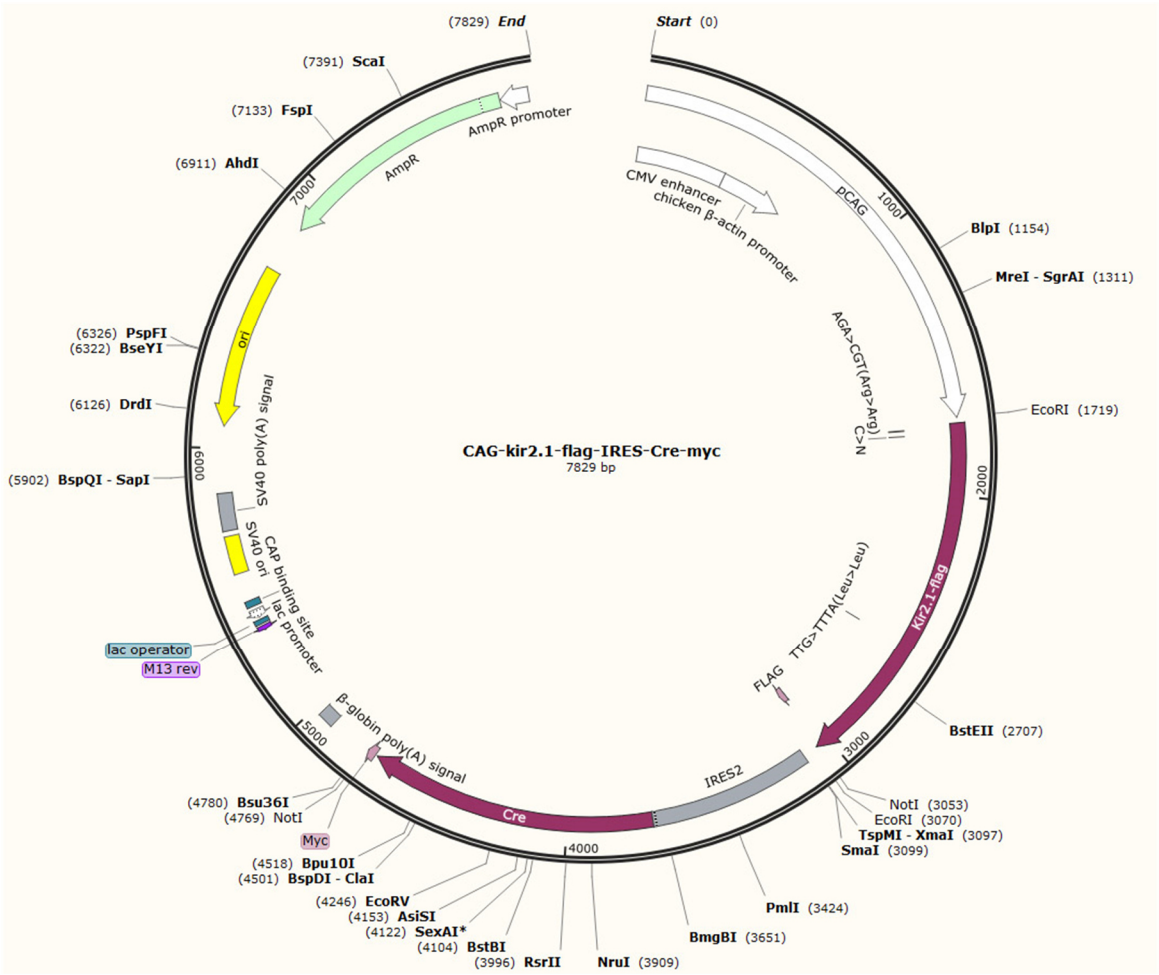


Figure 24: Plasmid map of pCAG-Kir2.1-IRES-Cre
(Figure provided by Professor Nobuhiko Yamamoto, University of Osaka Japan)

Stop-floxed DsRed

pCAG-DsRed (Figure 25) was a gift from Professor Connie Cepko (Harvard University, Cambridge, USA, Addgene plasmid #13769).

DNA was extracted from filter paper by incubating with 50 µl H_2O for 1h. Following steps were similar to pCAG-Kir2.1-IRES-Cre plasmid above.

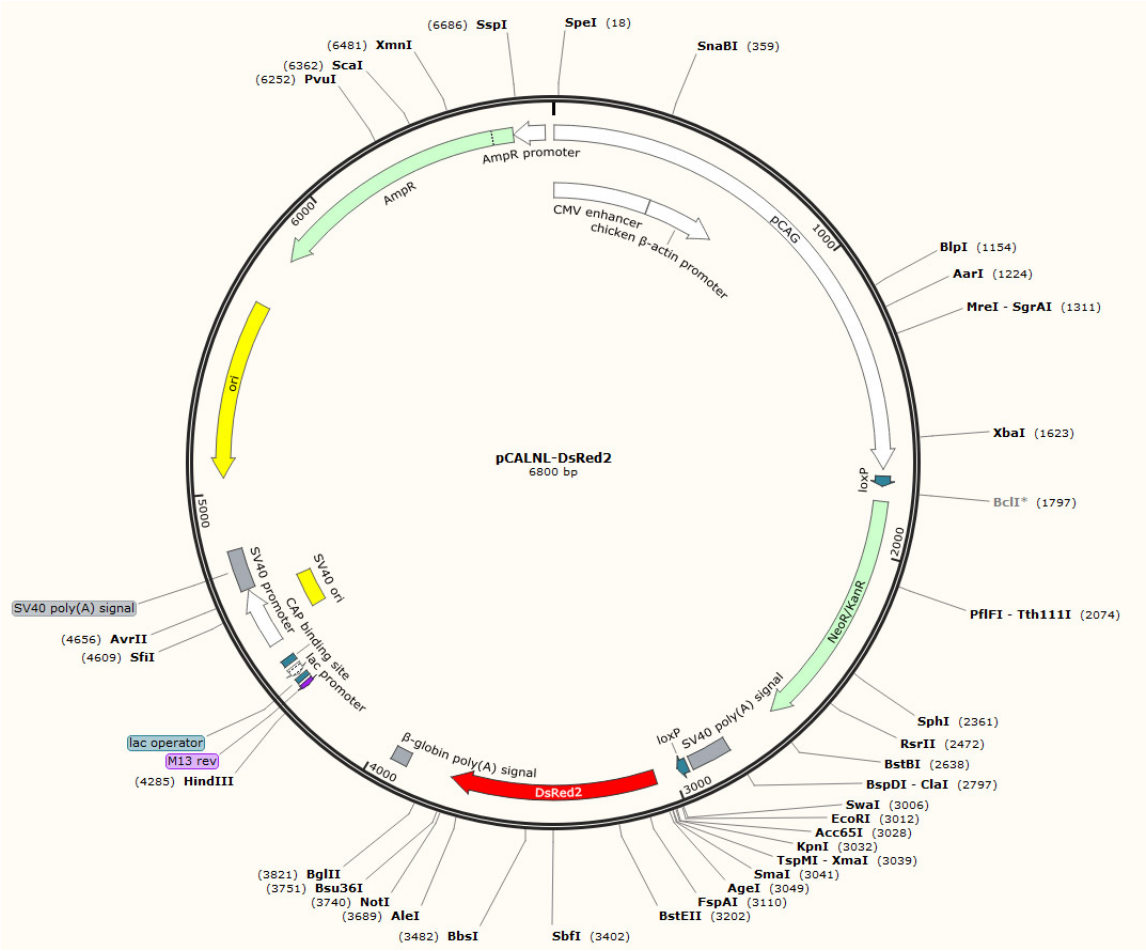


Figure 25: Plasmid map of stop-flox dsRed
(Figure provided by Professor Nobuhiko Yamamoto, University of Osaka, Japan)

pCAG-Kir2.1-T2A-tdTomato & pCAG-MutKir2.1-T2A-tdTomato

Bacteria containing plasmids were gifts from Professor Massimo Scanziani (then University of San Diego, now UCSF; Addgene plasmid # 60598 & #60644) and received as stab cultures (Figure 26, Figure 27). Bacteria were plated on agar-plates containing ampicillin and incubated overnight at 37°C. A non-conducting MutKir2.1-T2A-tdTomato plasmid was used as a control that included three point mutations: G144A, Y145A and G146A (Tinker, Jan, and Jan 1996; Xue, Atallah, and Scanziani 2014).

The T2A-Sequence is a peptide that induces co-translational cleavage (Trichas, Begbie, and Srinivas 2008).

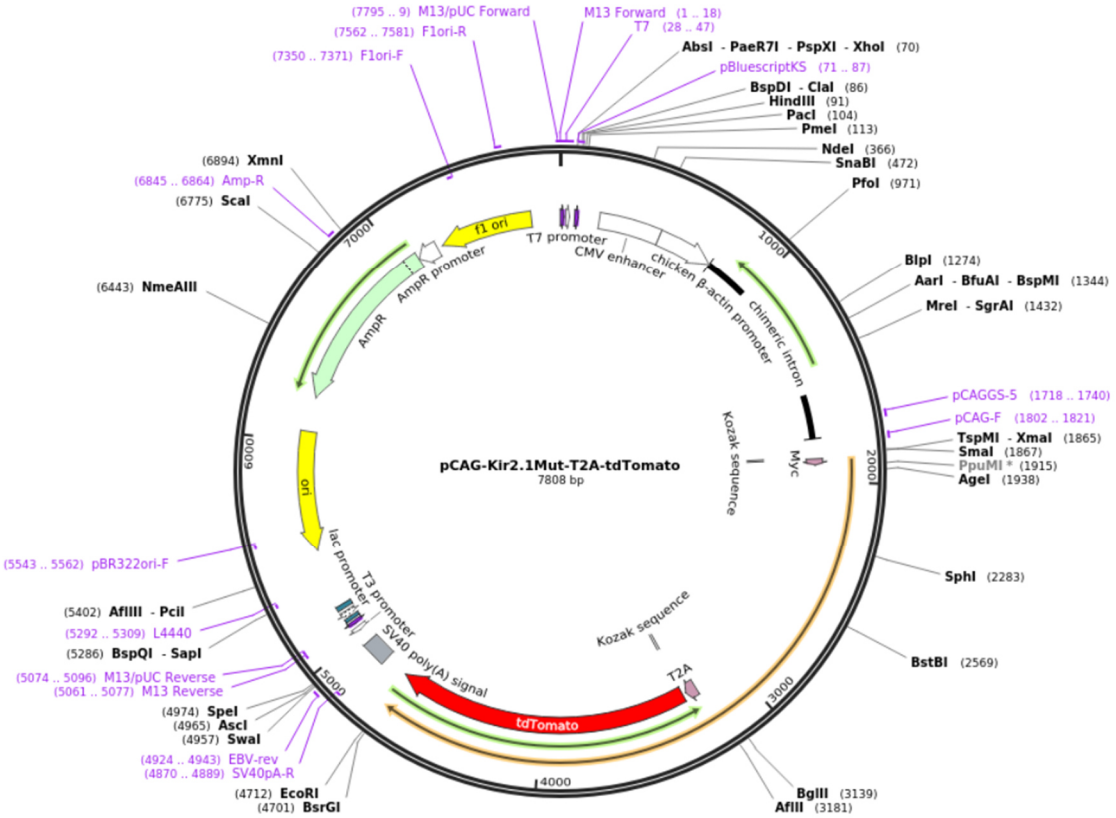


Figure 26: Plasmid map of MutKir2.1-T2A-tdTomato

The non-conducting control plasmid, MutKir2.1-T2A-tdTomato, is carrying the mutation GYG to AAA (144-146).

(Figure downloaded from Addgene: https://www.addgene.org/60598/)

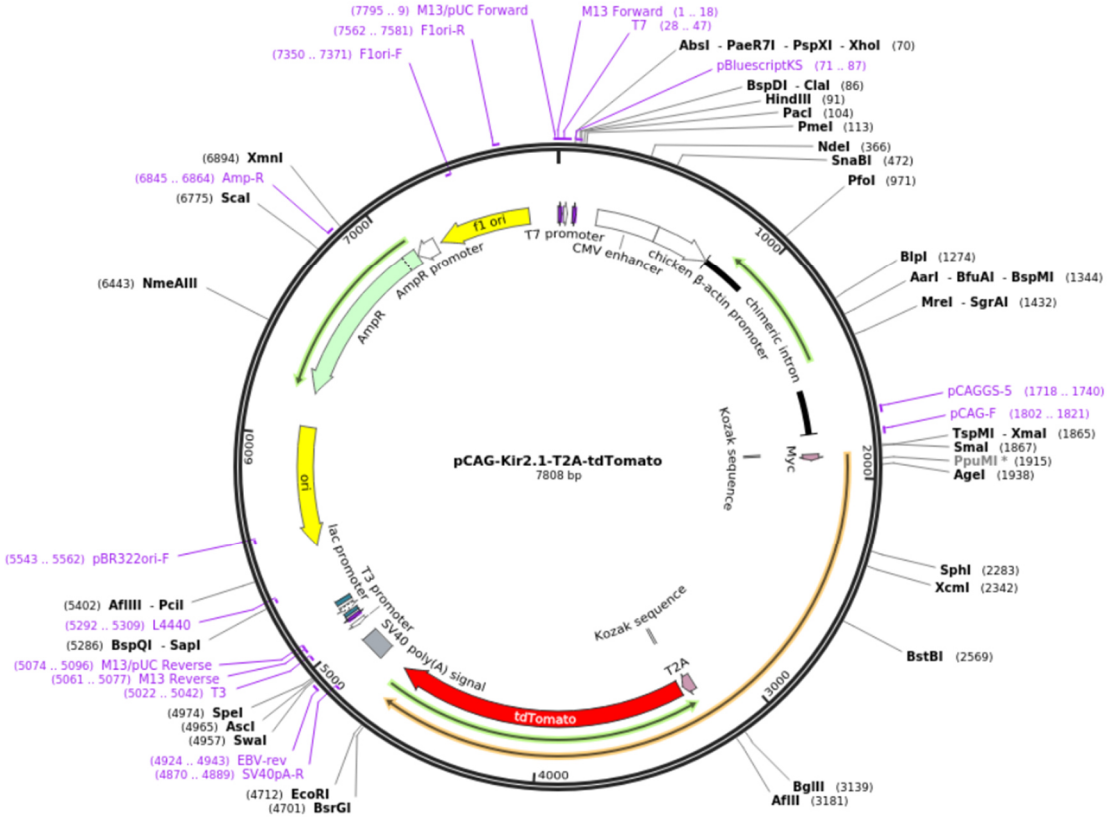


Figure 27: Plasmid map of Kir2.1-T2A-tdTomato
(Figure downloaded from Addgene: https://www.addgene.org/60644/)

3.2.3.2 Fibre analysis of cortical neurons electroporated with Kir2.1 and MutKir2.1

To assess myelination around fibres that originated from cortical projection neurons electroporated with Kir2.1, it was important to establish whether there are long range projections present consistently to be able to assess them. Therefore, I examined whether the tdTomato signal is similar in controls and in brains after Kir2.1 *in utero* electroporation (IUE) at E13.5 (Figure 28). For improved microscopic fibre analysis, brain sections were stained by immunohistochemistry for the red fluorescent protein dsRed to reinforce intrinsic tdTomato signal.

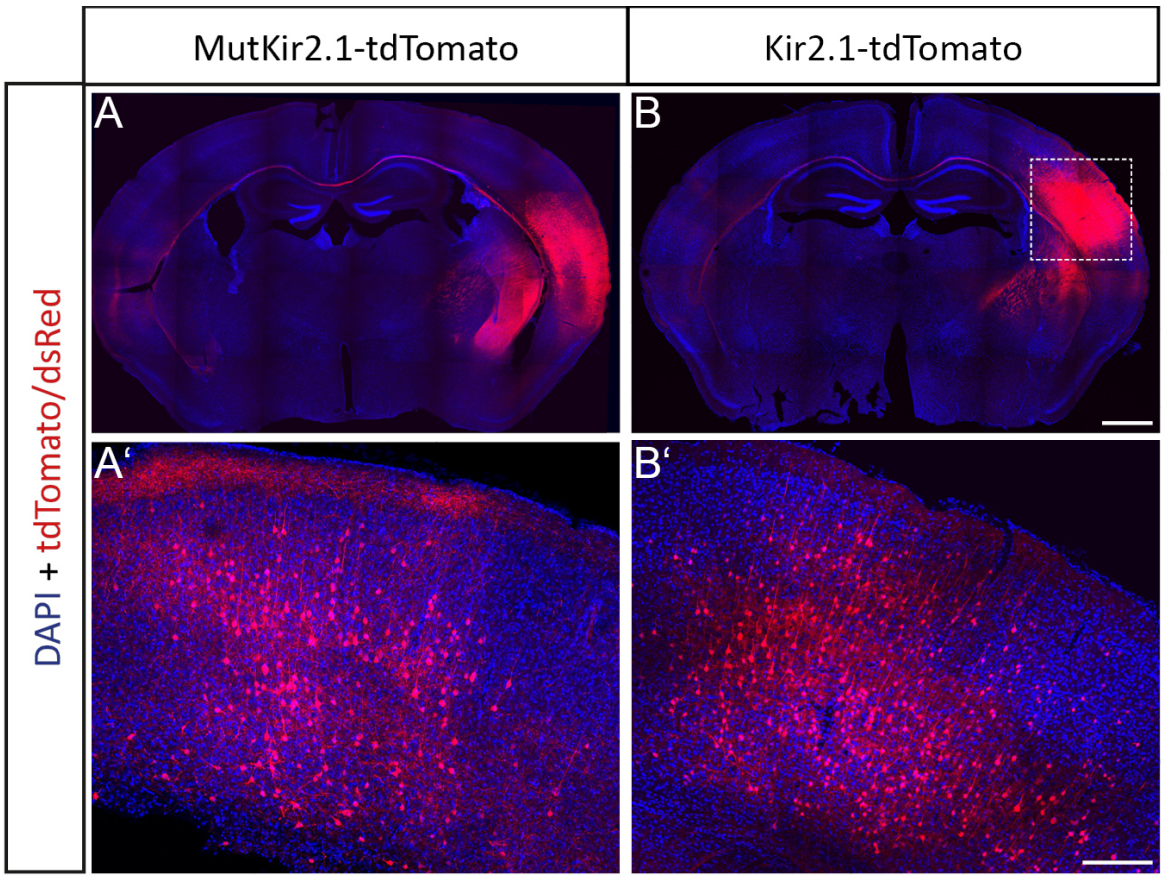


Figure 28: In utero electroporation in E13.5 embryos resulted in expression of experimental vectors in deep and superficial cortical layers at P14

By P14 cell bodies as well as their neurites are tdTomato/dsRed labelled after embryonic electroporation and sacrifice at P14. MutKir2.1 (A-A') and Kir2.1 (B-B') expressing cortical neurons can be seen in the corpus callosum projecting to the contralateral hemisphere where fibres sprout. Additionally, fibres also project to subcerebral areas like the thalamus via the striatum and the internal capsule (n=3/genotype). White box (B) indicates magnified region shown in A' and B'.
Scale bar overview (B) 1000 µm, (B') magnification 200 µm

IUEs were conducted at E13.5 and animals sacrificed postnatally at various ages up to P21 (timepoints chosen with regard to following myelin analysis in the corpus callosum, chapter 5). The majority of the electroporated cells were typically located in the somatosensory area of the cortex. For both control and experimental plasmid, tdTomato fluorescence was visible in several layers of the cortex with most of them in deeper layers (layers VI and V) of the cortex. Due to the inside-out

development of the cortex, earlier born cells are located deeper in the cortex (see 1.2). Hence, the earlier an electroporation is taking place during embryogenesis, the deeper the labelled cells will be in the cortex.

Figure 28 shows that fibres from cortical neurons project to the contralateral hemisphere via the corpus callosum and sprouting into the cortex of this hemisphere. They also project through the underlying white matter and striatum, the internal capsule and into the thalamus in both conditions.

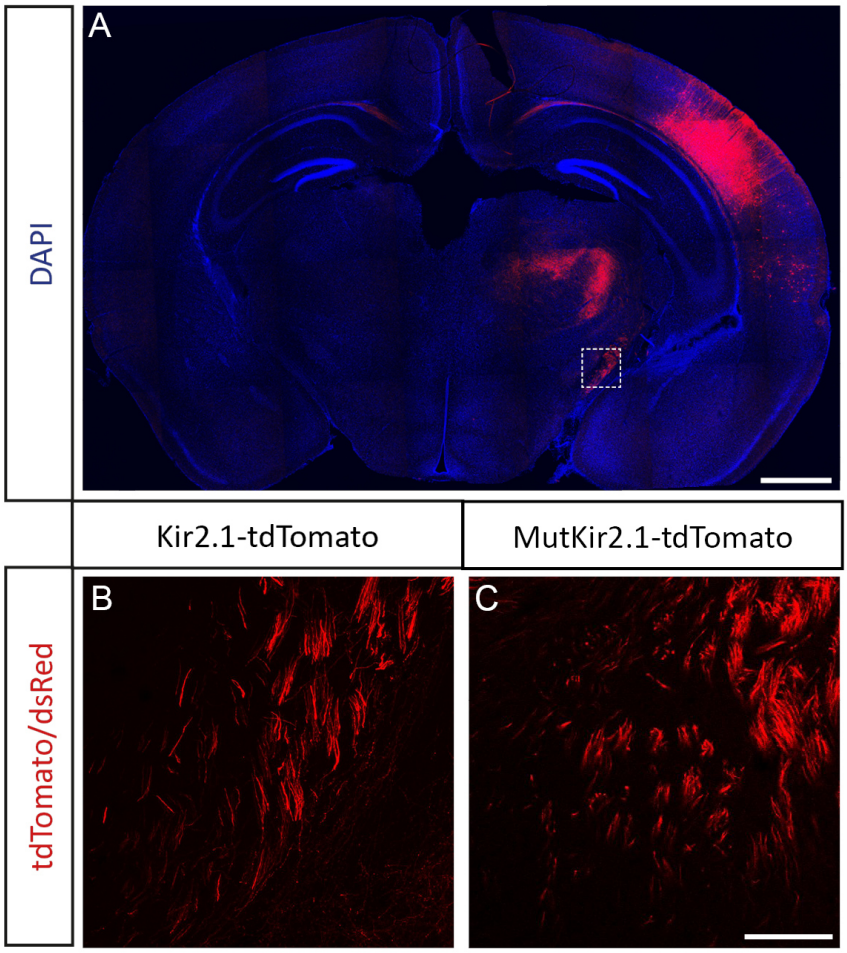


Figure 29: At P14 tdTomato/dsRed signal is visible in the cerebral peduncle after in utero electroporation at E13.5

LV corticospinal fibres project from the cortex through the cerebral peduncle into the dorsal corticospinal tract. tdTomato/dsRed positive fibres are visible in the cerebral peduncle (A) at P14 in Kir2.1-tdTomato (C) as well as in MutKir2.1-tdTomato (B) electroporated mice. White box in A indicates magnified region shown in B and C.
Scale bar overview (A) 1000 µm and (C) magnification 100 µm

In electroporations with control as well as experimental plasmids, tdTomato/dsRed labelled fibres can also be detected in the cerebral peduncle (Figure 29). This is an area where LV corticospinal fibres deviate from the rest of the internal capsule (containing layer V and VI projections) and purely layer V axons project through to enter the spinal cord. Therefore, I examined the spinal cord in order to answer the question, if the signal is strong enough to be also detected in LV long range projections of the spinal cord (Figure 30).

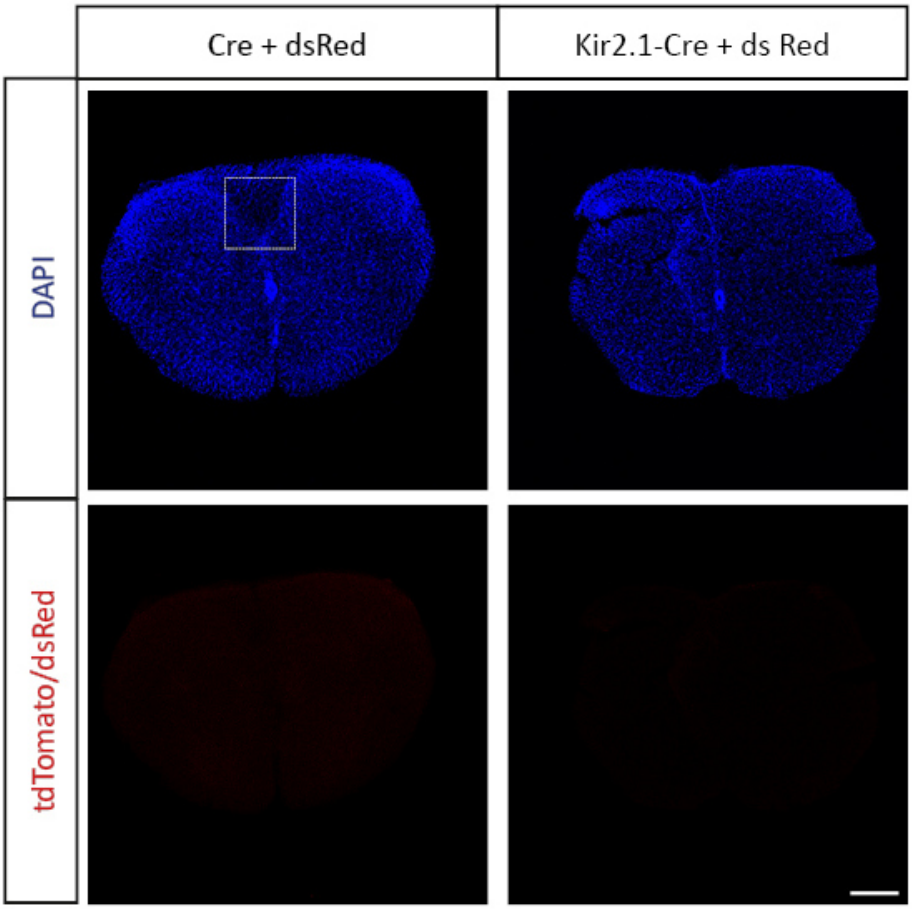


Figure 30: tdTomato/dsRed signal is not visible in the dorsal corticospinal tract after in utero electroporation at E13.5 examined at P14

LV corticospinal fibres project from the cortex through the cerebral peduncle into the dorsal corticospinal tract. tdTomato/dsRed positive fibres are visible in the cerebral peduncle at P14 but not in the dorsal corticospinal tract of C4-T4 in electroporated control and Kir2.1 animals examined in independent litters. White box in the first image indicates magnified region shown in the lower two panels.
Scale bar: 200 µm

However, despite a labelled cerebral peduncle, there was no tdTomato/dsRed signal detected in the upper spinal cord either in controls nor in Kir2.1 animals. In LV Snap25 cKOs and controls a tdTomato signal was present in the cerebral peduncle as well as the dorsal corticospinal tract where corticospinal LV fibres project through. After detecting a red signal in the cerebral peduncle following *in utero* electroporation, I therefore would have expected to also see a label in the dorsal corticospinal tract of the spinal cord (indicated with white box in Figure 30). Unfortunately, this was not the case and thus I concentrated my analysis on fibres in the brain.

In summary, results from first *in utero* electroporations showed unequal fluorescence intensity when vector backbones of experimental and control condition were not similar. Adaptation of the backbones resulted in similar fluorescence intensities, but discontinuous labelling did not result in satisfying results for following myelin analysis. Therefore, vectors have been changed completely from Cre-dependent co-electroporation of Kir2.1 and tdTomato to electroporation with only one plasmid that includes a self-cleaving T2A area. This also enabled us to use an improved control plasmid where a non-conducting MutKir2.1 channel is introduced.

3.3 Discussion

This chapter described the targeting and maintenance of projections that originate from cortical LV and LVI neurons that lack the ability to release synaptic vesicles in a regulated fashion due to the deficiency of Snap25. I also described Ntsr1-Cre extra-cortical labelling as well as targeting of projections from cortical projection neurons that have reduced activity due to Kir2.1 electroporation at the time of their birth at E13.5.

3.3.1 Targeting of LV and LVI Snap25 cKO fibres

First, the thalamic targeting of LV and LVI Snap25 cKO fibres were examined during the first three postnatal weeks due to previously published conflicting studies with siRNA and in Snap25 KO in axonal outgrowth during development (Molnár et al. 2002; Washbourne et al. 2002; Osen-Sand et al. 1993; Blakey et al. 2012). Both cortical layers, LV and LVI, innervate the thalamus by projecting through the internal capsule but then innervate distinct areas within the thalamus (Grant 2014). Studies have shown that thalamic targeting might be influenced by neuronal activity (Grant, Hoerder-Suabedissen, and Molnar 2016). Further targeting and branching, besides in the thalamus, was not studied in this thesis since it was not of specific interest. In general, it would be very interesting to study if the absence of Snap25 has an effect on the innervation of further targets and dendritic or axonal brancing.

Therefore, my question was whether cortical projection neurons develop and maintain their normal innervation pattern in the absence of the ability to release synaptic vesicles in an organised fashion after action potential in the absence of Snap25.

In the thalamus, LV targets higher order nuclei while LVI innervates both higher and first order nuclei (Sherman and Guillery 2011). By P8, the earliest time point studied, corticothalamic LV and LVI fibres already targeted their specific set of thalamic nuclei and there was no difference between the distribution of the projections that originated from Snap25 containing or Snap25 cKO cortical neurons. This similar pattern was obtained until P21, the oldest time point studied. Likewise, the cerebral peduncle, where corticospinal fibres pass through to project into the spinal cord, is tdTomato labelled by P8.

A previous study using the same mouse lines (Rpb4-Cre::tdTomato and Ntsr1-Cre::tdTomato) showed that at P2 corticothalamic fibres reach the thalamus and have nearly established their final innervation pattern by P6 (Grant, Hoerder-Suabedissen, and Molnar 2016). In particular, the dorsal Lateral Geniculate Nucleus (dLGN) was studied to which retinal fibres transmit spontaneous waves of activity (Mooney et al. 1996; Maffei and Galli-Resta 1990). It was shown that the waiting period in which LV and LVI fibres accumulate outside the dLGN is reduced after loss of retinal input by monocular enucleation (Grant, Hoerder-Suabedissen, and Molnar 2016). Furthermore, this study showed that the loss of retinal input to the dLGN also induces layer V fibres to enter the dLGN contrary to their normal innervation pattern. These results indicate how important peripheral neuronal activity can be for the timing and correct targeting of the thalamus.

Although there is no visible difference in thalamic nuclei targeting, distribution of the fibres in callosum, in internal capsule and cerebral peduncle labelling between LV and LVI Snap25 cKOs and their respective controls at P8, there is the possibility that genetic ablation of Snap25 and evoked neuronal activity causes an altered timing in targeting. This could be a delay in either reaching the thalamus and

cerebral peduncle before P2 or in establishing the innervation pattern around P6. To investigate this possibility, earlier timepoints would need to be chosen for further experiments.

Table 4: Summary of fluorescent LV and LVI fibre innervation in thalamus and cerebral peduncle

	first order		higher order		unclassified	
	LGN	VPM	LP	Po	TRN	Cerebral Peduncle
LV	-	-	+	+	-	+
LV Snap25 cKO	-	-	+	+	-	+
LVI	+	+	+	+	+	-
LVI Snap25 cKO	+	+	+	+	+	-

LV fibres innervate higher order nuclei whereas LVI innervates higher as well as first order nuclei. LV fibres project through LGN, VPM and TRN but do not arbourise in these regions. Corticothalamic LV fibres are visible in the cerebral peduncle
Abbreviations: TRN: thalamic reticular nucleus, v and dLGN: ventral and dorsal Lateral Geniculate Nucleus, VPM: ventral posterior-medial thalamic nucleus, LP: lateral posterior thalamic nucleus and Po: posterior thalamic nucleus.

This is also the case for fibres within the spinal cord. It is known that LV neurons send excess projections into the spinal cord but eliminate some of them during the first three postnatal weeks. However, little is known about the exact timing and regulatory mechanism of this process (O'Leary and Stanfield 1989; Koester and O'Leary 1992). The role of activity in the maintenance or elimination of these projections is not known. Whether the area-specific axonal side branch elimination occurs to the same extent in normal and LV Snap25 cKO is currently not known. My data suggests that at P21 there is no obvious difference between the corticospinal tract of LV Snap25 cKO mice and controls.

According to my experiments, the absence of Snap25 and thus the absence of evoked neurotransmitter release, did not influence the overall gross thalamic innervation pattern of LV and LVI fibres between P8 and P21. My results are in conflict with previously published in vitro studies using siRNA to reduce Snap25

expression where axon elongation defects were described (Osen-Sand, Catsicas, Staple, Jones, Ayala, Knowles, et al. 1993) and in support of previous in vivo studies where normal axonal outgrowth and branching has been described during embryonic development or in organotypic co-cultures (Blakey et al. 2012; Molnár et al. 2002; Washbourne et al. 2002).

In global Snap25 KO mice, it was shown that reciprocal thalamocortical projections develop in normal gross topography and immature synapses are formed by fibres lacking Snap25 (Molnár et al. 2002). Due to postnatal fatality of global Snap25 KO mice and premature neuronal degeneration *in vitro,* the study was unable to investigate this further (Washbourne et al. 2002).

LV and LVI are not just distinct in their innervation pattern but also in the kind of synapses they form to their downstream neighbours. LV corticothalamic fibres exhibit driver input to the thalamus whereas LVI cells provide modulator input (Sherman and Guillery 1998). Whether this is also true when Snap25 is absent exceeded the scope of this thesis. The question is currently under investigation in our laboratory for layer V synapses in the thalamus. It will be interesting to see if LV neurons keep their driver synapses without regulated vesicle release present and in which quantities.

Rbp4-Cre is expressed in both LV sublayers, upper LVa and lower LVb as well as in both neuron subtypes, Type I and II. I made similar observations for controls as well as Snap25 cKOs. Both sublayers have distinct projection targets. LVa is characterised by projections to the contralateral hemisphere or the ipsilateral striatum as well as other cortical regions and mainly consists of neurons with Type II morphology (Schubert et al., 2001; Hallman et al. 1988; Klein et al. 1986; Larsen et al., 2008; Veinante et al., 2000; Wise & Jones, 1977). Therefore, LVa cells

project through the corpus callosum where a tdTomato signal was detected in both genotypes. These neurons often have smaller dendrites that usually end in layer II/III of the cortex and a less complex dendritic morphology than neurons in LVb (Kasper, Larkman, and Lubke 1994). LVb neurons, mostly Type I neurons, have thick-tufted apical dendrites endling in layer I. They project to subcortical regions like the brainstem, spinal cord, superior colliculus, ipsilateral striatum and thalamus (Leary and Louis 1988; Veinante et al. 2000; Wise and Jones 1977). The presence of LVb cells can be seen in Figure 9 and Figure 11 where a tdTomato signal was detected in cortical LI (after P7 when remodelling was taking place) as well as in the cerebral peduncle leading to the spinal cord (Koester and O'Leary, 1992; Molnár and Cheung, 2006; Hattox and Nelson, 2007).

It was also tested, if the strength of Cre-expression (Rbp4 or Ntsr1) is similar between controls and the respective cKOs by measuring fluorescence intensity of tdTomato in LV or LVI. The results show that expression levels in both mouse lines are similar between controls and cKOs, indicating that introducing Rbp4- or Ntsr1-Cre does not change the recombination efficiency. Due to these results, I relied in the cell counts that were performed in our laboratory and others in the control mouse lines, stating that the effected cell population size is roughly 15% for LV and over 35 % for LVI (Olsen et al. 2012; Grant 2014). Cell counts were performed by adding a neuronal marker (NeuN) into the experimental paradigm to see overlap with tdTomato positive cells.

Hence, the lack of Snap25 expression does not alter which cell type is affected by Cre-expression, how many cells, nor does it lead to a missing subpopulation or projections of LV cells.

These observations were similar to the ones I made on the two subpopulations of LVI cells. Ntsr1-Cre is expressed in pyramidal neurons extending their dendrite to LI as well as in neurons that have dendrites in LVI and LV (Olsen et al. 2012; Bortone, Olsen, and Scanziani 2014). In Figure 20 a strong labelling of LV and LIV is visible that allows location of the barrels in S1. Additionally, the upper edge of the cortex is visible by tdTomato fibres ending in in the upper layers. Therefore, the two distinct LVI cells that are affected by Ntsr1-Cre as reported by Olsen and colleagues are affected in a similar way even if Snap25 and regulated vesicle release is missing.

Additionally to the cortical Cre expression, extra-cortical Cre expression was detected. In this thesis, extra-cortical Ntsr1-Cre expression was described in LVI Snap25 cKOs and controls and no obvious difference was observed. Rbp4-Cre is also expressed outside the cortex as described before by our laboratory (Grant 2014). Most of the identified areas in LV and LVI animals do not contribute to the long corticothalamic and corticospinal projections that were analysed in this thesis. Additionally, since the extra-cortical labelling was sparse compared to the cortical labelling, the Rbp4- and Ntsr1-Cre lines are suitable for studying layer V and layer VI corticothalamic projections.

The formation of the barrel field is dependent on the activity of the sensory periphery, transmission via the thalamus and through the thalamocortical projections (Feldman and Brecht 2005; Erzurumlu and Kind 2001; Fox 2002). Especially during the critical period, prior to P4, sensory deprivation has a big influence on the formation of the whisker barrels (Woolsey and Loos 1970; Fox 1992). In my two mouse lines, activity of LIV is not directly affected. LIV barrels get

their sensory information from the thalamus. Therefore, we would expect a correct barrel formation. However, the innervation of LV or LVI cells to LIV might be altered due to the lack of regulated vesicle release. Moreover, we observed no changes in the organisation of the conditional Snap25 KO where layer IV was specifically targeted (Six3-cre::Snap25fl/fl) (Hoerder-Suabedissen, Molnar and Paulsen, unpublished observation).

The barrels in LIV are made visible by the hollow formation of cell bodies in the underlying LV and LV neurite bundles in the septa of LIV. Even though LVI is not adjacent to LIV, the barrels are still visible by dense tdTomato signal ending in LV and denser neurite bundles that extend through LV into LIV. The visibility of the barrel field by indirect labelling of tdTomato signal in LV and LVI was identical in controls as well as Snap25 cKOs. The reduced vesicle release in Snap25 cKOs did therefore not lead to a visibly altered innervation pattern in the whisker barrel field of the somatosensory cortex at 2 months of age.

3.3.2 Impaired fibre maintenance in LV and LVI Snap25 cKOs after the third postnatal week

As shown above, the development of LV and LVI Snap25 cKO fibres appears normal during the first three postnatal weeks. But what happens after this time? Here, I observed and described a phenotype of impaired fibre maintenance in both mouse lines. Our laboratory described fibre degeneration in the brain and a decrease in tdTomato positive cells by 8 months in the primary somatosensory cortex of LV Snap25 cKO mouse line which was not observed at 2 months (Hoerder-Suabedissen, Korrell et al. 2018). Therefore, tdTomato positive cell bodies were also counted in LVI Snap25 cKOs. For the analysis, 9 months old

brains were used since the observed degeneration processes slower in LVI than in LV Snap25 cKOs. Additionally, fibre degeneration was observed in LVI Snap25 cKO brains to be compared with the findings in LV Snap25 cKOs. To expand the findings on LV Snap25 fibre maintenance in the brain, I studied tdTomato positive long-projection fibres in the spinal cord, which are not present in LVI Snap25 cKOs.

In LVI Snap25 cKO mice degeneration becomes first evident at around 2 months in fibre bundles like white matter and striatum. In LV Snap25 cKOs the first signs of fibre degeneration are visible at P23 in the spinal cord. In the brain of LV Snap25 cKO mice axonal swellings as well as tdTomato punctae are visible after the first month. Dendrites have been shown to stay intact into older ages. Some of the tdTomato punctae are synapses since they co-localize with the synaptic marker vesicular glutamate transporter 1 (Hoerder-Suabedissen, Korrell et al. 2018). The remaining observed discontinuous tdTomato punctae could be accumulation of tdTomato protein rather than neurodegeneration. Findings against this hypothesis are that 1) over time, the observed swellings and punctae exceed the size of an axon and 2) the loss of cell bodies. For LV Snap25 cKOs it has been shown that changes in Iba1 positive cells as well as increased autofluorescence accompany the observed degeneration. Both could be evidence of inflammation due to emerging cell debris. Activated microglia were present mostly in LV Snap 25 cKO brains when compared to controls. At 8 months, but not at 1.5 months, there tend to be more Iba1 positive cells in the deeper layers of the cortex in LV Snap25 cKOs compared to controls (Hoerder-Suabedissen, Korrell et al. 2018).

Additionally, an increased broad-spectrum autofluorescence was observed at 1.5 months that was significant at 8 months. It was concluded that the signal could be lipofuscin deposits that points towards an inflammatory reaction or premature ageing (Hoerder-Suabedissen, Korrell et al. 2018). Since the degeneration processes slower in LVI Snap25 cKOs compared to LV Snap25 cKOs we would expect that these effects might also be visible in LVI Sanap25 cKOs but at a later timepoint. In support of this hypothesis, no obvious signs of autofluorescence was observed at 9 months in LVI Snap25 cKOs, the oldest time point studied. Due to home office animal license restrictions in this mouse line, animals were never maintained for longer than one year after birth.

The question remains what the cause is of the impaired maintenance. In 2012 it was published that neuronal degeneration observed in cultures originating from a cysteine-string protein-a (CSPa – co-chaperone for SNARE complex) KO mouse is based on the defect function of Snap25. They showed that reduced levels of Snap25 impaired assembly of the SNARE complex which caused neurodegeneration (Sharma et al. 2012).

Before that in 2002, Washbourne and colleagues had already observed that neuronal cultures of the global Snap25 knock out mouse show signs of premature degeneration starting at 5 days *in vitro.* By supplying glutamate or AMPA to the cultures to promote synaptic activity or keep cells depolarised, the progressive degeneration could not be prevented. This, as well as the fact that the lack of neuronal activity in Kir2.1 fibres has not been reported to lead to premature degeneration, shows that the lack of neuronal activity itself is probably not responsible for the fibre degeneration. Washbourne concluded that Snap25

deficient neurons in culture might not be able to secrete sufficient neurotrophic or other factors for neighbouring neurons to survive (Washbourne et al. 2002). In the brain of Snap25 cKO mice there are many surrounding cells still capable of releasing such factors. However, Snap25 cKO neurons need to be able to absorb and transport neurotrophic factors. Therefore, it is also possible that impaired endocytosis or trafficking contributes to the impaired fibre maintenance when Snap25 is lacking. Supportive of the hypothesis to connect the cause of neurodegeneration to impaired endocytosis and trafficking is the observation that the timing of axonal fragmentation differs between the mouse lines (Figure 29).

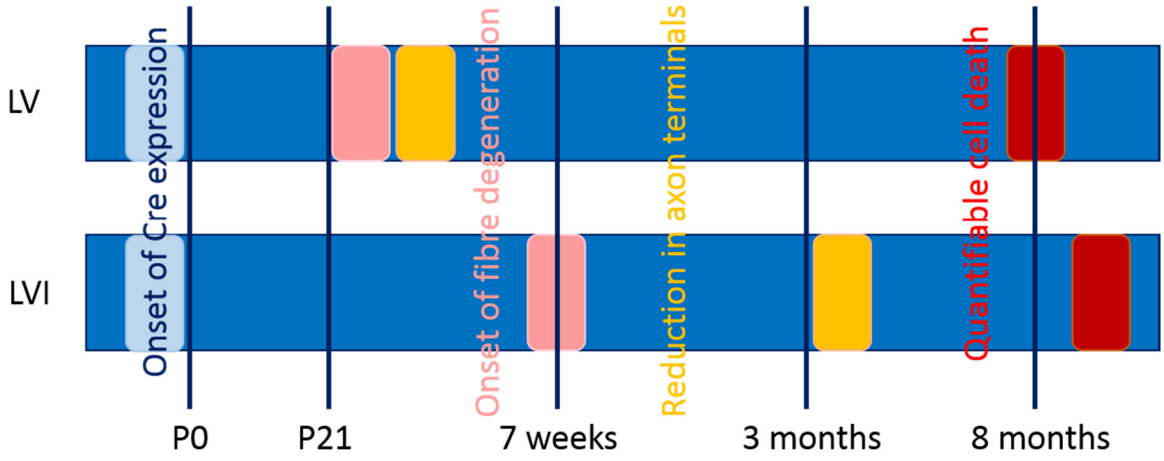


Figure 31: Timeline of Cre-expression and degenerative processes in the Rbp4-Cre (LV) and Ntsr1-Cre (LVI) strains following Snap25 knockdown

Cre-recombinase expression starts during late embryonic development. Fragmentation of distal axons is detectable from P21 in Rbp4-Cre cKO brains. A decrease in the density of terminal arbours in subcortical target structures is evident by P28 for Rbp4-Cre cKO brains. A reduction in the density of cortical Cre+ neurons was evident for both Rbp4-Cre and Ntst1-Cre cKO brains around 8-10mths of age.
Adapted from Hoerder-Suabedissen, Korrell et al. 2018

One possible explanation is the distance of projection targets. LV axons project out of the brain to the spinal cord where they innervate downstream neurons. This distance is much further than the one LVI axons must cover until they reach e.g. the thalamus. Essential survival signals or factors would be prevented from

reaching the distal axon areas leading to degeneration. Important neurotrophic factors are taken up by distal ends of axons. When released by postsynaptic neurons, neurotrophic factors bind to neurotrophin receptors (Trks) on synaptic endings. By endocytosis receptors as well as their ligands are taken up and then get transported retrogradely in vesicles to the cell bodies to signal for survival (Campenot and Macinnis 2003; Ginty and Segal 2002). This important neurotrophin signalling and transport mechanism from distal synaptic endings to cell bodies has been linked to neuronal death in neurodegenerative disorders (Williamson and Cleveland 1999; Gunawardena et al. 2001).

Bronk and colleagues described a reduction in endocytosis during evoked stimulation in neurons with Snap25 deletion. However, due to further experiments they concluded that Snap25 does not directly function in endocytosis (Bronk et al. 2007). Experiments with hippocampal neurons derived from LV Snap25 cKOs also pointed towards an impaired vesicle recycling (Hoerder-Suabedissen, Korrell et al. 2018). However, the degenerative phenotype is only occurring after three postnatal weeks and endocytosis of neurotrophic factors is especially important during development to survive in a competitive environment.

Impaired trafficking has been described in pancreatic β-cells lacking Snap25. This is also observed after the dominant mutation of Snap25 in the blind-drunk mouse (Jeans et al. 2007). If internal cell trafficking is impaired, cell cargo accumulates along axons and may lead to axonal swelling. Further reasons why impaired trafficking leads to neuronal degeneration are that supply of material might be failing or accumulation of toxic substances occurs (Chevalier-Larsen and Holzbaur 2006).

The impaired vesicle recycling as well as the impaired trafficking, could lead to impaired fibre maintenance ending in cell loss. Further experiments will be necessary to determine why neuronal degeneration occurs according to different timetable in different Snap25 cKO lines where different cortical projection neurons (Layer V, VI and VIb) lack the ability to release synaptic vesicles in a regulated fashion.

3.3.3 Targeting of projections originating from Kir2.1 electroporated cortical neurons

Manipulating electrical activity by Kir2.1 has been reported to influence axonal targeting and sprouting (see 1.8.2). For further experiments in my thesis, the presence of long projection axons needed to be given. Therefore, I analysed the targeting of Kir2.1 electroporated fibres in comparison to controls. In both cases, labelled fibres were seen in the contralateral hemisphere as well as in subcortical regions. A more detailed analysis, including fibre arborisation, was not conducted due to already existing literature on this method. A limitation of this study is that it was not tested how many neurons have been targeted in comparison to the whole neuronal population. This would have been possible by stained IUE brains not only with dsRed but also with a neuronal marker (e.g. NeuN). I have shown in later experiments (see 4.2.2) that IUE efficiency is similar between experimental conditions. However, it would have been useful to know the affected population to discuss the effect size that could have been observed. From visual judging when looking at microscope images, it is unlikely that more cells were targeted by IUE than by Rbp4- or Ntsr1-Cre expression, leading to the conclusion of far less than 40% of cells being affected. For a more accurate estimate, future experiments

should include cell counts of cells targeted by IUE in comparison to total neuronal cell counts in LV and LVI.

Electroporations at E13.5 to putative somatosensory cortex mostly affect deeper layers of the cortex but since this is the peak of neurogenesis, it fails to selectively label a specific neuronal population and most often do not only target one specific brain area. However, only LV neurons project out of the brain through the foramen magnum and into the spinal cord. For fibres to reach the spinal cord, they need to pass through the cerebral peduncle, a part of the midbrain where only LV from the cortex projects through. Therefore, the labelled fibres seen in the cerebral peduncle of electroporated brains arise from LV cells that should project to the basal pons and spinal cord. Although I observed consistent labelled fibres in cerebral peduncle, I could not detect labelled fibres in the spinal cord. It is worth noticing that during development almost all cortical areas descend axons into the spinal cord but not all areas maintain them. Anterior cortical areas, including M1, do maintain them while S1 axons get selectively eliminated (Larsen & Callaway 2006; O'Leary & Stanfield 1989; Koester & O'Leary 1992). Since mostly S1 was targeted by IUE (targeting M1 is not possible with forceps electrodes), tdTomato positive axons in the CP might originate from S1 at a timepoint of axonal remodelling that is taking place during the first three postnatal weeks. This could explain why a signal is still detectable in the CP but not in the spinal cord, since the mechanism of elimination is not yet known. It would be very interesting to study, if the CP signal disappears at a later time point to support this hypothesis.

Larsen and Callaway described that around P7, LV cells have still a quite simple descending axon to the spinal cord which becomes complex around P10 (Larsen and Callaway 2006). Therefore, by P14, LV axons should definitely be present in

the spinal cord and not only in the cerebral peduncle. To support this, in LV Snap25 mice as well as controls, tdTomato positive fibres are already present in the dorsal corticospinal tract at P14. The lack of a red signal in the spinal cord in electroporated brains could be based on the different amount of red fluorescent protein. This assumption is supported by the fact, that electroporated brains needed to be stained to strengthen the tdTomato (red) fibre signal. The amount of tdTomato protein is dependent on the promotor that controls the expression of the protein. All used expression vectors had a pCAG promotor. In the Rbp4-Cre mouse line, not only the upstream promotor is decisive but also Cre-expression. This difference in promotor could explain why there is no signal in the spinal cords of IUE animals at P14 while there is one in the LV Rbp4-Cre mouse line. Though, there are far more LV labelled cells in the Rbp4-Cre mouse line since both hemispheres are affected. Grant reported that 15% of neurons in LV are labelled with tdTomato after Rbp4-Cre expression at P6. We did not quantify how this compares to labelled LV cells after IUE.

In general, the red fluorescent proteins here, do not get actively transported into the axons but follow the law of diffusion (Jackson Laboratory). Hence, it could take a while until they reach the distal end of a long projection axon. However, I verified the presence of red fluorescent cells in the cortex at P4 indicating that the red fluorescence proteins had 10 days to reach the cervical part of the spinal cord.

Using my first set of plasmids (Kir2.1-Cre + Stop-dsRed and Cre + Stop-dsRed) red fibres were discontinuously labelled in controls as well as Kir2.1 affected cells. This could either point towards a fibre-maintaining problem due to the plasmids or towards irregular tdTomato signal. This signal was comparable to the beginning of

discontinuous labelling of LV and LVI Snap25 cKOs. However, the signal appeared like this already from the earliest time point checked (P12) and did not evolve after a juvenile state. Additionally, the red signal was discontinuous in a uniform way whereas in LV and LVI Snap25 cKO mice the red punctae where of different size. When using the second set of plasmids (pCAG-MutKir2.1-T2A-tdTom and pCAG-Kir2.1-T2A-tdTom) the labelling was continuous indicating that the problem was probably due to a discontinuous labelling of the tdTomato signal rather than a fibre maintenance issue.

3.3.4 Conclusion

In this chapter I described the innervation pattern of LV and LVI Snap25 cKO fibres, their maintenance as well as the innervation of Kir2.1 electroporated cells at E13.5. The analysis showed that despite the reduced neuronal activity - by either the lack of Snap25 or the presence of Kir2.1 - fibre outgrowth and correct targeting is taking place. These results lead me to the analysis of myelination around these fibres, which will be the focus of the next two chapters.

4 Onset of myelination under the influence of genetically reduced neuronal activity

4.1 Introduction

Following the first results chapter in which proper projection formation in Snap25 cKOs as well as neurons overexpressing Kir2.1 have has been established, in this chapter the timing of myelination during its onset and oligodendroglial density during development will be analysed. Analysis will include the examination of LV and LVI Snap25 cKOs. Additionally, at P14 the corpus callosum will be investigated for myelination in LV Snap25 cKOs as well as cortical cells electroporated with MutKir2.1 and Kir2.1. Comparing results from these two techniques might give further insights into different roles of neuronal activity (vesicular release vs exitability and spontaneous activity) in myelination and on oligodendroglial cells.

It has been shown *in vivo* (in zebrafish and mice) that genetic induced changes in neuronal activity can result in altered myelination or altered numbers of OPCs and oligodendrocytes (Hines et al. 2015; Mensch et al. 2015; Gibson et al. 2014; Mitew et al. 2018; Etxeberria et al. 2016). Despite several studies examine this, no study so far has looked at myelination and oligodendroglial density during development after reduced neuronal activity in deep cortical layers in mice in particular. Therefore, the aim of this chapter is to contribute to our understanding of the effect of reduced neuronal activity on myelination and cells responsible for myelination, oligodendroglial, in deep cortical layers and their projections in mice. First, in the introduction markers that have been used for the analysis of the oligodendroglial lineage, will be described. Second, the so far known influence of neuronal activity on oligodendrocyte development and myelinogenesis will be presented.

4.1.1 Marker of oligodendrocyte lineage

Cell-type specific markers allow to distinguish cell types and track their developmental progress in the CNS. In this thesis, Olig2 and CC1 were used as markers for the oligodendroglial cell lineage. Therefore, they will be the focus of this introduction.

4.1.1.1 Olig2 and CC1

OPCs develop from multi-potent neuronal stem cells. At this early stem cell stage, the OPC fate can lead them not only towards becoming oligodendrocytes but also astrocytes or neurons (Dawson et al., 2000; Hart et al, 1989; Nishiyama et al., 1999; Pringle et al., 1992; Stallcup 1981). Cells differentiating to immature oligodendrocytes under the positive influence of the insulin growth factor 1 (IGF-1), the cytokine ciliary neurotrophic factor (CNTF), and the thyroid hormone T3. They can be detected by the markers O4+ and GalC+ (galactocerebroside) (Bansal et al., 1992; Jones et al., 2003; Miron et al., 2011; Tosic et al., 1992). O4 can be used to detect oligodendrocyte progenitors as well as mature oligodendrocytes (Reynolds and Hardy 1997; Sommer and Schachner 1981). After maturation into myelinating oligodendrocytes, myelin proteins like PLP, MBP, CNP, MAG and MOG can be used for oligodendrocyte identification (Miron, Kuhlmann, and Antel 2011).

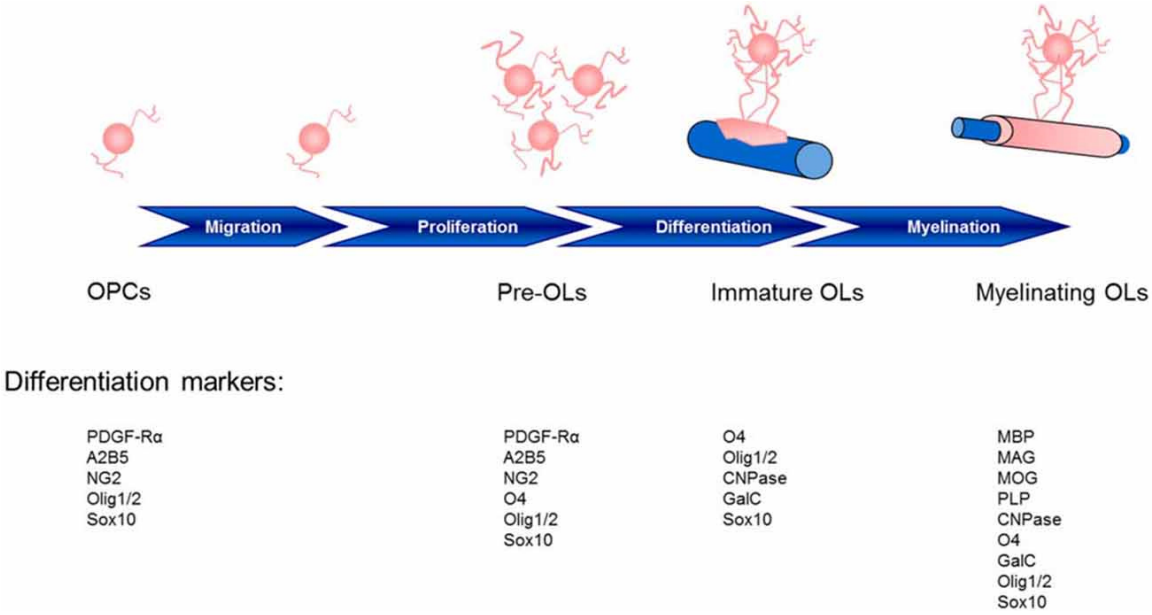


Figure 32: Stages of oligodendrocyte development and their markers in the oligodendroglial lineage

Migrating oligodendrocyte precursor cells (OPCs) proliferate and become pre-oligodendrocytes. They further differentiate into immature oligodendrocytes which do not yet myelinate axons, a definition for mature oligodendrocytes. Mature oligodendrocytes can be identified by myelin proteins like MBP, MAG, MOG, PLP and CNPase. The basic helix-loop-helix transcription factor Olig2 plays an essential role in the determination of the cell fate of the oligodendroglial lineage and thereby the generation of mature oligodendrocytes. PDGFRα and NG2 are important markers for the earlier stages within the development.
Figure from Marinelli et al. 2016

To generate myelin during development, precisely regulated processes are needed to form mature oligodendrocytes from precursor cells. Myelination is controlled by a gene regulatory program that involves the master transcription regulator Olig1 and 2, Myrf (myelin regulatory factor) and Sox10. Olig genes form a subgroup of the basic helix-loop-helix (bHLH) family that includes not only Olig1-4 but also Bhlhb4 and Bhlhb5 (Meijer et al. 2012). The bHLH motif mediates transcription factor dimerization and DNA targeting (Murre et al. 1994; Murre and Schonleber 1989). In mammals, Olig1 and 2 genes are in close proximity to each other in a well conserved chromosomal region (Frazer et al. 2001). Their names derived from

early *in situ* hybridization experiments that showed distinct expression in OPCs and oligodendrocytes (Lu et al. 2000; Zhou, Wang, and Anderson 2000). Olig1 and Olig2 are structurally conserved (especially the bHLH motifs) and have similar spatial and temporal expression patters. In contrast to Olig3, they are expressed exclusively in the CNS. Olig1 and 2 however differ in their subcellular localisation and they have distinct and non-overlapping biological functions (Lu et al., 2000; Takebayashi et al., 2000; Zhou et al., 2000).

It is known that Olig2 has a major role in oligodendrocyte development but the detailed role and importance of Olig1 is not as clear. Olig2 is one of the most consistent markers for the early stages of the oligodendrocyte lineages. It is expressed during all stages of early oligodendroglial development due to its importance in cell specification. However, its expression decreases with differentiation into oligodendrocytes (Kitada and Rowitch 2006).

Notably, most oligodendrocyte lineage cells in the spinal cord arise from the pMN (motor neuron progenitor) domain around E12.5 (Tripathi et al. 2011). Olig2 is extraordinary within the group of bHLH transcription factors with candidates that are normally either pro- or antimitotic. In contrast, Olig2 is necessary for sustaining progenitors in the pMN domain during motor neuron production for later gliogenesis. Later, Olig2 is additionally important for specification and differentiation of motor neurons and oligodendrocytes but shown to be less important for long-term myelin maintenance (Lee et al., 2005; Lu et al., 2002; Mei et al., 2013).

Importantly, OPCs can be detected in the forebrain from E13.5 onward. The newly generated cells express platelet-derived growth factor receptor α (PDGFRα) and transcription factor Sox10 (Tekki-Kessaris et al. 2001). Experiments with Olig2

knockouts showed that in the spinal cord, no PDGFRα /Sox10-positive cells can be found in Olig2 knockouts (Lu et al., 2002). In the brain of Olig2 knockouts however, PDGFRα /Sox10-positive cells can be found in reduced numbers in the brain probably due to compensation by Olig1. Double null mutants of Olig1 and 2 do not form any OPCs or oligodendrocytes in the CNS (Zhou and Anderson 2002). Inducing Olig2 expression by Doxycycline in Nestin-positive progenitor cells during murine prenatal development increased the generation of OPCs in the spinal cord as well as the brain even postnatally (Maire et al., 2010).

Since the early 2000s there is an emerging body of literature suggesting that Olig 1 and 2 are not only associated with developmental diseases like schizophrenia and Down syndrome but also with Alzheimer's disease and especially with malignant gliomas (Bouvier et al., 2003; Chakrabarti et al., 2010; Georgieva et al., 2006; Huang et al., 2008; Ligon, Fancy, Franklin, & Rowitch, 2006; Lu et al., 2018; Lu et al., 2001; Marie et al., 2001; Ohnishi et al., 2018; Sims et al., 2009). One possible explanation for the involvement of Olig2 in this form of brain cancer might be its early anti-neurogenic function (Meijer et al. 2012).

Of note, the Olig2 neurogenic bHLH transcription factor is continuously expressed throughout development and continues into adulthood. However, it has multiple roles during different stages of oligodendrocyte lineage specification. A possible explanation for the versatile role of Olig2 is phosphorylation given this transcription factor is especially rich in serine residues. Consequently, activity of Olig2 is susceptible to regulation by post-translational modification (Li et al., 2011; Prabakaran et al., 2012; Sun et al., 2011; Yu et al., 2012). Further research is needed to determine the pathways by which Olig2 is de- and phosphorylated.

The CC1 monoclonal-antibody is a commonly used antibody to specifically label mature oligodendrocyte cell bodies. Its ability to label cell bodies without labelling abundant myelin in the surroundings like most other myelin markers, is advantageous for oligodendrocyte quantification (Bhat et al. 1996; Fuss et al. 2000; Messersmith et al. 2000).

The antibody was originally raised against adenomatous polyposis coli (APC, clone CC1) which is mainly expressed in neurons (Bhat et al., 1994; Lang et al., 2013; Smith et al., 1993). However, it has been shown that in fact the antibody does not bind to APC, but rather to an unknown oligodendrocyte antigen (Brakeman et al., 1999; Lang et al., 2013). In 2016, Bin and colleagues showed that the previously unknown antigen is Quaking 7 (QKI7), a protein stabilising the mRNA necessary for myelin protein translation (Bin et al., 2016; Z. Li et al., 2000). QKI7 is a cytoplasmic, 40 kDA isoform of the RNA-binding protein Quaking (QKI) that is highly expressed in mature oligodendrocytes (Hardy et al. 1996; Artzt and Wu 2010).

4.1.2 Neuronal activity and the influence on oligodendrocyte development and myelinogenesis

Myelinogenesis depends on oligodendrocytes and starts around birth in the murine spinal cord and approximately P7 in the white matter tracts of the brain (Baumann and Pham-Dinh 2001; Foran and Peterson 1992). Murine developmental myelination in the brain is completed in nearly all regions between P45 and P60 (Baumann and Pham-Dinh 2001). *In vivo* studies in zebrafish have investigated the influence of reduced neuronal activity on myelin development. They showed that globally reduced neuronal activity did not affect myelin onset (Hines et al., 2015).

However, reduced synaptic vesicle release in a subset of neurons amongst active neurons resulted in hypomyelination of these silenced neurons. The researchers found that the hypomyelination was caused by a higher frequency of retracted sheath and shorter stabilized sheath (Hines et al. 2015; Mensch et al. 2015). A further zebrafish study on the influence of neuronal subtypes of activity dependent myelination strikingly revealed that distinct types of neurons show variable sensitivity to vesicular dependent myelination. This could not be explained by their properties since the analysed neuronal subgroups were very similar in neurotransmitter use, axon calibre, birth time, axon projections and are even myelinated by the same oligodendrocytes (Koudelka et al. 2016).

Together, these results led to the hypothesis that synaptic vesicle exocytosis in neurons is not necessary for the initial wrapping of oligodendrocytes. However, it can bias axon selection in some neuronal subtypes in a competitive way for nascent sheath stabilization during their short formation period (Hines et al. 2015; Mensch et al. 2015).

Interestingly, neuronal activity has not only an influence on the myelination capacity of oligodendrocytes but also on numbers and distribution of OPCs and oligodendrocytes (Mensch et al. 2015). Murine experiments showed that an increase in neuronal activity indeed is followed by changes in OPC and oligodendrocyte numbers as well as changes in myelination (Stedehouder et al. 2018). Furthermore, it has also been demonstrated, that these changes were necessary for motor learning and increase results in motor improvement (Gibson et al. 2014; McKenzie et al. 2014).

McKenzie and colleagues conditionally deleted myelin regulatory factor (MRF) in OPCs from experimental mice. Subsequently, the MRF-cKO mice were challenged

with a complex running wheel. In the control group an increase in OPC density as well as more mature oligodendrocytes were described. The observed change correlated with better performance compared to MRF deficient mice who failed to develop strategies to cope with the complex running wheel. Consequently, at least partially, OPC recruitment seems necessary for motor learning (McKenzie et al. 2014).

Furthermore, Gibson and colleagues stimulated layer V neurons via optogenetics in one hemisphere of the murine motor cortex. Their observations included increased OPC proliferation by examining Olig2 and PDGFRα cells, increased OPC differentiation and myelin thickness which correlated with improved swing speed of the correlated forelimb. These changes were not only observed in the motor cortex but also in the corpus callosum through which these neurons project to the contralateral hemisphere. Thus, their findings demonstrated that neuronal activity induced remodelling is not limited to the soma or synaptic endings (Gibson et al. 2014).

Interestingly, not only the effect of an increase in neuronal activity on OPC and oligodendrocyte numbers has been studied but also the effect of decreased neuronal activity by sensory deprivation in mice. Whisker trimming in neonatal mice led to a spatial alteration in OPC distribution and diminished myelination in the barrel cortex (Barrera et al., 2013; Mangin et al., 2012). However, monocular deprivation increased oligodendrogenesis without changes in OPC proliferation in the optic nerve. Myelin thickness and the number of myelinated axons were likewise unaffected. Nevertheless, conduction speed in the optic nerve was reduced after monocular deprivation which was accompanied by shorter internodal length (Etxeberria et al. 2016).

In conclusion, these experiments document that neuronal activity can have an influence on number and distribution of OPCs and oligodendrocytes and parameters of myelin, such as its thickness and internodal length thereby shaping activity dependent myelination.

4.1.3 Aims of this chapter

As described in the introduction of this chapter, previous studies reported an influence of increased and decreased neuronal activity on myelin as well as OPC and oligodendrocyte numbers (Gibson et al. 2014; Mitew et al. 2018; Mensch et al. 2015; Hines et al. 2015; Etxeberria et al. 2016; McKenzie et al. 2014). These activity dependent changes can influence certain behaviour, like motor behaviour, and may be necessary for learning or other changes in behaviour. In mice studies investigating decreased neuronal activity and myelination, the decrease was achieved by sensory deprivation after birth or genetic attenuation of synaptic glutamate release in the optic nerve (Barrera et al. 2013; Mangin et al. 2012; Sinclair et al. 2017; Etxeberria et al. 2016). Genetic reduction of vesicular release in mice in other parts of the CNS has not yet been studied. Hence, in this chapter I will investigate myelination in the corpus callosum at P14 after genetic reduction of neuronal activity in LV Snap25 cKOs as well as cortical cells electroporated with MutKir2.1 and Kir2.1 at E13.5. P14 as the timepoint for examination was chosen, since at the onse of myelination in the CC (at P12), no MBP immunoreactivity was seen in the area where electroporated fibres where (neither controls nor Kir2.1 fibres). An early developmental stage was also chosen because follow up experiments to this thesis were planned to include analysis of nodes of Ranvier. Individual nodal analysis is harder in regions with dense myelination like the CC.

Additionally, I will assess oligodendroglial density after genetical reduction of regulated vesicle release in LV and LVI Snap25 cKOs. As done by Gibson and Xiao after optogenetic stimulation of the motor cortex or self-training of a new motor skill, I will focus on one hand on the area where neuronal cell bodies are located that are affected by altered neuronal activity. On the other hand, I will investigate the striatum, an area where LV and LVI fibres project through (Gibson et al. 2014; Xiao et al. 2017). The reasoning for choosing these two regions was that there might be regional differences in oligodendroglial response to altered neuronal activity. OPC mitogens can be released by cell bodies as well as from axons and might be influenced by changes in neuronal activity (Fruttiger, Calver, and Richardson 2000). Furthermore, differences could be explained by varying origins of OPCs or different response to mitogens. This could then result in distinct responses to activity-regulating signals (Gibson et al. 2014; Yue 2006; Hill et al. 2013).

LV and LVI Snap25 cKO mice were sacrificed between P8 to P21 and the results compared to LV and LVI control animals. I will assess myelination by MBP mean fluorescence intensity while oligodendroglial density was assessed by Olig2 and CC1 quantification.

4.2 Results

4.2.1 Onset of myelination assessed by MBP in LV and LVI Snap25 cKOs

As described in the introduction of this chapter, cell-type specific markers can be used to differentiate cells and their developmental progress. Myelin basic protein is a marker for mature oligodendrocytes that form myelin. MBP is located in the cell processes where myelin membranes are formed. Therefore, analysis of myelin by MBP is done by fluorescence intensity measurement following immunohistochemistry rather than cell counting. Coronal brain sections from animals sacrificed at P8, P14 and P21 were examined for MBP immunoreactivity. Control and Snap25 cKO sections were stained simultaneously to ensure equal processing and imaged with identical settings. Age optimal settings were chosen, so that no signal overexposure occurred, and hence no comparisons between ages was undertaken.

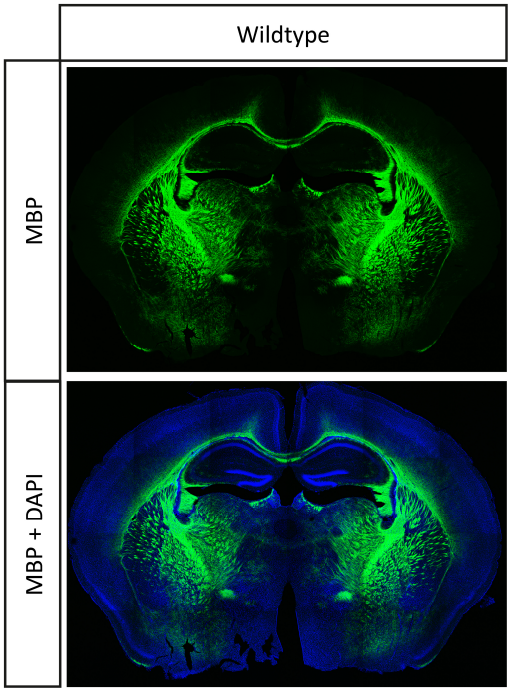


Figure 33: Myelin basic protein (MBP) immunoreactivity in a wildtype brain at P14 (medial cross section)

At P14, myelination assessed by MBP can be seen in major white matter tracts. The corpus callosum and the white matter tracts beneath the cerebral cortex are partially myelination. Additionally, deeper cortical layers start to get myelinated. Strong MBP signal can be detected in the internal capsule and the striatum as well as the anterior commissure. DAPI counterstain (lower panel) revealed the cytoarchitectonic boundaries of various structures, such as hippocampus, striatum, thalamus and cerebral cortex.

Around P7-P8, myelination starts in the internal capsule in the murine brain and continuously progresses during adolescence. P8 brains were used to assess onset of myelination and for observing progression of myelination during adolescence the timepoints P14 and P21 were analysed. Analysis was performed in two different regions: in the layer of the cortex where the cell bodies of LV and LVI Snap25 cKOs and controls were located as well as in the striatum, where their fibres project through.

4.2.1.1 Onset of myelination assessed by MBP immunoreactivity in LV Snap25 cKOs

Myelination starts in the murine brain after P7 and continuously progresses during adolescence until mature myelination is achieved in almost all brain regions between P45 and P60 (Baumann and Pham-Dinh 2001).

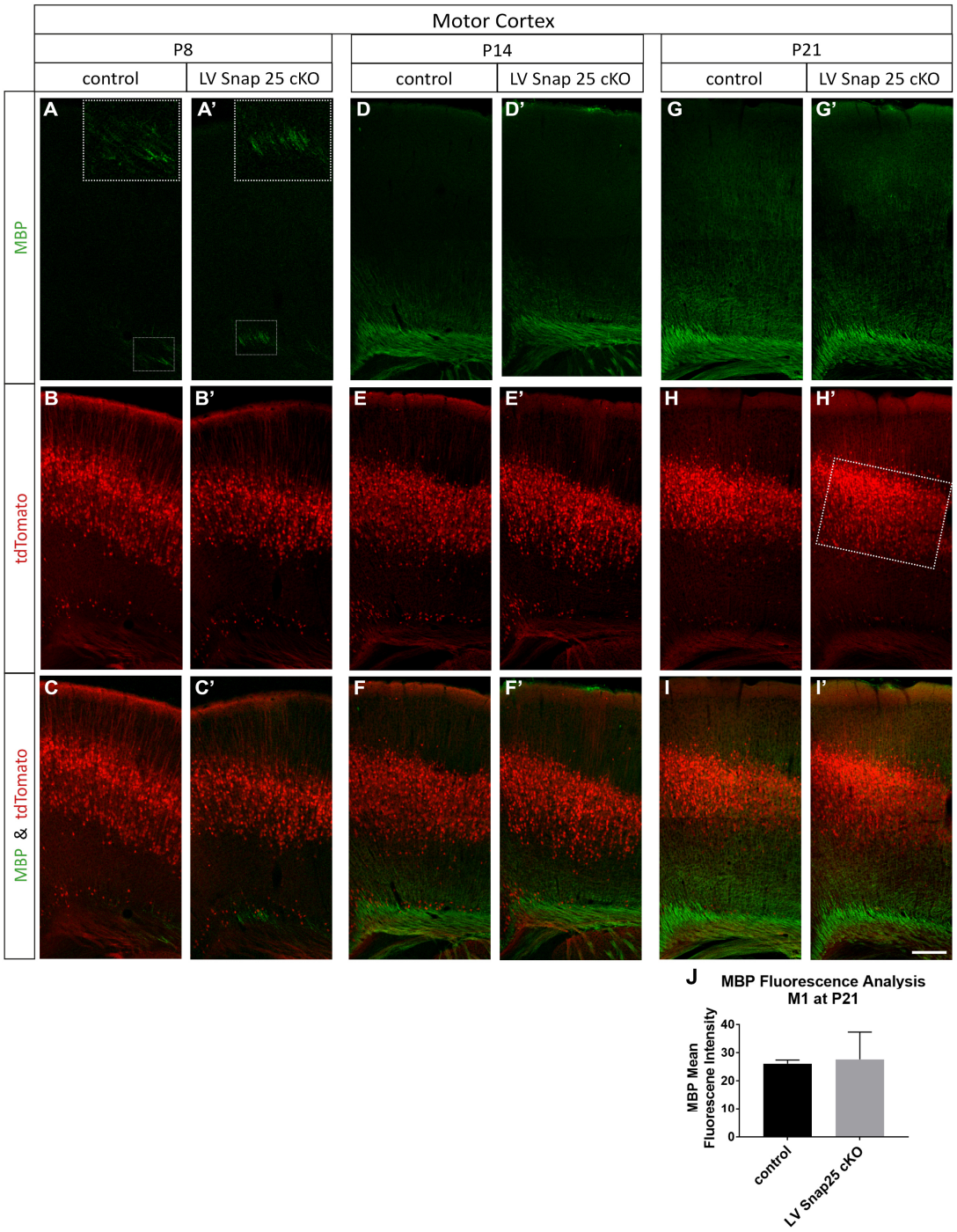


Figure 34: MBP immunoreactivity in LV Snap25 cKOs in M1 at P8, P14 and P21

A-A'). Myelin basic protein (MBP) immunoreactivity in the primary motor cortex (M1) in LV Snap25 cKOs and controls was only visible in the underlying white matter but not yet in LV at P8. White boxes indicate magnified area shown in the upper right corner. B-B') tdTomato positive LV cells in M1 of the cortex at P8 in LV Snap25 cKOs and controls. C-C') Overlay of tdTomato positive cells in cortical LV and MBP at P8 in both genotypes. D-D') Immunohistochemistry against mature oligodendrocyte marker myelin basic protein at P14 in LV Snap25 cKOs and controls showed MBP immunoreactivity spread into cortical LVI. E-E') tdTomato positive LV cells in M1 of the cortex at P14 in LV Snap25 cKOs and controls. F-F') Overlay of tdTomato positive cells and their projections in cortical LV and

MBP at P14 in both genotypes. G-G') MBP IHC at P21 in LV Snap25 cKOs and controls revealed detectable signal in LV. H-H') tdTomato positive LV cells in M1 of the cortex at P21 in LV Snap25 cKOs and controls. Box indicates quantification area. I-I') Overlay of tdTomato positive cells in cortical LV and MBP at P21 in both genotypes. J) Mean fluorescence intensity of MBP signal in LV of M1 is comparable at P21 between LV Snap25 cKOs (27.6 ± 9.72) and control (26.1 ± 1.29) (p= 0.700).
n=3/genotype, 2 sections/animal, unpaired t-test, values shown are mean ± SEM.
Scale bar: 200 µm

Figure 34 visualises the onset and progression of myelination in the motor cortex assessed by MBP from P8 to P21 in LV Snap25 cKOs and controls. At P8, MBP expression was weak and no MBP immunostaining detectable in the cortex yet, even though myelination had started in the white matter underlying the motor cortex (A-A'). By P14, more of the underlying white matter shows MBP immunoreactivity suggesting that this sector of white matter had been myelinated as well as parts of LVI, but myelination had not yet advanced as far into the cortex as to reach LV (D-D'). By P21, MBP can be detected in even more depth of the cortex including LV (G-G').

Since MBP immunoreactivity intensity should be assessed in LV and myelination had not reached this cortical area at P8 or P14, only P21 brains were used for MBP immunoreactivity intensity analysis in LV. For the analysis a box of the exact same size was drawn around LV in M1 that fitted the layer in all specimen examined.

The analysis showed that mean fluorescence intensity of MBP immunoreactivity signal in LV of M1 was comparable between LV Snap25 cKOs (27.6 ± 9.72) and control (26.1 ± 1.29) at P21 (p= 0.700).

Fibres from cell bodies located in LV of the cortex have long-range projections to subcortical areas. These projections extended through the striatum in large fibre fascicles where they were identifiable by tdTomato in LV controls and LV Snap25 cKOs and assessed for MBP immunoreactivity.

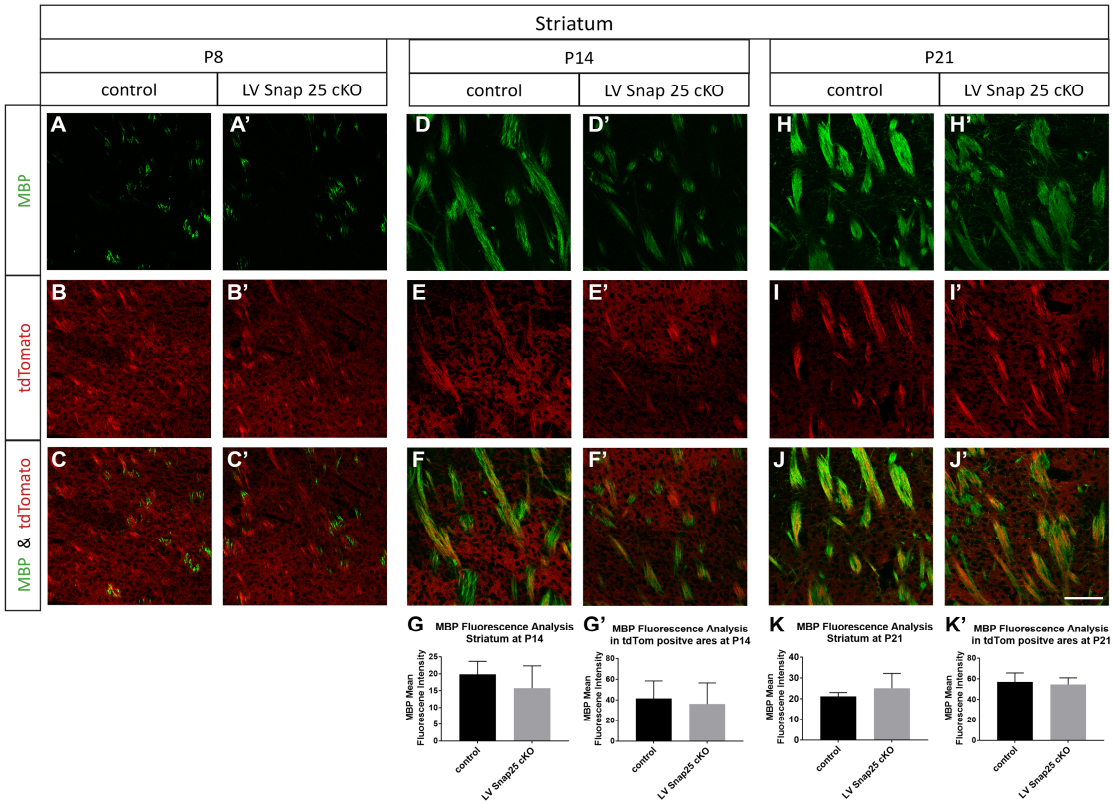


Figure 35: MBP immunoreactivity in striatal tissue of LV Snap25 cKOs and controls between P8 and P21

A-A') Signal of myelin basic protein IHC in the striatum at P8 in LV Snap25 cKOs. B-B') tdTomato positive fibres from LV cells projecting through the striatum at P8 in LV Snap25 cKOs and controls. C-C') Overlay of tdTomato positive fibres from LV cells and MBP positive areas at P8 in both genotypes. D-D') Immunohistochemistry against myelin basic protein at P14 in LV Snap25 cKOs and controls. E-E') LV tdTomato positive fibres in LV Snap25 cKOs and controls at P14. F-F') Overlay showing tdTomato positive in the striatum and MBP positive areas in both genotypes at P14. G) Overall mean fluorescence intensity of MBP immunoreactivity signal in the striatum at P14 in LV Snap25 cKOs (15.8 ± 6.6) was comparable to controls (19.8 ± 3.8) (p= 0.700). G') No difference seen in mean fluorescence intensity of MBP immunoreactivity in the tdTomato positive areas between LV Snap25 cKOs (36.3 ± 20.3) and controls (41.5 ± 17.02) (p= 0.700). H-H') MBP was visible in the striatum at P21 in LV Snap25 cKOs and controls. I-I') tdTomato positive fibres from LV cells at P21 in LV Snap25 cKOs and controls. J-J') Overlay of LV tdTomato positive fibre projections in striatal tissue and MBP immunopositive areas at P21 in both genotypes. K) Overall MBP mean fluorescence intensity in the striatum is similar at P21 in LV Snap25 cKOs (25.1 ± 7.0) when compared to controls (21.2 ± 1.9) (p> 0.999). K') Mean fluorescence intensity of MBP signal in tdTomato positive areas is comparable between LV Snap25 cKOs (54.6 ± 6.4) and control (57.0 ± 8.7) at P21 (p> 0.999).
n=3/genotype, 2-3 sections/animal, Mann-Whitney test, values shown are mean ± SEM.
Scale bar: 100 µm

In Figure 35 myelination in the striatum assessed by MBP immunoreactivity between P8 and P21 in LV Snap25 cKOs and controls is shown. The region of interest while imaging was chosen by using the whole field of view of the 20x magnification object. The view was set manually in the area with the highest density and intensity of tdTomato positive fibres independent of the signal in the green channel (MBP) for objectivity.

At P8, similar to M1, little MBP immunoreactivity was seen in the striatum (A-A'). By P14 myelination had progressed rapidly in the striatum covering most tdTomato positive fibre tracts (D-F'). By P21, all tdTomato positive fibre tracts were also MBP positive (H-J'). Quantitative analysis of MBP immunoreactivity was done at P14 and P21 in whole field of view as well as only in tdTomato positive areas to compare specific effects of affected neurons (G-G', K-K'). No difference was observed in the area that was covered by tdTomato positive fibres at P14 in the striatum (control: 0.0012 mm^2 ± 0.0004, cKO: 0.0006 mm^2 ± 0.0002) and P21 (control: 0.0009 mm^2 ± 0.0003, cKO: 0.0009 mm^2 ± 0.0001) between LV Snap25 cKOs and controls (P14: p= 0.457, P21: p= >0.9999).

At P14, there was neither a difference in overall mean fluorescence intensity of MBP immunoreactivity in LV Snap25 cKOs (15.8) compared to controls (19.7) nor in tdTomato positive areas only (G-G'). Similar to observations at P14, at P21 there was no difference in the overall mean fluorescence intensity or in the mean fluorescence intensity in tdTomato positive areas only (K-K').

In summary, no significant difference was found between controls and LV Snap25 cKOs from P8 to P21 in mean MBP immunoreactivity fluorescence intensity.

4.2.1.2 Onset of myelination assessed by MBP immunoreactivity in LVI Snap25 cKOs

Following my assesment of onset and progression of MBP immunoreactivity during murine development in LV Snap25 cKOs, LVI Snap25 cKOs were analysed in a similar manner.

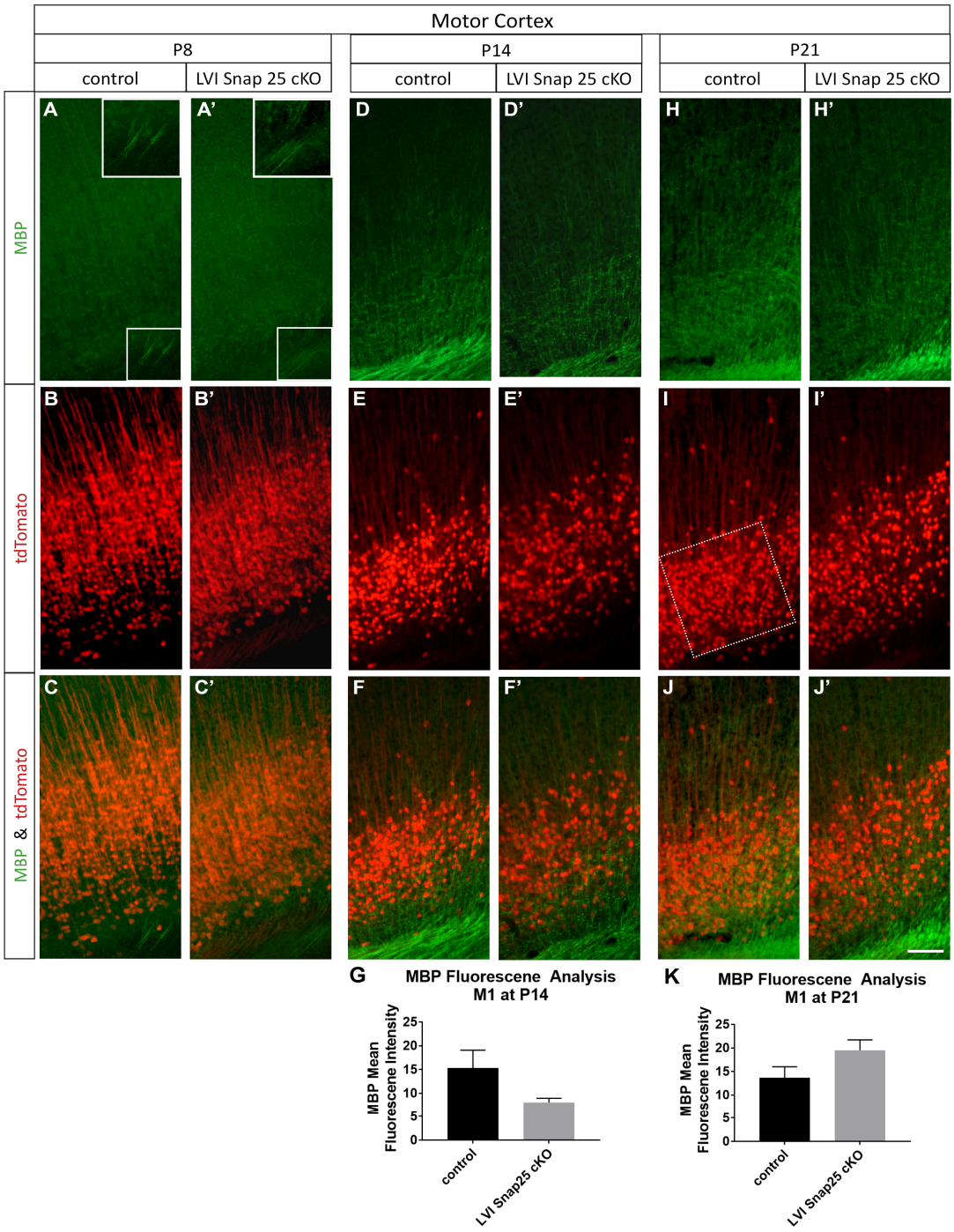


Figure 36: MBP immunoreactivity in LVI Snap25 cKOs and controls in M1 at P8, P14 and P21

A-A') MBP signal in the primary motor cortex (M1) at P8 in LVI Snap25 cKOs and controls was only detectable in the underlying white matter, and not within the cortex. White boxes indicate magnified area shown in the upper right corner. B-B') tdTomato positive cortical LVI cells at P8 in LVI Snap25 cKOs and controls. C-C') Overlay of tdTomato positive cells in LVI of the cortex and MBP in both genotypes at P8. D-D') MBP IHC at P14 in LVI Snap25 cKOs and controls showed MBP signal in LVI. E-E') tdTomato positive LVI cells in M1 of the cortex at P14 in LVI Snap25 cKOs and controls. F-F') Overlay of tdTomato positive cells in cortical LVI and MBP immunoreactivity at P14 in both genotypes. G) At P14, there was a trend towards a reduced mean fluorescence intensity signal of MBP in LVI Snap25 cKOs (8.1 ± 0.88) compared to controls (15.3 ± 3.75) (p= 0.200). H-H') Myelin basic protein at P21 in LVI Snap25 cKOs and controls. I-I') tdTomato positive LVI cells in M1 at P21 in LVI Snap25 cKOs and controls. Box indicates quantification area. J-J') Overlay of tdTomato positive cells in cortical LVI and MBP at P21 in both genotypes. K) Mean fluorescence intensity of MBP signal in LVI of M1 shows a trend towards an increase at P21 in LVI Snap25 cKOs (19.5 ± 2.2) when compared to controls (13.7 ± 2.3) (p= 0.400). n=3/genotype, 2-3 sections/animal, Mann-Whitney test, values shown are mean ± SEM. Scale bar: 100 µm

Figure 36 shows the onset and progression of myelination in the motor cortex assessed by MBP fluorescent immunoreactivity from P8 to P21 in LVI Snap25 cKOs. Similar to results in LV, only little MBP could be seen after immunohistochemistry at P8. There was no MBP immunoreactivity in the cortex yet, only in the white matter underlying the cortex (A-A'). By P14 more of the underlying white matter had been myelinated as well as LVI as visualised by MBP immunofluorescence (D-D'). By P21, myelination had reached even more depth within the cortex also reaching layers above the low LVI (G-G').

Since MBP immunoreactivity intensity should be assessed in LVI and myelination had not reached this cortical area at P8, only P14 and P21 brains were used for MBP intensity analysis in LVI. For the analysis a box of the exact same size was drawn around LVI in M1 that fitted the layer in all P14 or P21 specimen examined. The analysis showed a trend towards MBP mean immunofluorescence intensity being reduced in M1 of LVI Snap25 cKOs (8.1) compared to controls (15.3) at P14 (G) (p= 0.200). At P21, this trend dissapeard and LVI Snap25 cKOs (19.5) showed

a comparable mean fluorescence intensity compared to controls (13.7) (p= 0.400) (K).

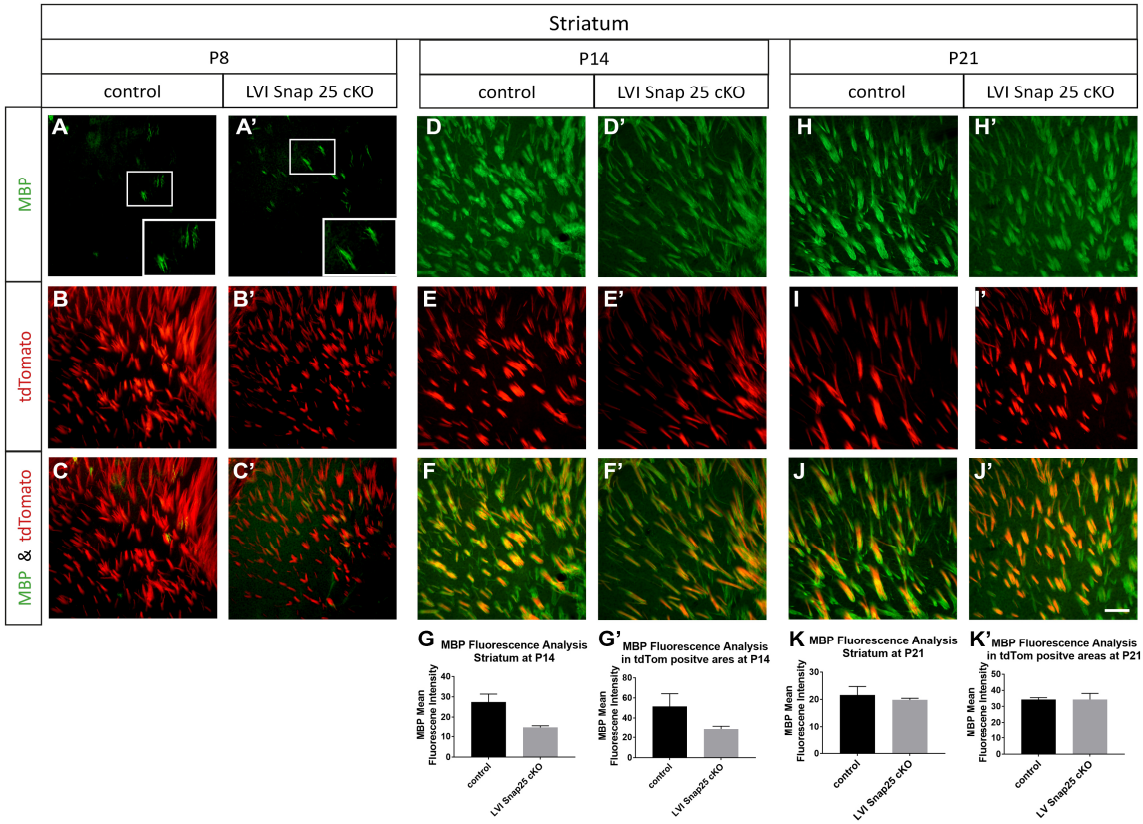


Figure 37: MBP immunoreactivity in the striatum at P8, P14 and P21 in LVI Snap25 cKOs and controls

A-A') IHC against myelin basic protein (MBP) in the striatum at P8 in LVI Snap25 cKOs and controls. White boxes indicate magnified area shown in the lower right corner. B-B') tdTomato positive fibres from LVI cells projecting through the striatum at P8 in LVI Snap25 cKOs and controls. C-C') Overlay of tdTomato positive fibres from LVI cells and MBP immunopositive areas at P8 in both genotypes. D-D') At P14 compared to P8, a more intense MBP immunosignal was detectable in LVI Snap25 cKOs and controls. E-E') tdTomato positive LVI fibres at P14 in LVI Snap25 cKOs and controls. F-F') Overlay of tdTomato positive fibres and MBP immunopositive areas at P14 in both genotypes. G) Overall mean fluorescence intensity of MBP immunoreactivity signal in the striatum was significantly reduced at P14 in LVI Snap25 cKOs (14.9 ± 0.82) compared to control (27.4 ± 3.97) (p= 0.100). G') In LVI Snap25 cKOs (29.1 ± 2.7) there was a trend towards a reduced mean fluorescence intensity signal of MBP in tdTomato positive areas of the striatum at P14 compared to control (51.5 ± 12.7) (p= 0.200). H-H') Myelin basic protein immunoreactivity at P21 in LVI Snap25 cKOs and controls. I-I') Signal of tdTomato positive fibres from LVI cells at P21 in LVI Snap25 cKOs and controls. J-J') Overlay of tdTomato positive fibres from LVI cells and MBP immunopositive areas at P21 in both genotypes. K) Overall mean fluorescence intensity of MBP immunoreactivity signal in the striatum was comparable at P21 between LVI Snap25 cKOs (19.8 ± 0.61) and control (21.6 ± 3.2) (p> 0.999). K') Mean fluorescence intensity of MBP immunosignal in the tdTomato positive

areas of the striatum was similar at P21 between LVI Snap25 cKOs (34.3 ± 3.9) and controls (34.2 ± 1.3) (p> 0.999).
n=3/genotype, 2 sections/animal, Mann-Whitney t-test, values shown are mean ± SEM.
Scale bar: 500 µm

As mentioned before, little MBP immunoreactivity could be detected in the striatum at P8. Figure 37 shows the onset of myelation as indicated by MBP immunoreactivity in the striatum at P8 and the progression to P14 and P21 in LVI Snap25 cKOs and controls. By P14 and P21, myelination had progressed rapidly in the striatum (D-F', H-J'). The region of interest is the whole field of view of the 20x object of the confocal microscope. The area set manually where the highest density and intensity of thTomato positive fibres were independent of the signal in the green channel (MBP) to exclude bias.

Since there was only little MBP immunoreactivity in the striatum at P8, only P14 and P21 brains were analysed for MBP immunoreactivity quantitatively (G-G', K-K'). MBP fluorescent immunoreactivity analysis was done in whole field of view as well as only in tdTomato positive areas. At P14 a significicant difference was observed in the area covered by tdTomato positive fibres in the striatum but not at P21 (P21 control: 0.012 mm^2 ± 0.0024, cKO: 0.009 mm^2 ± 0.0024, p= 0.629). LVI Snap25 cKOs had a smaller area covered by tdTomato postive fibres (0.007 mm^2 ± 0.0006) compared to controls at P14 (0.01 mm^2 ± 0.0007) (p= 0.027).

At P14, MBP mean immunofluorescence analysis showed a reduction in LVI Snap25 cKOs (14.9) compared to controls (27.4) (p= 0.100) (G). This trend persisted when analysing the MBP immunosignal in tdTomato positive areas, however, it did not reach significance (LV Snap25 cKOs: 29.1, controls: 51.5, p= 0.200) (G'). At P21 the trend disappeared and MBP mean immunofluorescence

intensity values were comparable between LVI Snap25 cKOs and controls overall as well as in tdTomato positive areas only (K-K').

4.2.2 Comparison of myelination in the Corpus Callosum around LV Snap25 cKO and Kir2.1 electroporated fibres measured by MBP immunoreactivity

After assessing myelination around LV and LVI Snap25 cKOs, myelination around Kir2.1 and MutKir2.1 as controls was examined. Animals were electroporated at E13.5 to target the cohort of cells that are generated for the deeper cortical layers to match the Cre expressing LV and LVI mouse lines (Rbp4-Cre and Ntsr1-Cre) that were used for the conditional Snap25 KO experiments.

Myelination starts in the corpus callosum (CC) around P12. However, no MBP immunoreactivity at P12 in the area of electroporated fibres in controls or in experimental animals were detected. Therefore, pups were sacrificed at P14 when myelin in the corpus callosum was visualisable via MBP immunohistochemistry in areas where tdTomato positive fibres from electroporated cells were also apparent. Since tdTomato positive LV fibres were also strongly visualisable in the corpus callosum, their myelination was also assessed by MBP immunoreactivity at P14 for comparison. tdTomato signal in the striatum of electroporated animals of both genotypes was too sparse to be used for quantitative analysis. Both methods used here reduced neuronal activity genetically but in different ways. Introducing Kir2.1 in neuronal cells reduces electrical excitation non-reversibly and chronically by increasing the potassium leakage current as well as spontaneous activity (Burrone, Byrne, and Murthy 2002; Johns et al. 1999; Hagihara et al. 2015). In the Snap25 cKO mouse lines, electrical excitation had not been altered but regulated synaptic vesicle release was reduced.

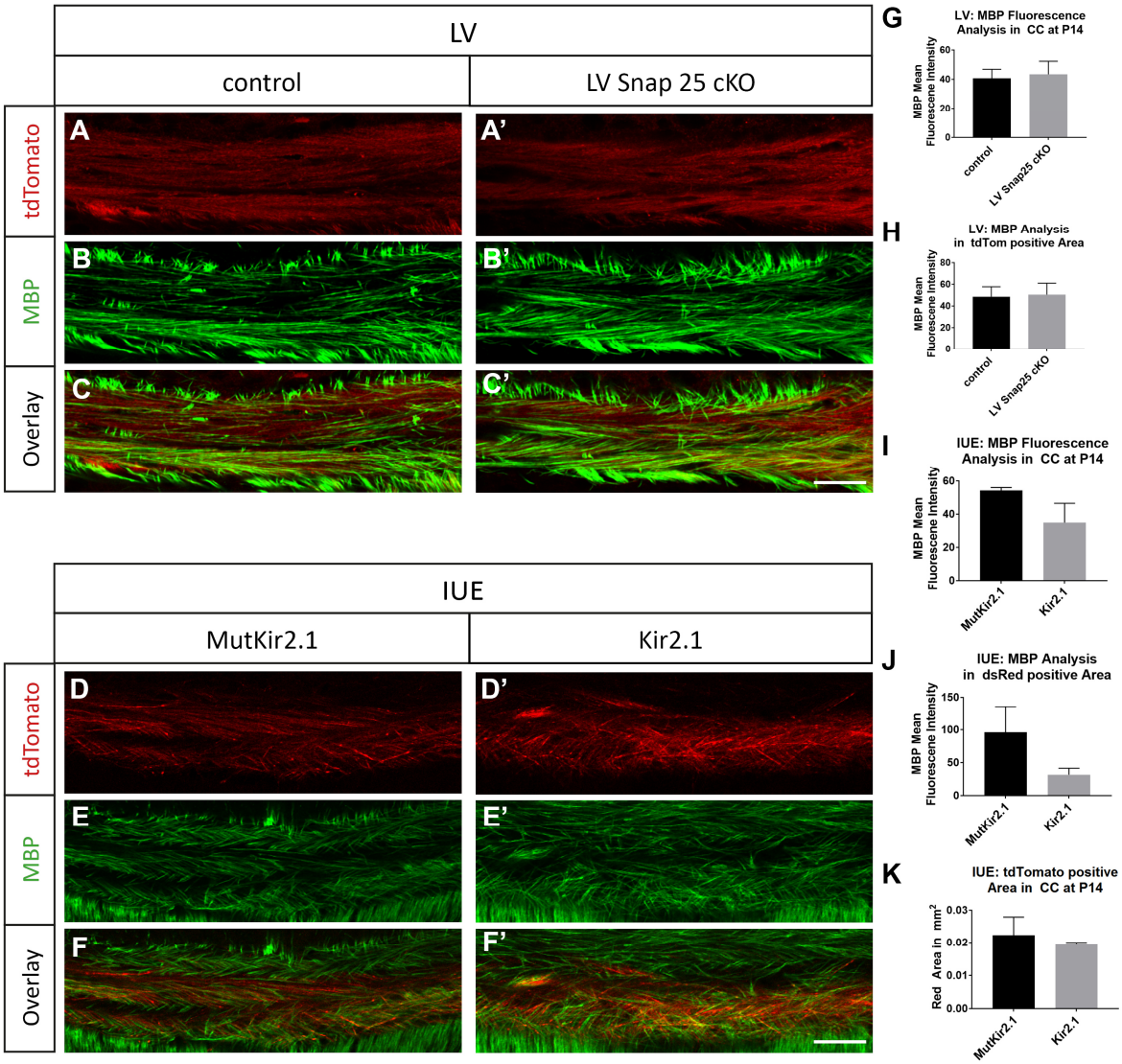


Figure 38: MBP immunoreactivity in LV Snap25 cKOs and LV controls as well as Kir2.1 and MutKir2.1 electroporations in the corpus callosum (CC) at P14

A-A') tdTomato positive fibres from LV cells projecting through the corpus callosum in LV Snap25 cKOs and controls. B-B') Immunohistochemistry against mature oligodendrocyte marker myelin basic protein (MBP) at P14 in LVI Snap25 cKOs and controls. C-C') Overlay of tdTomato positive fibres from LV cells projecting through the corpus callosum and MBP positive areas in both genotypes. D-D') Immunohistochemistry against tdTomato to identify electroporated fibres from MutKir2.1 and Kir2.1 electroporated cells at E13.5. E-E') MBP IHC after IUE with MutKir2.1 and Kir2.1. F-F') Overlay of tdTomato positive fibres from MutKir2.1 and Kir2.1 electroporated cells in the corpus callosum and MBP positive areas at P14. G) Overall mean fluorescence intensity of MBP signal was similar between LV Snap25 cKOs (43.5 ± 8.9) and controls (40.8 ± 6.1) (p> 0.999). H) MBP mean fluorescence intensity in tdTomato positive areas was comparable between LV Snap25 cKOs (50.5 10.51) and controls (48.5 ± 9.3) (p> 0.999). I) Overall MBP mean fluorescence intensity in Kir2.1 electroporated fibres (34.9 ± 11.6) was similar to MutKir2.1 (54.3 ± 1.7) (p= 0.500). J) The trend in reduced MBP mean fluorescence intensity persists in tdTomato positive areas in Kir2.1 electroporated fibres (31.8 ± 9.7) compared to MutKir2.1 (96.2 ± 38.4) at

P14 (p= 0.100). K) tdTomato positive area in the corpus callosum of MutKir2.1 (0.022 mm^2 ± 0.0056) and Kir2.1 (0.20 mm^2 ± 0.0003) electroporated fibres was similar between groups (p= 0.600).
n=3/genotype, 2 sections/animal, Mann-Whitney test, values shown are mean ± SEM.
Scale bar: 50 µm

In Figure 38 A-C' MBP as well as tdTomato immnunopositive fibres in the corpus callosum of LV Snap25 cKOs and controls are shown at P14. Analysis of MBP mean immunofluorescence intensity revealed no difference between genotypes in the corpus callosum (LV Snap25 cKO: 43.5, control: 40.8, p> 0.999) (G). If only MBP immunofluorescence signal was considered that was within tdTomato positive area, the same result was obtained (LV Snap25 cKO: 50.5, control: 48.5, p> 0.999) (H).

Figure 38 D-F' shows MBP IHC as well as tdTomato signal in the corpus callosum at P14 after IUE of MutKir2.1 and Kir2.1 at E13.5. Similar to results with LV Snap25 cKOs, in Kir2.1 electroporated animals (34.9) no difference between genotypes in the corpus callosum was observed in MBP mean immunofluorescence compared to MutKir2.1 control electroporations (54.3, p= 0.500) (I). When MBP in tdTomato positive areas only was considered a trend appeared towards less MBP in Kir2.1 electroporations (31.8) compared to MutKir2.1 (96.2) (p= 0.100). To compare if electroporations were equal between plasmids, the tdTomato positive area in the corpus callosum was measured. The results indicated that there was no difference between Kir2.1 (0.20mm^2) and MutKir2.1 (0.022mm^2) electroporated fibres in the corpus callosum (p= 0.600).

In summary, studying the onset and progression of myelination in LV and LVI Snap25 cKOs, did not reveal a major phenotype in both lines. However, in LVI

Snap25 cKOs there was a transient trend towards less MBP in the striatum compared to controls. MBP immunoreactivity was analysed in M1 the LVI lines from P14 onwards but only at P21 in the LV lines since myelination did not yet take place in cortical LV at P14. At P8 no MBP immunoreactivity was observed in the cortex of either of the two lines, but only in the underlaying white matter.

Myelination of fibres in the CC when neuronal activity was reduced, either through the lack of Snap25 or by overexpression of Kir2.1, led to no significant changes between experimental and control conditions. However, when IUEs were analysed, a trend towards less MBP immunoreactivity was observed in tdTomato positive areas.

4.2.3 Expression of oligodendrocyte lineage markers in LV and LVI Snap25 cKO

Cell-type specific markers can be used to distinguish cells and their developmental progress. Here, Olig2 and CC1 as markers of the oligodendrocyte lineage were used to quantify OPCs and pre-oligodendrocytes as well as mature oligodendrocytes. As such, immunohistochemistry (IHC) on coronal brain sections was performed from animals sacrificed at P8 and P21. Time points were chosen to either capture onset of myelination at P8 or track progress of myelination during adolescence (P21).

Marker expression was studied in the layer of the cortex where cell bodies from LV or LVI Snap25 cKOs and controls were located. In addition, the striatum was analysed, where LV and LVI fibres project through.

The region of interest was chosen in M1 as well as the striatum in all mouse lines through the whole field of view of the 20x confocal objective. In M1, the area was chosen so that the layer is in the middle of the field of view. In the striatum the region of interest was chosen in a similar way as done before when myelination itself was examined. In the red channel (tdTomato) the area of highest fibre density and intensity was searched for to exclude bias towards observations in the green channel (MBP).

4.2.3.1 Expression of Olig2 and CC1 in LV Snap25 cKOs

In order to examine Olig2 and CC1 expression in the motor cortex and the striatum of LV Snap25 cKOs compared to controls, immunohistochemistry was performed, and positively stained cells were counted from confocal images for cell density comparison. At P8, counting was done automatically in cell profiler for Olig2 (no

CC1 quantification at P8) whereas at P21, counting was conducted manually for Olig2 as well as for CC1.

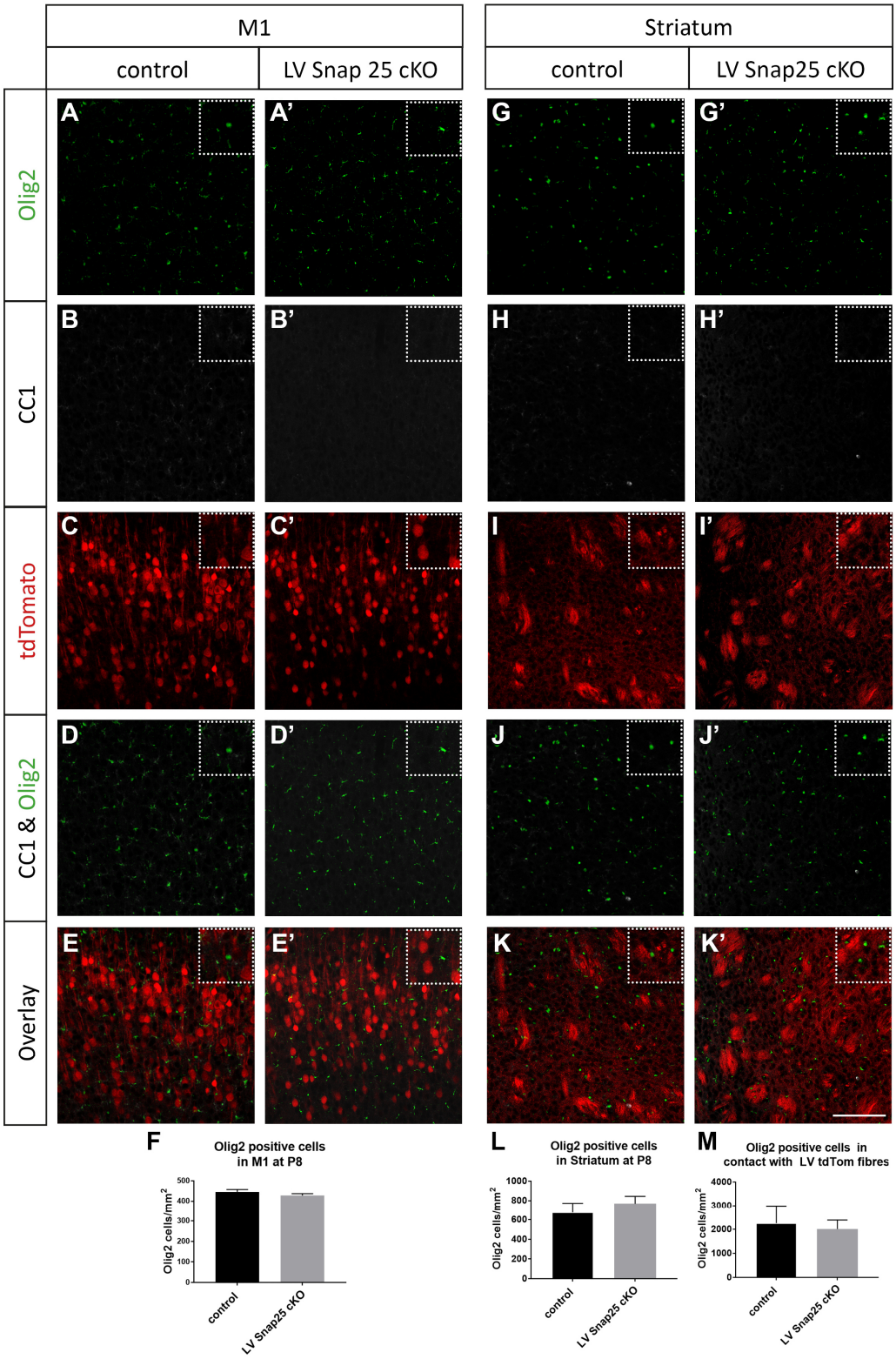
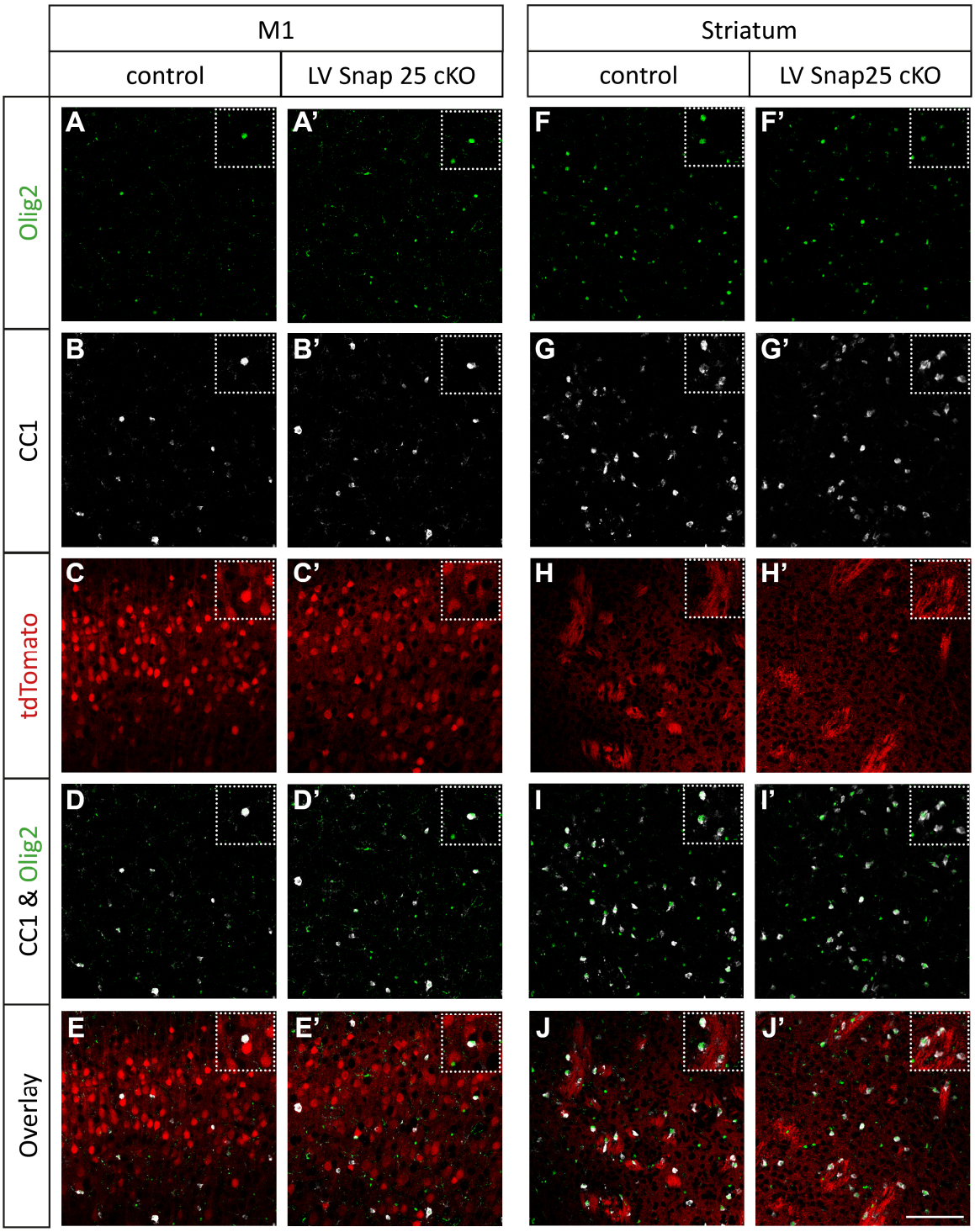


Figure 39: Expression of oligodendroglial markers Olig2 and CC1 in LV Snap25 cKOs at P8 in M1 and striatum

A-A') Immunohistochemistry against oligodendroglial lineage marker Olig2 in M1 revealed high immunoreactivity in controls and LV Snap25 cKO. B-B') Only very few CC1 positive cells were detected by IHC in M1 in both genotypes at P8. C-C') tdTomato positive cells in LV of the cortex. D-D') Overlay of CC1 and Olig2 positive cells. E-E') Overlay of tdTomato positive LV fibres, CC1 and Olig2 in LV Snap25 cKOs as well as controls. F) The density of Olig2 positive cells in M1 of LV Snap25 cKOs (428 cells/mm^2 ± 9) was comparable to the cell density in controls (446 cells/mm^2 ± 11) (p= 0.400). G-G') Olig2 IHC in the striatum revealed high density in controls and LVI Snap25 cKO. H-H') The mature oligodendrocyte marker CC1 was rarely detectable in the striatum in both genotypes at P8. I-I') tdTomato positive fibres projecting from LVI through the striatum to subcortical areas in both conditions. J-J') The overlay illustrated that there were no CC1 and Olig2 positive cells detected in the striatum in controls as well as LVI Snap25 cKOs. K-K') Overlay of tdTomato positive LV fibres, CC1 and Olig2 in LV Snap25 cKOs as well as controls. L) There was no difference in Olig2 positive cells in the striatum of LV Snap25 cKOs (767.5 cells/mm^2 ± 77.0) compared to controls (674.8 cells/mm^2 ± 97.2) (p= 0.700). M) There was also no difference if only cells were considered which were in contact with tdTomato positive LV fibres projecting through the striatum (LV Snap25 cKO: 2008 cells/mm^2 ± 377, controls: 2253 cells/mm^2 ± 738, p> 0.999).
White boxes show magnifications of single cells. n=3/genotype, 2-3 sections/animal counted, Mann-Whitney test, values shown are mean ± SEM.
Scale bar: 100 µm

Figure 39 shows the immunoreactivity of the oligodendrocyte lineage markers Olig2 and CC1 in M1 as well as the striatum at P8 of LV Snap25 cKOs compared to controls. Only very few CC1 positively stained cells were detected by IHC in M1 and striatum upon start of myelination at P8. Consequently, no CC1 quantification at P8 was conducted. In contrast, Olig2 was already detected by P8 (A-A' and F-F'). Comparison of Olig2 positive cells in LV Snap25 cKOs compared to controls did not show a significant difference in cell density at P8 (F, L, M). This applies for both, M1 and the striatum, where total cell density was analysed as well as cells that were in contact with LV tdTomato positive fibres projecting trough the striatum (K-K'). In M1, the cell density in controls (446 cells/mm^2) was comparable to LV Snap25 cKOs (428 cells/mm^2) (p= 0.400). There were comparable Olig2 positive cells (767.5 cells/mm^2) in the striatum of LV Snap25 cKOs and in controls (674.8 cells/mm^2) (p= 0.700). No difference was observed if only cells are considered

which were in contact with tdTomato positive LV fibres projecting through the striatum (LV Snap25 cKO: 2008 cells/mm^2, controls 2253 cells/mm^2, p> 0.999). The higher densities in red areas compared with overall image density suggest that Olig2 positive cells accumulate in tdTomato positive fibre areas.



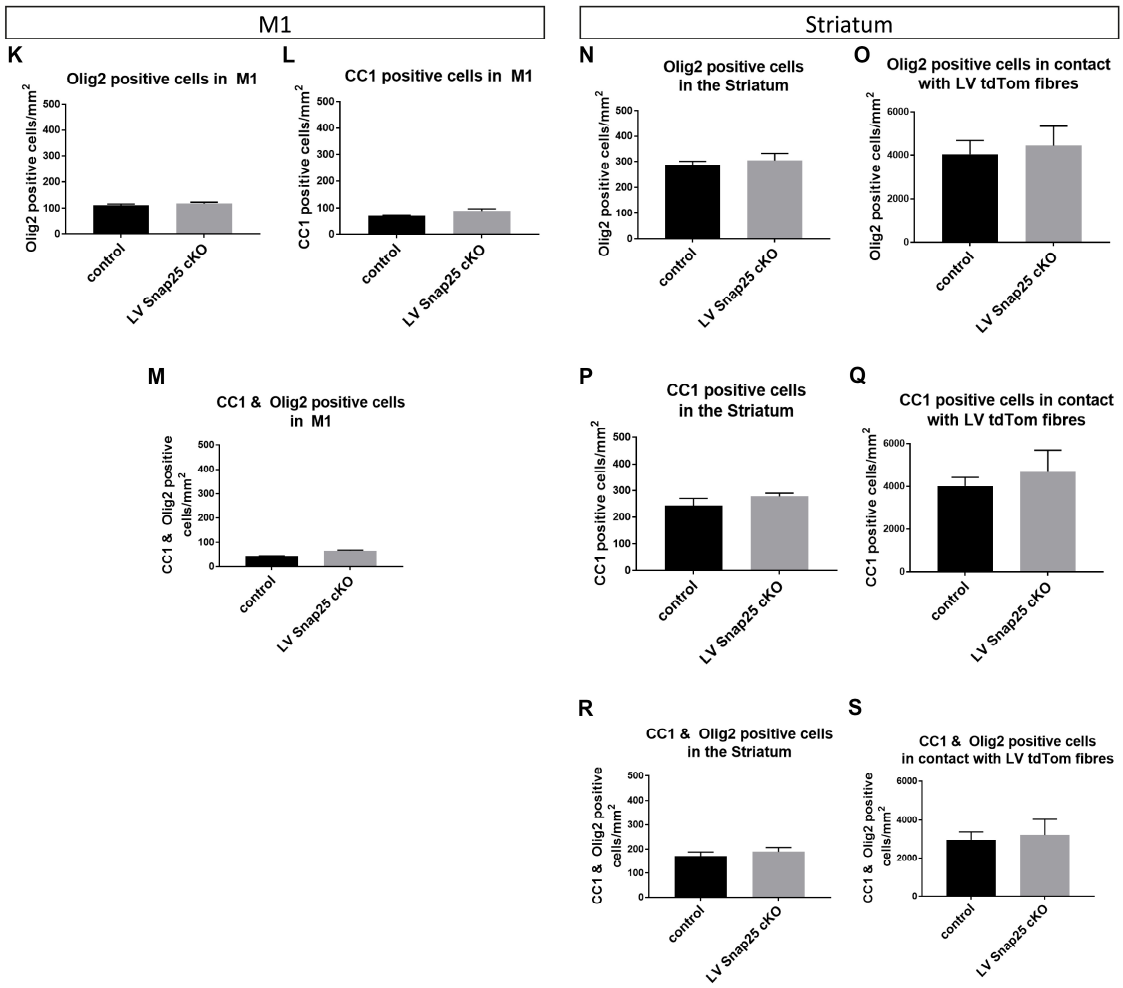


Figure 40: Expression of oligodendroglial markers Olig2 and CC1 in LV Snap25 cKOs at P21 in M1 and striatum

A-A') Visualisation of oligodendroglial lineage marker Olig2 in M1 of controls and LV Snap25 cKO by IHC. B-B') Immunohistochemistry against mature oligodendrocyte marker CC1 in M1 of both genotypes. C-C') Rbp4-Cre positive cells expressing tdTomato located in LV of the cortex. D-D') Double positive cells for CC1 and Olig2 in M1 of LV Snap25 cKOs and controls. E-E') Overlay of tdTomato positive LV cells, CC1 and Olig2 in LV Snap25 cKOs as well as controls. F-F') Olig2 IHC in the striatum revealed higher marker density than seen in M1 in controls as well as LVI Snap25 cKO at P21. G-G') IHC against CC1 also showed increased CC1 positive cells in the striatum compared to M1 in both genotypes at. H-H') tdTomato positive fibres projecting from LV in the striatum of both conditions. I-I') Double positive cells for CC1 and Olig2 in the striatum of LV Snap25 cKOs as well as controls. J-J') Overlay of tdTomato positive LV fibres, CC1 and Olig2 in LV Snap25 cKOs as well as controls. K) The density of Olig2 positive cells in M1 of LV Snap25 cKOs (112 cells/mm^2 ± 5) at P21 was comparable to the cell density in controls (118.3 cells/mm^2 ± 5) (p= 0.400). L) Despite a strong trend, CC1 positive cells in LV Snap25 cKOs were non-significantly increased (89.3 cells/mm^2 ± 8) with respect to controls (70 cells/mm^2 ± 1) (p= 0.100). M) CC1 positive cells which were also Olig2 positive show an increase in LV Snap25 cKOs (66 cells/mm^2 ± 3) relatively to controls (44.3 cells/mm^2 ± 0.67), (p= 0.100). N) The density of Olig2 positive cells in the striatum was comparable between LV Snap25 cKOs (304.7 cells/mm^2 ± 27) and controls (286.7 cells/mm^2 ± 14) (p= 0.600). O)

Density of Olig2 positive cells in the striatum contacting tdTomato positive LV fibres at P21 were comparable between genotypes (control: 4041 cells/mm^2 ± 637.3, LV Snap25 cKO: 4443 cells/mm^2 ± 893) without a significant difference (p> 0.999). P) CC1 positive cell density in Snap25 cKOs (278.3 cells/mm^2 ± 12) was comparable to controls (243.3 cells/mm^2 ± 28) in the striatum (p= 0.400). Q) CC1 positive cells in proximity to tdTomato positive LV fibres were similar in Snap25 cKOs (4680 cells/mm^2 ± 1019) compared to controls (4020 cells/mm^2 ± 408) in the striatum (p= 0.700). R) In contrast to M1, no significant difference in double positive cells for CC1 and Olig2 in LV Snap25 cKOs (189.7 cells/mm^2 ± 167) and controls (171 cells/mm^2 ± 18), was detected in the striatum (p= 0.500). S) Double positive CC1 and Olig2 cells in visible contact with LV tdTomato positive fibres projection through the striatum were similar in LV Snap25 cKOs (3211 cells/mm^2 ± 827) compared to controls (2959 cells/mm^2 ± 417) (p= 0.700).
White boxes show magnifications of single cells. n=3/genotype, 2 sections/animal counted, Mann-Whitney test, values shown are mean ± SEM.
Scale bar: 100 µm

To assess cell density of the oligodendroglial lineage at adolescence Olig2 as well as CC1 positive cells were analysed at P21. Similar to P8, analysis was performed in two different regions: LV of the motor cortex where cell bodies are located and the striatum where the axon of these cells project through.

Figure 40 shows the expression of the oligodendrocyte lineage markers Olig2 and CC1 in M1 as well as the striatum at P21 of LV Snap25 cKOs compared to controls. Contrary to P8, there were CC1 (B-B' and G-G') additionally to Olig2 (A-A' and F-F') positive cells detectable in both the motor cortex and the striatum.

Neither the comparison of Olig2 positively stained cells in M1 of LV Snap25 cKOs compared to controls revealed a significant difference in cell density at P21 (K) nor to comparison of CC1 cells (L). However, for CC1, a trend towards increased density in LV Snap25 cKOs is detectable (p= 0.100). Subsequent, cell density of cells which are positive for CC1 as well as Olig2 were also increased in LV Snap25 cKOs (66 cells/mm^2) compared to controls (44 cells/mm^2) (p= 0.100).

At P21 in the striatum, there was no difference in density of Olig2 positive cells in LV Snap25 cKOs (304.7 cells/mm^2) compared to controls (286.7 cells/mm^2). Olig2

positive cells in the striatum that were in close proximity to tdTomato positive LV fibres at P21 were relatively similar between genotypes. Similar to the density of Olig2 cells, density of CC1 positive cells was comparable in Snap25 cKOs (278.3 cells/mm^2) to controls (243.3 cells/mm^2) in the striatum. CC1 positive cells in contact with tdTomato positive LV fibres was also unchanged in Snap25 cKOs (4680 cells/mm^2) compared to controls (4020 cells/mm^2). In contrast to M1, there was no significant difference in CC1 and Olig2 double positively stained cells in LV Snap25 cKOs and controls located in the striatum. There was also no difference when only cells were included that were in visible contact with LV tdTomato positive fibres projecting through the striatum. The density of double positive CC1 and Olig2 cells in LV Snap25 cKOs was 3211 cells/mm^2 compared to 2959 cells/mm^2 in controls ($p= 0.700$).

Comparison of the Olig2 immunoreactive cell density between M1 and striatum showed that the density is only half as much in M1 compared to the striatum at P8 as well as P21. When comparing the CC1 density between M1 and striatum at P21 an over 3-fold higher density in the striatum can be observed than in M1. At P21, the density of double positive Olig2 and CC1 positive cells was 3.8-fold and 2.8-fold higher in the striatum than in M1 for controls and LV Snap25 cKOs respectively.

Comparison of the Olig2 cell density at P8 and P21 demonstrated that Olig2 density decreased between these ages. In the motor cortex, cell density did reduce approximately 3.5-fold from over 400 cells/mm^2 to circa 115 cells/mm^2. The same trend was observed in the striatum where Olig2 cell density drops approximately 2.5-fold in both genotypes, from 767.5 cells/mm^2 in LV Snap25 cKOs to 304.7

cells/mm^2 and from 674.8 cells/mm^2 to 286.7 cells/mm^2 in controls. In contrast, the density of Olig2 positive cells in contact with LV tdTomato positive fibres increased roughly 2-fold from P8 to P21 from around 2000 cells/mm^2 to circa 4000 cells/mm^2.

4.2.3.2 Expression of Olig2 and CC1 in LVI Snap25 cKOs

Density of Olig2 and CC1 positive cells in the motor cortex as well as the striatum was also analysed in the deeper layer below LV, in LVI Snap25 cKOs compared to controls at P8 and P21.

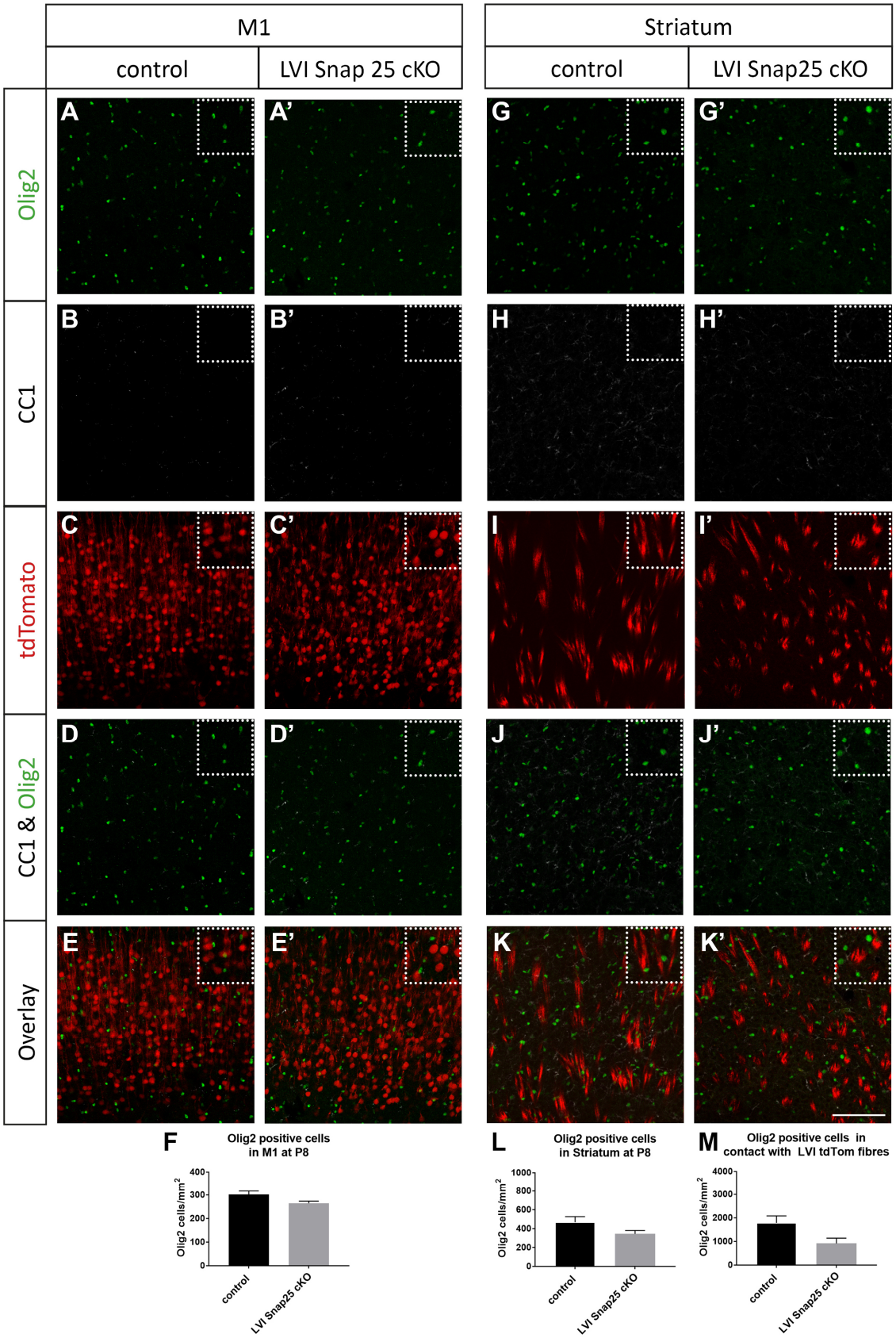
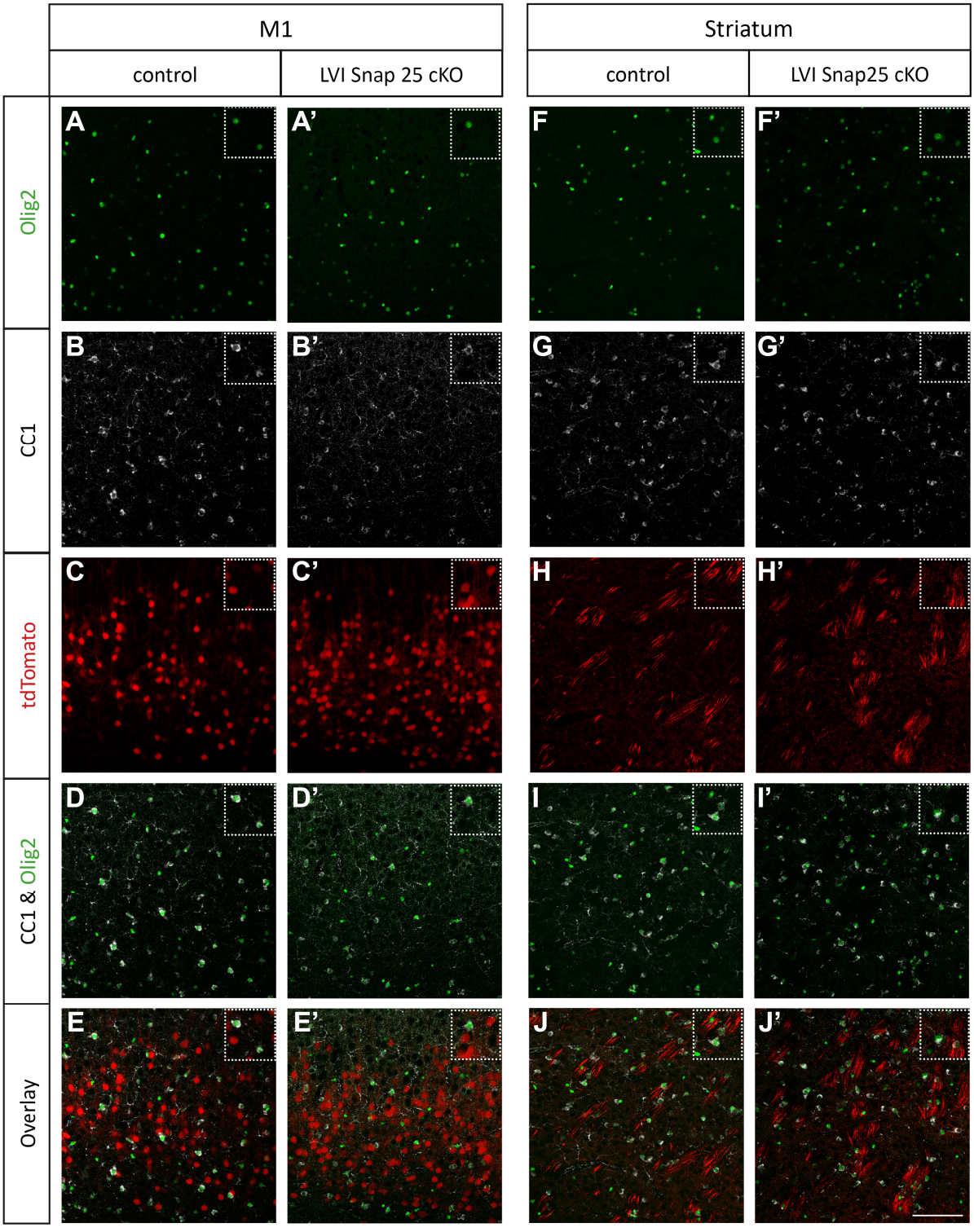


Figure 41: Immunoreactivity of Olig2 and CC1 in LVI Snap25 cKOs at P8 in the striatum

A-A') IHC against oligodendroglial lineage marker Olig2 in M1 revealed high density in controls and LV Snap25 cKO. B-B') Mature oligodendrocyte marker CC1 showed hardly any CC1 positive cells in the M1 in both genotypes at P8. C-C') tdTomato positive cells located in cortical LV. D-D') Overlay of CC1 and Olig2 positive cells. E-E') Overlay of tdTomato positive LV fibres, CC1 and Olig2 in LV Snap25 cKOs as well as controls. F) The density analysis of Olig2 positive cells in M1 at P8 showed a trend towards slightly less cells in of LV Snap25 cKOs (265 cells/mm^2 ± 9) compared to controls (302cells/mm^2 ± 15) (p= 0.200). G-G') In the striatum, the marker Olig2 was at high density in controls and LVI Snap25 cKO. H-H') After CC1 IHC, no CC1 positive cells were detected in the striatum in both genotypes at P8. I-I') tdTomato positive fibres projecting from LVI through the striatum to subcortical areas in both conditions. J-J') As seen in the overlay no CC1 and Olig2 positive cells were detectable since no CC1 positive cells were detected in the striatum in controls as well as LVI Snap25 cKOs. K-K') Overlay of tdTomato positive LVI fibres, CC1 and Olig2 in LVI Snap25 cKOs as well as controls. L) The analysis of Olig2 positive cells in LVI Snap25 cKOs demonstrated that cKOs had slightly less Olig2 positive cells (345 cells/mm^2 ± 35) in the striatum at P8 than controls (467.5 cells/mm^2 ± 59), (p= 0.100). M) Examination exclusively of Olig2 positive cells which were in contact with LVI tdTomato positive fibres projecting through the striatum revealed that with 917 ± 226 cells/mm^2 LVI Snap25 cKOs had less cells in contact with tdTomato positive LVI fibres than controls with 1788 ± 297 cells/mm^2 (p= 0.100).
White boxes show magnifications of single cells. n=3/genotype, 2-3 sections/animal, Mann-Whitney test, values shown are mean ± SEM.
Scale bar: 100 µm

Similar to the findings in the LV Snap25 cKOs and controls at P8, in LVI Snap25 cKOs and controls rarely any mature oligodendrocytes were detectable by CC1 immunohistochemistry (Figure 41, B-B' and G-G') but Olig2 positive cells (A-A', G-G'). Therefore, only Olig2 quantification at P8 was conducted in M1 and the striatum (F, L, M). Comparison of Olig2 positive cells in LVI Snap25 cKOs (265 cells/mm^2) compared to controls (302cells/mm^2) in M1 did not reveal a significant difference in abundance but a trend (p= 0.200). The analysis of Olig2 positive cells in the striatum of LVI Snap25 cKOs demonstrates that cKOs have slightly lower Olig2 positive cell density (345 cells/mm^2) than controls (467.5 cells/mm^2) (p= 0.100). Exclusive examination of Olig2 positive cells which were in contact with LVI tdTomato positive fibres projecting through the striatum (K-K') revealed that with

917.3 cells/mm^2 LVI Snap25 cKOs have fewer Olig2+ cells contacting tdTomato positive LVI fibres compared to controls (1788 cells/mm^2) (p= 0.100).



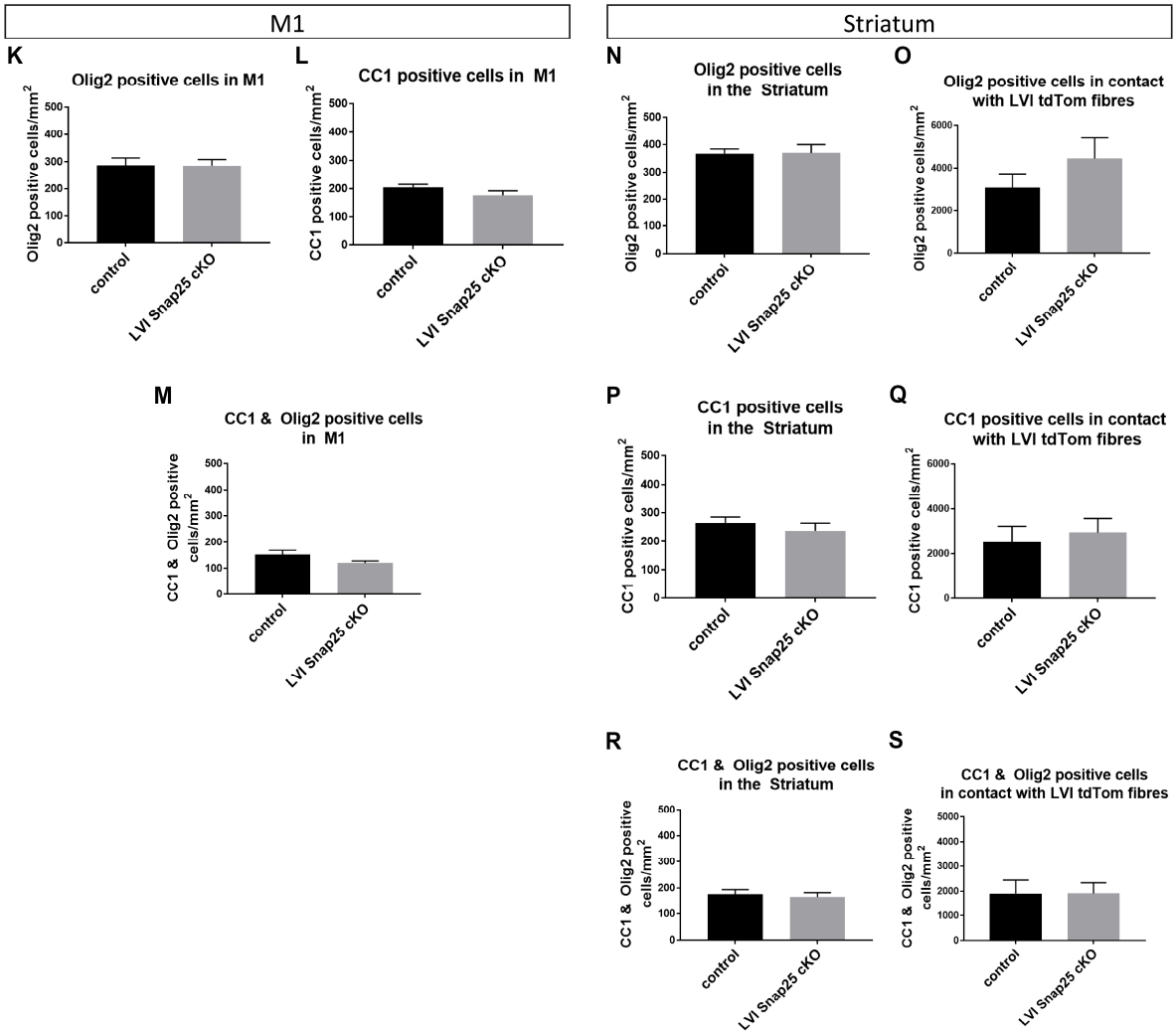


Figure 42: Immunoreactivity of Olig2 and CC1 in LVI Snap25 cKOs at P21 in M1 and striatum

A-A') Olig2 positive cells in M1 of controls and LVI Snap25 cKO. B-B') CC1 positively stained cells in M1 of both genotypes. C-C') Ntsr1-Cre positive cells expressing tdTomato located in LVI of the cortex. D-D') Double positive cells for CC1 and Olig2 in M1. E-E') Overlay of tdTomato positive LVI cells, CC1 and Olig2 in LVI Snap25 cKOs as well as controls. F-F') IHC against Olig2 in the striatum revealed higher density than in M1 in controls as well as LVI Snap25 cKO at P21. G-G') An increase in CC1 positive cell density was visible in the striatum compared to M1 in both genotypes. H-H') tdTomato positive fibres from LVI. I-I') Double positive cells for CC1 and Olig2 in the striatum of LVI Snap25 cKOs as well as controls. J-J') Overlay of tdTomato positive LVI fibres projecting from LVI through the striatum, CC1 and Olig2 in LVI Snap25 cKOs as well as controls. K) Analysis of Olig2 positive cells in M1 of Snap25 cKOs at P21 indicated that there is no difference to controls ($p > 0.999$). L) The density of CC1 positive cells in LVI Snap25 cKOs were (176.5 cells/mm^2 ± 16) comparable to controls (203.3 cells/mm^2 ± 12) ($p = 0.400$). M) CC1 positive cells which are also positive for Olig2 showed no significant difference between LVI Snap25 cKOs (120.3 cells/mm^2 ± 8) compared to controls (152 cells/mm^2 ± 17) ($p = 0.228$). N) Olig2 positive cells in the striatum were relatively similar in abundance for both genotypes without a significant difference ($p = 0.800$). O) There was no difference in Olig2

positive cells that were in close proximity with tdTomato positive LVI fibres in the striatum at P21 in LVI Snap25 cKOs (4449 cells/mm^2 ± 942) compared to controls (3073 cells/mm^2 ± 661) (p= 0.191). P) CC1 positive cells in Snap25 cKOs (237.8 cells/mm^2 ± 27) are comparable to controls (264.3 cells/mm^2 ± 22) in the striatum (p= 0.686). Q) No difference was observable in CC1 positive cells that were in contact with tdTomato positive LVI fibres in Snap25 cKOs (2690 ± 616 cells/mm^2) compared to controls (2507 cells/mm^2 ± 723) in the striatum (p= 0.413). R) In the striatum the density of double positive cells for CC1 and Olig2 was similar between genotypes (p= 0.686). S) The density of double positive CC1 and Olig2 that are in visible contact with LVI tdTomato positive fibres projecting through the striatum was comparable between genotypes (p= 0.886).
White boxes show magnifications of single cells. n=4/genotype, 2-3 sections/animal, Mann-Whitney test, values shown are mean ± SEM.
Scale bar: 100 µm

Like in LV Snap25 cKOs and controls at P21, CC1 can be detected in M1 as well as the striatum at P21 (Figure 42, B-B' and G-G') additionally to Olig2 positive cells (A-A' and F-F') in both genotypes. However, the density in M1 of cells which were positive for CC1 as well as Olig2 was not significantly increased in LVI Snap25 cKOs (120.3 cells/mm^2) compared to controls (152 cells/mm^2), (p= 0.228). The individual densities for Olig2 and CC1 in M1 were comparable between genotypes (K-L).

At P21 in the striatum, density of Olig2 positive cells is similar in LVI Snap25 cKOs (369.8 cells/mm^2) and in controls (369.8 cells/mm^2) in the whole field of view as well as Olig2 positive cells in contact with tdTomato positive LVI fibres (LVI Snap25 cKOs: 4449 cells/mm^2, control: 3073 cells/mm^2, (p= 0.191). The density of CC1 positive cells in the striatum was similar between genotypes overall as well as in LVI tdTomato positive areas. This was also visible for CC1 and Olig2 double positive cell densities.

Comparison of the Olig2 cell density between M1 and the striatum at P8 and P21 demonstrated that Olig2 density of LVI mouse lines in the striatum is approximately 1.3 times higher than in M1.

When comparing the CC1 density between M1 and striatum at P21 it is to see that the CC1 density in the striatum is 1.3 times higher than in M1 in both genotypes.

The density of Olig2 positive cells in contact with LVI tdTomato positive fibres increased in LVI controls around 2-fold from P8 to P21. In LVI Snap25 cKOs the increase was nearly 5-fold. At P21, the density of double positive Olig2 and CC1 positive cells in controls as well as LVI Snap25 cKOs was 1.5 times higher in the striatum than in M1.

To conclude, no major phenotype was observed when Olig2 and CC1 positive cells were examined in LV and LVI Snap25 cKOs compared to their respective controls during development (at P8 and P21).

At P8, rarely any CC1 positive cells (mature oligodendrocytes) were detected due to the just starting myelination in the brain. However, Olig2, as a marker for earlier stages, was already detected at P8 and showed declined expression by P21 in all conditions.

4.3 Discussion

In this chapter the onset of myelination as well as oligodendroglial density during development as well as adolescence was analysed in LV and LVI Snap25 cKOs. Furthermore, myelination in the corpus callosum in LV Snap25 cKOs as well as cortical cells electroporated with MutKir2.1 and Kir2.1 at E13.5 was explored at P14.

4.3.1 Onset of myelination under the influence of genetically reduced neuronal activity

Studies investigating how genetic reduction on neuronal activity influences myelination have been performed mostly in the zebrafish spinal cord (Hines et al. 2015; Mensch et al. 2015). *In vivo* studies of activity dependent myelination in mice focussed either on increasing neuronal activity or on sensory deprivation (Etxeberria et al. 2016; Gibson et al. 2014; Mitew et al. 2018; Sinclair et al. 2017). One study using genetic reduction of neurotransmitter examined the murine optic nerve. In this thesis, two different genetic methods were chosen to study the influence on activity dependent myelination in mice. Myelination was assessed around LV and LVI Snap25 cKOs as well as around Kir2.1 and MutKir2.1 by MBP mean immunofluorescence intensity analysis after immunohistochemistry. Myelin basic protein is located in the myelin membrane and thus provides a good marker for myelin, in contrast to CC1 and Olig2, which are expressed in the soma. Deshmukh and colleagues reported that MBP fluorescent measurements correlated with their results obtained by luxol fast blue stains in the autoimmune encephalomyelitis (EAE) model of relapsing-remitting multiple sclerosis validating MBP fluorescent measurements (Deshmukh et al. 2013). Similar to my method, they stained spinal cord sections with fluorescent antibodies against MBP followed

by confocal microscopy imaging for software evaluation which resulted in values indicating light intensity that were used for statistical analysis (Deshmukh et al. 2013 and personal correspondence with Brian Lawson, Scripps Research Institute).

Introducing Kir2.1 in neuronal cells reduces electrical excitation by increasing the potassium leakage current, leading to spontaneous neuronal activity (Burrone, Byrne, and Murthy 2002; Johns et al. 1999; Hagihara et al. 2015). In the Snap25 cKO mouse lines, electrical excitation was not altered but regulated synaptic vesicle release was reduced with spontaneous release still occurring.

4.3.1.1 Onset of myelination in LV and LVI Snap25 cKOs

In the murine CNS myelination onset takes place during the first postnatal week in the spinal cord and during the second postnatal week in the brain (Foran and Peterson 1992; Baumann and Pham-Dinh 2001). Given this timeframe, three timepoints at P8 (beginning of second postnatal week), P14 (beginning of third) and P21 (beginning of fourth) were selected for collection of coronal brain sections. Analysis was performed in two regions: in cortical layers LV and LVI (for LV and LVI Snap25 cKOs and controls respectively) and in the striatum, where they have projections. The rationale for this choice was that regional differences in activity dependent myelination might exist (Yue 2006; Hill et al. 2013; Fruttiger, Calver, and Richardson 2000). No comparison between ages P14 and P21 as well as LV and LVI lines were drawn as performed with Olig2 and CC1 cell counts. This was due to the reason that contrary to cell counts with absolute numbers to compare, MBP mean fluorescence intensity analysis after immunohistochemistry was performed on images taken with age optimal settings as well as optimal settings

for each individual immunohistochemistry. Brains of mice sacrificed at similar points in time were chosen since experiments in our laboratory showed that MBP intensity after immunohistochemistry was dependent on length of time between fixation and histological analysis.

Preliminary results showed no MBP staining at P6 in the areas of interest. In all genotypes first MBP signals were detected at P7, mostly at the junction of white matter underlying the cortex, striatum and internal capsule (data not shown). Therefore, MBP was assessed from P8 onward. At P8, slightly more MBP was visible in these areas without any obvious differences between LV and LVI Snap25 cKOs and their controls. MBP quantification at P8 was not conducted as cKO and control pups were taken from different litters due to the breeding scheme in place and birth determination is only precise within approximately 12 hours.

Myelination peaks during the third and fourth week of *ex utero* development (Foran and Peterson 1992). By P14 and P21, myelination in the striatum had progressed so far that most subcortical projections were strongly myelinated, including the majority of the tdTomato positive fibres from LV or LVI. In the cortex, myelination started from the underlying white matter and spread into the above cortex. Therefore, deeper cortical layers got myelinated first. By P14 myelination reached into LVI in M1 but not yet into upper LV. At P21, however, LV was myelinated. In M1 at P21, MBP mean fluorescence intensity analysis showed no difference between LV Snap25 cKOs and controls. Examination of the striatum showed no difference between genotypes at P14 or P21 when comparing LV Snap25 cKOs and controls.

In contrast, in LVI significant differences at P14 but not at P21 have been found. In M1 there was a trend towards less MBP intensity in LVI Snap25 cKOs versus controls without significance (p= 0.200). This trend vanished at P21 (p= 0.400).

When overall MBP mean fluorescence intensity was examined in the striatum at P14, LVI Snap25 cKOs had significantly less MBP immunoreactivity compared to controls when measured with a Mann-Whitney test for non-parametric samples (p=0.100) However, it is to keep in mind that this test can never become p< 0.100 with n= 3, a t-test would have indicated significance (p= 0.037). When only MBP immunoreactivity in tdTomato positive areas is considered the significance weakens and stays as a trend (p= 0.200).

It is to consider that at P14 in the striatum it was also the only instance when a significant difference between Snap25 cKOs and controls was seen in the area covered by tdTomato positive fibres (LVI Snap25 cKOs: 0.007 mm^2, controls: 0.01 mm^2, p= 0.027). Fibres project in relatively irregular pattern through the striatum. Hence, the imaging area can have an influence on the area covered. A significant decrease in the area covered by tdTomato positive LVI fibres might result in a significant reduction in MBP intensity due to the smaller area considered. However, experiments conducted by Ms Jolande Disser, a MSc student continuing my project, also showed a reduction in MBP intensity at P14 in the striatum without a reduction in the tdTomato positive area when imaged with at 40x objective (in contrast to my images taken with a 20x objective). This result supports the hypothesis, that the irregular pattern of fibres in the striatum are responsible for the significant difference rather than actual less fibres projecting through the striatum in LVI Snap25 cKOs compared to controls at P14. Furthermore, this hypothesis is supported by the finding that the area covered by tdTomato positive fibres in the

corpus callosum, where fibres extend in a more regular pattern, is similar between controls and LVI Snap25 cKOs. While Miss Disser also observed a reduced intensity in MBP mean fluorescence in the corpus callosum at P14, no such difference was seen in M1, similar to the results reported here by me.

A limitation of my study is that internodal length could not be observed. Changes in myelination could therefore not be assigned to either fewer axons being myelinated overall or each axon being less myelinated. So far, internodal length after reducing neuronal activity had only been studied in the optic nerve after monocular deprivation where a shorter internodal length was observed (Etxeberria et al. 2016). Therefore, further investigation in other brain regions achieved by different techniques are necessary to state further conclusions about the connection of internodal length and activity dependent myelination in the mammalian CNS.

A further limitation of my techniques is that Ntsr1- (LVI) as well as Rbp4- (LV) Cre is expressed in the whole cortical span affecting most major white matter tracts which prevents taking reference images in non-affected white matter tracts for normalisation. Even though there are many fibres (e.g. in the internal capsule and striatum) from the whole cortical span, the total amount of neuronal cells affected by either LV- or LVI-Cre expression (Rbp4 or Ntsr1) within one layer is probably well below 50% as tested before and might be even as low as 15% (Grant 2014). Having few cells affected also lowers the effect size that can be seen drastically. Therefore, future experiments measuring fluorescence intensity of MBP might be more likely to observe strong effects when promotors are used, that affect much more cells within the layer. The challenge would probably be to find a promoter that is layer specific enough but does not include too many different cell types since

this can drastically influence the outcome as shown in zebrafish (Koudelka, et al. 2016). Another approach would be to label even fewer cells to look at them individually to see an effect.

When comparing the experimental paradigm with studies in zebrafish, it is worth noting that the authors reduced neuronal activity globally, as well as only in a subset of cells, and also used both methods in combination with each other (Hines et al. 2015). As reported before, Ntsr1- (LVI) as well as Rbp4- (LV) Cre was not expressed in all LV and LVI cells but only in a subset. Additionally, projections through the white matter tracts were intermingled with projections from other brain regions. Therefore, the model used in this thesis is rather comparable to zebrafish findings when only subset of cells had reduced neuronal activity than global activity reduction.

Hines and colleagues describe that oligodendrocyte processes wrapping axons where VAMP2-dependent exocytosis was prevented retracted their sheath more frequently (and resulted in shorter stabilised sheath) during initial myelination (Hines et al. 2015). A disadvantage of using a mouse model in comparison with using e.g. zebrafish is that *in vivo* time-lapse imaging of deeper brain regions as used by Hines is not (yet) possible and hence such conclusion cannot be made in mice.

4.3.1.2 Myelination around MutKir2.1 and Kir2.1 electroporated fibres

After assessing myelination around LV and LVI Snap25 cKOs where regulated synaptic vesicle release was reduced in a subset of these projection neurons, myelination around less excitable Kir2.1 electroporated fibres was examined.

Animals were electroporated at E13.5 and sacrificed 14 days postnatally. In the corpus callous, myelin can first be detected at P11 (Sturrock 1980). At P14, tdTomato positive fibres from electroporated cells were at least partially myelinated when assessed with MBP immunohistochemistry which was not seen at P12.

Since LV Snap25 cKOs and controls had a strong tdTomato signal in the corpus callosum (much stronger than LVI Snap25 cKOs and controls as described in chapter 3), their myelination was also assessed at P14 for comparison.

Evaluation of overall MBP mean fluorescence analysis as well as in tdTomato positive areas only exhibited no difference between genotypes in the corpus callosum of LV Snap25 cKO compared to controls. This finding was in line with the analysis I conducted in the striatum where LV also displays projections.

In Kir2.1 electroporated animals a trend towards less MBP that did not reach significance in MBP mean fluorescence could be detected compared to MutKir2.1 control electroporations in tdTomato positive areas ($p= 0.100$). Post hoc analysis showed that 6 animals per group would be necessary for this trend to reach significance (ß set to 0.2 = 80%). Ms Jolande Disser, who repeated the experiments (on the same tissue obtained through my IUE surgeries) for comparison with the less prominent tdTomato positive fibres of LVI Snap25 cKOs in the corpus callosum, also observed no significant difference between Kir2.1 and MutKir2.1 electroporations ($p=0.54$). Her analysis included a ratio between MBP positive areas in the corpus callosum outside of tdTomato positive areas and MBP areas within tdTomato positive areas. When mean MBP intensity within that box differed more than one standard deviation from the mean MBP intensity of all the boxes the section was discarded as an outlier. By this method, the trend seen in my results towards less myelin around Kir2.1 fibres, vanished. Since no tdTomato

negative area is available in the corpus callosum of LV Snap25 cKOs, this method could have not been used there.

In utero electroporation is a challenging surgery technique that can result in varying outcomes. To evaluate whether the outcome of the surgery was suitable for tissue processing each brain was visually assessed for location and strength of fluorescent signal in the electroporation site after cutting. Variation in the electroporation site could occur by the placing angle of the electrode as well as when the embryo might move during the 5 pulses given (Martínez-Garay et al. 2016). Variation in the strength of the signal could arise from varying amount of plasmid injected, which was controlled by mouth pipetting during surgery, or the amount of plasmid in the injected solution. This latter source of variability was controlled by previous measurement of DNA concentrations. Measuring the tdTomato positive area in the corpus callosum, which indicated no difference between Kir2.1 and MutKir2.1 electroporated fibres, was an additional control step to ensure high surgery quality outcome.

In utero electroporation only targets a small subset of cells. This means that in the corpus callous, non-affected cell projections were also present. In zebrafish experiments have been conducted with silencing only a subset of neuronal cells as well as global silencing (an a combination of both) (Hines et al. 2015), but this has not yet been investigated in the mammalian CNS *in vivo*. Combining studies where only subsets of neurons are affected with global silencing might give further insights into activity dependent myelination in the murine nervous system. Additionally, an approach where more cells are targetd, might bare the possibility of a bigger effect size, as discussed before (see 3.3.3).

Due to the exigent surgery technique required for this experiment and limited time, all three control MutKir2.1 animals analysed came from a single litter. Contrary to the three animals for Kir2.1 analysis which originated from three different litters. Future experiments should be refined by collecting further MutKir2.1 control tissue from several litters as well as further Kir2.1 electroporated animals to increase statistical power which could consolidate the trend seen in my results.

A further limitation of my study is that internodal length could not be observed. In zebrafish it was shown that axons overexpressing Kir2.1 were less frequently selected for myelination but sheath length was not altered. In the murine study internodal length was only assessed after reduced neuronal activity in the optic nerve (Etxeberria et al. 2016). It was detected that long-term monocular deprivation as well as genetically reducing synaptic release of glutamate shortens myelin internode lengths. Our laboratory studied NoRs in Kir2.1 and MutKir2.1 electroporated fibres and preliminary results indicate that there might be fewer and shorter nodes in Kir2.1 (n=2) IUEs compared to controls. Fewer nodes might indicate towards fewer internodes whereas shorter nodes might be a compensation mechanism to increase action potential propagation (Arancibia-Cárcamo et al. 2017). Additional experiments will be needed to give further insights into internodal length after reduced neuronal activity in the mammalian CNS for example by 3D EM analysis (Tomassy et al. 2014).

An interesting study recently connected an increase in myelination after DREADD mediated stimulation to an increase in internode numbers and axonal arborization without changes in internodal length in parvalbumin interneurons. After chemogenetic stimulation myelination was found at higher order axonal branches

(Stedehouder et al. 2018). Previous experiments with Kir2.1 showed that axons may exhibit less branching after Kir2.1 introduction (Antonini and Stryker 1996; Antonini and Stryker 1993; Haruta and Hata 2007; Hua et al., 2005). Therefore, changes in axonal branching induced by altered neuronal activity could play a role for myelin quantity. However, since the corpus callosum is not one of the areas with the highest axon branching, this might be more important to consider when examining other areas of the cortex.

A further recent study by Mitew and colleagues investigated how reduced neuronal activity by Kir2.1 electroporations affects myelination in transcallosal projections arising from somatosensory cortex (Mitew et al. 2018). Though the experimental design was similar to that carried out in this chapter, Mitew and colleagues conducted *in utero* electroporations at a later timepoint, E15.5 rather than E13.5. Due to the reverse inside-out development of the cortex where earlier generated cells were located in deeper layers, later electroporations targeted upper cortical layers. Furthermore, they did not electroporate a mutated Kir2.1 plasmid as a control but only the fluorescent plasmid with GFP (Mitew et al. 2018). Without introducing a non-conducting Kir2.1 channel, it was not controlled for effects that could be caused by the introduction of this channel independent of its function. In Mitew's study animals were sacrificed at P20 and sagittal sections were analysed. Despite the fact that immuno-gold EM was performed for DREADDs experiments in their study (using GFP like done in IUEs), immuno-gold EM was not performed in Kir2.1 experiments, which would have been the gold standard, without giving a reason. Around Kir2.1 overexpressing fibres less MBP immunopositive rings were observed without a difference in total MBP around fibres in this area. They concluded that the decrease in myelination around Kir2.1 fibres derives from the

level of axonal selection since no difference in oligodendrocyte differentiation or OPC proliferation was found. Additionally, they argue that myelination is influenced by levels of neuronal activity in mammalian CNS like observed in zebrafish. Unfortunately, using Kir2.1, it cannot be distinguished if reduced neuronal excitability or absence of spontaneous vesicular release (or combination of both) is responsible for the observed effects. Mitew and colleagues state that the reduction in MBP positive rings were a result of reduced excitability, which can actually not be concluded from this experiment and should be subject to future experiments (Mitew et al. 2018).

Taking the data here presented into account, which show a trend but no significant result in a different subset of cortical cells, the influence of neuronal activity on myelination might not be apparent or as strongly apparent in all neuronal CNS cells or regions. In zebrafish, this was already shown when reticulospinal neurons displayed reduced myelin sheath numbers after tetanus-toxin expression to reduce synaptic vesicle release but not commissural primary ascending neurons (Koudelka et al., 2016). Future experiments might include analysis of oligodendroglial cells in the corpus callosum following Kir2.1 and MutKir2.1 electroporation of deep cortical layers like it has been done by Mitew and colleagues after IUE of upper cortical layers.

4.3.2 Oligodendrocyte lineage markers in LV and LVI Snap25 cKO

Cell-type specific markers can be used to identify cells and track their developmental trajectory. Here, Olig2 and CC1 were used as markers of the oligodendrocyte lineage to quantify oligodendroglial density at P8 and P21 for observation during myelination onset as well as at an adolescence timepoint.

Marker quantification was performed in two regions: in cortical layers LV and LVI (for LV and LVI Snap25 cKOs respectively) as well as in the striatum, where fibers originating from both of these layers display projections. The reasoning behind this choice was that there might be regional differences in oligodendroglial response to changes in neuronal activity. Differences could be due to differing origins of OPCs or varying response to mitogens which could also be reflected in distinct response to activity-regulating signals (Gibson et al. 2014; Yue 2006; Hill et al. 2013). Additionally, OPC mitogens can be released not only from axons but also from cell bodies which might be influenced by changes in neuronal activity (Fruttiger, Calver, and Richardson 2000).

Olig2 is one of the most consistent markers for the oligodendroglial cell lineage since it is expressed in all stages of oligodendrocyte development due to its importance in oligodendrocyte maturation (Lu et al. 2000; Zhou, Wang, and Anderson 2000). However, the expression reduces upon differentiation into mature, myelinating oligodendrocytes (Kitada & Rowitch 2006). Therefore, Olig2 can be seen as a marker for OPCs and pre-oligodendroytes, especially when cells are not additionally CC1 positive, as a marker for mature oligodendrocytes. Cells, which are Olig2 as well as CC1 positive, are considered mature oligodendrocytes. In the striatum, Olig2 and CC1 cell counting results were split into overall numbers/density as well as cells in visible contact with tdTomato positive fibres projecting through the striatum. This distinction indicated which cell bodies were in close proximity to affected LV or LVI fibres, however, it did not exclude that processes from cell bodies not in close proximity were in contact with tdTomato positive fibres and thereby sensing potential signals. PDGFRalpha is an alternative

marker which can be found on the cell surface of OPCs and pre-oligos to visualise processes via immunohistochemistry. However, PDGFRalpha was not used in this experiment, since preliminary experiments in existing tissue showed that PDGFRalpha was less suitable for quantification due to its non-somatic expression and tracing of cell processes would be needed.

The expression of Olig2 and CC1 was predictably age-dependent. Given that CC1 is a marker of mature oligodendrocytes, only very few CC1 positively stained cells were detected by IHC in M1 and striatum upon start of myelination at P8. In contrast, Olig2 could already be detected by P8. Of note, presence of OPCs and immature oligodendrocytes is required for the initiation of myelination. Comparison of Olig2 positive cells in LV and LVI Snap25 cKOs with their controls did not reveal a significant difference in cell density at P8. This was found for M1 as well as for the striatum, where total cell density was analysed as well as cells that were in contact with LV or LVI tdTomato positive fibres projecting through the striatum.
Like at P8, in the striatum and M1, no significant difference in Olig2 or CC1 density was detected between LV and LVI Snap25 cKOs and their controls at P21. Furthermore, in the striatum and in tdTomato positive areas, there was no significant difference in the density of double positive cells for CC1 and Olig2 between LV and LVI Snap25 cKOs and respective controls at P21. However, CC1 positive and Olig2 positive cell density was increased in M1 of LV Snap25 cKOs compared to controls ($p= 0.100$ in non-parametric Mann-Whitney test that can not detect smaller p-values with $n=3$. Parametric t-test p-value indicated significance with $p= 0.0019$) but not in LVI Snap25 cKOs. Olig2 as well as CC1 density seemed to increase in LV Snap25 cKOs compared to control in M1 at P21 but this trend did

not reach significance. Yet, when double positive cells were quantified and compared this difference was significant.

As mentioned before, PDGFRalpha can be used to label cells of the oligodendroglial lineage at a younger state that are not yet differentiated. It would have been beneficial to use this marker here in combination with CC1 and Olig2, to investigate weather the slight increase in mature oligodendrocytes is due to changes in proliferation or differentiation. This conclusion can not be drawn from only studying CC1 and Olig2, since none of these markers labels exclusively OPCs.

Examening the Olig2 positive cells it is to observe, that at P8 the density in the striatum as well as in M1 of LV controls was higher compared to P21 LV controls (M1 $p = <0.0001$, striatum $p = 0.017$). In LVI controls, there was a trend towards lower Olig2 density in the striatum ($p = 0.119$) but not in M1 ($p = 0.663$) during the development from P8 to P21.

Since Olig2 is a marker for all cells of the oligodendroglial lineage, the number should have been stable even when OPCs differentiate to mature oligodendrocytes, which took place between P8 and P21. However, the expression of Olig2 decreased with this differentiation and therefore might not get detected anymore (Kitada and Rowitch 2006). Additionally, the brain expands between P8 and P21 which could lead to a decrease in cell density if the total number of cells stays constant in a larger volume.

Interestingly, while LVs as well as LVIs exhibited less Olig2 cells at P21 than at P8, the reduction in M1 in LVs was much stronger (LV: 5-fold, LVI: 1.5-fold). This might have been due to the fact that in the deeper LVI OPCs already started

differentiating at P8 and therefore not as many were detected any more whereas this happened slightly later in the upper LV.

Notably, there was an increase in density of Olig2 positive cells in contact with tdTomato positive areas from P8 to P21 in the striatum despite a general decrease in Olig2 density between the ages, as described previously. It is likely, that this difference was based on the varying counting method between P8 and P21. At P8, Olig2 counts were conducted using a cell profiler script whereas at P21, cells were counted manually due to simultaneous counting of CC1 positive cells. The script was optimised for detecting a strong nuclear signal whereas CC1 is cytoplasmic and not as uniform as Olig2. At P21, double positive cells for Olig2 as well as CC1 were also counted for in contact with tdTomato positive areas, when cytoplasmic CC1 was within this area but not nuclear Olig2 stain.

The question whether neuronal activity has an effect on myelination had been tackled in a series of recent studies. Gibson and colleagues reported an increase in dividing cells positive for Olig2 in the optogenetically stimulated murine cortical layer V as well as in their projections through the corpus callosum 3h after stimulation. After 4 weeks, an increase in CC1 positive cells was found in both examined regions (Gibson et al. 2014). Additionally, chronic pharmacogenetic stimulation in S1 lead to an increased OPC proliferation one week after treatment as well as an increased density in CC1 positive cells and in the corpus callosum of mice (Mitew et al. 2018).

Studies about the role of sensory deprivation on myelination using whisker trimming and monocular deprivation, reported spatial alteration in OPC distribution

and increased oligodendrogenesis without changes in OPC proliferation, respectively (Etxeberria et al. 2016; Barrera et al. 2013; Mangin et al. 2012).

Table 5: Overview of oligodendroglial markers in key in vivo experiments manipulating neuronal activity either genetically or by sensory deprivation to observe activity dependent myelination

First Author, year	Species	Mode of Manipulation	Neuronal activity	Marker	Region	Result
Gibson et at, 2014	mice	Optogenetics LV	increased	Olig2	CC, M2	increase
				PDGFRalpha	M2	increase
				CC1	CC, M2	increase
				EdU (dividing cells)	Spinal Cord	No significant change
Mitew et al, 2018	mice	DREADD in upper cortical neurons	increased	PDGFRalpha	CC	increase
				ASPA (mature oligos)	CC	increase
		Kir2.1 IUE, upper cortical neurons	decreased	PDGFRalpha	CC	No significant change
				CC1	CC	No significant change
Etxeberria et al., 2016		Monocular Deprivation	decreased	PDGFRalpha	Optiv Nerve	decrease
				CC1	Optiv Nerve	increase
		VGlut2 cKO	decreased	CC1	Optiv Nerve	increase
Barrera et al., 2013	mice	Whisker trimming	decreased	Olig2	Barrel Field	No significant change
Mayoral et al., 2018	mice	Monocular Enucleation	decreased	Olig2	Optiv Nerve	No significant change
				CC1	Optiv Nerve	No significant change

In my thesis, the major effects reported after increasing or decreasing neuronal activity had not been observed. The lack of major effects after reduced regulated vesicle release from a subpopulation of LV and LVI cells on oligodendroglial density did not necessarily mean, that there was no effect on myelination after silencing other cortical cells or in other regions of the CNS. In zebrafish Koudelka and colleagues showed distinct responses to changes in neuronal activity dependent on specific neuronal types (Koudelka, et al. 2016). Since here only deeper cortical layers have been examined within the brain, effects in the spinal cord or when upper layers are affected cannot be excluded and should be further explored.

Additionally, it has been postulated that oligodendroglial cells might integrate information from several axons and myelinate accordingly (Mangin and Gallo 2010). If this is indeed the case, then being in contact with several active axons as

well as inactive ones, would probably not lead to an overall change of oligodendroglial cell numbers.

Experiments to analyse the oligodendroglial lineage further within LV and LVI Snap25 cKOs could include immunohistochemistry against PDGFRalpha and NG2, which are markers for early stages of oligodendrocyte development. However, this approach also has limitations: preliminary results with LV and LVI Sna25 cKOs and control tissue showed that tested NG2 antibodies needed shorter fixation of brain tissue for epitope binding and therefore fresh tissue needs to be collected which is time and cost intensive due to the breeding scheme. Also, as mentioned previously, quantification of PDGFRalpha can be challenging due to its spread expression outside the cell body.

In summary, spatial alteration of pre-myelinating oligodendenroglial distribution and increased oligodendrogenesis, as previously described after reductions in neuronal activity by sensory deprivation, was not observed after genetic reduction of vesicle release in subsets of LV and LVI neurons (Barrera et al., 2013; Mangin et al., 2012, Etxeberria et al. 2016). Earlier in this chapter it was shown, that the onset of myelination was not majorly affected in LV and LVI Snap25 cKOs during development at P8 and P21. However, at P14 some transient trends were observable. Therefore, investigating oligodendroglial density at P14 might result in some interesting findings if changes in myelin is regulated on the level of individual oligodendrocytes. Post hoc analysis showed that in several cases (MBP at P14 in M1 and Striatum in LVIs and Olig2 at P8 in the striatum of LVIs) only a few more animals (total n of 4-5) would be neccessary to reach significance where trends are indicated at the moment. My findings on myelination at P8 and P21 are in line

with the results of Olig2 and CC1 positive cells that also do not seem to be majorly affected in both Snap25 cKOs excluding that mature oligodendrocytes produce a changed amount of myelin compared to control conditions.

4.3.3 Conclusion

This chapter describes the timing of myelination onset in LV and LVI Snap25 cKOs as well as after MutKir2.1 and Kir2.1 electroporations. Oligodendroglial lineage marker density was then analysed in LV and LVI Snap25 cKOs. My analysis showed that there are mainly no significant changes in myelination or oligodendroglial lineage markers between genotypes. MBP analysis around Kir2.1 electroporated fibres showed a non-significant reduction compared to MutKir2.1 fibres in tdTomato positive areas.

5 Myelin characteristics and myelin maintenance surrounding axons originating from silenced cortical neurons

5.1 Introduction

After studying myelination onset as well as oligodendroglial cells during development, this chapter will focus on two specific myelin characteristics (g-ration and node or Ranvier) that define the formation of mature myelin. Additionally, myelination during impaired maintenance of fibres after Snap25 abolishing will be studied, since no study so far has looked at myelination in degenerating Snap25 lacking fibres. Alterations of Snap25 have been associated with neurological disorders of which some also show signes of changes in myelination, like shizophrenia (Fatemi, et al, 2001; Young et al., 1998, Lewis et al. 2003).

To obtain measurements for the g-ratio (myelin thickness in relation to fibre diameter) as well as for nodes, several protocols have been used until satisfactory results were gained which will be explained in this chapter as well. To observe alterations during premature aging of myelin ensheathed LVI Snap25 cKO fibres, myelin markers, tdTomato and inflammation markers were probed (protein and mRNA).

The main aim of this chapter is to address the current gap of *in vivo* knowledge in mice about reduced neuronal activity on the g-ratio as well as nodes. Current published studies about activity dependent myelination examining the g-ratio in mice mostly looked at increased neuronal activity in the brain or decrease neuronal activity in the optic nerve (Mitew et al. 2018; Gibson et al. 2014; Etxeberria et al. 2016). Although *in vivo* zebrafish studies looked at the spinal cord via EM when

examining myelination after reduced neuronal activity, no murine study did so far (Mensch et al. 2015).

In the introduction of this chapter literature will be reviewed about general conduction velocity in myelinated nerve fibres as well as the influence of activity dependent myelination on conduction speed. Since Caspr, as a paranodal protein, is used as a marker to analyse nodes in this chapter, it will also be briefly introduced.

5.1.1 Conduction velocity in myelinated nerve fibres

Accurate timing in the nervous system is essential to precisely regulate motor, sensory and cognitive functions (Almeida and Lyons 2017). This is especially apparent in demyelinating diseases where previous precisely balanced propagation velocity is lost and thereby impairs integration of motor and sensory information (Compston and Coles 2002; Tomasi, Caminiti, and Innocenti 2012; Innocenti, Vercelli, and Caminiti 2013). Although myelin can be partially restored in some diseases, remyelination around axons is often less thick compared to non-disease states (Blakemore and Murray 1980; Schroder 1972; Gledhill and Mcdonald 1977).

The timing of information arrival depends on conduction velocity which can be influenced in several ways in myelinated fibres. The axon diameter is an important factor in conduction velocity. Axons with larger calibres generally conduct action potentials faster due to the lower resistance to electrical current. It has been shown that myelination itself or myelinating glia cells can have an influence on the axon diameter, and vice versa, the axon diameter can also influence myelination (Friede 1972; Colello and Ztirich 1994; Windebank 1985). Another energy efficient factor

that has an influence on conduction velocity is the spacing and composition of nodes of Ranvier (internodal length) where saltatory conduction is taking place (Fields 2008; Waxman 1975; Hursh 1939; Wu et al. 2012; Huxley and Stampfli 1948; Arancibia-Cárcamo et al. 2017). Brivio and colleagues showed that not necessarily myelin sheaths but also axonal cytoskeleton was able to shape nodal length during development (Brivio et al. 2017). Additionally, the number of nodes as well as myelin thickness compared to the axon diameter (g-ratio) can impact conduction speed. Myelin sheath thickness is linearly related to the axon diameter (Hursh 1939, Friede and Bischhausen, 1982; Hildebrand and Hahn, 1978). Axonal diameter, however, cannot be the only determining factor if an axon gets myelinated or not since there are many axons in the corpus callosum which are not myelinated despite a sufficient diameter (Sturrock 1980). It might be possible that not all axons are myelinated because maximal propagation speed is not always desirable but a rather conduction velocity that leads to well-coordinated information integration. Early studies in Squid and the electric organs of electric fish have shown this, but results were replicated in smaller mammals as well (Pumphrey and Young 1938; Bennett 1970; Waxman 1971; Waxman, Pappas, and Bennett 1972; Lang and Rosenbluth 2018; Salami et al. 2003; Pelletier et al. 2018).

Several studies suggested that there is a specific myelin profile to achieve optimal conduction velocity. Optimal for most fibres does not necessarily mean maximal conduction velocity, since arrival of action potentials, for example synchronized with other signals, are most often more important than extremely fast arrival of information. Increasing internodal distance increases conduction velocity, but there is an optimal spacing of nodes along axons which leads to a flat maximum conduction velocity (Huxley and Stampfli 1948; Wu et al. 2012; Brill et al. 1977).

With regard to the g-ratio, there is also an optimal value by which conduction velocity is maximised, however, with large variations around the mean (Chomiak and Hu 2009; Fields 2008). Depending on the CNS region, these optimal myelin properties are more or less often met than in others. In the cortex and subcortical regions, studies showed that the structure of myelin is diverse (Tomassy et al. 2014; Peters and Sethares 1996; Mount and Monje 2017). Conversely, it was thought that the g-ratio in the optic nerve varies less. However, a recent study using 3D electron microscopy demonstrated that also in the optic nerve of adult rats there is significant variability of g-ratios additionally to variations in axon diameter and myelin ultrastructure along single axons (Giacci et al. 2018). The fibre diameter of an individual axon can be increased by up to 500% from its smallest to its largest diameter within a measured distance of 100µm. The g-ratio along an individual axon varies as well, which leads to the conclusion of heterogenous conduction velocity. This might be important for subtle adjustment to the neuronal circuit. Interestingly, this study did not find differences between the myelin thickness at extremities of internodes versus central regions as described previously during CNS development suggesting of a disappearance of this effect in adulthood (Giacci et al. 2018; Snaidero et al. 2014).

It is not completely understood how myelin thickness in the CNS is regulated. It was demonstrated that ERK1/ERK2 (extracelluar signal-regulated protein kinases1 and 2) and MAPK (mitogen-activated protein kinase) signalling controls myelin thickness (Ishii et al., 2012) and that myelin characteristics that influence conduction velocity can be activity-dependent in the CNS (Etxeberria et al. 2016; Mitew et al. 2018; Gibson et al. 2014).

Mice lacking ERK1 as well as ERK2 specifically in oligodendrocytes were unable to increase myelin thickness in proportion to the axon calibre after normal proliferation and differentiation. At this point, oligodendrocyte numbers were not affected but they failed to up-regulate mature myelin protein expression. Interestingly, if only one of the extracelluar signal-regulated protein kinases was missing, these effects were not observed (Ishii et al. 2012).

A murine study by Etxeberria and colleagues showed that internodal length is influenced by experience dependent activity (Etxeberria et al. 2016). In this study monocular deprivation was used to demonstrate that reduced neuronal activity of retinal ganglion cells results in decreased internodal length along their axons without influencing other myelin characteristics (including the g-ratio). Therefore, it was concluded that the observed significant reduction in conduction velocity was a direct result of the altered distance between nodes of Ranvier. Interestingly, myelination was not only affected in axons from the deprived eye. In the optic tract ipsilateral to the deprived eye, where most axons derive from the deprived eye, non-deprived axons (from the contralateral retina) also showed reduced internodal length. This points towards a secreted factor being responsible for the changes. By using a conditional VGluT2 KO mouse they were able to suggest glutamate as a possible mechanism. Vesicular glutamate transporter (VGluT2) is responsible for transporting glutamate into synaptic vesicles in retinal ganglion cells to be released upon neuronal activity. Conditional VGluT2 mice showed a similar phenotype to monocular deprivation animals, suggesting that the dominant effect of monocular deprivation is a reduction glutamate release.

Furthermore, a study on sensory deprivation in the auditory system reported thinner axons as well as thinner myelin in the trapezoid body when mice were

earplugged from the onset of hearing. They concluded that sensory activity in development as well as maintenance of myelin is needed since also plugging during adulthood decreased myelin (but only in the thickest trapezoid body fibers) (Sinclair et al. 2017)

Two other murine studies showed that neuronal activation in two differing areas of the cortex increased myelin thickness in the white matter underlying the stimulated areas (Gibson et al. 2014; Mitew et al. 2018). The studies mentioned used DREADD-mediated neuronal stimulation (Designer Receptors Exclusively Activated by Designer Drugs) in the somatosensory cortex and optogenetics in the motor cortex and both revealed increased myelin thickness detected by electron microscopy followed by g-ratio analysis. Gibson and colleagues showed that the observed changes after increased neuronal activity lead to improved motor output (faster hindlimb swing speed after cortical motor neuron stimulation) which could indicate an improved circuit function, but the study does not measure conduction speed in stimulated axons (Gibson et al. 2014).

Two publications investigating the influence of neuronal activity on nodes increased neuronal activity for their study (Trigo and Smith 2015; Huff et al. 2011). In spinal cord tissue of the guinea pig myelin was observed after electrical stimulation by laser-scanning coherent anti-Stokes Raman scattering (CARS) imaging. The authors reported paranodal myelin retraction at the nodes during 200 Hz electrical stimulation starting minutes after the onset of stimulation and continued for up to 10 min after stimulation has ended. However, the observed effect was reversed after 2 hours of recovery (Huff et al. 2011). In the peripheral nervous system of anaesthetised mice saphenous nerves and spinal roots were stimulated resulting in axonal herniating around the nodal membrane. This lead to

a displacing paranodal myelin as well as to a widening of the nodal gap within 2 hours after stimulation (Trigo and Smith 2015).

Taken these findings together, there is currently a lack of evidence how genetical reduction in activity levels changes myelin characteristics in cortical projections of the CNS.

5.1.2 Contactin associated protein 1

In this chapter Contactin Associated Protein (CASPR) as a paranodal marker will be used to analyse NoRs. Therefore, it is briefly introduced here.

CASPR 1 is a 190 kDA transmembrane protein. It is part of the CASPR family that consists of 5 protein members (CASPR 1-5), which are part of the neurexin superfamily. CASPR 1 is encoded by the CNTNAP1 gene. The protein is located in the neuronal membrane of paranodes of myelinated axons where it forms a complex with contactin (neuronal) and Neurofascin-155 (glial) to create a barrier between node and internode (Rios et al. 2000; Gollan et al. 2003; Sherman et al. 2005). A recent study indicated that CASPR is essential for mediating the temporal specification of neuron and astrocyte differentiation from radial glia cells in the developing murine cortex via Notch signalling. In the absence of Caspr in neuronal progenitor cells, the formation of neurons is delayed while astrocyte formation is premature (Wu et al. 2017).

5.1.3 Aims of this chapter

The formation of nodes of Ranvier as well as compact membrane structures are typical characteristics of mature and healthy myelin. Especially the latter one has been shown to be influenced by neuronal activity (Etxeberria et al. 2016; Gibson et al. 2014; Mitew et al. 2018). In contrast, reports about effects of neuronal activity on nodes of Ranvier are underrepresented given its importance in regulating conduction speed up to 20% based on the accumulation of ion channels (Arancibia-Cárcamo et al. 2017; Waxman 1975). Node diameter has been predicted to be an important factor in conduction velocity in the auditory system, the optic nerve as well as cortical axons (Arancibia-Cárcamo et al. 2017; Ford et al. 2015).

In this chapter, I aim to study the effect of abolished regulated neurotransmitter release on the formation of myelination (including g-ratio and nodal characteristics in LV Snap25 cKOs), as well as determining the effect that slowly progressing axonal degeneration has on the surrounding myelin in LVI Snap25 cKOs.

Firstly, I will analyse myelin around fibres lacking Snap25, which are incapable of regulated neurotransmitter release. This will be assessed by measuring the g-ratio of the dorsal corticospinal tract before the onset of degeneration in LV Snap25 cKOs at P18. Additionally, the formation of nodes of Ranvier will be assessed in LV Snap25 cKOs by studying the paranodes using Caspr immunoreactivity. This allows to measure paranodal width, nodal width as well as number of nodes in a selected field of view.

As established in chapter 3, the projections originating from cortical LV and LVI that have no functional Snap25 cKO innervate the thalamus like control fibres but

later show signs of axonal degeneration and eventual cell loss during their lifespan. Hence, an additional aspect of this chapter will be to examine the impact of degenerating, underlying axons on myelin in these Snap25 cKO mice. This chapter deals with myelin markers as well as inflammation markers in LVI Snap25 cKOs and controls during the process of degeneration in M1 and striatum at different ages and with various techniques to assess mRNA as well as protein levels.

5.2 Results

5.2.1 Testing post embedding immuno-gold stain for tdTomato on TEM sections for myelin quantification in LV Snap25 cKOs

In order to calculate the g-ratio in tdTomato positive fibres in controls and LV Snap25 cKOs within the dorsal corticospinal tract, it is necessary to be able to distinguish these fibres from tdTomato negative fibres. Rbp4-Cre tdTomato positive fibres from cortical LV are projecting through the dorsal corticospinal tract of the spinal cord. However, it is not known how many of the 15% Rbp4-Cre positive and how many of the 85% Rbp4-Cre negative cells in LV are projecting to the dorsal corticospinal tract or to other regions (Grant 2014; Hoerder-Suabedissen, Korrell et al. 2018). Hence, it is also unknown how many of these axons are tdTomato negative and how many are positive.

The goal of the initial experiment was to determine the abundance of tdTomato positive and negative axons and compare myelination of tdTomato positive control fibres to tdTomato positive LV Snap25 cKO fibres as well as to tdTomato negative fibres in the dorsal corticospinal tract. The dorsal corticospinal tract was chosen since a pure and parallel LV population projects through it which is also tdTomato positive.

Animals were sacrificed at P18 to maximise the time in which fibres could be myelinated but did not yet show obvious signs of degeneration when examined by confocal microscopy (at P23, see chapter 3 Figure 10). Murine spinal cord myelination was reported to start one day prior to birth and already shows a relatively mature pattern at P11 when visualised by Lac Z expression under the MBP promoter (Foran and Peterson 1992). For the present study, animals were transcardially perfused with PBS and 4% PFA, but no glutaraldehyde to keep

epitopes available for the following antibody binding. The tdTomato positive area of the upper thoracic part of spinal cords from controls as well as LV Snap25 cKOs were dissected out and processed for TEM. Subsequently, a contrast and immuno-gold stain was carried out with a dsRed antibody to detect red fluorescent proteins. Sections were imaged using a transmission electron microscope.

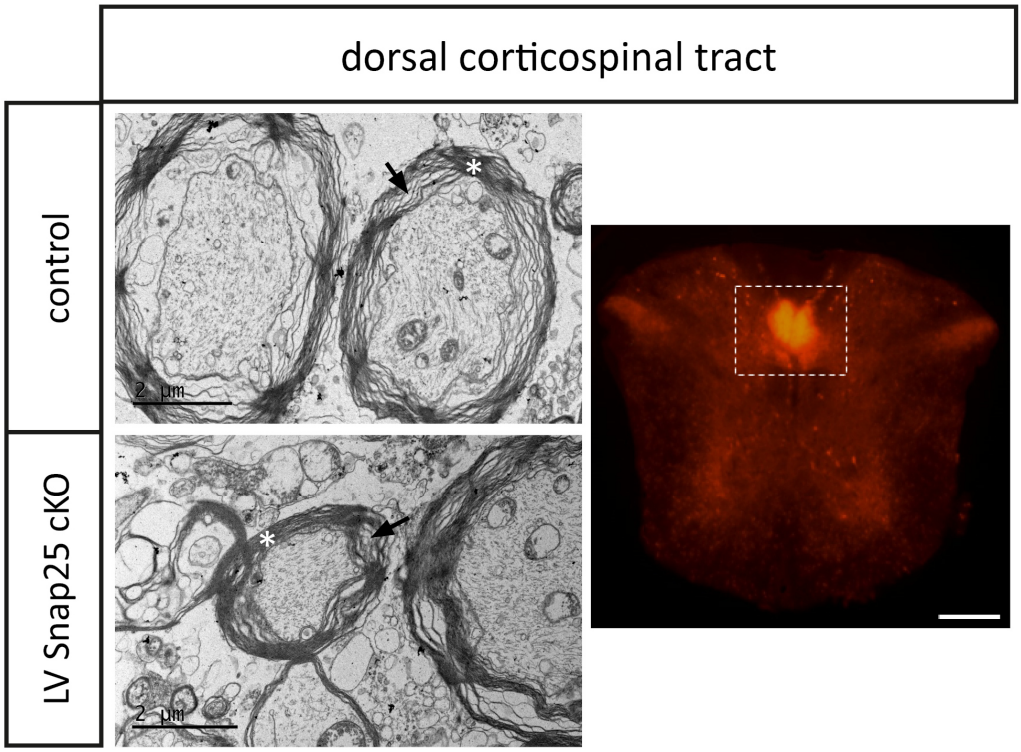


Figure 43: Transmission electron microscopy artefacts of myelin disintegration due to inefficient fixation on a coronal section through the spinal cord

tdTomato expressing projections in the dorsal corticospinal tract (region indicated with white box) originating from layer V cortical neurons appear red. The dorsal corticospinal tract was dissected out of the spinal cord to undergo processing for transmission electron microscopy. Ultra-thin sections were imaged revealing that both conditions, wildtype animals as well as LV Snap25 cKOs, showed disintegrated myelin. In some areas myelin was still compact (white asterisk) whereas in other areas of the same axon myelin layers were separated (black arrow). Myelin appears equally disintegrated independent of the genotype.
Scale bar EM images: 2 µm, overview: 200 µm

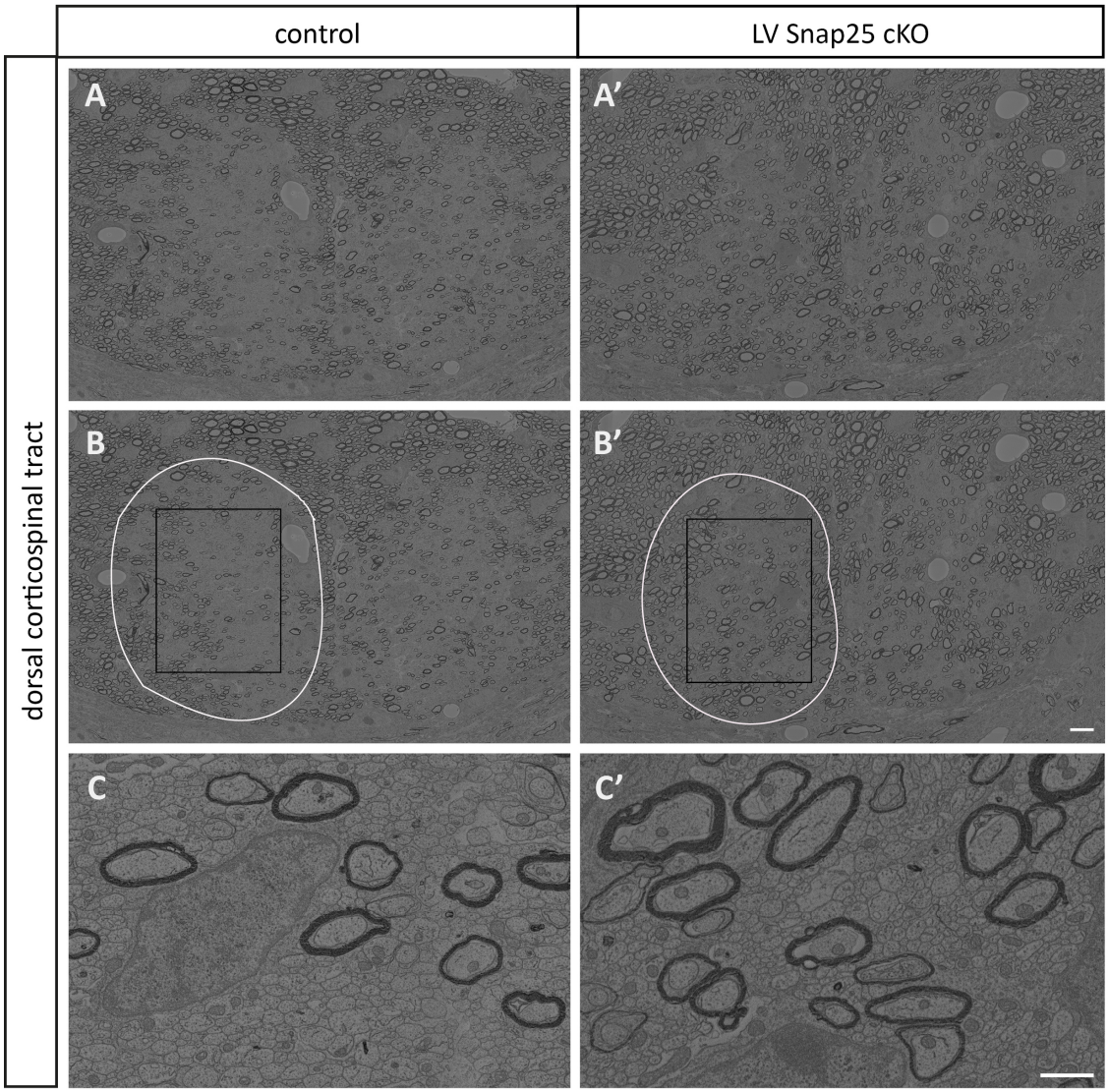
Figure 43 shows the transmission electron microscopy images of the spinal cord. Myelin disintegration is apparent by the lack of compaction. Myelin appears

disintegrated independent of the genotype. Additionally, no obvious gold-labelling is visible to distinguish tdTomato positive from tdTomato negative cells. The boundaries of the dorsal corticospinal tract are not recognizable within the visual area of the microscope, which made the determination of the correct area challenging. This accompanied by unsatisfying results regarding the myelin ultrastructure, lead to an adjustment of experimental design as described in the following section.

5.2.2 Reduced g-ratio in the dorsal corticospinal tract of LV Snap25 cKOs

Further experiments conducted in adult mice that were perfused with 2.5% glutaraldehyde in addition to 2% PFA showed an improvement of myelin quality. However, there was no detectable tdTomato gold-labelling. Therefore, the experimental design was adjusted. In the follow up experiments, mice were perfused with 2.5% glutaraldehyde in addition to 2% PFA and the g-ratio of all myelinated axons in a given area of the dorsal corticospinal tract was determined. Therefore, the examined fibre population contained tdTomato positive (originating from Rbp4-Cre positive layer V projection neurons) and other corticospinal neuronal populations. The ROI (region of interest) was chosen by drawing a box, while blinded to genotypes, of maximum size to capture as many axons in the dorsal corticospinal tract that fitted within the dorsal corticospinal tract of all analysed specimen.

The use of a scanning electron microscope allowed visualisation and correct identification of the whole dorsal corticospinal tract of the spinal cord (Figure 44, A).


control
LV Snap25 cKO
dorsal corticospinal tract
A
A'
B
B'
C
C'

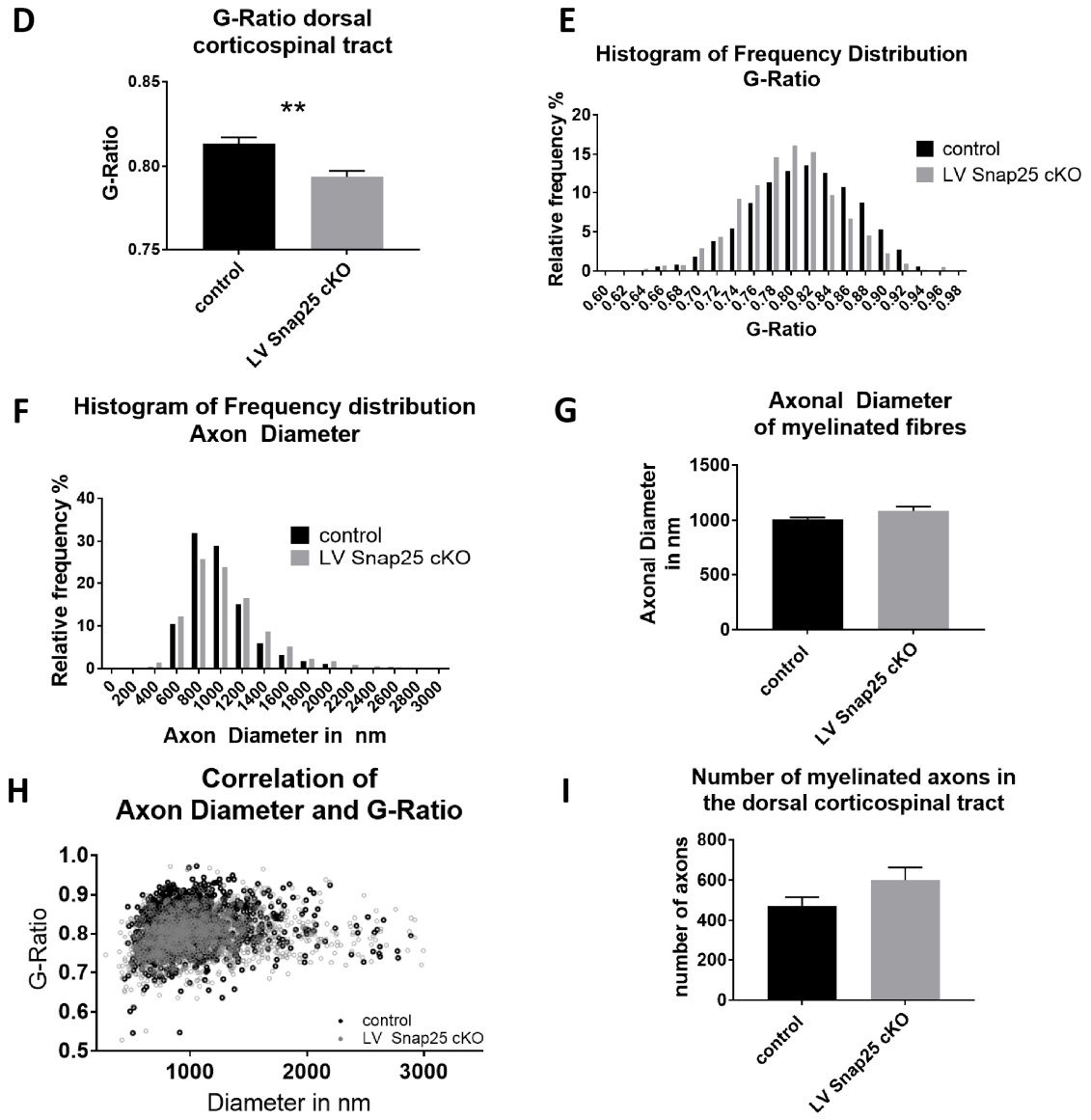


Figure 44: Lower g-ratio of LV Snap25 cKOs in comparison to controls in dorsal corticospinal tract at P18

G-Ratio was measured in a given area (32.5 µm x 42.5 µm) of the left and right part of the cervical dorsal corticospinal tract in controls as well as LV Snap25 cKOs. A-A') Representative overview of the area where the dorsal corticospinal tract is located of control (A) as well as LV Snap25 cKO (A') spinal cords (also see fluorescent image of previous Figure 43 where white square indicates dorsal corticospinal tract). B-B') Representative overview of the area containing dorsal corticospinal tract with left part of the dorsal corticospinal tract marked in white circles. Left area in which axons were counted for g-ratio quantification is marked with black rectangle. C-C') Magnification of axons in the dorsal corticospinal tract to see myelin of individual axons in LV Snap25 cKO and controls. D) The average g-ratio of LV Snap25 cKOs (0.794 ± 0.0036) is significantly less than the g-ratio of controls (0.813 ± 0.0037) (p= 0.0072). E) Histogram of frequency

distribution of g-ratios from controls (black) as well as LV Snap25 cKOs (grey). F) Histogram of frequency distribution of axon diameter from myelinated fibres. G) Axonal diameter of myelinated fibres did not reveal a significant difference between controls (1008 ± 18.6) and LV Snap25 cKOs (1086 ± 39.7) but a trend towards bigger diameters in LV Snap25 cKOs (p= 0.127). H) Scatter plot graphs display g-ratio in relation to axon diameter of individual fibers. I) Analysing the number of myelinated axons that were counted reveals a trend towards controls (472.4 ± 43.6) having fewer axons than LV Snap25 cKOs (600.8 ± 62.5) in the dorsal corticospinal tract per animal counted (p= 0.126).
Unpaired t-test, values given are mean ± SEM, n=5 control animals and n=4 LV Snap25 cKO animals. Scale bar overview: 5000 nm, magnification: 1000 nm

The usage of a scanning electron microscopy allowed for an easier identification of the dorsal corticospinal tract by viewing a larger area than a conventional transmission electron microscope can visualize (Figure 44). However, the identification of a sharp boundary of the dorsal corticospinal tract was not always possible. Therefore, a box sized 32.5 x 42.5 µm was chosen to fit in the dorsal corticospinal tract on both sides that were to be analysed. The application of high percentage of glutaraldehyde during the transcardial perfusion lead to a satisfying preservation of myelin so that a g-ratio quantification could be conducted. This g-ratio quantification in 5 controls and 4 LV Snap25 cKOs (around 500 axons/animal) revealed that LV Snap25 cKOS have a reduced g-ratio (0.794) compared to controls (0.813). The smaller the g-ratio, the more myelin surrounds an axon compared to its diameter. There was no significant difference in the axonal diameters of LV Snap25 cKOs and controls but a trend occurring that LV Snap25 cKOs have a bigger diameter compared to controls (p= 0.127). A trend (p= 0.126) could also been observed when assessing the number of myelinated axons that were counted. In LV Snap25 cKOs there were in average 600 myelinated axons per animal whereas in control animals only 472 were counted.

5.2.3 Nodes of Ranvier in LV Snap25 cKOs

Membrane compaction is an important characteristic for myelin to increase conduction speed and has been shown in EM images in the prior section. Another characterisation of mature myelin is the formation of highly organised compartments dividing each myelin segment into internode, juxtaparanode, paranode and node (Sherman and Brophy 2005). At the node of Ranvier, action potentials are renewed in a saltatory fashion to propagate along the axon. Therefore, each segment exhibits necessary and specific ion channels and associated proteins in a specific spatial formation (Buttermore, Thaxton, and Bhat 2013).

In my thesis, Caspr has been chosen to examine the formation of nodes of Ranvier in LV Snap25 cKOs. Caspr is located at the paranode and thereby enables to measure paranodal length directly as well as nodal width indirectly.

5.2.4.1 Fibre teasing of the dorsal corticospinal tract for NoR analysis

The aim of the experiment was to measure nodal width as well as internodal distance in LV Snap25 cKOs compared to control. Analysis of internodal length in brain sections requires imaging over longer distances in several depth to track axons that are not parallel to the cutting plane. Another technique that can be applied is fibre teasing where single fibres are separated from the tissue and placed on glass slides for analysis. The laboratory of Professor Brophy (Center for Neuroregeneration, Edinburgh Medical School) very kindly hosted me and taught me the technique. They use fibre teasing to examine nodes of Ranvier and internodal length in the ventral funiculus, a white matter tract in the ventral spinal cord. Fibre teasing of the dorsal corticospinal tract was performed where

corticospinal LV fibres project along the spinal cord, including tdTomato positive fibres in LV Snap25 cKOs and controls. Furthermore, this area was fristly chosen to strengthen the findings from EM in the spinal cord by adding information about internodal length. Unfortunately, the technique did not work when performed on the dorsal corticospinal tract at P18. As for the g-ratio analysis, this age was chosen to maximise the time in which fibres could be myelinated but did not yet show obvious signs of degeneration when examined by confocal microscopy. When observed under a fluorescence microscope, tdTomato positive fibres stayed agglutinated where they were meant to spread and stick to the adhesive slide surface like ventral funiculus fibres do.

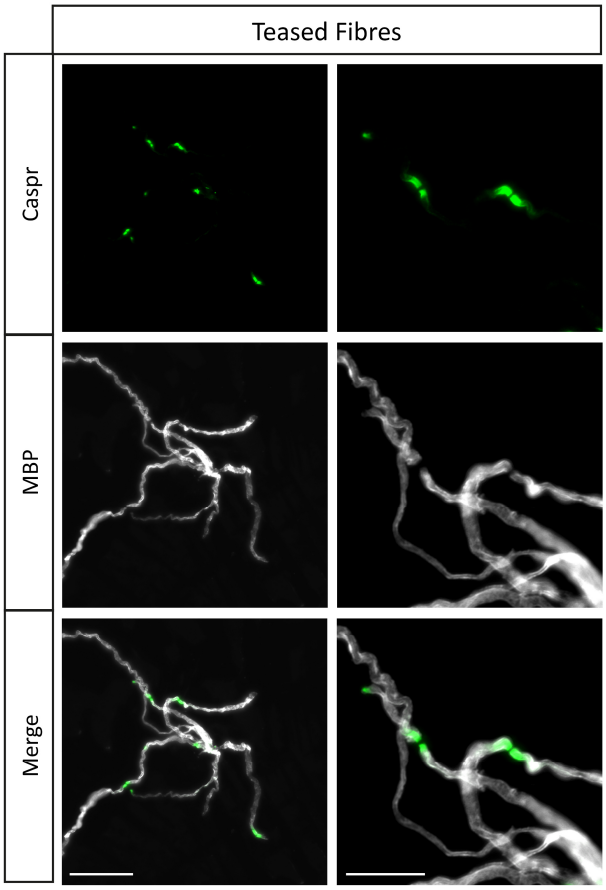


Figure 45: Attached teased fibres from the dorsal spinal cord after immunohistochemistry for MBP and Caspr at P18 of control animals

Teased and attached fibres were detectable under the fluorescent microscope after immunohistochemistry for MBP and Caspr. However, these fibres were never tdTomato positive.
Scale bar left: 50 µm, right: 20 µm

Attached fibres were myelinated as indicated by positive MBP immunoreactivity and nodes of Ranvier were visible by Caspr immunoreactivity (Figure 45). No tdTomato signal was detectable despite the fact that there should be tdTomato positive fibres present in the dorsal region of the spinal cord. Therefore, it is likely, that adhered fibres originate from the tissue surrounding the corticospinal tract.

5.2.4.2 Analysis of NoR parameters in the CC of LV Snap25 cKOs

Due to the above-mentioned difficulties with fibre adherence during teasing, the experimental setup was adjusted. Instead of parallel fibres in the dorsal corticospinal tract, fibres in the corpus callosum of coronal brain sections were examined regarding their nodal width. This region was chosen since there are parallel fibres positive for tdTomato in LV Snap25 cKOs as well as controls. The examination age was lowered to P14 to provide a sparse NoR density for optimal analysis. Additionally, this enables comparisons to future IUE experiments which do not exhibit tdTomato positive fibres in the dorsal corticospinal tract.

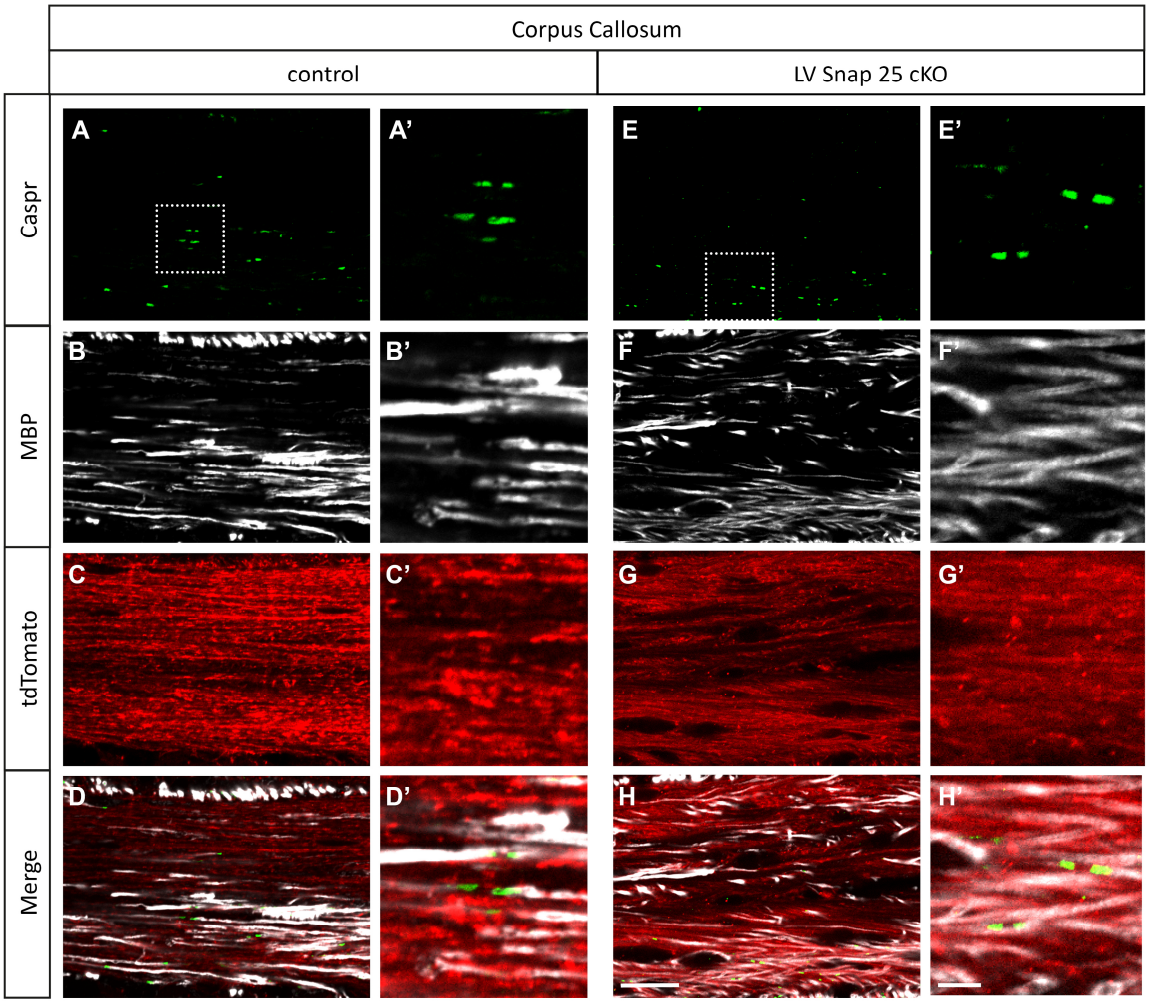


Figure 46: Regular Caspr immunoreactivity at nodes of Ranvier in the corpus callosum of LVI Snap25 cKO at P14

A-A') Caspr at the paranode of nodes of Ranvier in the corpus callosum in control animals. White box indicates magnified region indicated in A', B', C' and D'. B-B') MBP in the corpus callosum at P14 in control animals sparing nodes of Ranvier but being present at internodes. C-C') LV tdTomato positive fibres projection through the corpus callosum of control animals. D-D') Myelinated tdTomato positive fibres in the corpus callosum of control animals. Caspr (green) is located at the paranode, at the end of each internode where no MBP (white) can be found. E-E') Caspr at the paranode of nodes of Ranvier in the corpus callosum in LV Snap25 cKO. White box indicates magnified region indicated in E', F', G' and H'. F-F') MBP internodes in the corpus callosum in LV Snap25 cKOs sparing nodes of Ranvier. G-G') LV tdTomato positive fibres in the corpus callosum of LV Snap25 cKOs. H-H') Myelinated tdTomato positive fibres of LV Snap25 cKOs displaying Caspr at paranodes.

Images show a single plane of imaged z-stacks where two corresponding paranodes are in one plane that were used for analysis to demonstrate nodal density in the CC at P14. Scale bar left: 20 µm, magnification: 5 µm

Figure 46 shows laser scanning confocal micrographs of the corpus callosum at P14 after immunohistochemistry against MBP and Caspr. At P14, myelination is not yet completed in the murine brain, including the corpus callosum. The sparse myelination allowed to visualise internodes by MBP at tdTomato positive fibres ending in paranodes marked by Caspr. The gap between two paranodal Caspr stains is the nodal area where sodium channels are located.

Although the overall formation appeared visually normal, various distances of the node of Ranvier were analysed based on Caspr to determine if there are differences in the nodal structure between LV Snap25 cKOs and controls (Figure 47).

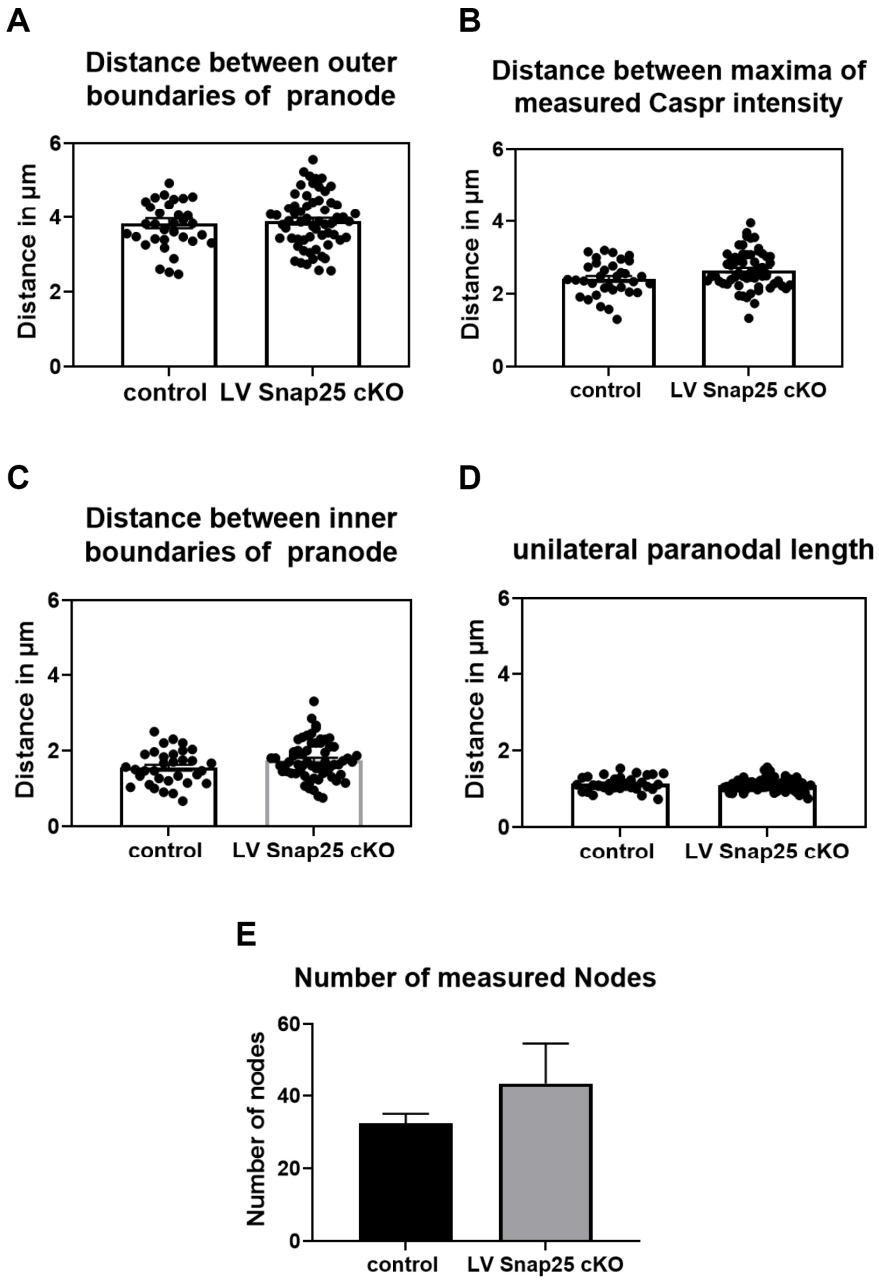


Figure 47: Nodal segmentation along axons is not affected at P14 in the corpus callosum when analysed based on Caspr immunoreactivity

A) The distance between the outer boundaries of the paranodes based on Caspr immunoreactivity signal in the corpus callosum is 3.7 (± 0.12) µm in controls and 3.9 (± 0.09) µm in LV Snap25 cKOs with no significant difference (p= 0.439). B) The distance between the maximum of Caspr intensity measured in each paranode is 2.3 µm (± 0.09) in controls and 2.6 µm (± 0.07) in LV Snap25 cKOs (p= 0.24). C) The distance between the inner boundaries of the paranodes based on Caspr signal in the corpus callosum is 1.5 µm (± 0.06) in controls and 1.7 µm (± 0.06) in LV Snap25 cKOs with no significant difference (p= 0.21). D) The unilateral paranodal length (heminode) based on Caspr signal in the corpus callosum is 1.1 µm in controls as well as in LV Snap25 cKOs (p = 0.93). E) In average 32 (± 2.7) nodes per control animal and 43 (± 11.3) per LV Snap25 cKO were measured. There was no significant difference between conditions (p= 0.60).
Nested t-test for A-D, Mann-Whitney test in E, values given are mean ± SEM, n=3/genotype

All measurements were performed in the corpus callosum at P14 from line measurement plots of confocal z-stack images. Measuring the outer boundaries of Caspr allows to examine the paranodal length. In LV Snap25 cKOs there is no significant difference of the overall length of the node (distance between outer boundaries) (Figure 47). Neither is there a significant difference when measuring the distance between maxima of Caspr stain at paranodes (p= 0.24), the inner nodal width (p= 0.21), the length of individual paranodes (heminode, controls & LV Snap25 cKOs: 1.1 µm, p= 0.93), nor when considering the average number of nodes counted per animal (p= 0.6).

Summing up the results from examine myelin thickness as well as node formation in LV Snap25 cKOs compared to controls, it is concluded that only myelin thickness in relation to axonal diameter (g-ratio) has been significantly altered in the spinal cord. Nodes, when assessed with the paranodal marker Caspr, did not show a significant difference between LV Snap25 cKOs and controls.

5.2.4 Protein and mRNA levels after degeneration of LVI Snap25 cKOs fibres

The last set of experiments undertaken in this thesis will especially deal with analysis of myelin markers when degeneration of fibres lacking Snap25 occure. As described in chapter 3, tdTomato positive axons in LV and LVI Snap25 cKOs became discontinuously labelled over different time courses in various regions of the CNS indicating degeneration of these fibres. Hence, I wanted to investigate if this has an effect on the surrounding myelin. Therefore, I processed 6 months old brain tissue for experimental usage in western blots (striatum) and qPCR (cortices of the same mice) to measure various protein and mRNA levels. Additionally, I measured mean fluorescence intensity of MBP and tdTomato from 6 and 9 months old LVI animals in two brain regions.

5.2.4.1 MBP protein-levels in western blot of striatal tissue do not reveal a detectable difference at 6 months

To assess if there is a quantifiable difference in MBP protein levels as a marker of myelin, a western blot was conducted and MBP protein levels normalised to the housekeeping gene GAPDH (Glyceraldehyde 3-phosphate dehydrogenase) for quantification.

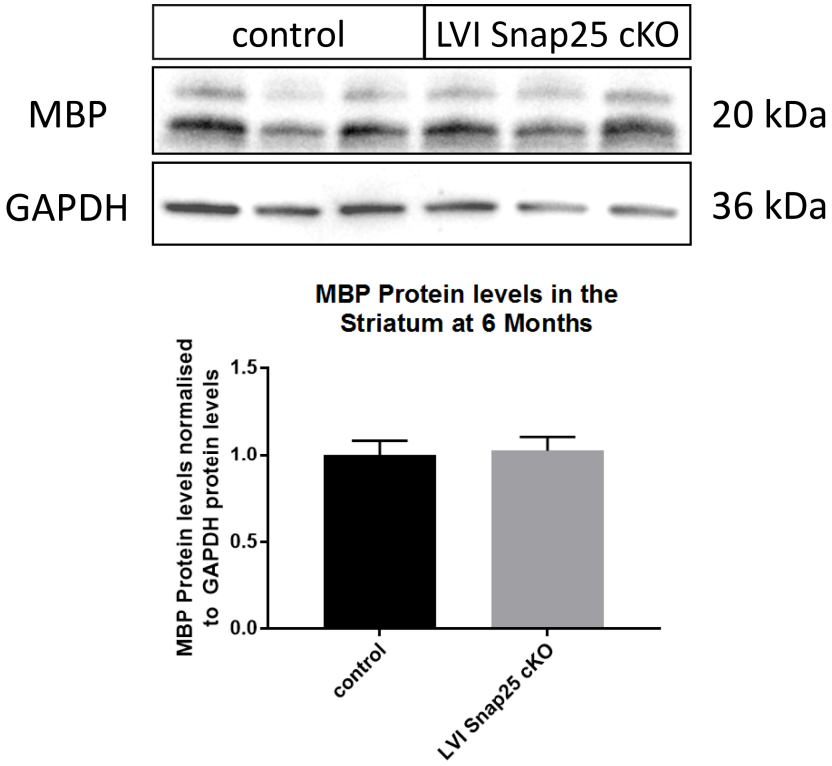


Figure 48: Quantitative western blot of myelin constituent MBP did not reveal a difference in MBP protein levels when normalised against the housekeeping gene GAPDH in striatal tissue at 6 months

The western blot of MBP shows two bands in each loaded lane. Murine MBP isoforms (14, 17, 18.5, 21.5) are between 14 and 21.5 kDa in which range the two MBP bands are detected (upper band at around 20 kDa, strongest band around 18 kDa). The loading control GAPDH, to which MBP levels have been normalised, shows comparative protein loading in all lanes. Quantification of 6 repetitions of this experiments indicate that there is no quantifiable difference between MBP levels in LVI Snap25 cKOs (1.003 ± 0.079) and controls (1.027 ± 0.081) at 6 months in the striatum (p 0.500).

One tailed Mann-Whitney test, values given are mean ± SEM, n=3/genotype

The western blot (Figure 48) shows bands for MBP as well as for GAPDH. Applying different antibodies against tdTomato protein did not result in a detectable band (data not shown). The quantification of MBP was conducted against the housekeeping gene GAPDH which showed comparative protein levels in all lanes. MBP exhibits two clear bands at around 20 kDa and 18 kDA (main band) with a third blurred underneath. These band areas match the 4 different murine MBP isoforms of 14, 17, 18.5 and 21.5 kDa.

The quantification following normalisation of MBP against GAPDH did not reveal a difference in MBP protein levels in striatal tissue at 6 months.

Next, our goal was to conduct qPCR (quantitative polymerase chain reaction) as a more sensitive technique to detect differences. Additionally, this enabled me to also target tdTomato levels, which was not possible in western blot as well as some more myelin and inflammation markers.

5.2.4.2 Analysis of oligodendroglial proteins and inflammation markers in LVI Snap25 cKOs at 6 months

Analysing qPCR data allows comparison of relative mRNA levels between conditions that have been normalised to a housekeeping gene. The aim was to examine if there is a detectable difference in mRNA levels of several oligodendrocyte genes at 6 months in cortical tissue in LVI Snap25 cKOs compared to controls when degeneration of underlaying tdTomato fibres is advanced. Additionally, two markers for inflammation (Iba1 and CD68) were tested to see if there is an increase in LVI Snap25 cKOs.

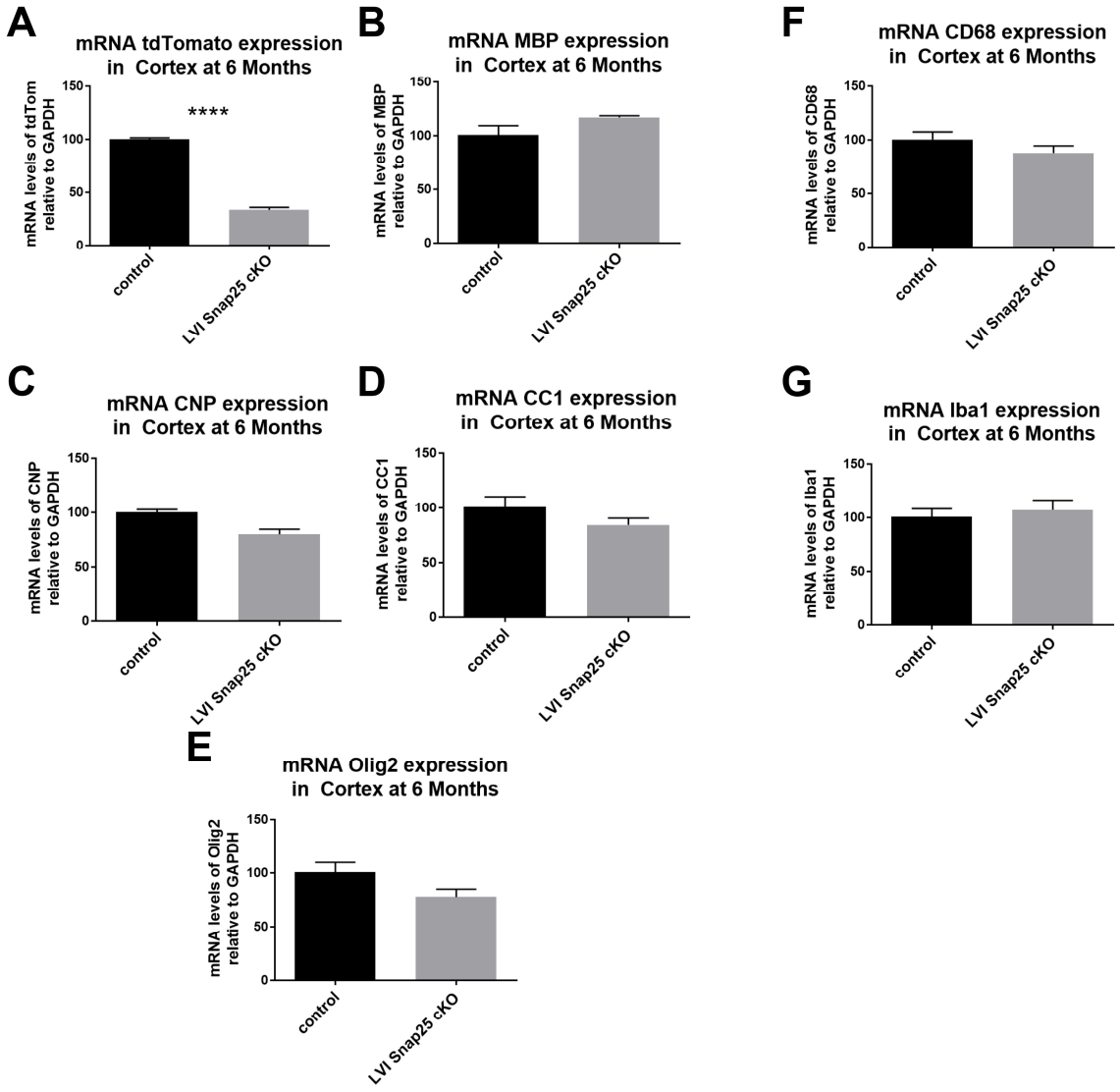


Figure 49: qPCR of mRNAs coding for myelin proteins or oligodendrocyte and inflammation markers of cortical tissue revealed significant difference in some mRNA levels

mRNA levels were normalised against housekeeping gene GAPDH. A) mRNA levels of tdTomato are significantly reduced (p= <0.0001) in LVI Snap25 cKOs (to 34%) at 6 months in the cortex when compared to controls. B) There is no significant difference in MBP mRNA levels between LVI Snap25 cKOs compared to controls (p= 0.464). The average MBP mRNA level in LVI Snap25 cKOs is slightly higher (117%) than in controls. C) CNP mRNA levels display a difference (p= 0.112) between control and LVI Snap25 cKO. In the cKOs CNP level is reduced (to 80%) compared to controls. D) CC1 mRNA levels are slightly reduced in LVI Snap25 cKOS (to 84%) compared to controls without a significant difference (p= 0.525). E) Olig2 mRNA levels show no difference between LVI Snap25 cKOs (78%) compared to controls (p= 0.464). F) CD68 mRNA levels are comparable between LVI Snap25 cKOS (to 88%) and controls (p= 0.525). G) There is no difference in Iba1 mRNA levels between genotypes (LVI Snap25 cKOs: 107%, p= 0.611).
t-test with adjusted p-values, values given are mean ± SEM, n=3/genotype

The analysis revealed that some mRNA levels of the examined proteins are significantly altered (Figure 49). The biggest difference, however, was neither seen in mRNA of oligodendrocytes nor degenerative and inflammation markers but in tdTomato. In the cortex of 6 months old LVI Snap25 cKOs mRNA levels of tdTomato were reduced to around 34%. The reduction in mRNA of tdTomato fits to the reduction in tdTomato that was observed in confocal images at 9 months of age (see chapter 3 and Figure 51).

Interestingly, mRNA levels of MBP as a marker for myelin and mature oligodendrocytes is not reduced but slightly increased in LVI Snap25 cKO to 117% without reaching significance (p= 0.464). Contrary to CNP (2',3'-Cyclic-nucleotide 3'-phosphodiesterase), which is also a marker for myelin and mature oligodendrocytes, was reduced to 80% (p= 0.112). CC1 is another marker that is mainly expressed in mature oligodendrocytes but not in myelin. The mRNA levels of CC1 are comparable between conditions (p= 0.525) as well as Olig2 levels (Oligodendrocyte transcription factor, a marker for the oligodendendroglial lineage, p= 0.464).

The proteins Iba1 (Ionized calcium binding adaptor molecule 1) and CD68 (Cluster of Differentiation 68) are markers for microglia and the macrophage lineage (Holness and Simmons 2018; Utans et al. 1995). Iba1 labels especially activated microglia in the case of injury and/or inflammation. I wanted to investigate if these mRNA levels are detectably upregulated in LVI Snap25 cKOs where tdTomato positive cells and corresponding fibres undergo degeneration which can cause inflammation. However, no significant difference was found when mRNA levels were analysed for Iba1 (p= 0.611) or CD68 (p= 0.525).

5.2.4.3 Reduced MBP/tdTomato-levels in degenerating LVI Snap25 cKOs at 6 and 9 months

As described in Chapter 3, fibres of LV as well as LVI Snap25 cKOs show signs of degeneration in adulthood. At 9 months, LVI Snap25 cKOs possess a circa 20% reduced number of tdTomato positive cells in M1 and a strongly reduced tdTomato signal in various brain regions (see chapter 3). I was interested in the MBP levels at 6 months (for comparison with western blot and qPCR analysis) and 9 months (when cell body loss was detected) in degenerating LVI Snap25 cKO brains compared to controls. Thus, I analysed MBP levels in the cortical area M1 where cell bodies are located as well as the striatum where descending axons project through at 6 and 9 months. The rational for this choice was based on the observation that fibre loss is visible much earlier than cell body loss. This led to the hypothesis that reduced signals will either earlier detectable or more detectable in the striatum than M1.

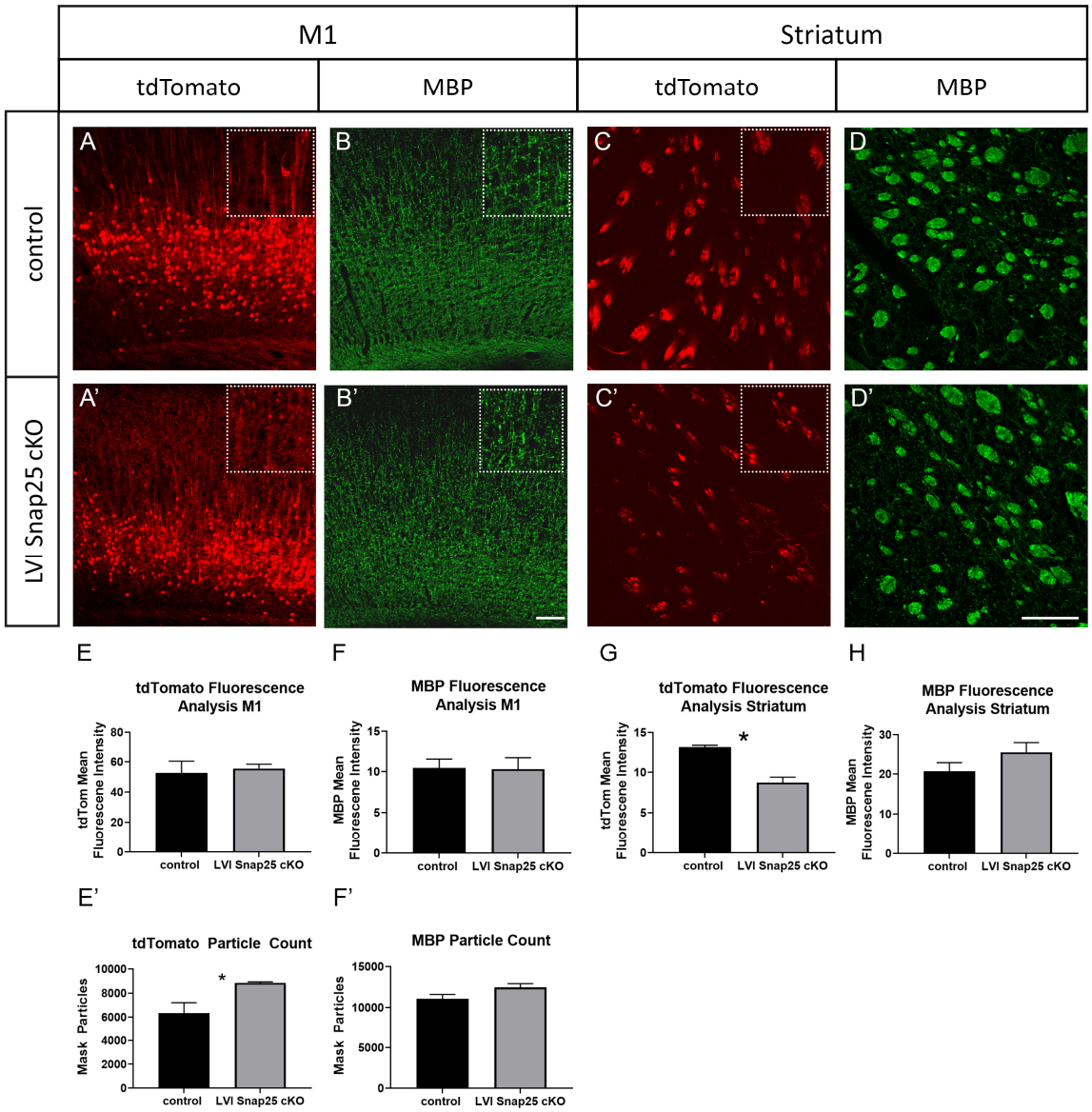


Figure 50: Reduced tdTomato signal intensity at 6 months in LVI Snap25 cKOs in the striatum

A-A') tdTomato signal in confocal images in M1 of LVI Snap25 cKOs and controls at 6 months. A disintegration of tdTomato signal is clearly visible E) Mean fluorescence intensity analysis of tdTomato in M1 reveals no difference in tdTomato levels in LVI Snap25 cKOs compared to controls (p= 0.50). E') Analysis of tdTomato particles in M1 shows significant more particles (less continuous neurits) in LVI Snap25 cKOs (8844 ± 84) compared to controls (6343 ± 859, p= 0.050). B-B') MBP signal after immunohistochemistry is observably altered, however not yet decreased in M1 of LVI Snap25 cKOs compared to controls. F) MBP mean fluorescence intensity does not show a difference between genotypes in M1 (p= 0.50). F') MBP particles in M1 do not show a significant increase in LVI Snap25 cKOs (12457 ± 466) compared to controls (11081 ± 527, p= 0.20). C-C') There are still some continuous fibres recognisable in LVI Snap25 cKOs compared to controls but several tdTomato punctae are visible. White boxes show

magnification of tdTomato positive fibre bundles. G) Mean fluorescence intensity analysis of tdTomato in the striatum shows a significantly loss in tdTomato signal in LVI Snap25 cKOs (8.7 ± 0.68) compared to controls (13.1 ± 0.23), (p= 0.050). D-D') MBP signal after immunohistochemistry in LVI Snap25 cKOs and controls in the striatum. H) MBP mean fluorescence intensity analysis does not indicate a significant difference in MBP signal of LVI Snap25 cKOs compared to controls (p= 0.20).
One-tailed Mann-Whitney test, values given are mean ± SEM, n=3/genotype, 3 sections/animal, scale bars: 100 µm

In Figure 50 M1 and striatum images taken with a confocal microscope are presented. Additionally, mean fluorescence image analysis of LVI Snap25 cKO and control brains at 6 months are shown and analysis of particles counted in M1. This was done since tdTomato signal in M1 is discontinuous with punctae present in LVI Snap25 cKOs compared to controls but especially because MBP signal seemed less continuous in cKOs. Both signals, MBP and tdTomato, are not yet reduced as seen in the mean fluorescence analysis of both proteins. The particle analysis, however, shows a significant increase meaning that LVI Snap25 cKOs have more tdTomato particles (deut to less continuous neurites, 8838 particles counted) compared to controls (6986 particles, p= 0.05). The similar analysis done for MBP shows no significant increase (controls: 10963 particles, LVI Snap25 cKOs: 12036, p= 0.2).

In the striatum tdTomato signal shows a significant reduction (around 33.6%) in LVI Snap25 cKOs when assessed by mean fluorescence intensity analysis without this effect also being present for MBP (Snap25 cKOs 25.4 ± 2.6, controls 20.7 ± 2.2, p= 0.20).

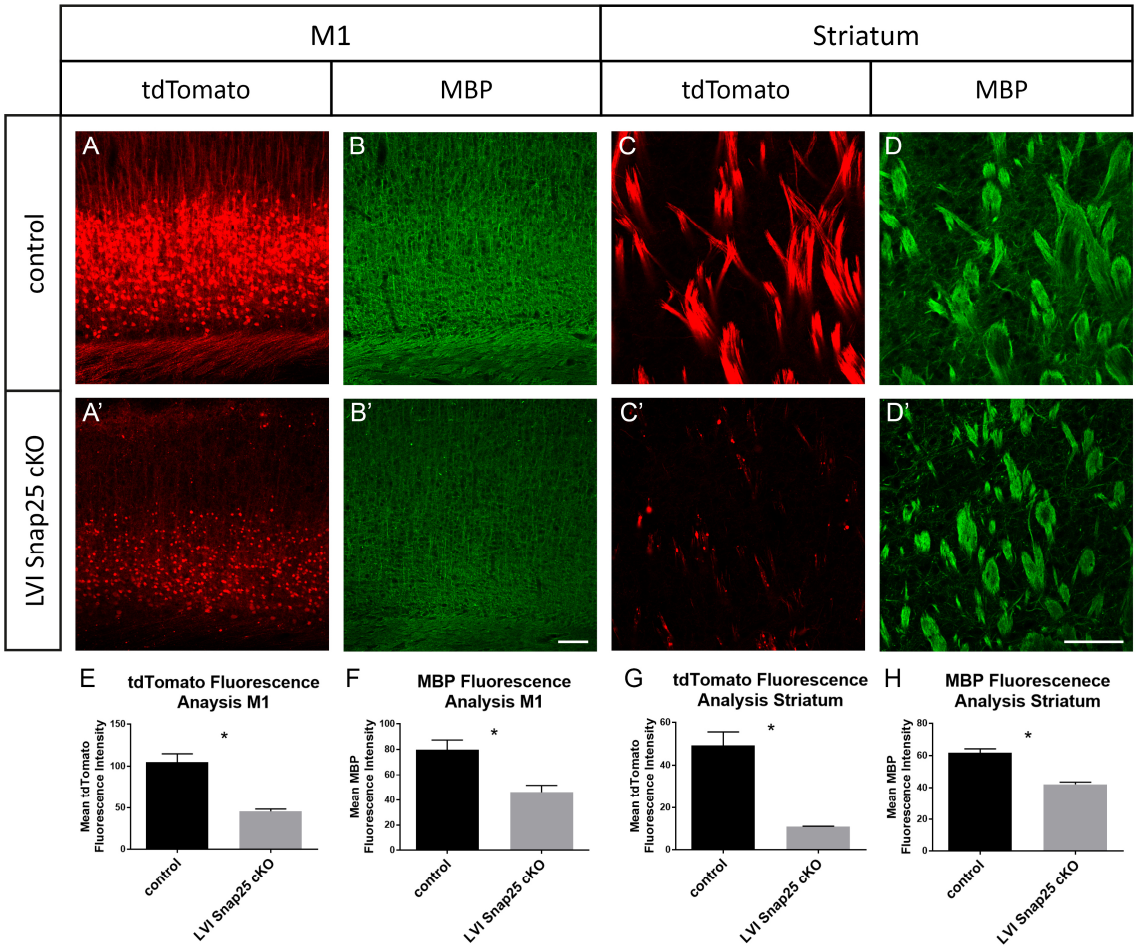


Figure 51: Reduced tdTomato and MBP signal intensity at 9 months in LVI Snap25 in primary motor cortex and striatum

A-A') tdTomato signal of confocal images is observably reduced in M1 of LVI Snap25 cKOs compared to controls at 9 months E) Mean fluorescence intensity analysis of tdTomato in M1 reveals reduced tdTomato signal in LVI Snap25 cKOs (45.6 ± 2.8) compared to controls (104.9 ± 9.8) (p= 0.050). B-B') MBP signal after immunohistochemistry is observably decreased in M1 of LVI Snap25 cKOs compared to controls. F) Analysis of MBP mean fluorescence intensity displays significant reduction in MBP signal in M1 of LVI Snap25 cKOs (46.5 ± 5.3) compared to controls (79.8 ± 7.6) (p= 0.050). C-C') There are no continuous tdTomato positive fibres recognisable anymore at 9 months in LVI Snap25 cKOs compared to controls but only tdTomato punctae are left. G) Mean fluorescence intensity analysis of tdTomato in the striatum reveals significantly reduced tdTomato signal in LVI Snap25 cKOs (10.99 ± 0.1) compared to controls (49.3 ± 6.3) (p= 0.050). D-D') MBP signal after immunohistochemistry is observably decreased in the striatum of LVI Snap25 cKOs compared to controls. H) Analysis of MBP mean fluorescence intensity in the striatum displays significant reduction in MBP signal of LVI Snap25 cKOs (42.2 ± 1.3) compared to controls (61.8 ± 2.5) (p= 0.050).

One-tailed Mann-Whitney test, values given are mean ± SEM, n=3/genotype, 2-3 sections/animal, scale bars: 100 µm

Figure 51 shows confocal images of M1 and striatum of LVI Snap25 cKO brains as well as controls after MBP immunohistochemistry at 9 months. There is a visually apparent reduction in tdTomato as well as MBP immunoreactivity in LVI Snap25 cKOs compared to controls in M1 as well as in the striatum. The mean fluorescence intensity analysis shows reductions of the tdTomato signals in M1 and striatum as well as reduced MBP levels in both regions. The biggest loss of mean fluorescence intensity was found in the tdTomato signal of the striatum where a 77.5% reduction was detected while MBP mean fluorescence intensity was reduced by 32.2%. In M1, the loss of tdTomato mean fluorescence intensity (56.2 %) also exceeded that of MBP (41.2%).

In conclusion, the results from degenerating LVI Snap25 cKO tissue showed that there is mainly a significant loss of tdTomato at 6 months. MBP mRNA or protein was not decreased at 6 months when probed by western blot or fluorescence intensity but at 9 months a decrease in fluorescence intensity can be observed.

5.3 Discussion

In this chapter myelin characteristics in LV and LVI Snap25 cKOs were described. Myelin thickness was determined in relation to fibre diameter and nodes of Ranvier were analysed by assessing different paranodal measurements by measuring the location of Caspr immunoreactivity. Additionally, myelin markers were probed to see alterations during premature aging of myelin ensheathed LVI Snap25 cKO fibres.

5.3.1 Decreased g-ratio in LVI Snap25 cKOs in the dorsal corticospinal tract at P18

G-ratios from LV Snap25 cKOs were calculated from EM measurements and compared to controls in the dorsal corticospinal tract at P18. The findings demonstrate that the average g-ratio is smaller (0.794) in LV Snap25 cKOs compared to the control mice (0.813). The g-ratio is known to decrease with increasing axon size, but there was no significant difference between axon diameters measured in the control (1008 µm) and cKO (1086 µm) spinal cord (p= p= 0.127). The distribution of g-ratios was overall shifted towards lower numbers across a range of values, but the correlation of axon diameter and g-ratio was not significantly altered, suggesting an effect across a range of axon diameters.

The decreased g-ratio in LV Snap25 cKOs implies that fibres are wrapped with more myelin in LV Snap25 cKOs than fibres in the control group which would lead to an increase in conduction velocity.

A prior study reported that 15% of LV cells express Rbp4-Cre in the somatosensory cortex at P6 (Grand and/or layer 5 paper). So far it is unclear, if this is comparable across ages and brain regions and therefore how it relates to the fibres in this

experiment that arise from the motor cortex at P18. It is also not shown how many of the cells expressing Rbp4-Cre in the motor cortex have collaterals into the spinal cord.

To answer this question of how many axons in the dorsal corticospinal tract are tdTomato positive, first EM experiments were conducted in combination with immune gold-labelling. Unfortunately, the experiment did not result in satisfactory myelin ultrastructure preservation. Additionally, the area of interest for quantification was difficult to identify. Myelin membrane is sensitive to disintegration during the perfusion process. Transcardial perfusion with PFA, which was sufficient for immunohistochemistry, was not sufficient for EM analysis. However, using glutaraldehyde, which is necessary for myelin preservation, prevents antibodies to bind to their epitopes during the labelling process (Dr Hayashi also had similar personal observations). Therefore, it is crucial to balance the amount of fixative in that a sufficient amount of fixation for myelin preservation is used while, at the same time, as little as possible is applied in order to ensure epitope exposure. This balance needs to be adjusted to each antibody since their ability to bind to their epitopes varies. Together with the fact that it was important to determine the area of interest, the dorsal corticospinal tract, it was challenging to combine high resolution EM to detect immuno-gold labelling with scanning the whole dorsal corticospinal tract.

Follow-up experiments by Dr Shuchi Hayashi from our laboratory enabled immuno-gold labelling of tdTomato in EM sections to assess layer V terminals in Po in thalamus within this mouse line. Hence, the protocol was not optimised for myelin and it is questionable if it would allow g-ratio quantification without further protocol changes.

Another attempt to identify the ratio of tdTomato positive fibres in the dorsal corticospinal tract for higher significance of EM results failed as well. By placing DiI into the motor cortex the overlap of tdTomato positive and DiI positive area should be compared in the dorsal corticospinal tract. DiI (1,1-Dioctadecyl-3,3,3,3-tetramethylindocarbocyanine perchlorate) is a fluorescent lipophilic dye which diffuses laterally and thereby labels cell membranes. DiI is thought to work only in young animals due to the increase in myelin lipids at older ages. However, experiments done in our laboratory could not prove this correlation between lack of carbocyanine dye labelling and onset of myelination. In my experiment, the DiI labelled cell membranes in the brain, however no labelling was observed in the spinal cord despite sufficient incubation times and conditions. The spinal cord displays relatively mature myelin patterns already at P11 while myelination in the brain is still strongly ongoing (Foran and Peterson 1992). This would support the hypothesis about the connection between DiI placement and myelination. Based on this assumption, myelination in the spinal cord was already too advanced to gain results at P12 when the placement was done.

Since all the attempts failed to determine the actual population ratio between tdTomato positive and negative fibres, we do not know how big the observed effect actually is. If only 15% of axons or less are affected and therefore show an altered g-ratio, this difference must be bigger than observed in the total average where 85% of not affected cells are included.

Hines and colleagues showed that in zebrafish VAMP2 dependent exocytosis in a subset of cells reduced sheath length. This effect disappeared when all neurons were electrically inactive. Therefore, they concluded that neuronal activity biases axon selection for myelination (Hines et al. 2015). In the dorsal corticospinal tract

Snap25 cKO axons extend alongside wildtype axons creating the competition that was needed to see activity dependent myelination in zebrafish and might play a role in mouse as well.

Hines and colleagues also demonstrated that myelin sheaths around silent axons are fewer and shorter. Here, we did not see a significant difference in the number of myelinated axons but a trend towards more axons being myelinated in LV Snap25 cKOs (600) versus controls (472). An increased number of myelinated axons counted in a cross section could indicate longer sheaths. Unmyelinated axons have not been counted due to the lower resolution of scanning electron microscopy in comparison to TEM. Future experiments might include 3D EM to visualise if shorter myelin sheaths are also present in the LV Snap25 cKO (Tomassy et al. 2014).

Recent findings challenged the former thinking that myelin along one individual axon is uniform by using modern imaging methods like 3D scanning EM (Tomassy et al. 2014; Giacci et al. 2018). This has been demonstrated in the optic nerve as well as for pyramidal neurons of the neocortex. For the spinal cord, the uniformity of myelin along axons has not yet been investigated. In the optic nerve it has been shown that not only myelin is not uniform but also that the fibre diameter is not. This is important when considering that the fibre diameter itself has an influence on the g-ratio (Giacci et al. 2018). Therefore, it is possible that 2D quantification, as performed in this thesis, is creating a confounded picture due to this irregularity along axons. Tomassy and colleagues also found that LV neurons are the most myelinated cells in the cortex compared to other layers. Additionally, LV neurons are not as affected by intermittent myelination as observed in layer II/III pyramidal

neurons. Contrary to upper layer neurons, deeper layer neurons have a longer pre-myelin axonal segment which can be dismissed since the axonal part in the spinal cord is far away from the cell body (Tomassy et al. 2014). Therefore, using 2D EM quantification on LV populations in the spinal cord was justifiable. Additionally, it has not yet been assessed if the effect of uneven myelination along axons might be ignorable when large numbers of axons are quantified as done in this thesis by measuring around 500 axons per animal.

To compare my findings with the current literature, it is important to know that no study so far has examined the effect of altered neuronal activity in murine spinal cord projections on myelin with electron microscopy. In zebrafish, Mensch and colleagues assessed activity dependent myelination by using EM in the spinal cord. A roughly 40% decrease was observed in the number of myelinated axons where synaptic exocytosis was disrupted (Mensch et al. 2015). The one murine study focusing on decreased neuronal activity in mice by monocular deprivation has not found an influence of decreased neuronal activity on myelin thickness in the optic nerve (Etxeberria et al. 2016). Two murine studies used EM to assess myelin thickness but focused on increased neuronal activity and the brain instead of the spinal cord (Gibson et al. 2014; Mitew et al. 2018). In these two murine studies an increase in neuronal activity by DREADD or optogenetics in the murine cortex resulted in an increase in myelin thickness (Gibson et al. 2014; Mitew et al. 2018). Mitew and colleagues used immuno-gold labelling of affected axons resulting in an observed effect double as big (difference of over 0.1) as observed by Gibson and colleagues (difference between groups roughly 0.05) when analysing a mixed population of affected and non-affected cells like performed in this thesis (it is

entirely possible that this is not only due to differences in methods but also in experimental reasons). Despite the fact that Gibson and colleagues also looked at dividing cells (EdU+) in the spinal cord and performed EM in their study, they did not perform EM in the spinal cord, due to a missing effect in dividing cells. However, it might be possible that changes in g-ratio occur, without changes in dividing cells by adaption of already existing oligodendrocytes.

In LV Snap 25 cKOs myelin thickness was increased in the dorsal corticospinal tract where fibres project through that do not have regulated neurotransmitter release. Zebrafish studies found that blocking synaptic vesicle release reduced the number of stabilised myelin sheaths during development and that sheaths were shorter in length (Hines et al. 2015; Mensch et al. 2015). This does not exclude a different thickness of the myelin wrap.

Importantly, it is noteworthy, that in zebrafish it has been shown that different subtypes of neurons (reticulospinal and commissural primary ascending (CoPA) neurons) that are similar to each other in several properties like axon calibre, birth time, long range axonal projection and myelin processes from the same oligodendrocyte still respond differently to changes in neuronal activity. While one subtype displayed fewer sheaths that were also 50% shorter, the other one was unaltered after reduction in neuronal activity by tetanus toxin expression (Koudelka et al. 2016). Targeting a different LV population (with another promotor than Rbp4 driving Cre expression), could result in different findings.

Due to this complexity that likely underlies activity dependent myelination, more studies are needed to look at various pathways to determine how the neuronal subtypes react to changes in neuronal activity. Those studies will most likely result

in varying findings dependent on which pathway is examined and which cells within this pathway. Therefore, more studies like this, were several subtypes are examined, will be needed.

5.3.2 Unchanged nodal parameters in the CC of LV Snap25 cKOs

Myelin thickness, as discussed in the previous section, is an important regulator of conduction velocity. Another one is the formation of nodes of Ranvier at which specialised proteins enable saltatory conduction of action potentials.

In this thesis, Caspr was used to examine the formation of nodes of Ranvier in LV Snap25 cKOs. Caspr is located at the paranode and thereby enables to measure paranodal length directly as well as nodal width indirectly. At the paranode myelin is anchored to the axon.

The initial aim was to measure nodal width as well as internodal distance in LV Snap25 cKOs compared to control. Therefore, fibre teasing of the dorsal corticospinal tract, through which tdTomato positive fibres in LV Snap25 cKOs and controls project, was performed. Unfortunately, fibre teasing of the dorsal corticospinal tract at P18 did not lead to the targeted result despite the fact, that I performed this technique successfully on the ventral funiculus. tdTomato positive fibres in the dorsal corticospinal tract stayed agglutinated instead of spreading and sticking to the adhesive slide surface.

In Figure 45 adhered fibres were shown that were immunoreactive for Caspr as well as MBP but no tdTomato positive fibres were detectable. These fibres are likely to originate from the surrounding white matter tissue like cuneate fasciculus. For fibre teasing fresh tissue, optimal tissue fixation as well as slide cover are crucial for the experiment to work. To exclude that the freshness of the tissue as

well as the used fixation method or the slide cover were the reason for the experiment not to work, I used ventral funiculus tissue from the same spinal cord as tdTomato fibre preparations. From the control tissue plenty of fibres were sticking to the slide without aggregating, proving that it must be the nature of the fibres in the dorsal corticospinal tract itself being responsible for the different behaviour in this experiment.

The experimental setting was adjusted in that tdTomato positive fibres in the corpus callosum were now analysed regarding their nodal width in LV Snap25 cKOs and compared to controls at P14. The reduced age provides sparse NoR density due to developing myelination during this timepoint for optimal analysis and provides optimal age for future comparisons with Kir2.1 IUE experiments. As described in chapter 3, the dorsal corticospinal tract does not exhibit tdTomato positive fibres after Kir2.1 IUE which would have prevented comparisons to LV Snap25 cKOs otherwise.

Several nodal measurements were taken based on Caspr immunoreactivity signal. Measurements taken were paranodal length, distance between outer paranodal boundaries, distance between Caspr maxima as well as heminodal paranode width (unilateral paranodal length) and finally the distance between inner paranodal boundaries was analysed to gain nodal width. Measurements were obtained blindly from line intensity profiles over Caspr regions of a 40x magnification confocal image. Optical slice thickness was set so that each node was sampled at least twice to ensure measuring at high Caspr intensity. A higher magnification (63x) can also be used with smaller optical slice thicknesses to sample nodes more often to may gain an even more accurate result. However, this would require higher laser power for imaging as well as longer (tile) scans to sample the same number of

nodes which leads to bleaching and outage of the section which lead to analysis from images taken with 40x objective.

There was no significant difference in the total number of nodes counted (controls: 32 nodes/animal vs LV Snap25 cKOs: 43 nodes/animal). However, the LV Snap25 cKOs group displays a relatively large SEM in the LV Snap25 cKOs of 11.3. This is due to the lowest number counted in one animal was 23 and the highest number counted in another of three animals was 62. When interpreting these numbers, it needs to be kept in mind, that only nodes horizontal to the focal plane were analysed to ensure both paranodes were visible. It is possible that small variations can arise from a minor angle in cutting coronal sections since fibres in the corpus callosum run mostly parallel to this plane.

Changes in the segmentation of mature myelin that is subdivided into internode, juxtaparanode, paranode and node can indicate changes in conduction velocity especially by alterations of ion channels distribution and/or amount (Waxman 1975; Wu et al. 2012).

In neurons that cannot release vesicles at their synaptic endings to communicate with other neurons by regulated neurotransmitter release, saltatory conduction might be altered due to less importance of their neuronal communication within their network. There was no significant difference in the number of nodes measured between LV Snap25 cKOs and controls. Changes in numbers of nodes of Ranvier would have pointed towards different internodal length and/or sheath number which influences conduction velocity. Analysis of the different Caspr parameters showed no significant difference in any of them. There were slight changes between conditions in the distance between the maximum of Caspr intensity measured in each paranode (controls: 2.3 µm, LV Snap25 cKOs: 2.6 µm)

without reaching significance (p= 0.24). Also, the inner nodal width was slightly bigger in LV Snap25 cKOs (1.7 µm) compared to controls (1.5 µm) without a significant difference (p= 0.21). Absolutely no difference was observed in the unilateral paranodal length (heminode, 1.1 µm in controls and LV Snap25 cKOs, p = 0.93).

This leads to the conclusion, that neither the node node itself, where sodium channels are located, nor the paranode, where myelin is anchored to the neuron, is influenced by reduction in neuronal activity. Simulations have shown that the NoR length can be a potential regulator of conduction speed (Arancibia-Cárcamo et al. 2017). However, due to the similarity between conditions this data suggests that if conduction velocity altered due to differences in g-ratio, nodes do most likely not contribute to changes in conduction speed.

5.3.3 Protein and mRNA levels after degeneration of LVI Snap25 cKOs fibres

In both Snap25 cKO mouse lines, premature degeneration of fibres lacking Snap25 in various CNS regions has been described (see chapter 3). So far, it had not been investigated what effect the degeneration in the mouse lines had on myelin.

Western blot, qPCR and quantitative confocal image analyses were conducted to provide information mainly about tdTomato and MBP protein as well as mRNA levels of LVI Snap25 cKO during ageing.

Analysis of MBP protein levels as a mature myelin marker by western blotting did not result in a detectable difference between LVI Snap25 cKO and control in striatal tissue at 6 months when normalised against the housekeeping gene GAPDH. MBP is an abundant protein in the striatum. It is possible that the amount lost due to degeneration of underlying LVI Snap25 cKO axons might be too little to detect in a

western blot. tdTomato in contrast, is specific to a subpopulation of LVI axons in this experiment. Hence, changes should have been more likely to be detected. Unfortunately, several tries with different antibodies suitable for detecting red fluorescent proteins (in immunohistochemistry) did not result in any bands for tdTomato on WBs. The same blots showed bands for MBP indicating that protein transfer etc all worked and sufficient protein amount is on the membrane for antibodies to bind. However, there is less tdTomato in the striatum than MBP due to its restriction to subpopulations of neurons. It might be possible that the amount of tdTomato protein in the striatum was not sufficient to produce a visible band but a cortex sample, where cell bodies, dendrites as well as axons containing tdTomato are located, could have. Cortex tissue of these brains was used for qPCR and therefore not available for western blots.

One explanation for the missing bands could be that some antibodies do not bind to proteins in the denaturing conditions of SDS-PAGE (sodium dodecyl sulfate polyacrylamide gel electrophoresis). In this case, the epitope is only recognised by the antibody when the native structure of the protein is preserved by fixation. This may explain why the sampled antibodies worked in immunohistochemistry when brain tissue was fixed by using PFA but failed to work in western blots after sample preparation that included denaturation. However, according to companies supplying the antibodies detecting tdTomato present in our laboratory, protein detection in western blots should be possible.

In line with the MBP results from western blotting, when MBP levels were analysed by quantitative confocal imaging at 6 months, there was no difference detected between LVI Snap25 cKOs and controls in the striatum and M1. Quantification of tdTomato signal showed a significant reduction in signal in the striatum but not yet

in M1. In M1 cell bodies of tdTomato positive neurons are located whereas in the striatum only fibres can be found. The fibre loss in this mouse line is more prominent and starts earlier than cell body loss. Therefore, observing a reduction in the striatum without yet observing one in M1 despite a discontinuous labelling is plausible. Additionally, the comparable tdTomato levels at 9 months in M1 between controls and cKOs underline the analysis done at P21 in M1, showing no difference in Cre-recombination efficiency.

At 9 months, MBP as well as tdTomato protein levels analysed by the same technique revealed significant differences for both proteins. In chapter 3, differences in tdTomato signal in the thalamus have already been detected between genotypes by this method. In this chapter, it became obvious that not only in the thalamus but also in the striatum and cortex of LVI Snap25 cKOs tdTomato signal is strongly reduced at 9 months when compared to controls. The reduction in tdTomato signal of LVI Snap25 cKOs that the statistical analysis reflects, is visually obvious in the images especially in the striatum where only punctae but no continuous tdTomato positive fibres were detectable. The striatum is also the area where the greatest reduction in tdTomato signal was measured with 77.5% at 9 months. At 6 months, the decrease in striatal tdTomato signal in LVI Snap25 cKOs compared to controls was only 33.6% indicating a worsening of the condition.

At 9 months, there is also a reduction in MBP immunoreactivity detected by quantitative confocal imaging in M1 and striatum. At 6 months, there was no quantifiable difference in MBP protein levels by western blotting in striatal tissue or by quantitative confocal image analysis in M1 and striatum. This finding indicates a loss in MBP proteins levels after 6 months. However, this late loss in MBP protein

levels of 32.2% in the striatum seems unlikely given the fact, that degeneration in this area was already observed at 2 months (see chapter 3).

After no difference was found in MBP proteins levels in western blot and image analysis despite progressive degeneration of LVI Snap25 cKO fibres at 6 months in the striatum, qPCR as a more sensitive technique was conducted in an attempt to detect smaller changes in MBP mRNA. In general, changes in mRNA, precursor to proteins, can be detected without changes in protein levels since not all cellular mRNA is translated into proteins. Further, using qPCR enabled me to also target additional markers as well as tdTomato mRNA levels, the latter protein having been undetectable by WB.

The tissue analysed with qPCR was cortical tissue from the same mice that were used for western blot analysis. tdTomato mRNA in LVI Snap25 cKOs showed a 34% significant reduction in mRNA levels when normalised to the housekeeping gene GAPDH, which was used for all normalisations in qPCR. Due to the implemented breeding scheme all control animals as well as all LVI Snap25 cKO animals were homozygous for the tdTomato gene excluding heterozygosity as a reason for the reduced mRNA levels. Additionally, all animals in both colonies were heterozygous for Cre also excluding different levels of Cre protein for being responsible for changes in tdTomato mRNA levels.

Four makers for the oligodendroglial lineage were also tested for alterations in their mRNA levels. MBP, CNP and CC1 are markers for mature oligodendrocytes whereas Olig2 is a transcription factor that determines oligodendroglial fate. In qPCR of 6 months old cortex tissue, CC1 and Olig2 are reduced, 84% and 78% respectively for LVI Snap25 cKOs but only CNP shows a statistical trend in its reduction to 80% compared to controls at 6 months. CNP has (SEM control: 2.8

and LVI Snap25 cKO: 4.5), compared to CC1 (SEM control: 9.5 and LVI Snap25 cKO: 6.3) and Olig2 (SEM control: 9.0 and LVI Snap25 cKO: 7.2), the lowest SEM. Interestingly, mRNA levels of MBP is not reduced but slightly increased in LVI Snap25 cKOs to 117% which was also detected by mean fluorescence analysis in the striatum at 6 months.

To conclude, qPCR as well as western botting revealed no significant reduction in MBP mRNA or protein levels as a marker for mature myelin at 6 months. At 9 months, a reduction in MBP protein was detected by using confocal images. Reduction in MBP levels would therefore only occur after 6 months. However, another marker, CNP, shows a trend towards reduction already reduced at 6 months. Note, that non-adjusted p-value indicated significance ($p= 0.020$), which disappeared after adjustment of p-values and became a trend ($p= 0.112$).

It is possible, that some myelin proteins might be more susceptible to myelin degeneration than others. Judging by the results for Olig2 mRNA, the oligodendroglial lineage does not seem to be significantly affected by ongoing degeneration and its influence on myelin. Due to neuronal loss, there is probably no need to replace lost myelin and therefore to increase oligodendrocyte numbers. Density of Olig2 and CC1 positive cells, as described in chapter 4, were also not influenced by a reduction in neuronal activity in LV and LVI cells in the motor cortex during development. Anyway, myelin could also be replaced by existing oligodendrocytes if their numbers are not altered.

It is worth mentioning, that in two out of three methods, protein and mRNA levels were normalised to a housekeeping gene that may also be affected by degeneration. Less cells because of degeneration would also mean less of housekeeping genes. Although there is some literature about housekeeping genes

in degenerating or injured tissue (like muscle or peripheral nervous system, Gambarotta et al. 2014; Yüzbaolu et al. 2010), no such literature was found on CNS degeneration. One study suggested to use a minimum of two housekeeping genes in cases of general degeneration to improve presumptions (Vandesompele et al. 2002).

GAPDH as well as myelin proteins are abundant proteins in the striatum and the cortex. tdTomato, however, is restricted to the affected cell population in both conditions and therefore less abundant. Changes in tdTomato due to degeneration are therefore more likely to be detectable than in myelin markers when compared to a housekeeping gene expressed in all surrounding cells. Small reduction in this number would still allow for tdTomato changes to be detectable in the analysis.

Alongside various markers for myelin, two inflammation markers were tested in the cortical tissue in both conditions, Iba1 (Ionized calcium binding adaptor molecule 1) and CD68 (Cluster of Differentiation 68). Since we observed neurodegeneration of LVI Snap25 cKO fibres, we expected mRNA levels of inflammation markers to be higher expressed in LVI Snap25 cKOs compared to controls due to arising cell debris that needs to be cleared (Neumann, Kotter, and Franklin 2009). Both makers showed slight changes without significant differences. Iba1 mRNA was slightly increased to 107% whereas CD68 mRNA decreased to 88%. Degeneration had started 4 months earlier to the time point tested in qPCR. In LV Snap25 cKOs immunohistochemistry against Iba1 showed that during the onset of degeneration at P48, no difference can be seen in Iba1 positive cell numbers. At 8 months, a non-significant increase can be seen comparable to the qPCR results of LVI Snap25 cKOs at 9 months. In LV Snap25 cKOs, Iba1 positive cells that displayed the morphology of activated microglia were more abundant in the deeper layer of

the cortex where LV cell bodies are located as well. Given the milder degenerative phenotype of LVI Snap25 cKOs, this was not assessed for LVI cKOs.

Additionally, I observed further signs of inflammation accompanying degeneration which were followed up by Dr Hoerder-Suabedissen. Autophagosomes and an increase in autofluorescence as possible lipofuscin deposits in the cortex of LV Snap25 cKOs were present. The increase in autofluorescence was already visible at P48 and significant at 8 months (Hoerder-Suabedissen, Korrell et al. 2018). In LV Snap25 cKOs the increase in broad spectrum autofluorescence was very obvious. In LVI Snap25 cKOs at 9 months there was no obvious increase in broad spectrum autofluroescence. Hence, we did not follow this up with dedicated imaging and analysis.

5.3.4 Conclusion

In this chapter I described the analysis of factors known to influence conduction velocity, such as g-ratio and nodes of Ranvier, in axons lacking Snap25. The analyses showed that LV Snap25 cKOs have a significant reduction in dorsal corticospinal tract g-ratio compared to controls and a significantly longer nodal width in the CC.

Additionally, in this chapter mRNA and protein levels of myelin proteins, tdTomato and inflammation markers in LVI Snap25 cKOs were assessed. The results showed that there is mainly a significant loss of tdTomato and CNP mRNA at 6 months. MBP mRNA or protein was not decreased at 6 months but at 9 months when assessed through fluorescence intensity analysis.

6 Discussion

The aim of my thesis was to contribute to our understanding of activity dependent myelination in the mammalian CNS with a particular focus on deep cortical layer projection neurons.

Each experimental chapter addressed different issues. First, postnatal axonal outgrowth, targeting and maintenance was studied in a subpopulation of murine cortical projection neurons after abolishing Snap25 expression or over-expression of Kir2.1. I observed, that postnatal axonal targeting was not affected when regulated synaptic vesicular release was abolished or neuronal activity was decreased. However, I found that fibre maintenance in Snap25 cKOs was impaired.

Second, oligodendroglial density and myelination was assessed after genetic abolition of regulated synaptic vesicular release between P8 and P21 in deep cortical layer neurons and their projections, or in the CC at P14 after neuronal Kir2.1 electroporation. No major difference was detected between experimental and control groups neither in myelination onset nor in density of oligodendroglial cells.

Finally, wider aspects of myelinated axon morphology were explored by investigating g-ratios in the dorsal corticospinal tract of LV Snap25 cKOs, nodes of Ranvier in the projections extending through the corpus callosum, and the impact of axonal degeneration on myelin in LV and/or LVI neurons where Snap25 was ablated. I observed a reduced g-ratio at P18 in the dorsal corticospinal tract that originates from LV neurons without seeing changes in nodal characteristics in the

corpus callosum fibres of LV Snap25 cKOs at P14. The impaired fibre maintenance in LVI Snap25 cKOs resulted in a decrease in myelin in adulthood.

6.1 Importance of activity dependent myelination

Myelination takes place mainly during development and is necessary for healthy brain physiology. The importance of myelination is obvious in demyelinating diseases such as Multiple Sclerosis (MS), but its dynamic nature during healthy adulthood has only recently started to emerge. This is exciting, as the possibility of modulating myelination long after first developmental myelination has taken place, for example by neuronal activity, might open new therapeutic approaches for patients. Many questions about developmental myelination, remyelination after demyelination as well as activity dependent myelination *in vivo* in mammals are still unsolved. One reason has historically been, and still is, the relative paucity of methods to link anatomical studies, e.g. post-mortem examinations or brain imaging, with processes at the cellular level, especially in humans. Employing mouse models is one way to overcome this gap. In 2014 and 2015, seminal studies were published on genetic manipulation of neuronal activity to observe adaptive myelination *in vivo* in zebrafish and mice (Hines et al. 2015; Mensch et al. 2015; Gibson et al. 2014). Since then, there has been a growing interest to learn more about activity dependent myelination at different stages. Previously, it has been proven that motor as well as spatial learning in adulthood involves myelin changes (Sampaio-Baptista et al. 2013; Blumenfeld-Katzir et al. 2011; McKenzie et al. 2014). Gibson investigated the opposite paradigm and looked if changes in myelination based on increased neuronal activity can result in improved motor behaviour (Gibson et al. 2014).

These studies revealed a new mechanism *in vivo* to permit brain changes, namely adaptive myelination (R. D Fields 2015). This phenomenon holds huge promise, as it represents a novel way by which brain tissue can be modified. In this sense, the discovery of adaptive myelination represents an important example of how basic research has the potential to elevate the platform of investigation that could lead to the discovery of new therapeutic treatments.

6.2 What are the mechanisms of activity-dependent myelination?

The current emerging body of literature investigating activity dependent myelination solves some of the early controversies, but it also gives rise to new questions (Colello et al., 1995; Demerens et al., 1996; Fukui et al., 1991; Gyllensten & Malmfors, 1963; Hayes & Meyer, 1989; Moore et al., 1976; Omlin, 1997; Shrager & Novakovic, 1995; Tauber et al., 1980). For example, one question that remains to be answered in detail is the mechanism underlying activity dependent myelination. It is likely that several mechanisms play a role in adaptive myelination as suggested after studies in zebrafish and that different outcomes are to be expected dependent on the experimental paradigm applied (Hines et al. 2015). Below, methods that have so far been used to alter neuronal activity in the context of studying activity dependent myelination *in vivo* and the consequential suggested mechanisms are briefly summarised.

Similarly to the murine model used in this thesis, neuronal activity was altered by influencing synaptic vesicle exocytosis in zebrafish. Vesicular release as a target in studying activity dependent myelination was based on studies where neurotransmitter communication via synapses was shown to be present as a mechanism of communication between neurons and oligodendroglial cells

(Paukert and Bergles 2006; Lin and Bergles 2004). Experiments in zebrafish indicated that synaptic vesicular release at synapses as well as at ensheathment sites participate in axon selection and participate in activity dependent myelination (Hines et al. 2015). Mensch et al concluded that single oligodendrocytes can adapt their myelination capacity in response to decrease or increase in synaptic vesicle release (Mensch et al. 2015).

These findings in zebrafish were strengthened by a subsequent report of attenuated glutamate release mimicking the phenotype of monocular deprivation in the optic nerve in mouse. This additional finding indicated that glutamate release might be a mechanism by which activity dependent myelination can be regulated in the murine CNS (Etxeberria et al. 2016). Yet, it is likely that utilising diverse methods of changing neuronal activity (e.g. increasing it as well as decreasing it, changing the pattern of action potential, changing regulated or non-regulated vesicular or non-vesicular transmitter release) will give variable results, probably also depending on the surroundings that silenced neurons are in (active vs non-active). Additionally, it is possible that several activity-dependent processes are in place, which has been shown to be the case in the zebrafish spinal cord. Synaptic vesicle release biases axon selection during development in a way that can be influenced by activity of surrounding axons. However, additional excitability dependent mechanism exist that are not influenced by activity of surrounding axons (Hines et al. 2015).

6.3 Various ways of myelin plasticity

Adaptive myelination can occur in many different ways. So far it is not completely understood, which neuronal changes result in which form of adaptive myelination. One has to distinguish between *de novo* myelination of former unmyelatined axons or axonal segments or adjustment of already existing sheath via internodal length, myelin thickness or nodal adjustments (R. D Fields 2015). LV and LVI projections as studied in this thesis are denser myelinated than upper layers (Tomassy et al. 2014). Moreover, layer V and layer VI could have a heterogeneous neuronal population with different projections in the populations identified through Rbp4-Cre and the Ntsr1-Cre expressions. The difference in pattern of myelination could affect adaptive myelination which can act by *de novo* myelination or by changes of already existing structures.

Individual features of myelin morphology can change independently of others. Due to the varying ways in which myelination can be adapted, specific set of experiments are needed to explore various possibilities. Further studies investigating adaptive myelination would need to take all these possibilities into account. Results showing that one myelin characteristic is not altered does not mean, that another one is also not affected. One example for this in my thesis is the result, that there was no difference between groups in the onset of myelination and oligodendroglial marker expression, however, nodal width was significantly affected. Ultimately, it needs to be proven whether the observed changes especially after increased neuronal activity lead to increased conduction speed and optimisation of the circuit function. The only study showing improved circuit function, measured by improved motor output (faster hindlimb swing speed after

cortical neuron stimulation), does not measure conduction speed in stimulated axons (Gibson et al. 2014).

6.4 Hypoactivity and activity independent mechanisms

Increase in neuronal activity by learning a new motor task for example, has been shown to affect myelination both in mice and human (Bengtsson et al., 2005; Carreiras et al., 2009; Pujol et al., 2006; Scholz et al., 2010; Sampaio-Baptista et al. 2013; Kaller et al. 2017). However, whether hypoactivity results in thinner myelin sheaths has not yet been shown. Those experiments are hard to control for, in human and in mice. The closest experimental set up so far to mimic hypoactivity is by studying social isolation. Prolonged social isolation of adult mice resulted in impaired myelination, cognitive and behavioural dysfunction as well as ultrastructural changes in prefrontal oligodendrocytes (Liu et al. 2012). While social re-integration of adult mice normalised these effects, re-integration of adolescent mice did not (Makinodan et al. 2012). Activity on neuronal levels in these experiments was not studied.

There are activity independent factors that could influence myelination. Experiments that showed myelination of carbon fibres as well as after global reduction of neuronal activity indicated towards a mechanism where neuronal activity is not solely responsible for activity dependent myelination. Axonal microenvironment such as spatial constraints have also been demonstrated to be an important determining factor in OPC development and myelination, independent of dynamic axonal signalling (Rosenberg et al. 2008). Since all axons are (more or less) active in a functioning CNS, this seems likely. Mechanisms based solely on

neuronal activation would otherwise result in myelination of all axons that would result in a misfunctioning coordination of signals because precise signal management is more important than conduction maximisation. Neuronal activity could help specify which axons need to get preferentially myelinated if there is an activity difference between axons in one area. Researchers suggested a two phase myelination process where oligodendrocyte-intrinsic (neuronal independent) and then neuronal adaptive mechanisms interplay for optimal outcome in myelination (Bechler et al. 2017). Fibre diameter has shown to be one determining factor for myelination decision (Bechler, Byrne, and Ffrench-Constant 2015). It is possible, that diameter as well as activity levels in combination influence myelination decisions further. However, most studies so far controlled for differences in fibre diameter and have not observed influences in fibre diameter on adaptive myelination (Hines et al. 2015; Mensch et al. 2015; Etxeberria et al. 2016; Mitew et al. 2018).

6.5 The role of diffusible molecules in activity-dependent myelination

LV and LVI neurons, as studied in this thesis, have long range projections so that OPCs and oligodendrocytes are located far away from synaptic endings where synaptic vesicles with transmitters and other soluble factors were traditionally thought to be released during neuronal activity. More recent studies have shown that neurotransmitters are also secreted along the axolemma in a vesicle dependent as well as vesicle-independent fashion (Fields & Ni 2010; Fields 2011; Stevens et al. 2002; Gudz 2006; Xiao et al. 2013). In zebrafish, an accumulation of vesicles has been reported at axon-glia contact sides suggesting an importance

of their cargo for myelination initiation (Hines et al. 2015). Future studies will likely attempt to address the identity and roles of specific vesicle cargoes. In addition to neurotransmitters, also neurotrophins have the potential to influence myelination at different stages (Xiao, Kilpatrick, and Murray 2009). Diffusible signals could be sensed by single oligodendrocytes via synapses or the accumulation of them in the surrounding could influence myelinating cells. One promising candidate for influencing adaptive myelination in the CNS via vesicular released neurotrophins is brain-derived-neurotrophic factor (BDNF) (Vondran et al. 2010; Wong et al. 2013; Lundgaard et al. 2013). While BDNF also influences axon growth, this diffusible molecule is known to be involved in synaptogenesis and synaptic remodelling, and therefore in learning and memory (Lu et al. 2013; Park and Poo 2012). In 2015 it was shown that VAMP2 and Snap25 mediate the vesicular release of BDNF in all subcellular domains of cortical pyramidal somatosensory neurons *in vivo* (Shimojo et al. 2015). Previously, it was largely unknown which SNAREs are involved in the secretion of neuronal proteins that are involved in experience-dependent plasticity.

BNDF is mainly secreted by neurons and astrocytes in a neuronal activity dependent manner and promotes CNS myelination by activating the receptor tyrosine kinase B (TrkB) (Xiao et al. 2010; Ghosh, Carnahan, and Greenberg 1994; Tao et al. 1998). In vivo, BDNF KO mice displayed reduced numbers of NG2 positive cells in the basal forebrain from embryonic development onwards without alterations in the number of CC1 positive oligodendrocytes. Additionally, immunohistochemistry against myelin markers exhibited reduced protein levels leading to the conclusion that BDNF is involved in oligodendrocyte differentiation (Vondran et al. 2010). Conditional deletion of TrkB in murine oligodendrocytes

during development resulted in an increase in OPC density while also exhibiting a reduction in myelin protein expression as well as myelin thickness in the white matter without altered numbers of mature oligodendrocytes and myelinated axons (Wong et al. 2013).

In studies examining adaptive myelination in zebrafish vesicle exocytosis was prevented by targeting VAMP2. The observed effects in these studies might therefore also be based on prevented neurotrophin release. Hence, also the effects on myelination in LV and LVI Snap25 cKOs could be mediated by dynamic changes in BDNF levels rather than activity related reasons. Experiments of our collaborators from the Barde laboratory, University of Cardiff, showed that BDNF levels in LV Snap25 cKOs are indeed increased compared to controls (Hayley Dingsdale, Yves-Alain Barde, Hoerder-Suabedissen, Molnár, unpublished observations). Although the increase in BDNF levels of LV Snap25 cKOs is in contrast to the finding that Snap25 is necessary for BDNF release, it could explain missing effects on MBP levels observed in this thesis. While a reduction in neuronal activity could give rise to signals impairing several myelin features, an increase in BDNF could initiate the opposite signals and thereby cancelling each other out. Altered levels of BDNF could also influence the maintenance of fibres in the Snap25 cKO mouse lines used in this thesis.

Similar effects like BDNF on myelination could be due to higher glutamate levels in Snap25 cKOs. It has been reported that in a forebrain glutamatergic neuron-specific Snap25 knockout mouse model significantly elevated extracellular glutamate levels were found in the cerebral cortex. These mice exhibited a typical schizophrenia-like phenotype (Yang et al. 2017). Glutamate has been suggested as a potential mechanism to influence activity dependent myelination by Etxeberria

after attenuation of it mimicked visual deprivation in the optic nerve (Etxeberria et al. 2016)

In conclusion, genetic cell-type specific manipulations in combination with manipulations of neurotrophin and neurotransmitter receptors in oligodendroglia cells might help to shed further light on the mechanisms underlaying adaptive myelination in different model organisms at different time points and different locations during development.

6.6 Future possibilities of influencing neuronal vesicular release

As shown in this thesis, genetic ablation of *Snap25* in a subset of cortical projection neurons leads to degeneration of axonal projections and ultimately to a loss of cell bodies. To examine long-term effects of reduced neuronal activity on myelination this model is therefore not optimal and other models where axon and cell degeneration is not observed are required. I did not observe similar signs of degeneration in the mice electroporated with Kir2.1. However, they were sacrificed at early postnatal periods. Previous literature using Kir2.1 did also not report axon degeneration and cell death making it a better model for long term observations.

A promising candidate for knock outs to observe long-term effects of reduced vesicle release on myelination is VAMP2 as it was used in zebrafish without degeneration reports. The third member of the trans SNARE complex necessary for synaptic vesicle exocytosis alongside Snap25 and VAMP2, is syntaxin. Syntaxin has been associated with reduced neuronal viability *in vitro* as well as *in vivo* which precludes its suitability for long-term observations (Kofuji et al. 2014; Vardar et al. 2016).

The Molnár laboratory has already investigated knock out mice that lack vesicle release included a Munc18 (mammalian uncoordinated-18) as well as Munc13 1,2,3 triple KO mice (DPhil Thesis Blakey, 2005). The aim was to observe effects of murine CNS neuronal activity to gain deeper insights into developmental disorders. Like the Snap25 null mutant, Munc18 and 13 KO embryos die immediately after birth due to a breathing deficit. This is due to the fact that all three proteins are essential components of the synaptic vesicle fusion complex (Varoqueaux et al. 2002; Washbourne et al. 2002, Blakey et al. 2007). While the Munc13 1,2,3 KO did not show any gross abnormalities, the Munc18 KO had considerable cell death in the region of the internal capsule, but not in thalamus or cortex.

Generating new conditional KO mouse lines (like Munc13 or 18 KO) is a time and cost intensive process and was therefore not within the scope of my thesis when degeneration of Snap25 cKOs was observed. Despite *in utero* electroporation being a challenging surgery, it is a useful technique because of a quicker adaption in experimental setup with changing plasmids than with generating a new transgenic mouse strain. A follow up approach would be to use the Cre-dependent Snap25 mouse lines to inject a Cre containing virus rather than to cross with mouse line where the Cre-promotor is expressed across whole layers. Virus injection enables to target specific cortical areas. This process has recently been adopted in the Molnár laboratory in collaboration with other laboratories but requires project licence from the home office and also extensive training similarly to the IUE is needed. By injecting only specific subregions of the cortex, regional differences for example in the different sensory areas could be studied followed by behaviour experiments that are tailored for a particular cortical region. Injections into specific

cortical areas would also allow to study the effects of abolished neuronal regulated vesicular release in other experimental set ups, besides adaptive myelination. With the current mouse model this is suboptimal since the promotors Rbp5 (LV) as well as Ntsr1(LVI) also display expression outside cortical areas like the cerebellum and hippocampus (Hoerder-Suabedissen, Korrell et al. 2018). Interestingly, basic motor behaviour tests conducted with LV Snap25 cKOs revealed relatively minor phenotype despite reducing neuronal activity in LV partially as well as the other cell types. Mice displayed hindlimb clasp which is a sign of upper motorneuron lesion (similar to mouse parkinsonism) and an inability to learn the rotarod, which could also be due to the extracortical Cre-expression.

Another potential research avenue is to generate a tamoxifen induced Snap25 cKO. Snap25cKO cells show earliest signs of degeneration in the fourth postnatal week (LV Snap25 cKO), approximately 4.5 weeks after Snap25 deletion by Cre expression. When examining the onset of myelination, tamoxifen-induced silencing would have to take place at the end of the first postnatal week and thereby probably pushing the onset of degeneration 2 weeks back allowing more time for analysis. Additionally, tamoxifen-induced Snap25 cKOs also would have the advantage that regulated vesicle release would not be reduced prenatally and could examine if reduced neuronal activity might only be influencing myelinating when it is reduced in a narrow time window rather than prenatally. This approach could then also be used to study reduced regulated vesicular release even at later time points in adulthood. Using a tamoxifen induced approach to reduce neuronal activity probably needs to include several time points since different studies suggest that oligodendrocytes have a limited time window in which they select axons for

myelination (Czopka, Ffrench-Constant, and Lyons 2013; Stevens, Tanner, and Fields 1998; Zalc and Fields 2000; Watkins et al. 2008). In the zebrafish spinal cord, it has been excluded that the time window is altered or influenced by neuronal activity. However, in the CNS and in mammals this has yet to be proven (Hines et al. 2015).

Notably, evoked synaptic vesicle release is severely reduced in Snap25 conditional knockout neurons when recorded in cultured hippocampal neurons but has not been determined *in vivo* at different ages (Hoerder-Suabedissen et al. 2018). Additionally, ablation of *Snap25* abolishes the regulated exocytosis, but does not affect spontaneous vesicle release or non-vesicular release (Washbourne et al. 2002). Thus, it cannot be excluded that the remaining vesicle release might be sufficient for essential signals to oligodendrocytes. Contrary to Snap25 ablation, Kir2.1 overexpression also reduces spontaneous activity additionally to reduced excitability (Yu et al. 2004; Johns et al. 1999; Hagihara et al. 2015). Overall outgrowth and targeting of IUE fibres seemed not to be affected after Kir2.1 electroporations compared to controls but detailed targeting and branching was not studied. Mitew and colleagues observed effects on adaptive myelination after Kir2.1 overexpression (Mitew et al. 2014). Further experiments are needed to distinguish if effects seen are only due to reduced excitability or the lack of spontaneous release or if both are needed in combination.

6.7 The influence of regional differences in adaptive myelination

This thesis examined subpopulations of neurons from deep layers of the cortex with subcortical long-range projections. It is known that different cell types within the zebrafish CNS displayed distinct sensitivity to activity dependent myelination

(Koudelka et al., 2016). It is a possibility that this also occurs in the mammalian CNS, but this has yet to be investigated. However, some studies seem to indirectly suggest this. For example, Gibson and colleagues observed a proliferative response of oligodendroglia in the deep layers of the cortex and subcortical projections after LV stimulation without a similar response in deep white matter projections down the cortico-spinal tract (Gibson et al. 2014). In this thesis, only brain white matter was studied for oligodendroglial density but not deep white matter projections. It is not to exclude that differences in sensitivity to adaptive myelination might even occur within one layer since layers are not formed out of uniform cell population. LV and LVI were targeted by using Rbp4- and Ntsr1-promotor driven Cre expression, respectively. Choosing different promotors that activate Cre expression in a changed neuronal subtype within these layers could result in different findings. It might even be possible that by exclusively targeting these promotors, axons from similar neuronal subtypes projected in close proximity to the same target so that all neurons in their surrounding are non-active and thereby simulating global reduced activity.

Additionally, is has been shown that myelin thickness and axon diameter is not uniform even along single axons (Giacci et al. 2018; Tomassy et al. 2014). Hence, regional differences along long-range projection axons are possible and could result in varying results of studies depending on the site of examination. Mitew and colleagues examined oligodendroglial cell density within the corpus callosum after Kir2.1 electroporations of upper cortical layers and found no change in the density of OPCs or mature oligodendrocytes at P20 (Mitew et al. 2018). This examination is still outstanding for deeper layers after similar electroporations. Targeting deep

versus superficial cortical populations might result in different outcomes since MBP measurements in this thesis were not identical to Mitew's findings.

6.8 Changes in myelin characteristics following changes in neuronal activity

When comparing the findings of this thesis with the current literature, a key distinction to keep in mind is that no previous study has looked at the effects of reduced regulated vesicular release in the murine CNS, and the only previous study has addressed this issue in the optic nerve and no other region. This study relied on conditionally ablating the *Vglut2* gene in retinal ganglion cells to genetically block vesicular glutamate release and did not find an effect of decreased neuronal activity on the g-ratio in the optic nerve (though an increase in oligodenrogenesis and shorter internode length was found, Etxeberria et al. 2016). In contrast to the results by Etxeberria and colleagues, my results in spinal cord projections from layer V cortical neurons with ablated Snap25 did show a reduced g-ratio in comparison with controls. I established these differences using electron microscopy, but no significant difference was found between groups in the average fibre diameters and myelinated fibres counted (although both values showed a trend of p= 0.126). This implies that Snap25 ablated or neighbouring WT fibres are wrapped with more myelin in LV Snap25 cKOs than fibres in the control group. Since no examination of oligodendroglial density in this region was conducted, it is not known if changes in OPC or oligodendrocyte numbers are responsible for the increase in formed myelin or if single oligodendrocytes adapted their myelination capacity. OPCs can differentiate into oligodendrocytes with or without prior division (Hughes et al. 2013). Further attempts should be made to identify how many cells

in the dorsal corticospinal tract are Cre/tdTomato positive. My attempts to use carbocyanine dye (DiI) tracing at P12 was unfortunately not successful to answer this question and neither was post-embedding immuno-gold EM.

In comparison with the currently available literature, increase in neuronal activity of three murine studies showed reduced g-ratios (Piscopo et al. 2018; Gibson et al. 2014; Mitew et al. 2018). Even subtle changes in g-ratio have been predicted to result in significant changes in conduction speed (Smith and Koles 1970). However, if the here observed reduction in g-ratio is restricted to projections with abolished Snap25 which do not contribute to regulated information transfer, changes in conduction speed should not influence neuronal circuit function.

Future experiments might include 3D EM to visualise myelin sheath length on axons originating from cells where Snap25 is ablated or after the firing was reduced by Kir2.1 electroporations. So far, internodal length after reducing neuronal activity had only been studied in the optic nerve after monocular deprivation where a shorter internodal length was observed and was associated with a significantly reduced conduction velocity (Etxeberria et al. 2016). Attempts to measure internodal length in my thesis by fibre teasing was not successful in the dorsal corticospinal tract despite success in other regions of the spinal cord. Number of nodes in a given area could be seen as an indirect measure of internodal length. In LVI Snap25 cKOs and Kir2.1 electroporations a reduction in the number of nodes was identified by another laboratory member, Jolande Disser, which was not present in LV Snap25 cKOs. Without changes in myelin**,** this could suggest that there are longer internodes, contrary to Etxeberria's findings in the optic nerve after reduced neuronal activity (Etxeberria et al. 2016). Longer internodes, up to a certain point, would lead to an increase in conduction velocity. Fibre tracing in

combination with immunohistochemistry could be an alternative method to 3D EM to measure internodal length for example in the corpus callosum where fibres run relatively parallel.

Our laboratory continued to study NoRs in the corpus callosum as an extension of my project. NoRs were analysed in Kir2.1 and MutKir2.1 electroporated fibres and LVI Snap25 cKOs additionally to my work in LV Snap25 cKOs. Preliminary results indicate a trend towards shorter nodes in Kir2.1 IUE compared to controls with samples size for Kir2.1 being only 2 (n=2). This trend was not observed in LVI Snap25 cKOs (Jolande Disser, Erasmus visiting student from University of Amsterdam). My results in LV Snap25 cKOs showed a contrary trend towards longer nodal width without changes in paranodal length. This might be an example how neuronal activity in the murine CNS can influence different neuronal populations in varying ways as shown in zebrafish (Koudelka et al. 2016).

Simulations of increased node diameter (by a fixed density in channels per area) showed that an increase in channels per node could increase current flow along an axon (Ford et al. 2015). It is to keep in mind that by introducing an additional potassium channel (like Kir2.1) that will be located at the NoR changes in nodal channel composition might be expected.

Further experiments will be needed to give deeper insights into internodal length as well as nodal width after various manipulations that reduces neuronal activity in the mammalian CNS and its implications for conduction velocity.

6.9 Conclusion

Ablating Snap25 to abolish regulated vesicular release and lowering excitability by introducing Kir2.1 both allow to achieve drastic change in neuronal activity.

Surprisingly, drastic changes in myelinated long-range projections were not always observed as a consequence of this change. One possibility is that such drastic changes in neuronal activity fail to elicit an effect as they are outside the normal physiological range. It might therefore be possible that smaller, naturalistic changes are sufficient to influence the network function in a meaningful way. Notably, seminal *in vitro* work has proven that specific firing patterns are needed in order to stimulate myelin formation via cell adhesion molecules (Stevens, Tanner, and Fields 1998). It might be possible that eliciting a specific firing pattern that is more likely to occur in a functioning network may result in a bigger effect than general silencing of fibres.

My thesis showed that the influence of neuronal activity on myelination in mice might not be apparent or as strongly apparent in cortical projections as it is in other cell types or CNS regions or in non-mammalian species. However, within this thesis I could not study all aspects due to time constrains. Future experiments will likely include analysis of oligodendroglial cells after silencing of deep cortical neurons in the corpus callosum as well as in deep white matter like it has been done by Mitew as well as Gibson and colleagues (Gibson et al. 2014; Mitew et al. 2018).

Due to the complexity that likely underlies activity dependent myelination, additional studies are needed to explore the various pathways that determine how the neuronal subtypes react to changes in neuronal activity. My thesis is on the forefront of nascent literature exploring the fascinating field of adaptive myelination as an additional mechanism of plasticity in the mammalian CNS.

References

Adrian. 1912. “The All-or-None Principle in Nerve.” *J Physiol*.

Aggarwal, Yurlova, Snaidero, Reetz, Frey, Zimmermann, Pähler, et al. 2011. “A Size Barrier Limits Protein Diffusion at the Cell Surface to Generate Lipid-Rich Myelin-Membrane Sheets.” *Developmental Cell*, August, 1–12. doi:10.1016/j.devcel.2011.08.001.

Agmon, a, and B W Connors. 1992. “Correlation between Intrinsic Firing Patterns and Thalamocortical Synaptic Responses of Neurons in Mouse Barrel Cortex.” *The Journal of Neuroscience* 12 (1): 319–29. doi:10.1523/JNEUROSCI.12-01-00319.1992.

Agmon, and Connors. 1989. “Repetitive Burst-Firing Neurons in the Deep Layers of Mouse Somatosensory Cortex.” *Neurosci Lett* 99: 137–41.

Aigner, Avossa, Diana, Barry, Barbarese, and Carson. 1997. “Transport and Localization Elements in Myelin Basic Protein MRNA.” *Journal of Cell Biology* 138: 1077–87.

Ainger, Avossa, Morgan, Hill, Barry, Barbarese, and Carson. 1993. “Transport and Localization of Exogenous Myelin Basic Protein MRNA Microinjected into Oligodendrocytes.” *J Cell Biol.* 123 (2): 431–41.

Allen, and Barres. 2009. “Glia — More than Just Brain Glue.” *Nature* 457 (February): 675–77.

Almeida, and Lyons. 2017. “On Myelinated Axon Plasticity and Neuronal Circuit Formation and Function.” *J Neurosci.* 37 (42): 10023–34. doi:10.1523/JNEUROSCI.3185-16.2017.

Althaus, Burgisser, Klöppner, Rohmann, Schröter, Schwartz, Siepl, and Neuhoff. 1987. “Oligodendrocytes Ensheath Carbon Fibres and Produce Myelin in Vitro.” *Glial-Neuronal Communication in Development and Regeneration*, 779–98.

Althaus, Montz, and Neuhoff. 1984. “Isolation and Cultivation of Mature Oligodendroglial Cells.” *The Science of Nature*, 309–15.

Ambrosini, Sicca, Brignone, Adamo, Napolitano, Servettini, Moro, et al. 2014. “Genetically Induced Dysfunctions of Kir2.1 Channels: Implications for Short QT3 Syndrome and Autism – Epilepsy Phenotype.” *Human Molecular Genetics* 23 (18): 4875–86. doi:10.1093/hmg/ddu201.

Anderson, Eisenstat, Shi, and Rubenstein. 1997. “Interneuron Migration from Basal Forebrain to Neocortex: Dependence on Dlx Genes.” *Science* 278 (October): 15–18.

Angevine, and Sidman. 1961. “Autoradiographic Study of Cell Migration during Histogenesis of Cerebral Cortex in the Mouse.” *Nature*.

Anthony, Klein, Fishell, and Heintz. 2004. “Radial Glia Serve as Neuronal Progenitors in All Regions of the Central Nervous System.” *Neuron* 41: 881–90.

Antonini, Antonella, and Michael P Stryker. 1993. “Rapid Remodeling of Axonal Arbors in the Visual Cortex.” *Science* 260 (June): 1819–22.

Antonini, and Stryker. 1996. “Plasticity of Geniculocortical Afferents Following Brief or Prolonged Monocular Occlusion in the Cat.” *The Journal of Comparative Neurology* 369 (1). John Wiley & Sons, Inc.: 64–82. doi:10.1002/(SICI)1096-9861(19960520)369:1<64::AID-CNE5>3.0.CO;2-I.

Antonio, Del Río, Martínez, and Auladell. 2000. “Developmental History of the Subplate and Developing White Matter in the Murine Neocortex. Neuronal Organization and Relationship with the Main Afferent Systems at Embryonic and Perinatal Stages.” *Cereb Cortex*, 784–801.

Arancibia-Cárcamo, Ford, Cossell, Ishida, Tohyama, and Attwell. 2017. “Node of Ranvier Length as a Potential Regulator of Myelinated Axon Conduction Speed.” *ELife* 6. doi:10.7554/eLife.23329.

Aronoff, Matyas, Mateo, Ciron, Schneider, and Petersen. 2010. “Long-Range Connectivity of Mouse Primary Somatosensory Barrel Cortex.” *Eur J Neurosci.* 31 (April): 2221–33. doi:10.1111/j.1460-9568.2010.07264.x.

Artzt, and Wu. 2010. “STAR Trek: An Introduction to STAR Family Proteins and Review of Quaking (QKI).” *Adv Exp Med Biol*.

Attwell, and Laughlin. 2013. “An Energy Budget for Signaling in the Grey Matter of the Brain.” *J Cereb Blood Flow Metab.*, no. March: 1133–45.

Auladell, Pérez-Sust, Supèr, and Soriano. 2000. “The Early Development of Thalamocortical and Corticothalamic Projections in the Mouse.” *Anat Embryol*, no. 201: 169–79.

Azevedo, Carvalho, Grinberg, Farfel, Ferretti, Leite, Filho, and Lent. 2009. “Equal Numbers of Neuronal and Nonneuronal Cells Make the Human Brain an Isometrically Scaled-Up Primate Brain.” *The Journal of Comparative Neurology* 541 (September 2008): 532–41. doi:10.1002/cne.21974.

Baas, Bourbeau, Sarliéve, Ittel, Dussault, and Puymira. 1997. “Oligodendrocyte Maturation and Progenitor Cell Proliferation Are Independently Regulated by Thyroid Hormone.” *Glia* 19 (4): 324–332.

Bain, Burnett-Hall, and Montgomerie. 1994. “SNARE Motif and Neurotoxins.” *Nature* 372: 415–16.

Ballabh, Braun, and Nedergaard. 2004. “The Blood-Brain Barrier: An Overview: Structure, Regulation, and Clinical Implications.” *Neurobiology of Disease* 16 (1): 1–13. doi:10.1016/j.nbd.2003.12.016.

Bansal, Stefansson, and Pfeiffer. 1992. “Proligodendroblast Antigen (POA), a Developmental Antigen Expressed by A007/O4-Positive Oligodendrocyte Progenitors Prior to the Appearance of Sulfatide and Galactocerebroside.” *Journal of Neurochemistry* 58 (6): 2221–29. doi:10.1111/j.1471-4159.1992.tb10967.x.

Baraban, Mensch, and Lyons. 2016. “Adaptive Myelination from Fish to Man.” *Brain Research* 1641: 149–61. doi:10.1016/j.brainres.2015.10.026.

Barbin, AIGROT, CHARLES, FOUCHER, GRUMET, SCHACHNER, ZALC, and LUBETZKI. 2004. “Axonal Cell-Adhesion Molecule L1 in CNS Myelination.” *Neuron Glia Biology* 1 (01). Cambridge University Press: 65–72. doi:10.1017/S1740925X04000092.

Barbour, and Callaway. 2008. “Excitatory Local Connections of Superficial Neurons in Rat Auditory Cortex.” *The Journal of Neuroscience* 28 (44): 11174–85. doi:10.1523/JNEUROSCI.2093-08.2008.

Bark, Hahn, Ryabinin, and Wilson. 1995. “Differential Expression of SNAP-25 Protein Isoforms during Divergent Vesicle Fusion Events of Neural Development.” *Proc Natl Acad Sci USA* 92 (February): 1510–14.

Barrera, Chu, Abramowitz, Steger, Ramos, and Brumberg. 2013. “Organization of Myelin in the Mouse Somatosensory Barrel Cortex and the Effects of Sensory Deprivation.” *Developmental Neurobiology* 73 (4): 297–314.

doi:10.1002/dneu.22060.
Barres, Burne, Holtmann, Thoenen, Sendtner, and Raff. 1996. “Ciliary Neurotrophic Factor Enhances the Rate of Oligodendrocyte Generation.” *Molecular and Cellular Neuroscience* 8 (2): 146–56. doi:https://doi.org/10.1006/mcne.1996.0053.
Barres, Hart, Coles, Burne, Voyvodic, Richardson, and Raff. 2018. “Cell Death and Control of Cell Survival in the Oligodendrocyte Lineage.” *Cell* 70 (1). Elsevier: 31–46. doi:10.1016/0092-8674(92)90531-G.
Based. 1998. “The Synaptic SNARE Complex Is a Parallel Four-Stranded Helical Bundle.” *Nature Structural Biology* 5 (9): 765–69.
Baudry, Davis, and Anderson. 1991. *Long-Term Potentiation - A Debate of Current Issues*. 1st ed.
Bauer, Moos, Horssen, Witte, Valk, Altenhein, Luhmann, and White. 2012. “Myelin Basic Protein Synthesis Is Regulated by Small Non-coding RNA 715.” *EMBO Rep.* 13 (9). Nature Publishing Group: 827–34. doi:10.1038/embor.2012.97.
Baumann, and Pham-Dinh. 2001. “Biology of Oligodendrocyte and Myelin in the Mammalian Central Nervous System.” *Physiological Reviews* 81 (2): 871–927. http://www.ncbi.nlm.nih.gov/pubmed/11274346.
Bechler, Byrne, and Ffrench-Constant. 2015. “CNS Myelin Sheath Lengths Are an Intrinsic Property of Oligodendrocytes.” *Current Biology* 25 (18). The Authors: 2411–16. doi:10.1016/j.cub.2015.07.056.
Bechler, Swire, and Ffrench-Constant. 2017. “Intrinsic and Adaptive Myelination-A Sequential Mechanism for Smart Wiring in the Brain.” *Developmental Neurobiology*, 1–12. doi:10.1002/dneu.22518.
Beeman, David. 2014. *Hodgkin-Huxley Model*. *Encyclopedia of Computational Neuroscience*. doi:10.1007/978-1-4614-7320-6_127-3.
Bengtsson, Nagy, Skare, Forsman, Forssberg, and Ullén. 2005. “Extensive Piano Practicing Has Regionally Specific Effetcs on White Matter Development.” *Nature Neuroscience*, 1148–50.
Bennett. 1970. “Comparative Physiology: Electric Organs.” *Annual Review of Physiology*.
Bergles, Dwight E, and William D Richardson. 2019. “Oligodendrocyte Development and Plasticity,” 1–28.
Bergles, Roberts, Somogyi, and Jahr. 2000. “Glutamatergic Synapses on Oligodendrocyte Precursor Cells in the Hippocampus.” *Nature* 405 (6783): 187–91. doi:10.1038/35012083.
Berry, and Rogers. 1965. “The Migration of Neuroblasts in the Developing Cerebral Cortex.” *Journal of Anatomy* 99 (Pt 4). England: 691–709.
Bhat, Axt, Fosnaugh, Smith, Johnson, Hill, Kinzler, and Baraban. 1996. “Expression of the APC Tumor Suppressor Protein in Oligodendroglia.” *Glia* 174: 169–74.
Bhat, Baraban, Johnson, and Eipper. 1994. “High Levels of Expression of the Tumor Suppressor Gene APC High Levels of Expression during Development of the Rat Central Nervous System.” *The Journal of Neuroscience* 14 (May).
Biase, De, Kang, Baxi, Fukaya, Pucak, Mishina, Calabresi, and Bergles. 2011. “NMDA Receptor Signaling in Oligodendrocyte Progenitors Is Not Required for Oligodendrogenesis and Myelination.” *Journal of Neuroscience* 31 (35): 12650–62. doi:10.1523/JNEUROSCI.2455-11.2011.
Bin, Harris, and Kennedy. 2016. “The Oligodendrocyte-specific Antibody ‘CC1’

Binds Quaking 7." *Journal of Neurochemistry*, 181–86. doi:10.1111/jnc.13745.
Binzegger, Tom, Rodney J Douglas, Kevan A C Martin, and Ch- Zu. 2004. "A Quantitative Map of the Circuit of Cat Primary Visual Cortex." *The Journal of Neuroscience* 24 (39): 8441–53. doi:10.1523/JNEUROSCI.1400-04.2004.
Blakemore, and Murray. 1980. "Quantitative Examination of Internodal Length of Remyelinated Nerve Fibres in the Central Nervous System." *Journal of Neurological Science*, 273–84.
Blakey, Wilson, and Molnár. 2012. "Termination and Initial Branch Formation of SNAP-25 Deficient Thalamocortical Fibres in Heterochronic Organotypic Co-Cultures." *Eur J Neurosci* 35 (10): 1586–94. doi:10.1111/j.1460-9568.2012.08120.x.Termination.
Blumenfeld-Katzir, Pasternak, Dagan, and Assaf. 2011. "Diffusion MRI of Structural Brain Plasticity Induced by a Learning and Memory Task." *PLoS ONE* 6 (6). doi:10.1371/journal.pone.0020678.
Boggs. 2006. "Myelin Basic Protein: A Multifunctional Protein." *Cellular and Molecular Life Sciences : CMLS* 63 (17): 1945–61. doi:10.1007/s00018-006-6094-7.
Boggs, Rangaraj, Heng, Liu, and Harauz. 2011. "Biochimica et Biophysica Acta Myelin Basic Protein Binds Microtubules to a Membrane Surface and to Actin Fi Laments in Vitro: Effect of Phosphorylation and Deimination." *BBA - Biomembranes* 1808 (3). Elsevier B.V.: 761–73. doi:10.1016/j.bbamem.2010.12.016.
Bond, Pessia, Xia, Lagrutta, Kavanaugh, and Adelman. 1994. "Cloning and Expression of a Family of Inward Rectifier Potassium Channels." *Receptors & Channels* 2 (3). England: 183–91.
Bortone, Olsen, and Scanziani. 2014. "Translaminar Inhibitory Cells Recruited by Layer 6 Corticothalamic Neurons Suppress Visual Cortex." *Neuron* 82 (2). Elsevier Inc.: 474–85. doi:10.1016/j.neuron.2014.02.021.
Boschert, Shaughnessy, Dickinson, Tessari, Bendotti, and Catsicas. 1996. "Developmental and Plasticity-Related Differential Expression of Two SNAP-25 Isoforms in the Rat Brain." *The Journal of Comparative Neurology* 193: 177–93.
Bourassa, Pinauit, and Deschqnes. 1995. "Corticothalamic Projections from the Cortical Barrel Field to the Somatosensory Thalamus in Rats : A Single-Fibre Study Using Biocytin as an Anterograde Tracer." *Eur J Neurosci.* 7 (June 1994): 19–30.
Bouvier, Bartoli, Aguirre-Cruz, Virard, Colin, Fernandez, Gouvernet, and Figarella-Branger. 2003. "Shared Oligodendrocyte Lineage Gene Expression in Gliomas and Oligodendrocyte Progenitor Cells." *Journal of Neurosurgery* 99: 344–50.
Brakeman, Gu, Wang, Dolin, and Baraban. 1999. "Neuronal Localization of the Adenomatous Polyposis Coli Tumor Suppressor Protein." *Neuroscience* 91 (2): 661–72.
Bredt, Wangt, Cohen, Gugginot, and Ii. 1995. "Cloning and Expression of Two Brain-Specific Inwardly Rectifying Potassium Channels." *Proc. Natl Acad. Sci. USA* 92 (July): 6753–57.
Bremaud, West, and Thomson. 2007. "Binomial Parameters Differ across Neocortical Layers and with Different Classes of Connections in Adult Rat and Cat Neocortex." *PNAS*.

Briggs. 2010. “Organizing Principles of Cortical Layer 6.” *Frontiers in Neural Circuits* 4 (February): 1–8. doi:10.3389/neuro.04.003.2010.
Briggs, and Callaway. 2001. “Layer-Specific Input to Distinct Cell Types in Layer 6 of Monkey Primary Visual Cortex.” *The Journal of Neuroscience* 21 (10): 3600–3608.
Brightman, and Reese. 1969. “Junctions between Intimately Apposed Cell Membranes in the Vertebrate Brain.” *Journal of Cell Biology*.
Brill, Waxman, Moore, and Joyner. 1977. “Conduction Velocity and Spike Configuration in Myelinated Fibres : Computed Dependence on Internode Distance.” *Journal of Neurology*, 769–74.
Brivio, Faivre-Sarrailh, Peles, Sherman, and Brophy. 2017. “Assembly of CNS Nodes of Ranvier in Myelinated Nerves Is Promoted by the Axon Cytoskeleton.” *Current Biology* 27 (7). Elsevier Ltd.: 1068–73. doi:10.1016/j.cub.2017.01.025.
Brodmann, Korbinian. 1909. *Vergleichende Lokalisationslehre Der Großhirnrinde*. Leipzig.
Bronk, Dea, Wilson, Liu, Su, Kavalali, Wilson Mc, and X Liu. 2007. “Differential Effects of SNAP-25 Deletion on Ca2+ -Dependent and C 2+ - Independent Neurotransmission.” *J Neurophysiol.*, 794–806. doi:10.1152/jn.00226.2007.
Brose, Petrenko, Sudhof, and Jahntt. 1992. “Synaptotagmin: A Calcium Sensor on the Synaptic Vesicle Surface.” *Science.* 256 (May): 1021–26.
Brown, and Hestrin. 2009. “Intracortical Circuits of Pyramidal Neurons Reflect Their Long-Range Axonal Targets.” *Nature* 457 (7233). Nature Publishing Group: 1133–36. doi:10.1038/nature07658.
Burrone, Byrne, and Murthy. 2002. “Multiple Forms of Synaptic Plasticity Triggered by Selective Suppression of Activity in Individual Neurons.” *Nature.* 420 (November). doi:10.1038/nature01179.1.
Butler, Dantzker, Shah, and Callaway. 2001. “Development of Visual Cortical Axons: Layer-Specific Effects of Extrinsic Influences and Activity Blockade.” *The Journal of Comparative Neurology* 331 (August 2000): 321–31.
Buttermore, Thaxton, and Bhat. 2013. “Organization and Maintenance of Molecular Domains in Myelinated Axons.” *Journal of Neuroscience Research* 91 (5): 603–22. doi:10.1002/jnr.23197.
Cai, Jun, Yingchuan Qi, Xuemei Hu, Min Tan, Zijing Liu, Jianshe Zhang, Qun Li, Maike Sander, and Mengsheng Qiu. 2014. “Generation of Oligodendrocyte Precursor Cells from Mouse Dorsal Spinal Cord Independent of Nkx6 Regulation and Shh Signaling.” *Neuron* 45 (1). Elsevier: 41–53. doi:10.1016/j.neuron.2004.12.028.
Campenot, and Macinnis. 2003. “Retrograde Transport of Neurotrophins: Fact and Function.” *J Neurobiol.*, no. April: 217–29. doi:10.1002/neu.10322.
Cancedda, Fiumelli, Chen, and Poo. 2007. “Excitatory GABA Action Is Essential for Morphological Maturation of Cortical Neurons In Vivo.” *The Journal of Neuroscience* 27 (19): 5224–35. doi:10.1523/JNEUROSCI.5169-06.2007.
Carlos, De, López-Mascaraque, and Valverde. 1996. “Dynamics of Cell Migration from the Lateral Ganglionic Eminence in the Rat.” *The Journal of Neuroscience : The Official Journal of the Society for Neuroscience* 16 (19): 6146–56.
Carreiras, Seghier, Baquero, Estévez, Lozano, Devlin, and Price. 2009. “An Anatomical Signature for Literacy.” *Nature* 461 (7266): 983–86.

doi:10.1038/nature08461.
Castelfranco, and Hartline. 2015. “The Evolution of Vertebrate and Invertebrate Myelin: A Theoretical Computational Study.” *J Comput Neurosci*, 521–38. doi:10.1007/s10827-015-0552-x.
Castillo, B Y J D E L, and B Katz. 1954. “Quantal Components of the End-Plate Potential.” *Journal of Physiology*, 560–73.
Catsicas, Larhammar, Blomqvistt, Sanna, Milner, and Wilson. 1991. “Expression of a Conserved Cell-Type-Specific Protein in Nerve Terminals Coincides with Synaptogenesis.” *Proc Natl Acad Sci USA* 88 (February): 785–89.
Catterall, William A. 1999. “Interactions of Presynaptic Ca 2 + Channels and Snare Proteins in Neurotransmitter Release.” *Annals of the New York Academy of Sciences*, 144–59.
Chagnac-Amitai, Luhmann, and Prince. 1990. “Burst Generating and Regular Spiking Layer 5 Pyramidal Neurons of Rat Neocortex Have Different Morphological Features.” *J Comp Neurol.* 2965984313.
Chakrabarti, Best, Cramer, Carney, Isaac, Galdzicki, and Haydar. 2010. “Olig1 and Olig2 Triplication Causes Developmental Brain Defects in Down Syndrome.” *Nature Neuroscience* 13 (8). Nature Publishing Group: 927–34. doi:10.1038/nn.2600.
Chang, Nishiyama, Peterson, Prineas, and Trapp. 2000. “NG2-Positive Oligodendrocyte Progenitor Cells in Adult Human Brain and Multiple Sclerosis Lesions.” *J. Neurosci.* 20: 6404–12.
Chapman, An, Barton, and Jahn. 1994. “SNAP-25, a t-SNARE Which Binds to Both Syntaxin and Synaptobrevin via Domains That May Form Coiled Coils.” *J Biol Chem.* 269 (44): 27427–32.
Chari, D M, and W F Blakemore. 2002. “New Insights into Remyelination Failure in Multiple Sclerosis: Implications for Glial Cell Transplantation.” *Mult. Scler.* 8: 271–77. http://dx.doi.org/10.1191/1352458502ms842oa.
Charles, Hernandez, Stankoff, Aigrot, Colin, Rougon, Zalc, and Lubetzki. 2000. “Negative Regulation of Central Nervous System Myelination by Polysialylated-Neural Cell Adhesion Molecule.” *PNAS*.
Chen, Abrams, Pinhas, and Brumberg. 2009. “Morphological Heterogeneity of Layer VI Neurons in Mouse Barrel Cortex.” *Journal of Comparative Neurology* 512 (6). Wiley Online Library: 726–46. doi:10.1002/cne.21926.
Chen, Xu, Huang, Huang, Ge, and Hu. 2017. “N-Cadherin Is Involved in Neuronal Activity-Dependent Regulation of Myelinating Capacity of Zebrafish Individual Oligodendrocytes In Vivo.” *Mol Neurobiol*, no. 96. Molecular Neurobiology: 6917–30. doi:10.1007/s12035-016-0233-4.
Chernoff. 1981. “Shiverer: An Autosomal Recessive Mutant Mouse with Myelin Deficiency.” *The Journal of Heredity* 72 (2). United States: 128.
Chevalier-Larsen, and Holzbaur. 2006. “Axonal Transport and Neurodegenerative Disease.” *(BBA) - Molecular Basis of Disease* 1762: 1094–1108. doi:10.1016/j.bbadis.2006.04.002.
Chevée, and Brown. 2018. “The Development of Local Circuits in the Neocortex: Recent Lessons from the Mouse Visual Cortex.” *Current Opinion in Neurobiology* 53: 103–9. doi:10.1016/j.conb.2018.06.009.
Chevée, Robertson, Cannon, Brown, and Goff. 2018. “Variation in Activity State, Axonal Projection, and Position Define the Transcriptional Identity of Individual Neocortical Projection Neurons.” *Cell Reports* 22 (2): 441–55.

doi:10.1016/j.celrep.2017.12.046.
Chomiak, and Hu. 2009. “What Is the Optimal Value of the G-Ratio for Myelinated Fibers in the Rat CNS? A Theoretical Approach.” *PLoS ONE* 4 (11). doi:10.1371/journal.pone.0007754.
Chong, Rosenberg, Fancy, Zhao, and Shen. 2012. “Neurite Outgrowth Inhibitor Nogo-A Establishes Spatial Segregation and Extent of Oligodendrocyte Myelination.” *PNAS* 109 (4). doi:10.1073/pnas.1113540109.
Christophe, Doerflinger, Lavery, Charpak, Audinat, Doerflinger, and Lavery. 2018. “Two Populations of Layer V Pyramidal Cells of the Mouse Neocortex: Development and Sensitivity to Anesthetics.” *Journal of Neurophysiology*, 3357–67. doi:10.1152/jn.00076.2005.
Chung, Kim, Kim, Kim, Jeong, Cha, Bae, Park, Lee, and Park. 2013. “Indian Hedgehog b Function Is Required for the Specification of Oligodendrocyte Progenitor Cells in the Zebrafish CNS.” *J Neurosci.* 33 (4): 1728–33. doi:10.1523/JNEUROSCI.3369-12.2013.
Citri, and Malenka. 2008. “Synaptic Plasticity: Multiple Forms, Functions, and Mechanisms.” *Neuropsychopharmacology Reiews*, 18–41. doi:10.1038/sj.npp.1301559.
Clemente, Ortega, Melero-Jerez, and Castro. 2013. “The Effect of Glia – Glia Interactions on Oligodendrocyte Precursor Cell Biology during Development and in Demyelinating Diseases.” *Frontiers in Neuroscience* 7 (December): 1–15. doi:10.3389/fncel.2013.00268.
Colello. 2011. “Myelin - Encyclopedia of Clinical Neuropsychology.” In , edited by Jeffrey S Kreutzer, John DeLuca, and Bruce Caplan, 1690–91. New York, NY: Springer New York. doi:10.1007/978-0-387-79948-3_339.
Colello, Devey, Imperato, and Pott. 1995. “The Chronology of Qligodendrocyte Differentiation in the Rat Optic Nerve: Evidence for a Signaling Step Initiating Myelination in the CNS.” *The Journal of Neuro* 15 (November).
Colello, R J, and U Pott. 1997. “Signals That Initiate Myelination in the Developing Mammalian Nervous System.” *Molecular Neurobiology* 15 (c).
Colello, and Ztirich. 1994. “The Role of Oligodendrocytes and Myelin on Axon Maturation Developing Rat Retinofugal Pathway.” *The Journal of Neuroscience* 74 (May).
Collarini, Pringle, Mudhar, Stevens, Kuhn, Monuki, Lemke, and Richardson. 1991. “Growth Factors and Transcription Factors in Oligodendrocyte Development.” *Journal of Cell Science. Supplement* 15. England: 117–23.
Compston, and Coles. 2002. “Multiple Sclerosis.” *The Lancet* 359: 1221–31.
Condliffe, Corradini, Pozzi, Verderio, and Matteoli. 2010. “Endogenous SNAP-25 Regulates Native Voltage-Gated Calcium Channels in Glutamatergic Neurons.” *The Journal of Biological Chemistry* 285 (32): 24968–76. doi:10.1074/jbc.M110.145813.
Constantinople, and Bruno. 2013. “Deep Cortical Layers Are Activated Directly by Thalamus.” *Science.* 340 (June): 1591–95.
Cornell-bell, Finkbeiner, Cooper, and Smith. 1988. “Glutamate Induces Calcium Waves in Cultured Astrocytes: Long-Range Glial Signaling.” *Science* 247 (24).
Czopka, Ffrench-Constant, and Lyons. 2013. “Individual Oligodendrocytes Have Only a Few Hours in Which to Generate New Myelin Sheaths in Vivo.” *Developmental Cell* 25 (6). Elsevier Inc.: 599–609. doi:10.1016/j.devcel.2013.05.013.

Damer, and Creutz. 1994. “Synergistic Membrane Interactions of the Two C2 Domains of Synaptotagmin.” *The Journal of Biological Chemistry* 269 (49): 31115–23.

Dantzker, and Callaway. 1998. “The Development of Local , Layer-Specific Visual Cortical Axons in the Absence of Extrinsic Influences and Intrinsic Activity.” *The Journal of Neuroscience* 18 (11): 4145–54.

Dantzker, J, and E Callaway. 2000. “Laminar Sources of Synaptic Input to Cortical Inhibitory Interneurons and Pyramidal Neurons.” *Nature Neuroscience* 3 (7): 701–7. doi:10.1038/76656.

Dart, Leyland, Spencer, Stanfield, Sutcliffe, Box, and Le. 1998. “The Selectivity Filter of a Potassium Channel , Murine Kir2 . 1 , Investigated Using Scanning Cysteine Mutagenesis.” *J Physiol.* 1.

Davies, Imbrici, Fialho, Herd, Bilsland, Weber, Mueller, et al. 2005. “Andersen-Tawil Syndrome: New Potassium Channel Mutations and Possible Phenotypic Variation.” *Neurology* 65 (7): 1083 LP-1089. http://n.neurology.org/content/65/7/1083.abstract.

Davis, Stewart, Friedman, and Buchsbaum. 2013. “White Matter Changes in Schizophrenia: Evidence for Myelin-Related Dysfunction.” *Arch Gen Psychiatry.* 60 (May 2003): 443–56.

Dawson, Levine, and Reynolds. 2000. “NG2-Expressing Cells in the Central Nervous System: Are They Oligodendroglial Progenitors?” *Journal of Neurosciene Reserach* 479 (May): 471–79.

Dawson, Polito, Levine, and Reynolds. 2003. “NG2-Expressing Glial Progenitor Cells: An Abundant and Widespread Population of Cycling Cells in the Adult Rat CNS.” *Molecular and Cellular Neuroscience* 24 (2): 476–88. doi:https://doi.org/10.1016/S1044-7431(03)00210-0.

Day, Carr, Ulrich, Ilijic, Tkatch, and Surmeier. 2005. “Dendritic Excitability of Mouse Frontal Cortex Pyramidal Neurons Is Shaped by the Interaction among HCN, Kir2, and K Leak Channels.” *The Journal of Neuroscience* 25 (38): 8776–87. doi:10.1523/JNEUROSCI.2650-05.2005.

Demerens, Stankoff, Logak, Anglade, Allinquant, Couraud, Zalc, and Lubetzki. 1996. “Induction of Myelination in the Central Nervous System by Electrical Activity.” *Proceedings of the National Academy of Sciences of the United States of America* 93 (18): 9887–92. http://www.pubmedcentral.nih.gov/articlerender.fcgi?artid=38524&tool=pmcentrez&rendertype=abstract.

Deshmukh, Tardif, Lyssiotis, Green, Kerman, Kim, Zanabhan, et al. 2013. “A Regenerative Approach to the Treatment of Multiple Sclerosis.” *Nature* 502 (7471). Nature Publishing Group: 327–32. doi:10.1038/nature12647.

Diamond, Heimendahl, and Knutsen. 2008. “‘Where’ and ‘What’ in the Whisker Sensorimotor System.” *Nature Reviews Neuroscience* 9 (august): 601–13. doi:10.1038/nrn2411.

Diamond, Jones, and Powell. 1969. “The Projection of the Auditory Cortex upon the Diencephalon and Brain Stem in the Cat.” *Brain Research* 15: 305–40.

Do, Wischmeyer, Karschin, Brockhaus, Ballanyi, Derst, and Karschin. 1998. “Kir2 .4: A Novel K+ Inward Rectifier Channel Associated with Motoneurons of Cranial Nerve Nuclei.” *The Journal of Neuroscience* 18 (11): 4096–4105.

Dodge, and Rahamimoff. 1967. “Co-Operative Action a Calcium Ions in Transmitter Release at the Neuromuscular Junction.” *Journal of Physiology*, 419–32.

Donaldson, Plaster, Tristani-firouzi, Fu, and Pta. 2003. “Defective Potassium Channel Kir2.1 Trafficking Underlies Andersen-Tawil Syndrome.” *J Biol Chem.* 278 (51): 51779–85. doi:10.1074/jbc.M310278200.

Economo, Von, and Koskinas. 1927. “Die Cytoarchitektonik Der Hirnrinde Des Erwachsenen Menschen.” *Journal of Anatomy* 61 (Pt 2): 264–66.

Edgar, Mazor, Rinon, Blumenthal, Golan, Buzhor, Livnat, et al. 2013. “LifeMap Discovery TM: The Embryonic Development , Stem Cells , and Regenerative Medicine Research Portal” 8 (7). doi:10.1371/journal.pone.0066629.

Emery, Agalliu, Cahoy, Watkins, Dugas, Mulinyawe, Ibrahim, Ligon, Rowitch, and Barres. 2009. “Myelin Gene Regulatory Factor Is a Critical Transcriptional Regulator Required for CNS Myelination.” *Cell* 138 (1). Elsevier Ltd: 172–85. doi:10.1016/j.cell.2009.04.031.

Engvig, Fjell, Westlye, Moberget, Sundseth, Larsen, and Walhovd. 2010. “Effects of Memory Training on Cortical Thickness in the Elderly.” *NeuroImage* 52 (4). Elsevier Inc.: 1667–76. doi:10.1016/j.neuroimage.2010.05.041.

Enriquez-Barreto, Palazzetti, Brennaman, and Maness. 2012. “Neural Cell Adhesion Molecule, NCAM, Regulates Thalamocortical Axon Pathfinding and the Organization of the Cortical Somatosensory Representation in Mouse.” *Front Mol Neurosci.* 5 (June): 1–13. doi:10.3389/fnmol.2012.00076.

Erzurumlu, and Kind. 2001. “Neural Activity: Sculptor of ‘barrels’ in the Neocortex.” *Trends in Neurosciences* 24 (10): 589–95. doi:10.1016/S0166-2236(00)01958-5.

Etxeberria, Hokanson, Dao, Mayoral, Mei, Redmond, Ullian, and Chan. 2016. “Dynamic Modulation of Myelination in Response to Visual Stimuli Alters Optic Nerve Conduction Velocity.” *Journal of Neuroscience* 36 (26): 6937–48. doi:10.1523/JNEUROSCI.0908-16.2016.

Fatt, and Katz. 1951. “Spontaneous Subthreshold Activity at Motor Nerve Endings.” *Journal of Physiology*.

Feldman, and Brecht. 2005. “Map Plasticity in Somatosensory Cortex.” *Science* 310 (November): 810–16.

Fields. 2005. “Myelination: An Overlooked Mechanism of Synaptic Plasticity?” *The Neuroscientist*, 528–31. doi:10.1177/1073858405282304.

———. 2008. “White Matter in Learning, Cognition and Psychiatric Disorders.” *Trends Neurosci.* 31. Nature Publishing Group: 361–70. http://dx.doi.org/10.1016/j.tins.2008.04.001.

Fields, and Ni. 2010. “Nonsynaptic Communication Through ATP Release from Volume-Activated Anion Channels in Axons.” *Science Signaling* 3 (142): ra73-ra73. doi:10.1126/scisignal.2001128.

Fields, R. D. 2015. “A New Mechanism of Nervous System Plasticity: Activity-Dependent Myelination.” *Nature Reviews Neuroscience* 16 (12). Nature Publishing Group: 756–67. doi:10.1038/nrn4023.

Fields, R.Douglas, and Beth Stevens. 2000. “ATP: An Extracellular Signaling Molecule between Neurons and Glia.” *Trends in Neurosciences* 23 (12). Elsevier: 625–33. doi:10.1016/S0166-2236(00)01674-X.

Fields, R D. 2011. “Nonsynaptic and Nonvesicular ATP Release from Neurons and Relevance to Neuron-Glia Signaling.” *Seminars in Cell and Developmental Biology* 22 (2): 214–19. doi:10.1016/j.semcdb.2011.02.009.

Fields, and Stevens-graham. 2002. “New Insights into Neuron-Glia Communication” 298 (October): 556–63.

Finean, Hawthorne, and Patterson. 1957. “Structural and Chemical Differences between Optic and Sciatic Nerve Myelins.” *Journal of Neurochemistry* 1: 256–59.

Foran, and Peterson. 1992. “Myelin Acquisition in the Central Nervous System of the Mouse Revealed by an MBP-Lac Z Transgene.” *The Journal of Neuroscience : The Official Journal of the Society for Neuroscience* 12 (12): 4890–97.

Ford, Alexandrova, Cossell, Stange-Marten, Sinclair, Kopp-Scheinpflug, Pecka, Attwell, and Grothe. 2015. “Tuning of Ranvier Node and Internode Properties in Myelinated Axons to Adjust Action Potential Timing.” *Nature Communications* 6. Nature Publishing Group: 1–14. doi:10.1038/ncomms9073.

Foster, Connors, and Waxman. 1982. “Rat Optic Nerve: Electrophysiological, Pharmacological and Anatomical Studies during Development.” *Developmental Brain Research* 3: 371–86.

Fox. 1992. “A Critical Period for Experience-Dependent Barrel Cortex Synaptic Plasticity in Rat.” *The Journal of Neuroscience*, no. May: 1626–36.

Fox, K. 2002. “Anatomical Pathways and Molecular Mechanisms for Plasticity in the Barrel Cortex.” *Neuroscience* 111 (4): 799–814. doi:10.1016/S0306-4522(02)00027-1.

Franklin, and Ffrench-Constant. 2008. “Remyelination in the CNS: From Biology to Therapy.” *Neuron-Glia Interactions* 9 (NoveMbeR): 839–55. doi:10.1038/nrn2480.

Frassoni, C, F Inverardi, S Coco, B Ortino, C Grumelli, D Pozzi, C Verderio, and M Matteoli. 2005. “Analysis of SNAP-25 Immunoreactivity in Hippocampal Inhibitory Neurons during Development in Culture and in Situ.” *Neuroscience.* 131: 813–23. doi:10.1016/j.neuroscience.2004.11.042.

Frazer, Sheehan, Stokowski, Chen, Cheng, Fodor, Cox, and Patil. 2001. “Evolutionarily Conserved Sequences on Human Chromosome 21.” *Genome Research*, 1651–59. doi:10.1101/gr.198201.1.

Friede. 1972. “Control of Myelin Formation by Axon Caliber (With a Model of the Control Mechanism).” *The Journal of Comparative Neurology* 144: 233–52.

Frost, and Caviness. 1980. “Tagential Organization of Thalamic Projections to the Neocortex in the Mouse.” *The Journal of Comparative Neurology* 194 (2): 369–93. doi:10.1002/cne.901940206.

Frühbeis, Fröhlich, Kuo, Amphornrat, Thilemann, Saab, Kirchhoff, et al. 2013. “Neurotransmitter-Triggered Transfer of Exosomes Mediates Oligodendrocyte – Neuron Communication.” *PLOS Biology* 11 (7). doi:10.1371/journal.pbio.1001604.

Fruttiger, Calver, and Richardson. 2000. “Platelet-Derived Growth Factor Is Constitutively Secreted from Neuronal Cell Bodies but Not from Axons.” *Current Biology* 10 (20): 1283–86. doi:10.1016/S0960-9822(00)00757-0.

Fukui, Hayaska, Bedi, Ozaki, and Takeuchi. 1991. “Quantitative Study of the Development of the Optic Nerve in Rats Reared in the Dark during Early Postnatal Life.” *J. Anat.*, 37–47.

Fünfschilling, Supplie, Mahad, Boretius, Saab, Edgar, Bastian G Brinkmann, et al. 2012. “Glycolytic Oligodendrocytes Maintain Myelin and Long-Term Axonal Integrity.” *Nature* 485 (April): 517. http://dx.doi.org/10.1038/nature11007.

Fuss, Mallon, Phan, Ohlemeyer, Kirchhoff, Nishiyama, and Macklin. 2000.

"Purification and Analysis of in Vivo-Differentiated Oligodendrocytes Expressing the Green Fluorescent Protein." *Dev. Biol.* 274: 259–74. doi:10.1006/dbio.1999.9574.

Galli, and Maffei. 1988. "Spontaneous Impulse Activity of Rat Retinal Ganglion Cells in Prenatal Life Localizaion of an Arg-Gly-Asp Recognition Site Within an Integrin Adhesion Receptor." *Science* 242: 21–22.

Galloway, and Moore. 2016. "MiRNAs As Emerging Regulators of Oligodendrocyte Development and Differentiation." *Frontiers in Cell and Developmental Biology* 4 (June): 1–8. doi:10.3389/fcell.2016.00059.

Gambarotta, Ronchi, Friard, Galletta, Perroteau, and Geuna. 2014. "Identification and Validation of Suitable Housekeeping Genes for Normalizing Quantitative Real-Time PCR Assays in Injured Peripheral Nerves." *PLoS ONE* 9 (8): 1–7. doi:10.1371/journal.pone.0105601.

García-Moreno, and Molnár. 2015. "Subset of Early Radial Glial Progenitors That Contribute to the Development of Callosal Neurons Is Absent from Avian Brain." *Proceedings of the National Academy of Sciences* 112 (36): E5058–67. doi:10.1073/pnas.1506377112.

García, De Marco, Karayannis, and Fishell. 2013. "Neuronal Activity Is Required for the Development of Specific Cortical Interneuron Subtypes." *Nature* 472 (7343): 351–55. doi:10.1038/nature09865.Neuronal.

Gasser, and Erlanger. 1927. "The Grouping of the Peripheral Nerve Fibres on the Basis of Their Psychological Characteristics." *Acta Psychatrica Scandinavica*.

Georgieva, Moskvina, Peirce, Norton, Bray, Jones, Holmans, et al. 2006. "Convergent Evidence That Oligodendrocyte Lineage Transcription Factor 2 (OLIG2) and Interacting Genes Influence Susceptibility to Schizophrenia." *PNAS* 103 (33): 12469–74.

Gerfen, Paletzki, and Heintz. 2013. "GENSAT BAC Cre-Recombinase Driver Lines to Study the Functional Organization of Cerebral Cortical and Basal Ganglia Circuits." *Neuron* 80 (6). Elsevier Inc.: 1368–83. doi:10.1016/j.neuron.2013.10.016.

Ghosh, Carnahan, and Greenberg. 1994. "Requirement for BDNF in Activity-Dependent Survival of Cortical Neurons." *Science* 263 (5153): 1618–23. doi:10.1126/science.7907431.

Giacci, Bartlett, Huynh, Kilburn, Dunlop, and Fitzgerald. 2018. "Three Dimensional Electron Microscopy Reveals Changing Axonal and Myelin Morphology along Normal and Partially Injured Optic Nerves." *Scientific Reports*, no. November 2017. Springer US: 1–12. doi:10.1038/s41598-018-22361-2.

Gibson, Purger, Mount, Goldstein, Lin, Wood, Inema, et al. 2014. "Neuronal Activity Promotes Oligodendrogenesis and Adaptive Myelination in the Mammalian Brain." *Science* 344 (6183): 1–27. doi:10.1126/science.1252304.Neuronal.

Gilbert. 1983. "Microcircuitry of the Visual Cortex." *Ann Rev INeurosc*, no. 6: 217–47. doi:10.1126/science.1153276.

Gilbert, and Kelly. 1975. "The Projections of Cells in Different Layers of the Cat ' s Visual Cortex." *J Comp Neur* 163: 81–106.

Ginty, and Segal. 2002. "Retrograde Neurotrophin Signaling: Trk-Ing along the Axon" 4: 268–74. doi:10.1016/S0959-4388(02)00326-4.

Gledhill, and Mcdonald. 1977. "Morphological Characteristics of Central Demyelination and Remyelination: A Single-Fiber Study." *Ann Neurol*, 552–60.

Goerge, Heinen, Bru, Rajan, Preisig-mu, Veh, and Derst. 2002. “Heteromerization of Kir2.x Potassium Channels Contributes to the Phenotype of Andersen’s Syndrome.” *PNAS* 99 (11).

Goldman, Steven A, and Nicholas J Kuypers. 2015. “How to Make an Oligodendrocyte,” 3983–95. doi:10.1242/dev.126409.

Gollan, Salomon, Salzer, and Peles. 2003. “Caspr Regulates the Processing of Contactin and Inhibits Its Binding to Neurofascin.” *JCB Reports* 163 (6): 1213–18. doi:10.1083/jcb.200309147.

Gong, Doughty, Harbaugh, Cummins, Hatten, Heintz, and Gerfen. 2007. “Targeting Cre Recombinase to Specific Neuron Populations with Bacterial Artificial Chromosome Constructs.” *The Journal of Neuroscience* 27 (37): 9817–23. doi:10.1523/JNEUROSCI.2707-07.2007.

Gong, Shiaoching, Chen Zheng, Martin L Doughty, Kasia Losos, Nicholas Didkovsky, Uta B Schambra, Norma J Nowak, et al. 2003. “A Gene Expression Atlas of the Central Nervous System Based on Bacterial Artificial Chromosomes.” *Nature* 425.

Grant. 2014. “The Development of Corticothalamic and Corticotectal Connections in the Murine Visual System.” Oxford University.

Grant, Hoerder-Suabedissen, and Molnar. 2016. “The Regulation of Corticofugal Fiber Targeting by Retinal Inputs.” *Cerebral Cortex* 26 (3): 1336–48. doi:10.1093/cercor/bhv315.

Grant, Hoerder-Suabedissen, and Molnár. 2012. “Development of the Corticothalamic Projections.” *Frontiers in Neuroscience* 6 (May): 53. doi:10.3389/fnins.2012.00053.

Greenhill, Ranson, Fox, Greenhill, Ranson, and Fox. 2015. “Hebbian and Homeostatic Plasticity Mechanisms in Regular Spiking and Intrinsic Bursting Cells of Cortical Layer 5.” *Neuron* 88 (3). The Authors: 539–52. doi:10.1016/j.neuron.2015.09.025.

Greer. 2013. “Autoimmune T-Cell Reactivity to Myelin Proteolipids and Glycolipids in Multiple Sclerosis.” *Multiple Sclerosis International* 2013 (October): 1–16. doi:10.1155/2013/151427.

Griffths, Klugmann, Anderson, Yool, Thomson, Schwab, Schneider, et al. 1998. “Axonal Swellings and Degeneration in Mice Lacking the Major Proteolipid of Myelin.” *Science* 5: 1610–13.

Grubb, and Burrone. 2010. “Activity-Dependent Relocation of the Axon Initial Segment Fine-Tunes Neuronal Excitability.” *Nature* 465 (7301). Nature Publishing Group: 1070–74. doi:10.1038/nature09160.

Gudz, Komuro, and Macklin. 2006. “Glutamate Stimulates Oligodendrocyte Progenitor Migration Mediated via an Alphav Integrin/Myelin Proteolipid Protein Complex.” *Journal of Neuroscience* 26 (9): 2458–66. doi:10.1523/JNEUROSCI.4054-05.2006.

Guillery. 1995. “Anatomical Evidence Concerning the Role of the Thalamus in Corticocortical Communication: A Brief Review.” *Journal of Anatomy*, 583–92.

Gunawardena, Goldstein, Diego, Jolla, and Strooper. 2001. “Disruption of Axonal Transport and Neuronal Viability by Amyloid Precursor Protein Mutations in Drosophila” 32: 389–401.

Guo, and Lu. 2003. “Interaction Mechanisms between Polyamines and IRK1 Inward Rectifier K+ Channels.” *Journal of General Physiology* 122 (November). doi:10.1085/jgp.200308890.

Gyllensten, and Malmfors. 1963. “Myelinization of the Optic Nerve and Its Dependence on Visual Function — A Quantitative Investigation in Mice.” *J. Embryol. Exp. Morphol.* 11 (March): 255–66.

Hagihara, Murakami, Yoshida, Tagawa, and Ohki. 2015. “Neuronal Activity Is Not Required for the Initial Formation and Maturation of Visual Selectivity.” *Nature Neuroscience* 18 (12). doi:10.1038/nn.4155.

Hallman, Schofield, and Lin. 1988. “Dendritic Morphology and Axon Collaterals of Corticotectal, Corticopontine, and Callosal Neurons in Layer V of Primary Visual Cortex of the Hooded Rat.” *Journal of Comparative Neurology* 160: 149–60.

Hanson, and Landmesser. 2004. “Normal Patterns of Spontaneous Activity Are Required for Correct Motor Axon Guidance and the Expression of Specific Guidance Molecules.” *Neuron* 43 (5). Cell Press: 687–701. doi:10.1016/J.NEURON.2004.08.018.

Harauz, and Boggs. 2013. “What Is Myelin Basic Protein and What Does It Do? The Classic MBP Isoforms Arise from the Gene in the Oligodendrocyte Lineage (Golli) in Differentiated Oligodendrocytes,” 334–61. doi:10.1111/jnc.12195.

Hardy, Loushin, Jr, Chen, Ebersole, Lazzarini, and Artzt. 1996. “Neural Cell Type-Specific Expression of QKI Proteins Is Altered in Quaking Viable Mutant Mice.” *The Journal of Neuroscience* 16 (24): 7941–49.

Harris, and Attwell. 2012. “The Energetics of Central Nervous System White Matter.” *The Journal of Neuroscience* 32 (1): 356–71. doi:10.1523/JNEUROSCI.3430-11.2012.The.

Harris, and Shepherd. 2015. “The Neocortical Circuit: Themes and Variations.” *Nat Neurosci.* 18 (2). doi:10.1038/nn.3917.

Hart, Richardson, Heldin, Westermark, and Raff. 1989. “PDGF Receptors on Cells of the Oligodendrocyte-Type-2 Astrocyte (O-2A) Cell Lineage.” *Development* 603: 595–603.

Hartline, and Colman. 2007. “Rapid Conduction and the Evolution of Giant Axons and Myelinated Fibers.” *Current Biology* 17 (1): R29-35. doi:10.1016/j.cub.2006.11.042.

Hartman, Kenichi N, Sumon K Pal, Juan Burrone, and Venkatesh N Murthy. 2006. “Activity-Dependent Regulation of Inhibitory Synaptic Transmission in Hippocampal Neurons.” *Nature-Neuroscience* 9 (5). doi:10.1038/nn1677.

Haruta, and Hata. 2007. “Report Experience-Driven Axon Retraction without Binocular Imbalance in Developing Visual Cortex.” *CellPress*, 37–42. doi:10.1016/j.cub.2006.10.064.

Hatanaka, and Murakami. 2002. “In Vitro Analysis of the Origin, Migratory Behavior, and Maturation Of.” *The Journal of Comparative Neurology* 14 (April): 1–14. doi:10.1002/cne.10421.

Hattox, and Nelson. 2007. “Layer V Neurons in Mouse Cortex Projecting to Different Targets Have Distinct Physiological Properties,” 3330–40. doi:10.1152/jn.00397.2007.

Hayashi, Yamasaki, Nauenburg, Binz, and Niemann. 1995. “Disassembly of the Reconstituted Synaptic Vesicle Membrane Fusion Complex in Vitro” 14 (10): 2317–25.

Haydon, and Hendry. 1982. “Nerve Impulse Blockage in Squid Axons by N-Alkanes: The Effect of Axon Diameter.” *Journal of Physiology*, 393–403.

Hayes, and Meyer. 1989. “Impulse Blockade by Intraocular Tetredetoxin During Optic Regeneration in Goldfish: HRP-EM Evidence That the Fomation of Normal Numbers of Optic Synapses and the Elimination of Exuberant Optic Fibers Is Activity Independent.” *The Journal of Neuroscience*, no. April.

He, and Lu. 2013. “Coordinated Control of Oligodendrocyte Development by Extrinsic and Intrinsic Signaling Cues.” *Neuroscience Bulletin* 29 (2): 129–43. doi:10.1007/s12264-013-1318-y.

Hedstrom, and Rasband. 2006. “Intrinsic and Extrinsic Determinants of Ion Channel Localization in Neurons.” *Journal of Neurochemistry* 98 (5): 1345–52. doi:10.1111/j.1471-4159.2006.04001.x.

Hepp, Perraut, Chasserot-Golaz, Galli, Aunis, Langley, and Grant. 1999. “Cultured Glial Cells Express the SNAP-25 Analogue SNAP-23.” *Glia* 187 (January): 181–87.

Herculano-Houzel. 2009. “The Human Brain in Numbers: A Linearly Scaled-up Primate Brain.” *Frontiers in Human Neuroscience* 3 (November): 1–11. doi:10.3389/neuro.09.031.2009.

Hevner, Shi, Justice, Hsueh, Sheng, Smiga, Bulfone, et al. 2001. “Tbr1 Regulates Differentiation of the Preplate and Layer 6.” *Neuron* 29: 353–66.

Hibino, Inanobe, Furutani, Murakami, and Findlay. 2018. “Inwardly Rectifying Potassium Channels : Their Structure , Function , and Physiological Roles,” 291–366. doi:10.1152/physrev.00021.2009.

Hill, Patel, Medved, Reiss, and Nishiyama. 2013. “NG2 Cells in White Matter But Not Gray Matter Proliferate in Response to PDGF.” *Journal of Neuroscience* 33 (36): 14558–66. doi:10.1523/JNEUROSCI.2001-12.2013.

Hines, Ravanelli, Schwindt, Scott, and Appel. 2015. “Neuronal Activity Biases Axon Selection for Myelination in Vivo.” *Nature Neuroscience* 18 (5): 683–89. doi:10.1038/nn.3992.

Hoerder-Suabedissen, Anna, and Zoltán Molnár. 2013. “Molecular Diversity of Early-Born Subplate Neurons.” *Cerebral Cortex* 23 (6): 1473–83. doi:10.1093/cercor/bhs137.

Hoerder-Suabedissen, Korrell, Hayashi, Jeans, Ramirez, Grant, Christian, Kavalali, Wilson, and Molnár. 2018. “Cell-Specific Loss of SNAP25 from Cortical Projection Neurons Allows Normal Development but Causes Subsequent Neurodegeneration,” no. August: 1–12. doi:10.1093/cercor/bhy127.

Hoerder-Suabedissen, and Molnár. 2012. “Morphology of Mouse Subplate Cells with Identified Projection Targets Changes with Age.” *The Journal of Comparative Neurology* 520 (1): 174–85. doi:10.1002/cne.22725.

Hofherr, Fakler, and Klöcker. 2005. “Selective Golgi Export of Kir2.1 Controls the Stoichiometry of Functional Kir2.x Channel Heteromers,” 1935–43. doi:10.1242/jcs.02322.

Hohenstein, and Roche. 2001. “SNAP-29 Is a Promiscuous Syntaxin-Binding SNARE” 171: 167–71. doi:10.1006/bbrc.2001.5141.

Holness, and Simmons. 2018. “Molecular Cloning of CD68, a Human Macrophage Marker Related to Lysosomal Glycoproteins.” *Blood*.

Holz, A, and M E Schwab. 1997. “Developmental Expression of the Myelin Gene MOBP in the Rat Nervous System.” *Journal of Neurocytology* 26 (7). United States: 467–77.

Hoogland, Welker, and Van der Loos. 1987. “Organization of the Projections from

Barrel Cortex to Thalamus in Mice Studied with Phaseolus Vulgaris-Leucoagglutinin and HRP." *Experimental Brain Research* 68 (1). Germany: 73–87.
Hoopfer, Mclaughlin, Watts, Schuldiner, Leary, Luo, Way, and Francisco. 2006. "Wlds Protection Distinguishes Axon Degeneration Following Injury from Naturally Occurring Developmental Pruning," 883–95. doi:10.1016/j.neuron.2006.05.013.
Hoover, Hoffer, Alloway, John, Hoffer, and Alloway. 2018. "Projections From Primary Somatosensory Cortex to the Neostriatum: The Role of Somatotopic Continuity in Corticostriatal Convergence," 1576–87.
Horio, Morishige, Takahashi, and Kurachi. 1996. "Differential Distribution of Classical Inwardly Rectifying Potassium Channel MRNAs in the Brain: Comparison of IRK2 with IRK1 and IRK3 IRK1" 379: 239–43.
Hosaka, Hanawa, Washizuka, Chinushi, Yamashita, Yoshida, Komura, Watanabe, and Aizawa. 2018. "Function, Subcellular Localization and Assembly of a Novel Mutation of KCNJ2 in Andersen's Syndrome." *Journal of Molecular and Cellular Cardiology* 35 (4). Elsevier: 409–15. doi:10.1016/S0022-2828(03)00046-4.
Howng, Avila, Emery, Traka, Lin, Watkins, Cook, et al. 2010. "ZFP191 Is Required by Oligodendrocytes for CNS Myelination" 6: 301–11. doi:10.1101/gad.1864510.Since.
Hu, Ang, Karsak, Hu, Cui, Duka, Takeda, et al. 2003. "F3/Contactin Acts as a Functional Ligand for Notch during Oligodendrocyte Maturation." *Cell* 115: 163–75.
Huang, Tang, Tang, Xu, He, Li, Xu, et al. 2008. "Positive Association between OLIG2 and Schizophrenia in the Chinese Han Population." *Human Genetics*, 659–60. doi:10.1007/s00439-007-0434-z.
Hubel, Wiesel, LeVay, Barlow, and Gaze. 1977. "Plasticity of Ocular Dominance Columns in Monkey Striate Cortex." *Soc, R Britain, Great* 409: 377–409.
Huff, Shi, Sun, Wu, Shi, and Cheng. 2011. "Real-Time CARS Imaging Reveals a Calpain-Dependent Pathway for Paranodal Myelin Retraction during High-Frequency Stimulation." *PloS One* 6 (3): e17176. doi:10.1371/journal.pone.0017176.
Hughes, Kang, Fukaya, and Bergles. 2013. "Oligodendrocyte Progenitors Balance Growth with Self-Repulsion to Achieve Homeostasis in the Adult Brain." *Nat Neurosci* 16 (6): 668–76. doi:10.1038/nn.3390.Oligodendrocyte.
Hursh. 1939. "Conduction Velocity and Diameter of Nerve Fibers." *American Journal of Physiology-Legacy Content* 127 (1). American Physiological Society: 131–39. doi:10.1152/ajplegacy.1939.127.1.131.
Huxley, and Stampfli. 1948. "Evidence for Saltatory Conduction in Peripheral Myelinated Nerve Fibres." *Journal of Physiology*, no. 1946: 315–39.
Igarashi, Kozaki, Terakawa, and Komiya. 1996. "Growth Cone Collapse and Inhibition of Neurite Growth by Botulinum Neurotoxin C1: A t-SNARE Is Involved in Axonal Growth" 134 (1): 205–15.
Igarashi, Tagaya, and Komiya. 1997. "The Soluble N-Ethylmaleimide-Sensitive Factor Attached Protein Receptor Complex in Growth Cones: Molecular Aspects of the Axon Terminal Development" 17 (4): 1460–70.
Ince-dunn, Hall, Hu, Ripley, Huganir, Olson, and Tapscott. 2006. "Regulation of Thalamocortical Patterning and Synaptic Maturation by NeuroD2." *Neuron* 49:

683–95. doi:10.1016/j.neuron.2006.01.031.
Innocenti, and Clarke. 1983. “Multiple Sets of Visual Cortical Neurons Projecting Transitorily Trough the Corpus Callosum.” *Neuroscience Letters* 41: 27–32.
Innocenti, Vercelli, and Caminiti. 2013. “The Diameter of Cortical Axons Depends Both on the Area of Origin and Target,” no. April: 2178–88. doi:10.1093/cercor/bht070.
Ishibashi, Tomoko, Kelly a. Dakin, Beth Stevens, Philip R. Lee, Serguei V. Kozlov, Colin L. Stewart, and R. Douglas Fields. 2006. “Astrocytes Promote Myelination in Response to Electrical Impulses.” *Neuron* 49 (6): 823–32. doi:10.1016/j.neuron.2006.02.006.
Ishii, Fyffe-maricich, Furusho, Miller, and Bansal. 2012. “ERK1/ERK2 MAPK Signaling Is Required to Increase Myelin Thickness Independent of Oligodendrocyte Differentiation and Initiation of Myelination.” *The Journal of Neuroscience* 32 (26): 8855–64. doi:10.1523/JNEUROSCI.0137-12.2012.
Itoh, Ozaki, Stevens, and Fields. 1997. “Activity-Dependent Regulation of N-Cadherin in DRG Neurons: Differential Regulation of N-Cadherin, NCAM, and L1 by Distinct Patterns of Action Potentials.” *Journal of Neurobiology* 33 (6): 735–48. doi:10.1002/(SICI)1097-4695(19971120)33:6<735::AID-NEU3>3.0.CO;2-A.
Jacob, Petreanu, Wright, Svoboda, and Fox. 2012. “Regular Spiking and Intrinsic Bursting Pyramidal Cells Show Orthogonal Forms of Experience-Dependent Plasticity in Layer V of Barrel Cortex.” *Neuron* 73 (2). Elsevier Inc.: 391–404. doi:10.1016/j.neuron.2011.11.034.
Jahn, and Südhof. 1999. “Membrane Fusion and Exocytosis,” 863–911.
Jäkel, and Dimou. 2017. “Glial Cells and Their Function in the Adult Brain: A Journey through the History of Their Ablation.” *Frontiers in Cellular Neuroscience* 11 (February): 1–17. doi:10.3389/fncel.2017.00024.
Jeans, Oliver, Johnson, Capogna, Vikman, Babbs, Partridge, et al. 2007. “A Dominant Mutation in Snap25 Causes Impaired Vesicle Trafficking, Sensorimotor Gating, and Ataxia in the Blind-Drunk Mouse” 104 (7): 2431–36.
Jensen, and Yong. 2016. “Activity-Dependent and Experience-Driven Myelination Provide New Directions for the Management of Multiple Sclerosis.” *Trends in Neurosciences* 39 (6). Elsevier Ltd: 356–65. doi:10.1016/j.tins.2016.04.003.
Jepson, Vought, Gross, Gan, Austen, Frantz, Zwahlen, Lowe, Markland, and Krauss. 2012. “LINGO-1, a Transmembrane Signaling Protein, Inhibits Oligodendrocyte Differentiation and Myelination Through” 287 (26): 22184–95. doi:10.1074/jbc.M112.366179.
Johansson, Momma, Clarke, Lendahl, and Frise. 1999. “Identification of a Neural Stem Cell in the Adult Mammalian Central Nervous System.” *Cell* 96: 25–34.
Johns, Marx, Mains, O’Rourke, and Marbán. 1999. “Inducible Genetic Suppression of Neuronal Excitability.” *The Journal of Neuroscience* 19 (5): 1691–97. http://www.ncbi.nlm.nih.gov/pubmed/10024355.
Jones, E, and T Powell. 1970. “Electron Microscopy of the Somatic Sensory Cortex of the Cat. I. Cell Types and Synaptic Organization.” *Philos Trans R Soc Lond B Biol Sci* 257 (812): 1–11.
Jones, Jolson, Cuta, Mariash, and Anderson. 2003. “Triiodothyronine Is a Survival Factor for Developing Oligodendrocytes.” *Molecular and Cellular Endocrinology* 199 (1–2): 49–60. doi:10.1016/S0303-7207(02)00296-4.
Jones, Kang, Wheeler, Lindquist, Papallo, Sabatini, Golland, and Carpenter. 2008.

"CellProfiler Analyst: Data Exploration and Analysis Software for Complex Image-Based Screens." *BMC Bioinformatics* 9: 1–16. doi:10.1186/1471-2105-9-482.

Jones, and Powell. 1968. "The Projection of the Somatic Sensory Cortex upon the Thalamus in the Cat." *Brain Research* 10.

Jones, and Rakic. 2010. "Radial Columns in Cortical Architecture: It Is the Composition That Counts." *Cerebral Cortex* 20 (10): 2261–64. doi:10.1093/cercor/bhq127.

Kaller, Lazari, Blanco-duque, Sampaio-baptista, and Johansen-berg. 2017. "Myelin Plasticity and Behaviour — Connecting the Dots." *Current Opinion in Neurobiology* 47. Elsevier Ltd: 86–92. doi:10.1016/j.conb.2017.09.014.

Kamholz, Toffenetti, and Lazzarini. 1988. "Organization and Expression of the Human Myelin Basic Protein Gene." *Journal of Neuroscience Research* 21 (1). Wiley Subscription Services, Inc., A Wiley Company: 62–70. doi:10.1002/jnr.490210110.

Káradóttir, and Attwell. 2007. "Neurotransmitter Receptors in the Life and Death of Oligodendrocytes." *Neuroscience* 145 (4). IBRO: 1426–38. doi:10.1016/j.neuroscience.2006.08.070.

Kasper, Larkman, and Lubke. 1994. "Pyramidal Neurons in Layer 5 of the Rat Visual Cortex . I . Correlation Among Cell Morphology, Intrinsic Electrophysiological Properties, and Axon Targets." *Journal of Comparative Neurology* 474: 459–74.

Katz. 1987. "Local Circuitry of Identified Projection Neurons in Cat Visual Cortex Brain Slices" 7 (April).

Katz, and Shatz. 1996. "Synaptic Activity and the Construction of Cortical Circuits." *Science* 274.

Kennedy, and Raz. 2009. "Aging White Matter and Cognition: Differential Effects of Regional Variations in Diffusion Properties on Memory, Executive Functions, and Speed." *Neuropsychologia* 47 (3): 916–27. doi:10.1016/j.neuropsychologia.2009.01.001.

Kessaris, Nicoletta, Matthew Fogarty, Palma Iannarelli, Matthew Grist, Michael Wegner, and William D Richardson. 2006. "Competing Waves of Oligodendrocytes in the Forebrain and Postnatal Elimination of an Embryonic Lineage." *Nat Neurosci* 9 (2). Nature Publishing Group: 173–79. http://dx.doi.org/10.1038/nn1620.

Kiritani, Wickersham, Seung, and Shepherd. 2012. "Hierarchical Connectivity and Connection-Specific Dynamics in the Corticospinal – Corticostriatal Microcircuit in Mouse Motor Cortex" 32 (14): 4992–5001. doi:10.1523/JNEUROSCI.4759-11.2012.

Kistler. 2002. "Spike-Timing Dependent Synaptic Plasticity: A Phenomenological Framework." *Biological Cybernetics* 87 (5–6): 416–27. doi:10.1007/s00422-002-0359-5.

Kitada, and Rowitch. 2006. "Transcription Factor Co-Expression Patterns Indicate Heterogeneity of Oligodendroglial Subpopulations in Adult Spinal Cord." *Glia*, no. March: 35–46. doi:10.1002/glia.

Klein, Mooney, Fish, and Rhoadd. 1986. "The Structural and Functional Characteristics of Striate Cortical Neurons That Innervate the Superior Colliculus and Lateral Posterior Nucleus in Hamster" 17 (1).

Klugmann. 1997. "Assembly of CNS Myelin in the Absence of Proteolipid Protein."

Neuron 18. Nature Publishing Group: 59–70. http://dx.doi.org/10.1016/S0896-6273(01)80046-5.

Koenning, Jackson, Hay, Faux, Kilpatrick, Willingham, and Emery. 2012. "Myelin Gene Regulatory Factor Is Required for Maintenance of Myelin and Mature Oligodendrocyte Identity in the Adult CNS" 32 (36): 12528–42. doi:10.1523/JNEUROSCI.1069-12.2012.

Koester, and O'Leary. 1992. "Functional Distinctions Classes of Cortical by Class-Specific Projection Neurons Develop Dendritic Sculpting of an Early Common Pattern." *The Journal of Neuroscience* 12 (April).

Kofuji, Fujiwara, Sanada, Mishima, and Akagawa. 2014. "HPC-1/Syntaxin 1A and Syntaxin 1B Play Distinct Roles in Neuronal Survival." *Journal of Neurochemistry* 130 (4): 514–25. doi:10.1111/jnc.12722.

Koudelka, Sigrid, Matthew G G. Voas, Rafael G G. Almeida, Marion Baraban, Jan Soetaert, Martin P P. Meyer, William S S. Talbot, and David A a. Lyons. 2016. "Individual Neuronal Subtypes Exhibit Diversity in CNS Myelination Mediated by Synaptic Vesicle Release." *Current Biology* 26 (11). The Authors: 1447–55. doi:10.1016/j.cub.2016.03.070.

Koudelka, Voas, Almeida, Meyer, Talbot, Lyons, Koudelka, et al. 2016. "Individual Neuronal Subtypes Exhibit Diversity in CNS Myelination Mediated by Synaptic Vesicle Report Individual Neuronal Subtypes Exhibit Diversity in CNS Myelination Mediated by Synaptic Vesicle Release." *Current Biology* 26 (11). The Authors: 1447–55. doi:10.1016/j.cub.2016.03.070.

Koyamaa, Morishige, Takahashi, Zanelli, Fassb, and Kurachia. 1994. "Molecular Cloning, Functional Expression and Localization of a Novel Inward Rectifier Potassium Channel in the Rat Brain." *FEBS Letters* 341: 303–7.

Krämer-Albers, Bretz, Tenzer, Winterstein, Möbius, Berger, Nave, Schild, and Trotter. 2007. "Oligodendrocytes Secrete Exosomes Containing Major Myelin and Stress-Protective Proteins: Trophic Support for Axons?" *PROTEOMICS – Clinical Applications* 1 (11). WILEY-VCH Verlag: 1446–61. doi:10.1002/prca.200700522.

Kramer, Schardt, and Nave. 2001. "Membrane Traffic in Myelinating Oligodendrocytes." *Microscopy Research and Technique* 52 (6). United States: 656–71. doi:10.1002/jemt.1050.

Kriegstein, and Noctor. 2004. "Patterns of Neuronal Migration in the Embryonic Cortex." *Trends in Neurosciences* 27 (7). doi:10.1016/j.tins.2004.05.001.

Kubicki, M, H Park, C F Westin, P G Nestor, R V Mulkern, S E Maier, M Niznikiewicz, et al. 2005. "DTI and MTR Abnormalities in Schizophrenia: Analysis of White Matter Integrity." *NeuroImage* 26: 1109–18. doi:10.1016/j.neuroimage.2005.03.026.

Kubo, Baldwin, Jan, and Jan. 1993. "Primary Structure and Functional Expression of a Mouse Inward Rectifier Potassium Channel." *Nature* 362: 127–133.

Kukley, Maria, Estibaliz Capetillo-Zarate, and Dirk Dietrich. 2007. "Vesicular Glutamate Release from Axons in White Matter." *Nature Neuroscience* 10 (3): 311–20. doi:10.1038/nn1850.

Kumar, and Ohana. 2008. "Inter- and Intralaminar Subcircuits of Excitatory and Inhibitory Neurons in Layer 6a of the Rat Barrel Cortex." *Journal of Neurop* 100: 1909–22. doi:10.1152/jn.90684.2008.Inter-.

Lane, and Liu. 1997. "Characterization of the Palmitoylation Domain of SNAP-25."

Lang, Maeda, Bannerman, Xu, Horiuchi, Pleasure, and Guo. 2013. "Adenomatous

Polyposis Coli Regulates Oligodendroglial Development." *J Neuros* 33 (7): 3113–30. doi:10.1523/JNEUROSCI.3467-12.2013.Adenomatous.
Lang, and Rosenbluth. 2018. "Role of Myelination in the Development of a Uniform Olivocerebellar Conduction Time." *J Neurophysiol*, 2259–70.
Lappe-Siefke, Goebbels, Gravel, Nicksch, Lee, Braun, Griffiths, and Nave. 2003. "Disruption of Cnp1 Uncouples Oligodendroglial Functions in Axonal Support and Myelination." *Nature Genetics* 33 (3): 366–74. doi:10.1038/ng1095.
Larsen, DeLaine D, and Edward M Callaway. 2006. "Development of Layer-Specific Axonal Arborizations in Mouse Primary Somatosensory Cortex." *The Journal of Comparative Neurology* 494 (3). United States: 398–414. doi:10.1002/cne.20754.
Larsen, Wickersham, and Callaway. 2008. "Retrograde Tracing with Recombinant Rabies Virus Reveals Correlations between Projection Targets and Dendritic Architecture in Layer 5 of Mouse Barrel Cortex." *Frontiers in Neural Circuits* 1 (March): 1–7. doi:10.3389/neuro.04.005.2007.
Lau, C Geoffrey, Yukihiro Takayasu, Alma Rodenas-ruano, Ana V Paternain, Juan Lerma, Michael V L Bennett, and R Suzanne Zukin. 2010. "SNAP-25 Is a Target of Protein Kinase C Phosphorylation Critical to NMDA Receptor Trafficking" 30 (1): 242–54. doi:10.1523/JNEUROSCI.4933-08.2010.
Lazari, Koudelka, and Sampaio-Baptista. 2018. "Experience-Related Reductions of Myelin and Axon Diameter in Adulthood." *Journal of Neurophysiology*, September. American Physiological Society. doi:10.1152/jn.00070.2018.
Leary, and Louis. 1988. "Cortical Axons Branch to Multiple Subcortical Targets by Interstitial Axon Budding: Implications for Target Recognition and 'Waiting Periods'" 1: 901–10.
Lee, Leach, Redmond, Chong, Mellon, Tuck, Feng, Corey, and Chan. 2012. "A Culture System to Study Oligodendrocyte Myelination-Processes Using Engineered Nanofibers." *Nature Methods* 9 (9): 917–22. doi:10.1038/nmeth.2105.A.
Lee, Lee, Ruiz, and Pfaff. 2005. "Olig2 and Ngn2 Function in Opposition to Modulate Gene Expression in Motor Neuron Progenitor Cells." *Genes & Development*, 282–94. doi:10.1101/gad.1257105.to.
Lee, Youngjin, Brett M Morrison, Yun Li, Sylvain Lengacher, Mohamed H Farah, Paul N Hoffman, Yiting Liu, et al. 2012. "Oligodendroglia Metabolically Support Axons and Contribute to Neurodegeneration." *Nature* 487 (7408). Nature Publishing Group: 443–48. doi:10.1038/nature11314.
Lefort, Tomm, Sarria, and Petersen. 2009. "Article The Excitatory Neuronal Network of the C2 Barrel Column in Mouse Primary Somatosensory Cortex." *Cell Press* 61 (2). Elsevier Inc.: 301–16. doi:10.1016/j.neuron.2008.12.020.
Levay, Stryker, and Shatz. 1978. "Ocular Dominance Columns and Their Development in Layer IV of the Cat's Visual Cortex: A Quantitative Study." *The Journal of Comparative Neurology*, 223–44.
Lévesque, Charara, Gagnon, Parent, and Deschênes. 1996. "Corticostriatal Projections from Layer V Cells in Rat Are Collaterals of Long-Range Corticofugal Axons." *Brain Reserach* 709: 311–15.
Levine, and Patrick. 1987. "Light and Electron Microscopic Localization of a Cell Surface Antigen (NG2) in the Rat Cerebellum: Association with Smooth Protoplasmic Astrocytes." *The Journal Fo Neuroscience* 7 (September).
Li, Brus-Ramer, Martin, and McDonald. 2010. "Electrical Stimulation of the

Medullary Pyramid Promotes Proliferation and Differentiation of Oligodendrocyte Progenitor Cells in the Corticospinal Tract of the Adult Rat." *Neuroscience Letters* 479 (2). Elsevier Ireland Ltd: 128–33. doi:10.1016/j.neulet.2010.05.043.

Li, Faria, Andrew, Nitarska, and Richardson. 2011. "Phosphorylation Regulates OLIG2 Cofactor Choice and the Motor Neuron-Oligodendrocyte Fate Switch." *Neuron* 69 (5). Elsevier Inc.: 918–29. doi:10.1016/j.neuron.2011.01.030.

Li, Zhang, Li, and Feng. 2000. "Destabilization and Mislocalization of Myelin Basic Protein MRNAs in Quaking Dysmyelination Lacking the QKI RNA-Binding Proteins." *The Journal of Neuroscience* 20 (12): 4944–53.

Ligon, Fancy, Franklin, and Rowitch. 2006. "Olig Gene Function in CNS Development and Disease." *Glia*, no. July 2005: 1–10. doi:10.1002/glia.20273.

Lin, and Bergles. 2004. "Synaptic Signaling between GABAergic Interneurons and Oligodendrocyte Precursor Cells in the Hippocampus." *Nature Neuroscience* 7 (1): 24–32. doi:10.1038/nn1162.

Liu, Cai, Hu, Tan, Qi, German, Rubenstein, Sander, and Qiu. 2003. "Region-Specific and Stage-Dependent Regulation of Olig Gene Expression and Oligodendrogenesis by Nkx6 . 1 Homeodomain Transcription Factor," 6221–31. doi:10.1242/dev.00868.

Liu, Dietz, DeLoyht, Pedre, Kelkar, Kaur, Vialou, et al. 2012. "Impaired Adult Myelination in the Prefrontal Cortex of Socially Isolated Mice." *Nature Neuroscience* 15 (12): 1621–23. doi:10.1038/nn.3263.

Llano, and Sherman. 2009. "Differences in Intrinsic Properties and Local Network Connectivity of Identified Layer 5 and Layer 6 Adult Mouse Auditory Corticothalamic Neurons Support a Dual Corticothalamic Projection Hypothesis." *Cerebal Cortex*, no. December 2009. doi:10.1093/cercor/bhp050.

Lopatin, Makhina, and Nichols. 1994. "Potassium Channel Block by Cytoplasmic Polyamines as the Mechanism of Intrinsic Rectification." *Nature*.

López-Bendito, and Molnár. 2003. "Thalamocortical Development: How Are We Going to Get There?" *Nature Reviews Neuroscience* 4 (4): 276–89. doi:10.1038/nrn1075.

Lozsadi, and Guillery. 1996. "The Course and Termination of Corticothalamic Fibres Arising in the Visual Cortex of the Rat." *European Journal of Neuroscience* 8 (1985): 2416–27.

Lu, and MacKinnon. 1994. "Electrostatic Tuning of Mg2+ Affinity in an Inward-Rectifier K+ Channel." *Letters to Nature*.

Lu, Nagappan, Guan, Nathan, and Wren. 2013. "BDNF-Based Synaptic Repair as a Disease-Modifying Strategy for Neurodegenerative Diseases." *Nature Reviews Neuroscience* 14 (6). Nature Publishing Group: 401–16. doi:10.1038/nrn3505.

Lu, Park, Noll, Cha, Alberta, Yuk, Alzamora, et al. 2018. "The Oligodendroglial Lineage Marker OLIG2 Is Universally Expressed in Diffuse Gliomas." *Journal of Neuropathology and Experimental Neurology* 63 (5): 499–509.

Lu, Park, Noll, Chan, Alberta, Yuk, Alzamora, et al. 2001. "Oligodendrocyte Lineage Genes (OLIG) as Molecular Markers for Human Glial Brain Tumors." *PNAS*.

Lu, Sun, Zhu, Ma, Garcia, Stiles, and Rowitch. 2002. "Common Developmental Requirement for Olig Function Indicates a Motor Neuron/Oligodendrocyte

Connection." *Cell* 109 (1): 75–86. doi:https://doi.org/10.1016/S0092-8674(02)00678-5.
Lu, Yuk, Alberta, Zhu, Pawlitzky, Chan, Mcmahon, Stiles, and Rowitch. 2000. "Sonic Hedgehog – Regulated Oligodendrocyte Lineage Genes Encoding BHLH Proteins in the Mammalian Central Nervous System." *Neuron* 25: 317–29.
Lubetzki, Demerens, Anglade, Villarroya, Frankfurter, Lee, and Zalc. 1993. "Even in Culture , Oligodendrocytes Myelinate Solely Axons." *Proc. Natl Acad. Sci. USA* 90 (July): 6820–24.
Lundgaard, Luzhynskaya, Stockley, Wang, Evans, Swire, Volbracht, et al. 2013. "Neuregulin and BDNF Induce a Switch to NMDA Receptor-Dependent Myelination by Oligodendrocytes." *PLoS Biology* 11 (12). doi:10.1371/journal.pbio.1001743.
Luskin, and Shatz. 1985. "Neurogenesis of the Cat's Primary Visual Cortex." *Journal of Comparative Neurology* 631.
Ma, Zerangue, Lin, Collins, Yu, Jan, and Jan. 2001. "Role of ER Export Signals in Controlling Surface Potassium Channel Numbers." *Science* 291 (5502): 316 LP-319. http://science.sciencemag.org/content/291/5502/316.abstract.
Madisen, Zwingman, Sunkin, Oh, Zariwala, Gu, Ng, et al. 2009. "A Robust and High-Throughput Cre Reporting and Characterization System for the Whole Mouse Brain." *Nature Neuroscience* 13 (1). Nature Publishing Group: 133–40. doi:10.1038/nn.2467.
Maffei, and Galli-Resta. 1990. "Correlation in the Discharges of Neighboring Rat Retinal Ganglion Cells during Prenatal Life." *Proceedings of the National Academy of Sciences of the United States of America* 87 (April): 2861–64. doi:10.1073/pnas.87.7.2861.
Maire, Wegener, Kernion, and Oumemar. 2010. "Gain-of-Function of Olig Transcription Factors Enhances Oligodendrogenesis and Myelination." *Stem Cells*, 1611–22. doi:10.1002/stem.480.
Makinodan, Rosen, Ito, and Corfas. 2012. "A Critical Period for Social Experience-Dependent Oligodendrocyte Maturation and Myelination." *Science* 337 (6100): 1357–60. doi:10.1126/science.1220845.
Malatesta, Hack, Hartfuss, Kettenmann, Klinkert, Kirchhoff, and Go. 2003. "Neuronal or Glial Progeny: Regional Differences in Radial Glia Fate." *Neuron* 37: 751–64.
Malatesta, Hartfuss, and Götz. 2000. "Isolation of Radial Glial Cells by Fluorescent-Activated Cell Sorting Reveals a Neuronal Lineage." *Development* 5263: 5253–63.
Malone, Gary, Yang, Miglioretti, Houdayer, Thakor, and McDonald. 2013. "Neuronal Activity Promotes Myelination via a CAMP Pathway." *Glia* 61 (6): 843–54. doi:10.1002/glia.22476.
Mangin, and Gallo. 2010. "The Curious Case of NG2 Cells: Transient Trend or Game Changer?" *ASN Neuro* 3 (1): AN20110001. doi:10.1042/AN20110001.
Mangin, Li, Scafidi, and Gallo. 2012. "Experience-Dependent Regulation of NG2 Progenitors in the Developing Barrel Cortex." *Nature Neuroscience* 15 (9). Nature Publishing Group: 1192–94. doi:10.1038/nn.3190.
Marie, Sanson, Mokhtari, Leuraud, Kujas, Delattre, Poirier, Zalc, and Hoang-Xuan. 2001. "OLIG2 as a Specific Marker of Oligodendroglial Tumour Cells." *The Lancet* 358: 298–300.

Marin-Padilla. 1971. “Early Prenatal Ontogenesis of the Cerebral Cortex (Neocortex) of the Cat (Felis Domestica). A Golgi Study. I. The Primordial Neocortical Organization.” *Zeitschrift Fur Anatomie Und Entwicklungsgeschichte* 134 (2). Germany: 117–45.

Marinelli, Bertalot, Zusso, Skaper, and Giusti. 2016. “Systematic Review of Pharmacological Properties of the Oligodendrocyte Lineage.” *Frontiers in Cellular Neuroscience* 10 (February): 1–19. doi:10.3389/fncel.2016.00027.

Markram, Henry, Maria Toledo-Rodriguez, Yun Wang, Anirudh Gupta, Gilad Silberberg, and Caizhi Wu. 2004. “Interneurons of the Neocortical Inhibitory System.” *Nature Reviews. Neuroscience* 5 (10): 793–807. doi:10.1038/nrn1519.

Markram, Muller, Ramaswamy, Reimann, Defelipe, Hill, Segev, et al. 2015. “Reconstruction and Simulation of Neocortical Reconstruction and Simulation of Neocortical Microcircuitry,” 456–92. doi:10.1016/j.cell.2015.09.029.

Marner, Lisbeth, Jens R. Nyengaard, Yong Tang, and Bente Pakkenberg. 2003. “Marked Loss of Myelinated Nerve Fibers in the Human Brain with Age.” *Journal of Comparative Neurology* 462 (2): 144–52. doi:10.1002/cne.10714.

Martínez-Garay, García-Moreno, Vasistha, Marques-Smith, and Molnár. 2016. “In Utero Electroporation Methods in the Study of Cerebral Cortical Development.” In *Prenatal and Postnatal Determinants of Development. Neuromethods*. Vol. 109. doi:10.1007/978-1-4939-3014-2.

Mason, and Larkman. 1990. “Correlations Between Morphology and Electrophysiology Pyramidal Neurons in Slices of Rat Visual Cortex.” *The Journal of Neuroscience* 70 (May): 1415–28.

Matsuda, Saigusa, and Irisawa. 1987. “Ohmic Conductance through the Inwardly Rectifying K Channel and Blocking by Internal Mg2+.” *Nature*.

Matsumoto, Naoyuki, Maki Hoshiko, Noriyuki Sugo, Yugo Fukazawa, and Nobuhiko Yamamoto. 2016. “Synapse-Dependent and Independent Mechanisms of Thalamocortical Axon Branching Are Regulated by Neuronal Activity.” *Developmental Neurobiology* 76 (3): 323–36. doi:10.1002/dneu.22317.

Mayer, Bhakoo, and Noble. 1994. “Ciliary Neurotrophic Factor and Leukemia Inhibitory Factor Promote the Generation , Maturation and Survival of Oligodendrocytes in Vitro” 153: 143–53.

McKenzie, Ohayon, Li, Paes de Faria, Emery, Tohyama, and Richardson. 2014. “Motor Skill Learning Requires Active Central Myelination.” *Science* 346 (6207): 318–22. doi:10.1126/science.1254960.

McMorris, and Dubois-Dalcq. 1988. “Insulin-like Growth Factor I Promotes Cell Proliferation and Oligodendroglial Commitment in Rat Glial Progenitor Cells Developing in Vitro.” *Journal of Neuroscience Research* 21 (2–4). Wiley Subscription Services, Inc., A Wiley Company: 199–209. doi:10.1002/jnr.490210212.

McMorris, and McKinnon. 1996. “Regulation of Oligodendrocyte Development and CNS Myelination by Growth Factors: Prospects for Therapy of Demyelinating Disease.” *Brain Pathology* 6 (3). Blackwell Publishing Ltd: 313–29. doi:10.1111/j.1750-3639.1996.tb00858.x.

Mei, Wang, Liu, Niu, Wang, He, Etxeberria, Chan, and Xiao. 2013. “Stage-Specific Deletion of Olig2 Conveys Opposing Functions on Differentiation and Maturation of Oligodendrocytes.” *The Journal of Neuroscience* 33 (19): 8454–

62. doi:10.1523/JNEUROSCI.2453-12.2013.
Meijer, Kane, Mehta, Liu, Harrington, Taylor, Stiles, and Rowitch. 2012. “Separated at Birth? The Functional and Molecular Divergence of OLIG1 and OLIG2.” *Nat Rev Neurosci*. Nature Publishing Group. doi:10.1038/nrn3386.
Mekki-Dauriac, Agius, Kan, and Cochard. 2002. “Bone Morphogenetic Proteins Negatively Control Oligodendrocyte Precursor Specification in the Chick Spinal Cord” 5130: 5117–30.
Mensch, Sigrid, Marion Baraban, Rafael Almeida, Tim Czopka, Jessica Ausborn, Abdeljabbar El Manira, and David a Lyons. 2015. “Synaptic Vesicle Release Regulates Myelin Sheath Number of Individual Oligodendrocytes in Vivo.” *Nature Neuroscience* 18 (5): 6–10. doi:10.1038/nn.3991.
Messersmith, Murtie, Le, Frost, and Armstrong. 2000. “Fibroblast Growth Factor 2 (FGF2) and FGF Receptor Expression in an Experimental Demyelinating Disease With Extensive Remyelination.” *J Neurosci Res* 256 (April): 241–56.
Meyer, Wimmer, Hemberger, Bruno, Kock, Frick, Sakmann, and Helmstaedter. 2010. “Cell Type-Specific Thalamic Innervation in a Column of Rat Vibrissal Cortex,” no. October. doi:10.1093/cercor/bhq069.
Meyersburg, and Post. 1979. “An Holistic Developmental View of Neural and Psychological Processes.” *Brit J Psychat*.
Mi, Deerinck, Jones, Ellisman, and Schwarzl. 1996. “Inwardly Rectifying K+ Channels That May Participate in K+ Buffering Are Localized in Microvilli of Schwann Cells.” *The Journal of Neuroscience* 76 (8): 2421–29.
Miller. 2002. “Regulation of Oligodendrocyte Development in the Vertebrate CNS.” *Progress in Neurobiology* 67: 451–67.
Miron, Kuhlmann, and Antel. 2011. “Cells of the Oligodendroglial Lineage, Myelination, and Remyelination.” *Biochimica et Biophysica Acta (BBA) - Molecular Basis of Disease* 1812 (2): 184–93. doi:http://dx.doi.org/10.1016/j.bbadis.2010.09.010.
Misson, Austin, Takahashi, Cepko, and Caviness. 1991. “The Alignment of Migrating Neural Cells in Relation to the Murine Neopallial Radial Glial Fiber System.” *Cerebral Cortex* 1 (3). United States: 221–29.
Mitew, Gobius, Fenlon, Mcdougall, Hawkes, Xing, Bujalka, et al. 2018. “Pharmacogenetic Stimulation of Neuronal Activity Increases Myelination in an Axon-Specific Manner.” *Nature Communications*. Springer US, 1–16. doi:10.1038/s41467-017-02719-2.
Mitew, Hay, Peckham, Xiao, Koenning, and Emery. 2014. “Mechanisms Regulating the Development of Oligodendrocytes and Central Nervous System Myelin.” *Neuroscience* 276. IBRO: 29–47. doi:10.1016/j.neuroscience.2013.11.029.
Miyata, Kawaguchi, Okano, and Ogawa. 2001. “Asymmetric Inheritance of Radial Glial Fibers by Cortical Neurons.” *Neuron* 31: 727–41.
Mizuno, Hirano, and Tagawa. 2007. “Evidence for Activity-Dependent Cortical Wiring: Formation of Interhemispheric Connections in Neonatal Mouse Visual Cortex Requires Projection Neuron Activity.” *The Journal of N* 27 (25): 6760–70. doi:10.1523/JNEUROSCI.1215-07.2007.
Mochida. 2011. “Activity-Dependent Regulation of Synaptic Vesicle Exocytosis and Presynaptic Short-Term Plasticity.” *Neuroscience Research* 70 (1). Elsevier Ireland Ltd and Japan Neuroscience Society: 16–23. doi:10.1016/j.neures.2011.03.005.
Molnár. 2013. “Cortical Columns.” In *Neural Circuit Development and Function in*

the Heathy and Diseased Brain, 109–29. Elsevier Inc. doi:10.1016/B978-0-12-397267-5.00137-0.

Molnár, and Cheung. 2006. “Towards the Classification of Subpopulations of Layer V Pyramidal Projection Neurons.” *Neuroscience Research* 55 (2): 105–15. doi:10.1016/j.neures.2006.02.008.

Molnár, López-Bendito, Small, Partridge, Blakemore, and Wilson. 2002. “Normal Development of Embryonic Thalamocortical Connectivity in the Absence of Evoked Synaptic Activity.” *The Journal of Neuroscience : The Official Journal of the Society for Neuroscience* 22 (23): 10313–23. http://www.ncbi.nlm.nih.gov/pubmed/12451131.

Molyneaux, Arlotta, Menezes, and Macklis. 2007. “Neuronal Subtype Specification in the Cerebral Cortex.” *Nature Reviews. Neuroscience* 8 (6): 427–37. doi:10.1038/nrn2151.

Monteggia, Lin, Adachi, and Kavalali. 2018. “Behavioral Analysis of SNAP-25 and Synaptobrevin-2 Haploinsufficiency in Mice.” *Neuroscience*. IBRO. doi:10.1016/J.NEUROSCIENCE.2018.08.014.

Mooney, Penn, Gallego, and Shatz. 1996. “Thalamic Relay of Spontaneous Retinal Activity Prior to Vision.” *Neuron* 17 (5): 863–74. doi:10.1016/S0896-6273(00)80218-4.

Moore, Kalil, and Richards. 1976. “Development of Myelination in Optic Tract of the Cat.” *J Comp Neurol*, 125–36.

Morishige, Takahashi, Jahangir, Yamada, Koyama, Zanelli, and Kurachi. 1994. “Molecular Cloning and Functional Expression of a Novel Brain-Specific Inward Rectifier Potassium Channel.” *FEBS Letters* 346: 251–56.

Mount, and Monje. 2017. “Wrapped to Adapt: Experience-Dependent Myelination.” *Neuron* 95 (4). Elsevier Inc.: 743–56. doi:10.1016/j.neuron.2017.07.009.

Mountcastle. 1956. “Modality and Topographic Properties of Single Neurons of Cat’s Somatic Sensory Cortex.”

Mountcastle, V. 1997. “The Columnar Organization of the Neocortex.” *Brain* 120 (4): 701–22. doi:10.1093/brain/120.4.701.

Murre, Bain, Dijk, Engel, Furnari, Massari, Matthews, Ouong, Rivera, and Stuiver. 1994. “Structure and Function of Helix-Loop-Helix Proteins.” *BBA* 1218: 129–35.

Murre, Cornelis, and Patrick Schonleber. 1989. “A New DNA Binding and Dimerization Motif in Lmmunoglobulin Enhancer Binding , Daughterless, MyoD, and Myc Proteins.” *Cell* 56: 777–83.

Naka, and Adesnik. 2016. “Inhibitory Circuits in Cortical Layer 5” 10 (May): 1–16. doi:10.3389/fncir.2016.00035.

Nave. 2010. “Myelination and the Trophic Support of Long Axons.” *Nat Rev Neurosci* 11 (4). Nature Publishing Group: 275–83. http://dx.doi.org/10.1038/nrn2797.

Neumann, Kotter, and Franklin. 2009. “Debris Clearance by Microglia: An Essential Link between Degeneration and Regeneration.” *Brain : A Journal of Neurology*, 288–95. doi:10.1093/brain/awn109.

Nishiyama, Chang, and Trapp. 1999. “NG2+ Glial Cells: A Novel Glial Cell Population in the Adult Brain.” *Journal of Neuropathology and Experimental Neurology*, no. June.

Noctor, Flint, Weissman, Dammerman, and Kriegstein. 2001. “Neurons Derived from Radial Glial Cells Establish Radial Units in Neocortex.” *Letters to Nature*

409 (February): 714–20.
Noctor, Flint, Weissman, Wong, Clinton, and Kriegstein. 2002. “Dividing Precursor Cells of the Embryonic Cortical Ventricular Zone Have Morphological and Molecular Characteristics of Radial Glia.” *The Journal of Neuroscience* 22 (8): 3161–73.
Noctor, Martínez-cerdeño, Ivic, and Kriegstein. 2004. “Cortical Neurons Arise in Symmetric and Asymmetric Division Zones and Migrate through Specific Phases.” *Nature Neuroscience* 7 (2): 136–44. doi:10.1038/nn1172.
Norton, and Oduslo. 1973. “Myelination in Rat Brain: Changes in Myelin Composition during Brain Maturation.” *Journal of Neurochemestry* 21: 759–73.
Novitch, Chen, and Jessell. 2001. “Coordinate Regulation of Motor Neuron Subtype Identity and Pan-Neuronal Properties by the BHLH Repressor Olig2” 31: 773–89.
O’Leary, D D, and S E Koester. 1993. “Development of Projection Neuron Types, Axon Pathways, and Patterned Connections of the Mammalian Cortex.” *Neuron* 10 (6). United States: 991–1006.
O’Leary, and Stanfield. 1989. “Selective Elimination of Axons Extended by Developing Neurons Is Dependent on Regional Locale: Experiments Fetal Cortical Transplants.” *The Journal of Neuroscience*, no. July: 2230–46.
Oberlaender, Kock, Bruno, Ramirez, Meyer, Dercksen, Helmstaedter, and Sakmann. 2012. “Cell Type-Specific Three-Dimensional Structure of Thalamocortical Circuits in a Column of Rat Vibrissal Cortex,” no. October: 2375–91. doi:10.1093/cercor/bhr317.
Ohnishi, Sawa, Tsuda, Sawamura, Itoh, Iwasaki, and Nagashima. 2018. “Expression of the Oligodendroglial Lineage-Associated Markers Olig1 and Olig2 in Different Types of Human Gliomas.” *Neurology, Journal of Neuropathology and Experimental* 62 (10): 1052–59.
Okada, and Matsuda. 2008. “Chronic Lentiviral Expression of Inwardly Rectifying K+ Channels (Kir2.1) Reduces Neuronal Activity and Downregulates Voltage-Gated Potassium Currents in Hippocampus” 156: 289–97. doi:10.1016/j.neuroscience.2008.07.038.
Olsen, Bortone, Adesnik, and Scanziani. 2012. “Gain Control by Layer Six in Cortical Circuits of Vision.” *Nature* 482 (7387). Nature Publishing Group: 47–52. doi:10.1038/nature10835.
Omlin. 1997. “Optic Disc and Optic Nerve of the Blind Cape Mole-Rat (Georychus Capensis): A Proposed Model for Naturally Occurring Reactive Gliosis.” *Brain Reserach Bulletin* 44 (5): 627–32.
Orentas, Hayes, Dyer, and Miller. 1999. “Sonic Hedgehog Signaling Is Required during the Appearance of Spinal Cord Oligodendrocyte Precursors” 2429: 2419–29.
Osen-Sand, Catsicas, Staple, Jones, Ayala, and Knowles. 1993. “Inhibition of Axonal Growth by SNAP-25 Antisense Oligonucleotides in Vitro and in Vivo.”
Osen-Sand, Catsicas, Staple, Jones, Ayala, Knowles, Grenningloh, and Catsicas. 1993. “Inhibition of Axonal Growth by SNAP-25 Antisense Oligonucleotides in Vitro and in Vivo.” *Nature* 364 (6436): 445–48. http://dx.doi.org/10.1038/364445a0.
Osen-Sand, Staple, Naldi, Schiavo, Rossetto, Petitpierre, Malgaroli, Montecucco, and Catsicas. 1996. “Common and Distinct Fusion Proteins in Axonal Growth

and Transmitter Release" 234.
Oumesmar, Vignais, and Evercooren. 1997. "Developmental Expression of Platelet-Derived Growth Factor Alpha-Receptor in Neurons and Glial Cells of the Mouse CNS." *The Journal of Neuroscience* 17 (1): 125–39.
Oyler, Higgins, Hart, Battenberg, Billingsley, Bloom, and Wilson. 1989. "The Identification of a Novel Synaptosomal-Associated Protein, SNAP-25, Differentially Expressed by Neuronal Subpopulations." *J Cell Biol.* 109 (6): 3039–52.
Oyler, Polli, Wilsont, and Billingsley. 1991. "Developmental Expression of the 25-KDa Synaptosomal-Associated Protein (SNAP-25) in Rat Brain" 88 (June): 5247–51.
Pajevic, Basser, and Fields. 2014. "Role of Myelin Plasticity in Oscillations and Synchrony of Neuronal Activity." *Neuroscience* 276. IBRO: 135–47. doi:10.1016/j.neuroscience.2013.11.007.
Paolicelli, Bolasco, Pagani, Maggi, Scianni, Panzanelli, Giustetto, et al. 2011. "Synaptic Pruning by Microglia Is Necessary for Normal Brain Development" 333 (September): 1456–59.
Park, and Poo. 2012. "Neurotrophin Regulation of Neural Circuit Development and Function." *Nature Reviews Neuroscience* 14 (1). Nature Publishing Group: 7–23. doi:10.1038/nrn3379.
Park, Solomon, and Vartanian. 2001. "Growth Factor Control of CNS Myelination." *Developmental Neuroscience* 23 (4–5): 327–37. doi:10.1159/000048716.
Patneau, Doris K., Paul W. Wright, Christine Winters, Mark L. Mayer, and Vittorio Gallo. 1994. "Glial Cells of the Oligodendrocyte Lineage Express Both Kainate- and AMPA-Preferring Subtypes of Glutamate Receptor." *Neuron* 12 (2): 357–71. doi:10.1016/0896-6273(94)90277-1.
Paukert, and Bergles. 2006. "Synaptic Communication between Neurons and NG2+cells." *Current Opinion in Neurobiology* 16 (5): 515–21. doi:10.1016/j.conb.2006.08.009.
Pedraza, Fidler, Staugaitis, and Colman. 1997. "The Active Transport of Myelin Basic Protein into the Nucleus Suggests a Regulatory Role in Myelination" 18: 579–89.
Peles, and Salzer. 2000. "Molecular Domains of Myelinated Axons." *Current Opinion in Neurobiology* 10 (5): 558–65. doi:10.1016/S0959-4388(00)00122-7.
Pelletier, Pare, Guillaume, and Pare. 2018. "Uniform Range of Conduction Times From the Lateral Amygdala to Distributed Perirhinal Sites." *Journal of Neurophysiology*, 1213–21.
Perin, Berger, and Markram. 2011. "A Synaptic Organizing Principle for Cortical Neuronal Groups" 108 (13): 5419–24. doi:10.1073/pnas.1016051108.
Pesaresi, Soon-Shiong, French, Kaplan, Miller, and Paus. 2016. "Axon Diameter and Axonal Transport: In Vivo and in Vitro Effects of Androgens," 191–201. doi:10.1016/j.neuroimage.2015.04.048.Axon.
Peters, and Sethares. 1996. "Myelinated Axons and the Pyramidal Cell Modules in Monkey Primary Visual Cortex." *The Journal of Comparative Neurology* 255.
Petreanu, Mao, Sternson, and Svoboda. 2009. "The Subcellular Organization of Neocortical Excitatory Connections." *Nature* 457 (7233). Nature Publishing Group: 1142–45. doi:10.1038/nature07709.
Piscopo, Weible, Rothbart, Posner, and Niell. 2018. "Changes in White Matter in

Mice Resulting from Low-Frequency Brain Stimulation." *Proceedings of the National Academy of Sciences* 115 (27): 201802160. doi:10.1073/pnas.1802160115.

Plaster, Tawil, Tristani-firouzi, Canu, Tsunoda, Donaldson, Iannaccone, et al. 2001. "Mutations in Kir2.1 Cause the Developmental and Episodic Electrical Phenotypes of Andersen's Syndrome." *Cell* 105: 511–19.

Pointer-Keenan, Lee, Hallok, Tan, Zand, and Ramamoorthy. 2004. "Investigation of the Interaction of Myelin Basic Protein with Phospholipid Bilayers Using Solid-State NMR Spectroscopy." *Chemistry and Physics of Lipids* 132 (1): 47–54. doi:https://doi.org/10.1016/j.chemphyslip.2004.09.004.

Polverini, Arisi, Cavatorta, Berzina, Cristofolini, Fasano, Riccio, and Fontana. 2003. "Interaction of Myelin Basic Protein with Phospholipid Monolayers : Mechanism of Protein Penetration" 1 (8): 872–77.

Poncet, Soula, Trousse, Kan, Hirsinger, Pourquié, Duprat, and Cochard. 1996. "Induction of Oligodendrocyte Progenitors in the Trunk Neural Tube by Ventralizing Signals: Effects of Notochord and Floor Plate Grafts, and of Sonic Hedgehog." *Mechanisms of Development* 60 (1): 13–32. doi:https://doi.org/10.1016/S0925-4773(96)00595-3.

Popko. 2003. "Notch Signaling : A Rheostat Regulating Oligodendrocyte Differentiation ?" *Developmental Cell* 1 (2002): 668–69.

Prabakaran, Lippens, Steen, and Gunawardena. 2012. "Post-Translational Modification : Nature's Escape from Genetic Imprisonment and the Basis for Dynamic Information Encoding." *Interdiscip Rev Syst Biol Med* 4 (December). doi:10.1002/wsbm.1185.

Price, Aslam, Tasker, and Gillies. 1997. "Fates of the Earliest Generated Cells in the Developing Murine Neocortex." *Journal of Comparative Neurology* 377 (3): 414–22. doi:10.1002/(SICI)1096-9861(19970120)377:3<414::AID-CNE8>3.0.CO;2-5.

Pringle, Mudhar, Collarini, and William. 1992. "PDGF Receptors in the Rat CNS: During Late Neurogenesis, PDGF Alpha- Receptor Expression Appears to Be Restricted to Glial Cells of the Oligodendrocyte Lineage." *Development* 551: 535–51.

Pringle, Yu, Guthrie, Roelink, Lumsden, Peterson, and Richardson. 1996. "Determination of Neuroepithelial Cell Fate: Induction of the Oligodendrocyte Lineage by Ventral Midline Cells and Sonic Hedgehog" 42 (0142): 30–42.

Pruss, Derst, Lommel, and Veh. 2005. "Differential Distribution of Individual Subunits of Strongly Inwardly Rectifying Potassium Channels (Kir2 Family) in Rat Brain." *Molecular Brain Reserach* 139: 63–79. doi:10.1016/j.molbrainres.2005.05.006.

Pujol, Soriano-Mas, Ortoz, Sebastián-Gallés, Losilla, and Deus. 2006. "Myelinaton of Language-Related Areas in the Developing Brain." *Neurology* 66: 339–43.

Pumphrey, and Young. 1938. "THE RATES OF CONDUCTION OF NERVE FIBRES OF VARIOUS DIAMETERS IN CEPHALOPODS." *Journal of Experimental Biology*, no. January.

Purves, Augustine, and Fitzpatrick. 2001. "Neuroscience. 2nd Edition." In .

Qi, Cai, Wu, Wu, Lee, Fu, Rao, and Sussel. 2001. "Control of Oligodendrocyte Differentiation by the Nkx2 . 2 Homeodomain Transcription Factor" 2733: 2723–33.

Rah, Bas, Colonell, Mishchenko, Karsh, Fetter, Myers, et al. 2013.

"Thalamocortical Input onto Layer 5 Pyramidal Neurons Measured Using Quantitative Large-Scale Array Tomography." *Frontiers in Neural Circuits*. https://www.frontiersin.org/article/10.3389/fncir.2013.00177.

Rakic. 1972. "Mode of Cell Migration to the Superficial Layers of Fetal Monkey Neocortex." *Journal of Comparative Neurology* 145 (1): 61–83. doi:10.1002/cne.901450105.

Ranvier. 1871. "Contributions à l'histologie et à La Physiologie Des Nerfs Périphériques." *Comptes Rendus de l'Académie Des Sciences* 73: 1168–71.

Ravichandran, Veerasamy, Ashish Chawla, and Paul A Roche. 1996. "Identification of a Novel Syntaxin- and Synaptobrevin / Expressed in Non-Neuronal Tissues." *The Journal of Biological Chemistry* 271 (23): 23–27.

Readhead, Popko, Takahashi, Shine, Saavedra, Sidman, and Hood. 1987. "Expression of a Myelin Basic Protein Gene in Transgenic Shiverer Mice: Correction of the Dysmyelinating Phenotype." *Cell* 48 (4): 703–12. http://www.ncbi.nlm.nih.gov/pubmed/2434242.

Reynolds, and Hardy. 1997. "Oligodendroglial Progenitors Labeled With the O4 Antibody Persist in the Adult Rat Cerebral Cortex In Vivo." *Journal of Neuroscience Reserach* 470: 455–70.

Richardson, Kessaris, and Pringle. 2006. "Oligodendrocyte Wars." *Nature Reviews. Neuroscience* 7 (1): 11–18. doi:10.1038/nrn1826.

Rieske, Azizi, Augelli, Gaughan, and Krynska. 2007. "A Population of Human Brain Parenchymal Cells Express Markers of Glial, Neuronal and Early Neural Cells and Differentiate into Cells of Neuronal and Glial Lineages." *European Journal of Neuroscience* 25 (1): 31–37. doi:10.1111/j.1460-9568.2006.05254.x.

Rios, Melendez-Vasquez, Einheber, Lustig, Grumet, Hemperly, Peles, and Salzer. 2000. "Contactin-Associated Protein (Caspr) and Contactin Form a Complex That Is Targeted to the Paranodal Junctions during Myelination." *The Journal of Neuroscience* 20 (22): 8354 LP-8364. http://www.jneurosci.org/content/20/22/8354.abstract.

Rosenberg, Kelland, Tokar, De La Torre, and Chan. 2008. "The Geometric and Spatial Constraints of the Microenvironment Induce Oligodendrocyte Differentiation." *Proceedings of the National Academy of Sciences* 105 (38): 14662–67. doi:10.1073/pnas.0805640105.

Rosenbluth. 1980. "Central Myelin in the Mouse Mutant Shiverer." *J. Comp. Neurol.* 194. Nature Publishing Group: 639–48. http://dx.doi.org/10.1002/cne.901940310.

Rosenmund, Stevens, and Zellula. 1996. "Definition of the Readily Releasable Pool of Vesicles at Hippocampal Synapses" 16 (1995): 1197–1207.

Rouiller, Tanné, Moret, Kermadi, Boussaoud, and Welker. 1998. "Dual Morphology and Topography of the Corticothalamic Terminals Originating From the Primary , Supplementary Motor , and Dorsal Premotor Cortical Areas in Macaque Monkeys." *The Journal of Comparative Neuroscience* 185 (February): 169–85.

Rudy, Fishell, Lee, and Hjerling-Leffler. 2011. "Three Groups of Interneurons Account for Nearly 100% of Neocortical GABAergic Neurons." *Developmental Neurobiology* 71 (1): 45–61. doi:10.1002/dneu.20853.

Saab, Tzvetavona, Trevisiol, Baltan, Dibaj, Kusch, Möbius, et al. 2016. "Oligodendroglial NMDA Receptors Regulate Glucose Import and Axonal Energy Metabolism Article Oligodendroglial NMDA Receptors Regulate

Glucose Import and Axonal Energy Metabolism." *Cell*, 119–32. doi:10.1016/j.neuron.2016.05.016.
Sahara, Yanagawa, O'Leary, and Stevens. 2012. "The Fraction of Cortical GABAergic Neurons Is Constant from near the Start of Cortical Neurogenesis to Adulthood." *The Journal of Neuroscience : The Official Journal of the Society for Neuroscience* 32 (14): 4755–61. doi:10.1523/JNEUROSCI.6412-11.2012.
Sakmann, and Trube. 1984. "Conductance Properties of Single Inwardly Rectifying Potassium Channels in Ventricular Cells from Guinea-Pig Heart." *Journal of Pysiology*, 641–57.
Salami, Itami, Tsumoto, and Kimura. 2003. "Change of Conduction Velocity by Regional Myelination Yields Constant Latency Irrespective of Distance between Thalamus and Cortex." *PNAS*.
Salzer. 1997. "Clustering Sodium Channels at the Node of Ranvier: Close Encounters of the Axon-Glia Kind." *Neuron* 18 (6): 843–46. doi:10.1016/S0896-6273(00)80323-2.
Sampaio-Baptista, Khrapitchev, Foxley, Schlagheck, Scholz, Jbabdi, DeLuca, et al. 2013. "Motor Skill Learning Induces Changes in White Matter Microstructure and Myelination." *Journal of Neuroscience* 33 (50): 19499–503. doi:10.1523/JNEUROSCI.3048-13.2013.
Schindelin, Arganda-Carreras, Frise, Kaynig, Longair, Pietzsch, Preibisch, et al. 2012. "Fiji: An Open-Source Platform for Biological-Image Analysis." *Nature Methods* 9 (7): 676–82. doi:10.1038/nmeth.2019.
Schmidt, and Lent. 1987. "Effects of Prenatal Irradiation on the Development of Cerebral Cortex and Corpus Callosum of the Mouse." *Journal of Comparative Neurology* 264 (2): 193–204. doi:10.1002/cne.902640205.
Schmithorst, V.J., M. Wilke, Dardzinski, B.J., and S.K. Holland. 2005. "COGNITIVE FUNCTIONS CORRELATE WITH WHITE MATTER ARCHITECTURE IN A NORMAL PEDIATRIC POPULATION: A," no. 2: 139–47.
Scholz, Klein, Behrens, and Johansen-Berg. 2010. "Training Induces Changes in White Matter Architecture." *Nat Neurosci* 12 (11): 1370–71. doi:10.1038/nn.2412.Training.
Schram, Melnyk, Pourrier, Wang, and Nattel. 2002. "Kir2.4 and Kir2.1 K+ Channel Subunits Co-Assemble: A Potential New Contributor to Inward Rectifier Current Heterogeneity." *Journal of Physiology*, 337–49. doi:10.1113/jphysiol.2002.026047.
Schroder. 1972. "Altered Ratio between Axon Diameter and Myelin Sheath Thickness in Regenerated Nerve Fibers." *Brain Reserach* 45 (September 1971): 49–65.
Schubert, Staiger, Cho, Ko, Zilles, and Luhmann. 2001. "Layer-Specific Intracolumnar and Transcolumnar Functional Connectivity of Layer V Pyramidal Cells in Rat Barrel Cortex" 21 (10): 3580–92.
Schulz, Cruz, and Moscarello. 1988. "Endogenous Phosphorylation of Basic Protein in Myelin of Varying Degrees of Compaction." *Biochemistry* 27 (20). United States: 7793–99.
Seidl. 2014. "Regulation of Conduction Time along Axons." *Neuroscience* 276. IBRO: 126–34. doi:10.1016/j.neuroscience.2013.06.047.
Seidl, and Rubel. 2016. "Systematic and Differential Myelination of Axon Collaterals in the Mammalian Auditory Brainstem." *Glia* 64 (4): 487–94.

doi:10.1002/glia.22941.
Sernagor, and Grzywacz. 1996. “Influence of Spontaneous Activity and Visual Experience on Developing Retinal Receptive Fields.” *Current Biology : CB* 6: 1503–8. doi:10.1016/S0960-9822(96)00755-5.
Sharma, Burre, Bronk, Zhang, Xu, and Su. 2012. “CSP a Knockout Causes Neurodegeneration by Impairing SNAP-25 Function.” *Journal of Cell Biology* 31 (4): 829–41. doi:10.1038/emboj.2011.467.
Sherman, and Brophy. 2005. “Mechanisms of Axon Ensheathment and Myelin Growth.” *Nature Reviews Neuroscience* 6 (9): 683–90. doi:10.1038/nrn1743.
Sherman, and Guillery. 1998. “On the Actions That One Nerve Cell Can Have on Another: Distinguishing ‘“Drivers”’ from ‘“Modulators.”’” *PNAS* 95 (June): 7121–26.
Sherman, S. M., and R. W. Guillery. 2002. “The Role of the Thalamus in the Flow of Information to the Cortex.” *Philosophical Transactions of the Royal Society B: Biological Sciences* 357 (1428): 1695–1708. doi:10.1098/rstb.2002.1161.
Sherman, Tait, Melrose, Johnson, Zonta, Court, Macklin, et al. 2005. “Neurofascins Are Required to Establish Axonal Domains for Saltatory Conduction.” *Neuron* 48 (5). United States: 737–42. doi:10.1016/j.neuron.2005.10.019.
Shimojo, Courchet, Pieraut, Torabi-Rander, Sando, Polleux, and Maximov. 2015. “SNAREs Controlling Vesicular Release of BDNF and Development of Callosal Axons.” *Cell Reports* 11 (7). The Authors: 1054–66. doi:10.1016/j.celrep.2015.04.032.
Shin, Shin, McManus, Ptáček, and Fu. 2009. “Dicer Ablation in Oligodendrocytes Provokes Neuronal Impairment in Mice.” *Annals of Neurology* 66 (6). Wiley Subscription Services, Inc., A Wiley Company: 843–57. doi:10.1002/ana.21927.
Shirasu, Kimura, Kataoka, and Takahashi. 2000. “VAMP-2 Promotes Neurite Elongation and SNAP-25A Increases Neurite Sprouting in PC12 Cells” 37: 265–75.
Shoykhet, Doherty, and Simons. 2000. “Coding of Deflection Velocity and Amplitude by Whisker Primary Afferent Neurons: Implications for Higher Level Processing.” *Somatosensory & Motor Research* 17 (2). England: 171–80.
Shrager, and Novakovic. 1995. “Control of Myelination, Axonal Growth, and Synapse Formation in Spinal Cord Explants by Ion Channels and Electrical Activity” 88: 68–78.
Simons, and Trotter. 2007. “Wrapping It up: The Cell Biology of Myelination.” *Current Opinion in Neurobiology* 17: 533–40.
Sims, Hollingworth, Moskvina, Dowzell, Donovan, Powell, Lovestone, et al. 2009. “Neuroscience Letters Evidence That Variation in the Oligodendrocyte Lineage Transcription Factor 2 (OLIG2) Gene Is Associated with Psychosis in Alzheimer ’ s Disease.” *Neuroscience Letters* 461: 54–59. doi:10.1016/j.neulet.2009.05.051.
Sinclair, Fischl, Alexandrova, Heß, Grothe, Leibold, and Kopp-Scheinpflug. 2017. “Sound-Evoked Activity Influences Myelination of Brainstem Axons in the Trapezoid Body.” *The Journal of Neuroscience* 37 (34): 3728–16. doi:10.1523/JNEUROSCI.3728-16.2017.
Skou. 1957. “The Influence of Some Cations on an Adenosine Triphosphatase from Peripheral Nerves.” *BBA - Biochimica et Biophysica Acta* 23 (C): 394–401. doi:10.1016/0006-3002(57)90343-8.

Slavena, Johansson, Ericsson, Janson, Beraki, Stanic, Sven Ove O, Martin A Wikstro, and Christina Bark. 2008. “An Ancient Duplication of Exon 5 in the Snap25 Gene Is Required for Complex Neuronal Development/Function.” *PLoS Genetics* 4 (11). doi:10.1371/journal.pgen.1000278.

Smith, De Avila, Paez, Spreuer, Wills, Jones, Boggs, and Harauz. 2012. “Proline Substitutions and Threonine Pseudophosphorylation of the SH3 Ligand of 18.5-KDa Myelin Basic Protein Decrease Its Affinity for the Fyn-SH3 Domain and Alter Process Development and Protein Localization in Oligodendrocytes.” *Journal of Neuroscience Research* 90 (1). Wiley Subscription Services, Inc., A Wiley Company: 28–47. doi:10.1002/jnr.22733.

Smith, Johnson, Bryan, Hills, Markowitz, Willson, Paraskeva, et al. 1993. “The APC Gene Product in Normal and Tumor Cells.” *Proc. Natl Acad. Sci. USA* 90 (April): 2846–50.

Smith, and Koles. 1970. “Myelinated Thickness Nerve Fibers: Computed Velocity Effect of Myelin on Conduction.” *Physiology* 219 (5): 5–7.

Smith, Paez, Spreuer, Campagnoni, Boggs, Campagnoni, and Harauz. 2011. “Classical 18.5-and 21.5-KDa Isoforms of Myelin Basic Protein Inhibit Calcium Influx into Oligodendroglial Cells, in Contrast to Golli Isoforms.” *Journal of Neuroscience Research* 89 (4). Wiley Subscription Services, Inc., A Wiley Company: 467–80. doi:10.1002/jnr.22570.

Snaidero, Möbius, Czopka, Hekking, Mathisen, Verkleij, Goebbels, et al. 2014. “Myelin Membrane Wrapping of CNS Axons by PI(3,4,5)P3-Dependent Polarized Growth at the Inner Tongue.” *Cell*, 277–90. doi:10.1016/j.cell.2013.11.044.

Sommer, and Schachner. 1981. “Monoclonal Antibodies (O1 to O4) to Oligodendrocyte Cell Surfaces - An Immunocytological Study in the Central Nervous System.”

Songyang, Fanning, Fu, Xu, Marfatia, Chishti, Crompton, Chan, Anderson, and Cantley. 1997. “Recognition of Unique Carboxyl-Terminal Motifs by Distinct PDZ Domains.” *Science* 275 (5296): 73 LP-77. http://science.sciencemag.org/content/275/5296/73.abstract.

Sørensen, Varoqueaux, Nehring, Brose, Wilson, and Neher. 2003. “Differential Control of the Releasable Vesicle Pools by SNAP-25 Splice Variants and SNAP-23.” *Cell* 114: 75–86.

Squire, Allaman, and Magistretti. 2013. “Fundamental Neuroscience (Fourth Edition).” In *Fundamental Neuroscience (Fourth Edition)*, edited by Darwin Berg, Floyd E Bloom, Sascha du Lac, Anirvan Ghosh, and Nicholas C B T - Fundamental Neuroscience (Fourth Edition) Spitzer, 261–84. San Diego: Academic Press. doi:https://doi.org/10.1016/B978-0-12-385870-2.00012-3.

Staiger, Zilles, and Freund. 1996. “Distribution of GABAergic Elements Postsynaptic to Ventroposteromedial Thalamic Projections in Layer IV of Rat Barrel Cortex.” *European Journal of Neuroscience* 8 (1994): 2273–85.

Stallcup. 1981. “The NG2 Antigen, a Putative Lineage Marker: Immunofluorescent Localization in Primary Cultures of Rat Brain.” *Development Biology* 165: 154–65.

Stanfield, B B., and D.M. O’Leary. 1985a. “The Transient Corticospinal Projection from the Occipital Cortex during the Postnatal Development of the Rat.” *Journal of Comparative Neurology* 238 (2): 236–48. doi:10.1002/cne.902380210.

Stanfield, Davies, Sheltonti, Khan, Brammartt, Standen, Conleyt, and Lej. 1994. “The Intrinsic Gating of Inward Rectifier K+ Channels Expressed from the Murine IRKI Gene Depends on Voltage, K+ and Mg2+.” *The Journal of Physiology*, 1–7.

Stanfield, and O’Leary. 1985b. “Fetal Occipital Cortical Neurons Transplanted to the Rostral Cortex Can Extend and Maintain a Pyramidal Tract Axon.” *Nature*.

Staugaitis, Smith, and Colman. 1990. “Expression of Myelin Basic Protein Isoforms in Nonglial Cells.” *The Journal of Cell Biology* 110 (5): 1719–27. http://www.pubmedcentral.nih.gov/articlerender.fcgi?artid=2200185&tool=pmcentrez&rendertype=abstract.

Steck, and Schaeren-Wiemers Hartung. 1998. “Demyelinating Inflammatory Neuropathies, Including Guillain–Barré Syndrome.” *Current Opinion in Neurology*.

Stedehouder, Brizee, Shpak, and Kushner. 2018. “Activity-Dependent Myelination of Parvalbumin Interneurons Mediated by Axonal Morphological Plasticity.” *The Journal of Neuroscience*, 0074-18. doi:10.1523/JNEUROSCI.0074-18.2018.

Steegmaier, Yang, Yoo, Huang, Shen, Yu, Luo, and Scheller. 1998. “Three Novel Proteins of the Syntaxin/SNAP-25 Family” 273 (51): 34171–79.

Steingard, Renshaw, Hennen, Lenox, Cintron, Young, Connor, Au, and Yurgelun-todd. 2002. “Smaller Frontal Lobe White Matter Volumes in Depressed Adolescents.” *Biological Physiology*.

Stevens, Porta, Haak, Gallo, and Fields. 2002. “Adenosine: A Neuron-Glial Transmitter Promoting Myelination in the CNS in Response to Action Potentials.” *Neuron* 36 (5): 855–686.

Stevens, Tanner, and Fields. 1998. “Control of Myelination by Specific Patterns of Neural Impulses.” *The Journal of Neuroscience : The Official Journal of the Society for Neuroscience* 18 (22): 9303–11.

Stockklausner, and Klo. 2003. “Surface Expression of Inward Rectifier Potassium Channels Is Controlled by Selective Golgi Export” 278 (19): 17000–5. doi:10.1074/jbc.M212243200.

Stockklausner, Ludwig, Ruppersberg, and Klo. 2001. “A Sequence Motif Responsible for ER Export and Surface Expression of Kir2.0 Inward Rectifier K(+) Channels” 493: 2–6.

Stolt, Rehberg, Ader, Lommes, Riethmacher, Schachner, Bartsch, and Wegner. 2002. “Terminal Differentiation of Myelin-Forming Oligodendrocytes Depends on the Transcription Factor Sox10,” 165–70. doi:10.1101/gad.215802.tive.

Sturrock. 1980. “Myelination of the Mouse Corpus Callosum.” *Neuropathology and Applied Neurobiology*, no. January: 415–20.

Südhof, and Rizo. 2011. “Synaptic Vesicle Exocytosis.” *Cold Spring Harbor Perspectives in Biology* 3 (12): 1–14. doi:10.1101/cshperspect.a005637.

Sun, Meijer, Alberta, Mehta, Kane, Tien, Fu, et al. 2011. “Phosphorylation State of Olig2 Regulates Proliferation of Neural Progenitors.” *Neuron* 69 (5). Elsevier Inc.: 906–17. doi:10.1016/j.neuron.2011.02.005.

Swadlow. 1985. “Physiological Properties of Individual Cerebral Axons Studied in Vivo for as Long as One Year.” *Journal of Neurophysiology* 54 (5): 1346–62. doi:n/a.

Swadlow, H A. 1994. “Efferent Neurons and Suspected Interneurons in Motor Cortex of the Awake Rabbit: Axonal Properties, Sensory Receptive Fields, and

Subthreshold Synaptic Inputs." *Journal of Neurophysiology* 71 (2): 437–53. doi:10.1523/JNEUROSCI.

Takahashis, Morishiges, Jahangirs, and Yamadas. 1994. "Molecular Cloning and Functional Expression of CDNA Encoding a Second Class of Inward Rectifier Potassium Channels in the Mouse Brain *." *Journal of Biological Chemistry* 269 (37): 23274–79.

Takebayashi, Hirohide, and Kazuhiro Ikenaka. 2015. "Oligodendrocyte Generation During Mouse Development." doi:10.1002/glia.22863.

Takebayashi, Yoshida, Sugimori, and Kosako. 2000. "Dynamic Expression of Basic Helix-Loop-Helix Olig Family Members: Implication of Olig2 in Neuron and Oligodendrocyte Differentiation and Identifcation of a New Member, Olig3." *Mechanisms of Development* 99: 143–48.

Tamamaki, Fujimori, and Takauji. 1997. "Origin and Route of Tangentially Migrating Neurons in the Developing Neocortical Intermediate Zone." *The Journal of Neuroscience : The Official Journal of the Society for Neuroscience* 17 (21): 8313–23. doi:10.1523/JNEUROSCI.17-21-08313.1997.

Tao, Finkbeiner, Arnold, Shaywitz, and Greenberg. 1998. "Ca2+influx Regulates BDNF Transcription by a CREB Family Transcription Factor-Dependent Mechanism." *Neuron* 20 (4): 709–26. doi:10.1016/S0896-6273(00)81010-7.

Tauber, Waehneldt, and Neuhoff. 1980. "Myelination in Rabbit Optic Nerves Is Accelerated by Artificial Eye Opening." *Neuroscience Letters* 16: 235–38.

Tekki-Kessaris, Woodruff, Hall, Gaffield, Kimura, Stiles, Rowitch, and Richardson. 2001. "Hedgehog-Dependent Oligodendrocyte Lineage Specification in the Telencephalon." *Development* 2554: 2545–54.

Thomson. 2010. "Neocortical Layer 6, a Review" 4 (March): 1–14. doi:10.3389/fnana.2010.00013.

Tinker, Jan, and Jan. 1996. "Regions Responsible for the Assembly of Inwardly Rectifying Potassium Channels." *Cell* 87: 857–68.

Tomasi, Caminiti, and Innocenti. 2012. "Areal Differences in Diameter and Length of Corticofugal Projections." *Cerebral Cortex*, no. April: 1463–72. doi:10.1093/cercor/bhs011.

Tomassy, Berger, Chen, Kasthuri, Hayworth, Vercelli, Seung, Lichtman, and Arlotta. 2014. "Distinct Profiles of Myelin Distribution Along Single Axons of Pyramidal Neurons in the Neocortex." *Science* 344 (6181): 319–24. doi:10.1126/science.1249766.

Tosic, Torch, Comte, Dolivo, Honegger, and J Matthieu. 1992. "Triiodothyronine Has Diverse and Multiple Stimulating Effects on Expression of the Major Myelin Protein Genes." *Journal of Neurochemistry* 59 (5). Wiley/Blackwell (10.1111): 1770–77. doi:10.1111/j.1471-4159.1992.tb11009.x.

Touahri, Yacine, Nathalie Escalas, Bertrand Benazeraf, Philippe Cochard, Cathy Danesin, and Cathy Soula. 2012. "Sulfatase 1 Promotes the Motor Neuron-to-Oligodendrocyte Fate Switch by Activating Shh Signaling in Olig2 Progenitors of the Embryonic Ventral Spinal Cord" 32 (50): 18018–34. doi:10.1523/JNEUROSCI.3553-12.2012.

Trapp, and Nave. 2008. "Multiple Sclerosis: An Immune or Neurodegenerative Disorder?" *Annual Review of Neuroscience* 31 (1). Annual Reviews: 247–69. doi:10.1146/annurev.neuro.30.051606.094313.

Travis. 1998. "Cortical and Cognitive Development in 4th, 8th and 12th Grade Students. The Contribution of Speed of Processing and Executive Functioning

to Cognitive Development." *Biological Physiology* 48: 37–56.
Trichas, Begbie, and Srinivas. 2008. "Use of the Viral 2A Peptide for Bicistronic Expression in Transgenic Mice." *BMC Biology* 13: 1–13. doi:10.1186/1741-7007-6-40.
Trigo, and Smith. 2015. "Axonal Morphological Changes Following Impulse Activity in Mouse Peripheral Nerve in Vivo: The Return Pathway for Sodium Ions." *The Journal of Physiology* 593 (4): 987–1002. doi:10.1113/jphysiol.2014.279331.
Tripathi, Clarke, Burzomato, Kessaris, Anderson, Attwell, and Richardson. 2011. "Dorsally and Ventrally Derived Oligodendrocytes Have Similar Electrical Properties but Myelinate Preferred Tracts." *The Journal of Neuroscience* 31 (18): 6809–19. doi:10.1523/JNEUROSCI.6474-10.2011.
Tristani-Firouzi, Jensen, Donaldson, Sansone, Meola, Hahn, Bendahhou, et al. 2002. "Functional and Clinical Characterization of KCNJ2 Mutations Associated with LQT7 (Andersen Syndrome)" 110 (3): 381–88. doi:10.1172/JCI200215183.Introduction.
Trotter, Karram, and Nishiyama. 2010. "NG2 Cells: Properties , Progeny and Origin Cell Lineage." *Brain Research Reviews* 63 (1–2). Elsevier B.V.: 72–82. doi:10.1016/j.brainresrev.2009.12.006.
Uhlhaas, and Singer. 2006. "Neural Synchrony in Brain Disorders: Relevance for Cognitive Dysfunctions and Pathophysiology." *Neuron* 52 (1): 155–68. doi:10.1016/j.neuron.2006.09.020.
Ullian, Sapperstein, Christopherson, and Barres. 2001. "Control of Synapse Number by Glia." *Science* 291 (5504): 657–61. doi:10.1126/science.291.5504.657.
Utans, Arceci, Yamashita, and Russell. 1995. "Cloning and Characterization of Allograft Inflammatory Factor-1 : A Novel Macrophage Factor Identified in Rat Cardiac Allografts with Chronic Rejection." *Clin. Invest.* 95 (June): 2954–62.
Vallstedt, Klos, and Ericson. 2014. "Multiple Dorsoventral Origins of Oligodendrocyte Generation in the Spinal Cord and Hindbrain." *Neuron* 45 (1). Elsevier: 55–67. doi:10.1016/j.neuron.2004.12.026.
Vandesompele, De Preter, Pattyn, Poppe, Van Roy, De Paepe, and Speleman. 2002. "Accurate Normalization of Real-Time Quantitative RT-PCR Data by Geometric Averaging of Multiple Internal Control Genes." *Genome Biology* 3 (711): 34–1. doi:10.1186/gb-2002-3-7-research0034.
Vardar, Chang, Arancillo, Wu, Trimbuch, and Rosenmund. 2016. "Distinct Functions of Syntaxin-1 in Neuronal Maintenance, Synaptic Vesicle Docking, and Fusion in Mouse Neurons." *The Journal of Neuroscience* 36 (30): 7911–24. doi:10.1523/JNEUROSCI.1314-16.2016.
Varoqueaux, Sigler, Rhee, Brose, Enk, Reim, and Rosenmund. 2002. "Total Arrest of Spontaneous and Evoked Synaptic Transmission but Normal Synaptogenesis in the Absence of Munc13-Mediated Vesicle Priming." *Proceedings of the National Academy of Sciences* 99 (13): 9037–42. doi:10.1073/pnas.122623799.
Veinante, Lavalle, Giffard, and Giffard. 2000. "Corticothalamic Projections From Layer 5 of the Vibrissal Barrel Cortex in the Rat." *J Comp Neurol.* 204 (March): 197–204.
Verkhratsky, and Steinhäuser. 2000. "Ion Channels in Glial Cells." *Brain Research. Brain Research Reviews* 32 (2–3): 380–412. doi:10.1016/S0165-0173(99)00093-4.

Virchow. 1856. “Gesammelte Abhandlungen Zur Wissenschaftlichen Medizin.” *Zeitschrift Für Psychiatrie*.
Vogel, and Roche. 1999. “SNAP-23 and SNAP-25 Are Palmitoylated in Vivo” 410: 407–10.
Vojvodic. 1989. “Target Size Regulates Calibre and Myelination of Sympathetic Axons.” *Letters to Nature* 342.
Vondran, Clinton-Luke, Honeywell, and Dreyfus. 2010. “BDNF +/- Mice Exhibit Deficits in Oligodendrocyte Lineage Cells of the Basal Forebrain.” *Glia* 58 (7): 848–56. doi:10.1002/glia.20969.
Wake, Hiroaki, Philip R Lee, and R Douglas Fields. 2011a. “Control of Local Protein Synthesis and Initial Events in Myelination By.” *Science* 333 (September): 1647–52.
Wake, Lee, and Fields. 2011b. “Control of Local Protein Synthesis and Initial Events in Myelination by Action Potentials.” *Science* 333 (6049): 1647–51. doi:10.1126/science.1206998.
Wang, Sdrulla, Bush, Nofziger, Hicks, Weinmaster, and Barres. 1998. “Notch Receptor Activation Inhibits Oligodendrocyte Differentiation” 21: 63–75.
Wang, Witkin, Hao, Bankaitis, Scherer, and Baldini. 1997. “Syndet Is a Novel SNAP-25 Related Protein Expressed in Many Tissues.” *J Cell Sci.* 513: 505–13.
Wang, Zhang, Zhou, Zhou, Yang, Duan, Xiong, and Ding. 2007. “Activity-Dependent Development of Callosal Projections in the Somatosensory Cortex.” *The Journal of Neuroscience* 27 (42): 11334–42. doi:10.1523/JNEUROSCI.3380-07.2007.
Washbourne, Pellizzari, Baldini, Wilson, and Montecucco. 1997. “Botulinum Neurotoxin Types A and E Require the SNARE Motif in SNAP-25 for Proteolysis.” *FEBS Letters* 418 (1–2). Federation of European Biochemical Societies: 1–5. doi:10.1016/S0014-5793(97)01328-8.
Washbourne, Thompson, Carta, Costa, Mathews, Lopez-Benditó, Molnár, et al. 2002. “Genetic Ablation of the T-SNARE SNAP-25 Distinguishes Mechanisms of Neuroexocytosis.” *Nature Neuroscience* 5 (1): 19–26. doi:10.1038/nn783.
Watkins, Emery, Mulinyawe, and Barres. 2008. “Distinct Stages of Myelination Regulated by γ-Secretase and Astrocytes in a Rapidly Myelinating CNS Coculture System.” *Neuron* 60 (4). Elsevier Inc.: 555–69. doi:10.1016/j.neuron.2008.09.011.
Waxman. 1971. “An Ultrastructural Study of the Pattern of Myelination of Preterminal Fibers in Teleost Oculomotor Nuclei, Electromotor Nuclei, and Spinal Cord.” *Brain Reserach* 27: 189–201.
Waxman, Pappas, and Bennett. 1972. “Morphological Correlates of Functional Differentiation of Nodes of Ranvier along Single Fibers in the Neurogenic Electric Organ of the Knife Fish Stern Archus.” *J Cell Biol*, 210–24.
Waxman, S G. 1975. “Integrative Properties and Design Principles of Axons.” *International Review of Neurobiology* 18 (C). Academic Press: 1–40. doi:10.1016/S0074-7742(08)60032-X.
Weiler, Wood, Yu, Solla, and Shepherd. 2008. “Top-down Laminar Organization of the Excitatory Network in Motor Cortex.” *Nature Neuroscience* 11 (3). doi:10.1038/nn2049.
Weimann, Zhang, Levin, and Devine. 1999. “Cortical Neurons Require Otx1 for the Refinement of Exuberant Axonal Projections to Subcortical Targets.” *Neuron*

24: 819–31.
Weimbs, Low, Chapin, Mostov, Bucher, and Hofmann. 1997. “A Conserved Domain Is Present in Different Families of Vesicular Fusion Proteins : A New Superfamily.” *Cell Biology* 94 (April): 3046–51.
White, Gonsior, Krämer-Albers, Stöhr, Hüttelmaier, and Trotter. 2008a. “Activation of Oligodendroglial Fyn Kinase Enhances Translation of MRNAs Transported in HnRNP A2-Dependent RNA Granules.” *The Journal of Cell Biology* 181 (4): 579–86. doi:10.1083/jcb.200706164.
White, Robin, Constantin Gonsior, Eva-Maria Krämer-Albers, Nadine Stöhr, Stefan Hüttelmaier, and Jacqueline Trotter. 2008b. “Activation of Oligodendroglial Fyn Kinase Enhances Translation of MRNAs Transported in HnRNP A2-Dependent RNA Granules.” *The Journal of Cell Biology* 181 (4): 579–86. doi:10.1083/jcb.200706164.
Wilent, and Contreras. 2004. “Synaptic Responses to Whisker Deflections in Rat Barrel Cortex as a Function of Cortical Layer and Stimulus Intensity.” *The Journal of Neuroscience* 24 (16): 3985–98. doi:10.1523/JNEUROSCI.5782-03.2004.
Williamson, and Cleveland. 1999. “Slowing of Axonal Transport Is a Very Early Event in the Toxicity of ALS-Linked SOD1 Mutants to Motor Neurons.” *Nature Neurosci.* 2. Nature Publishing Group: 50–56.
Wilson, Baetge, and Stallcup. 1981. “Antisera Specific for Cell Lines with Mixed Neuronal and Glial Properties” 153: 146–53.
Wilson, and Chiu. 1990. “Ion Channels in Axon and Schwann Cell Membranes at Paranodes of Mammalian Myelinated Fibers Studied with Patch Clamp.” *Journal of Neuroscience*, no. October.
Wimmer, Bruno, Kock, Kuner, and Sakmann. 2010. “Dimensions of a Projection Column and Architecture of VPM and POm Axons in Rat Vibrissal Cortex,” no. October: 2265–76. doi:10.1093/cercor/bhq068.
Windebank. 1985. “Myelination Determines the Caliber of Dorsal Root Ganglion Neurons in Culture.” *Journal of Neuroscience*, 1563–69.
Winterstein, and Trotter. 2008. “Distinct Endocytic Recycling of Myelin Proteins Promotes Oligodendroglial Membrane Remodeling,” 834–42. doi:10.1242/jcs.022731.
Wise, and Jones. 1977. “Cells of Origin and Terminal Distribution of Descending Projections of the Rat Somatic Sensory Cortex.”
Wong, Xiao, Kemper, Kilpatrick, and Murray. 2013. “Oligodendroglial Expression of TrkB Independently Regulates Myelination and Progenitor Cell Proliferation.” *Journal of Neuroscience* 33 (11): 4947–57. doi:10.1523/JNEUROSCI.3990-12.2013.
Wood, Vella, and Moscarello. 1984. “Interaction between Human Myelin Basic Protein and Lipophilin.” *Neurochemical Research* 9 (10). United States: 1523–31.
Woolsey, and Van der Loos. 1970. “The Structural Organization of Layer IV in the Somatosensory Region (S I) of Mouse Cerebral Cortex: The Description of a Cortical Field Composed of Discrete Cytoarchitectonic Units.” *Brain Research* 17: 205–42.
Wu, Li, Huang, Chen, Huang, Liu, Zhao, et al. 2017. “Caspr Controls the Temporal Specification of Neural Progenitor Cells through Notch Signaling in the Developing Mouse Cerebral Cortex.” *Cerebral Cortex* 27 (2): 1369–85.

http://dx.doi.org/10.1093/cercor/bhv318.
Wu, Williams, Delaney, Sherman, and Brophy. 2012. “Report Increasing Internodal Distance in Myelinated Nerves Accelerates Nerve Conduction to a Flat Maximum.” *Current Biology* 22 (20). Elsevier Ltd: 1957–61. doi:10.1016/j.cub.2012.08.025.
Xiao, Hu, Yang, Guo, Li, Shen, Liu, Aijun, Dan, and He. 2013. “NMDA Receptor Couples Rac1-GEF Tiam1 to Direct Oligodendrocyte Precursor Cell Migration.” *Glia* 61 (12): 2078–99. doi:10.1002/glia.22578.
Xiao, Kilpatrick, and Murray. 2009. “The Role of Neurotrophins in the Regulation of Myelin Development.” *Neurosignals* 17 (4): 265–76. https://www.karger.com/DOI/10.1159/000231893.
Xiao, Ohayon, Mckenzie, Sinclair-Wilson, JWright, Fudge, Emery, Li, and Richardson. 2017. “Rapid Production of New Oligodendrocytes Is Required in the Earliest Stages of Motor Skill Learning” 19 (9): 1210–17. doi:10.1038/nn.4351.Rapid.
Xiao, Wong, Willingham, van den Buuse, Kilpatrick, and Murray. 2010. “Brain-Derived Neurotrophic Factor Promotes Central Nervous System Myelination via a Direct Effect upon Oligodendrocytes.” *Neurosignals* 18 (3): 186–202. https://www.karger.com/DOI/10.1159/000323170.
Xu, Yu, Perlik, Tobin, Zweig, Jones, and Zuo. 2010. “Rapid Formation and Selective Stabilization of Synapses for Enduring Motor Memories.” *Nature* 462 (7275): 915–19. doi:10.1038/nature08389.Rapid.
Xue, Atallah, and Scanziani. 2014. “Equalizing Excitation-Inhibition Ratios across Visual Cortical Neurons.” *Nature* 511 (7511): 596–600. http://www.nature.com/authors/editorial_policies/license.html#terms.
Yamada, and Kuba. 2016. “Structural and Functional Plasticity at the Axon Initial Segment.” *Frontiers in Cellular Neuroscience* 10 (October): 1–7. doi:10.3389/fncel.2016.00250.
Yamada, Uesaka, Hayano, Tabata, and Kano. 2010. “Role of Pre- and Postsynaptic Activity in Thalamocortical Axon Branching.” *PNAS*. doi:10.1073/pnas.0900613107.
Yamaguchi, Seki, Imayoshi, Tamamaki, Hayashi, Tatebayashi, and Hitoshi. 2016. “Neural Stem Cells and Neuro/Gliogenesis in the Central Nervous System: Understanding the Structural and Functional Plasticity of the Developing, Mature, and Diseased Brain.” *Journal of Physiological Sciences* 66 (3). Springer Japan: 197–206. doi:10.1007/s12576-015-0421-4.
Yang, Li, Qiu, Zhang, Lu, Chen, Zhao, et al. 2013. “Effects of an Enriched Environment on Myelin Sheaths in the White Matter of Rats during Normal Aging: A Stereological Study.” *Neuroscience* 234: 13–21. doi:10.1016/j.neuroscience.2013.01.003.
Yang, Zhang, Shi, Zhou, Wan, Wang, Wan, Li, Wang, and Fei. 2017. “Brain-Specific SNAP-25 Deletion Leads to Elevated Extracellular Glutamate Level and Schizophrenia-Like Behavior in Mice” 2017. Hindawi. doi:10.1155/2017/4526417.
Yu, Chen, Kim, Wang, Zhao, He, Liu, et al. 2013. “Olig2 Targets Chromatin Remodelers to Enhancers to Initiate Oligodendrocyte Differentiation.” *Cell* 152 (1–2). Elsevier Inc.: 248–61. doi:10.1016/j.cell.2012.12.006.
Yu, Power, Barnea, Donnell, Brown, Osborne, Axel, and Gogos. 2004. “Spontaneous Neural Activity Is Required for the Establishment and

Maintenance of the Olfactory Sensory Map." *Neuron* 42: 553–66.
Yue. 2006. "A Critical Role for Dorsal Progenitors in Cortical Myelination." *Journal of Neuroscience* 26 (4): 1275–80. doi:10.1523/JNEUROSCI.4717-05.2006.
Yüzbaolu, Onbalar, Kocaefe, and ÖzgüÇ. 2010. "Assessment of Housekeeping Genes for Use in Normalization of Real Time PCR in Skeletal Muscle with Chronic Degenerative Changes." *Experimental and Molecular Pathology* 88 (2): 326–29. doi:10.1016/j.yexmp.2009.12.007.
Zalc, and Fields. 2000. "Do Action Potentials Regulate Myelination?" *The Neuroscientist* 6 (1): 5–13. doi:10.1177/107385840000600109.
Zaritsky, Eckman, Wellman, Nelson, and Schwarz. 2000. "Targeted Disruption of Kir2.1 and Kir2.2 Genes Reveals the Essential Role of the Inwardly Rectifying K(+) Current in K(+)-Mediated Vasodilation." *Circulation Reserach*, 160–67.
Zarrinpar, and Callaway. 2005. "Local Connections to Specific Types of Layer 6 Neurons in the Rat Visual Cortex." *Journal of Neurophysiology*, 1751–61. doi:10.1152/jn.00974.2005.
Zhang, and Desche. 1997. "Intracortical Axonal Projections of Lamina VI Cells of the Primary Somatosensory Cortex in the Rat : A Single-Cell Labeling Study." *The Journal of Neuroscience* 17 (16): 6365–79.
Zhao, He, Han, Yu, Ye, Chen, Hoang, et al. 2010. "Article MicroRNA-Mediated Control of Oligodendrocyte Differentiation." *Neuron* 65 (5). Elsevier Ltd: 612–26. doi:10.1016/j.neuron.2010.02.018.
Zhou, and Anderson. 2002. "The BHLH Transcription Factors OLIG2 and OLIG1 Couple Neuronal and Glial Subtype Specification." *Cell* 109: 61–73.
Zhou, Choi, and Anderson. 2001. "The BHLH Transcription Factor Olig2 Promotes Oligodendrocyte Differentiation in Collaboration with Nkx2 . 2" 31: 791–807.
Zhou, Wang, and Anderson. 2000. "Identification of a Novel Family of Oligodendrocyte Lineage-Specific Basic Helix – Loop – Helix Transcription Factors." *Neuron* 25: 331–43.
Zhou, Xiao, and Liu. 2000. "Participation of Syntaxin 1A in Membrane Trafficking Involving Neurite Elongation and Membrane Expansion" 328: 321–28.
Ziskin, Nishiyama, Rubio, Fukaya, and Bergles. 2007. "Vesicular Release of Glutamate from Unmyelinated Axons in White Matter." *Nature Neuroscience* 10 (3): 321–30.
Zuchero, and Barres. 2013. "Intrinsic and Extrinsic Control of Oligodendrocyte Development." *Current Opinion in Neurobiology* 23 (6): 914–20. doi:https://doi.org/10.1016/j.conb.2013.06.005.